MODELLING PURE THORIUM BUNDLE IMPLEMENTATION IN THE CANDU-6 REACTOR

MODELLING PURE THORIUM BUNDLE IMPLEMENTATION IN THE CANDU-6 REACTOR

By SHAUN SIA HO YEE, B. Sc.

A Thesis Submitted to the School of Graduate Studies in Partial Fulfilment of the Requirements for the Degree Master of Applied Science

McMaster University © Copyright by Shaun Sia Ho Yee, June 2015

McMaster University MASTER OF APPLIED SCIENCE (2015) Hamilton, Ontario (Engineering Physics)

TITLE: Modelling pure thorium bundle implementation in the CANDU-6 reactor

AUTHOR: Shaun Sia Ho Yee, B. Sc. (University of Calgary)
SUPERVISOR: Professor John C. Luxat
NUMBER OF PAGES: ix, 147

Abstract

Fuels comprised of the element thorium have become increasingly popular with researchers and the public as the next generation fuel due to its ability to produce its own fissile element (U-233) and generate lower concentrations of heavy actinides. The use of thorium can possibly lead to a self-sustaining cycle whereby the addition of fissile material is not required and that the fuel can breed sufficient amounts of U-233 for a continuous supply. Research into thorium use in CANDU reactors has mainly been focused on using driver elements such as U-235 or Pu-239 to initiate the nuclear reaction by taking advantage of bundle design or by mixing the thorium and driver fuel together; however, these methods have added complexities and may not lead to a pure thorium fuel cycle, but extend the life of current nuclear fuels used.

This thesis will investigate a simpler means of utilizing thorium for the intent of breeding U-233 through the use of pure thorium bundles in a once-through cycle by the ways of a heterogeneous core loading in a CANDU-6 reactor model. A 3x3 multi-cell model using DRAGON 3.06K will simulate the dual fuel model by having the centre lattice enclosing the thorium bundle and the outer eight lattices enclosing the enriched uranium bundles as the driver fuel. Next, the diffusion code DONJON 3.02E is used to produce time-average, instantaneous, and initial startup full-core simulations. As well, a brief look at the refuelling operations on the thorium channels will be done.

The presence of a thorium bundle places a negative reactivity load on the multi-cell, but causes a positive insertion of reactivity for a coolant void and shutdown scenario. In the full-core modelling, the final core configuration chosen shows that thorium channels should be located in the inner core rather than in the most outer channels to produce a flattening effect on the radial profile. Thorium channels will require a combination of SEU and thorium bundles in an attempt to maintain channel power levels. Specifically, the use of 4, 6, or 8 Th bundles were investigated. The most optimal core performance shown has a radial form factor of 0.816, a total average core burnup of 18.32 GWd/t, and operates within designed power limits.

It is possible to implement pure thorium bundles into a reactor set in a dual fuel mode. A careful consideration of where thorium bundles should be located in the core can help flatten the radial power distribution and help the reactor operate within the operating licensing parameters without the use of adjuster rods while breeding U-233 for a future thorium fuel cycle.

Acknowledgements

I would like to thank all the people who have helped and supported my graduate studies. It would not have been possible without them.

Firstly, I would like to express my sincere gratitude to Dr. John C. Luxat for taking me as his student. His guidance throughout my studies and thesis has been a tremendous help and an enlightening experience. I would like to also thank my defense committee, Dr. Buijs, Dr. Day, and Dr. Novog, for taking their time to read my thesis and providing valuable comments. Their input into my work is greatly appreciated.

I would also like to thank my mother and father, Chi Hung Mai and Jan Ng Yee, for their support in my decision to move to Hamilton to pursue my studies and making sure I stayed happy and healthy. As well, I would like to thank my brothers, my aunt, and my two cousins for their continual support .

I would also like to send gratitude to my friends back home for their unwavering support and help. Also, I would like to thank my friends and colleagues at McMaster University for their assistance and for making my studies enjoyable. Special thanks to David Hummel for his supply of codes and technical expertise. Thank you all for making this chapter of my life a great experience.

Contents

List of Figures

List of Tables

List of Abbreviations and Symbols

β	Beta Particle
$\chi(E)$	Fission Energy Spectrum
ϵ	Enrichment(%)
η	Number of Neutrons causing Fission
ν	Average Number of Fission Neutrons Produced
$\overrightarrow{r}$	Neutron Position
ϕ	Angular Neutron Flux
Σ	Macroscopic Cross-Section (cm$^-$1)
σ	Microscopic Cross-Section (cm^2)
$\widehat{\Omega}$	Direction Unit Vector
E	Neutron Energy
$GW_e(y)$	Giga-Watt Electric Year
Mg	Mega-gram
MW_e	Mega-Watt Electric
n	Neutron
s	Neutron Source
t	Time
v	Neutron Speed
2D	Two Dimensional
3D	Three Dimensional

AECL Atomic Energy of Canada Limited

BOC Beginning of Cycle

BS Bundle Shift

CANDU Canada Deuterium Uranium

CPPF Channel Peak Powr Factor

DU Depleted Uranium

DUPIC Direct Use of Pressurized Water Reactor Spent Fuel in CANDU

EOC End of Cycle

FP Fission Product

KAERI Korean Atomic Energy Research Institute

MA Minor Actinide

NU Natural Uranium

PUREX Plutonium Uranium Redox Extraction

PWR Pressurized Water Reactor

SEU Slightly Enriched Uranium

SSET Self-Sustaining Equilibrium Thorium

THOREX Thorium Extraction

UO_2 Uranium Oxide

The work presented in this thesis has been a cumulation of work performed by Shaun S.H. Yee. Information contributed by other authors used herein are duly referenced.

Chapter 1

Introduction

Nuclear energy is currently the most ideal method for sustaining the increasing levels of power consumption in the world and for reducing the quantity of carbon and toxic gas emissions. The current method of producing commercial nuclear energy is through fission. Unlike its fossil fuel counterpart, the nuclear fuel cycle produces significantly lower carbon emissions, which has become an increasingly popular attribute for energy production. The majority of current reactors in the world utilize a varying composition of U-235/238 oxides as its fuel. The fuel undergoes a 'once-through' concept where it is burned in the core and then sent off for long-term storage. As a result, the accumulation of spent nuclear fuel has been a growing concern. Ongoing research has looked into taking spent fuel out of storage and reprocessing it to extract the viable materials still left behind and incorporating it into new fuel bundles. This method, however, can be dangerous due to the high radioactivity of spent fuel bundles and expensive from the added costs to operate such a facility [1]. In order to curb the increasing amounts of spent fuel and mitigate the costs and risks associated with reprocessing, a plausible direction would be to investigate a new type of fuel, such as thorium.

1.1 Thorium

Thorium-232 can be a substitute for U-238 in the fuel for current reactors; however, there is an absence of fissile elements which is unlike the uranium fuel cycle that naturally contains $\sim 0.71\%$ fissile U-235. Instead, fertile Th-232 requires a neutron source to transmutate it into the fissile element U-233. A driver material like U-235 or Pu-239 is therefore required to initiate the production of U-233. After the absorption of a neutron, thorium decays to protactinium-233, which in turn decays to U-233 with a half-life of 27 days. The reaction equations of the process are shown below [2].

$$Th - 232 + n \rightarrow Th - 233 \rightarrow Pa - 233 + \beta^{-} \tag{1.1}$$

$$Pa - 233 \rightarrow U - 233 + \beta^{-} \tag{1.2}$$

There are several benefits to using thorium as a reactor fuel. For example, thorium ore is about three to four times more abundant than uranium [3]. Some countries, such as India, do not have a rich supply of uranium like in Canada, but have an over-abundance of thorium [4]. These countries would therefore benefit themselves if they could utilize their own natural resources [4].

In terms of neutronics, thorium is a better breeder material as it has a thermal neutron absorption cross-section that is three times higher than that of U-238 (shown later in Figure 2.1) [3]. Furthermore, the average thermal neutron produced (η) from the fission of U-233 is 2.29 neutrons while U-235 produces approximately 2.07 at the same thermal energy range [5]. Therefore, η-1, the excess neutrons available for other fissions or absorptions, is higher for U-233 than U-235 and thus U-233 is a suitable driver material for a thorium fuel bundle. As well, the material properties of thorium oxide provides an increase in intrinsic safety operations of the reactor due to it having a 50% higher conductivity than UO_2, a melting point of 3300°C, and a propensity to resist oxidation [2]. Furthermore, since thorium is one of the lighter elements in the actinide series, it would require numerous successive neutron absorptions to produce heavier elements when used, therefore inevitably lowering the amount of heavy element waste produced.

Table 1.1: Thermal neutronic characteristics of fissile isotopes

Isotopes	σ_f (barn)	σ_c (barn)	ν	$\eta = \nu\sigma_f/\sigma_a$
^{233}U	531	46	2.49	2.29
^{235}U	582	101	2.42	2.07
^{239}Pu	743	270	2.87	2.11

Due to thorium's superior neutronics outlined in Table 1.1 [5], a self-sustaining equilibrium thorium (SSET) cycle can be introduced into the CANDU system. This is accomplished by operating the reactor with only thorium enriched U-233 fuel such that it breeds a quantity of U-233 equal to or greater than the initial value. An SSET cycle is the ultimate way to conserving U-235 since no topping of fissile elements is required [3]. The only topping material needed is the addition of thorium to replace what was depleted from before. The caveat is that the fuel bundles must be continuously reprocessed due to the build-up of actinides and fission products, which inhibits a sustained nuclear chain reaction. Furthermore, reprocessing thorium bundles and the frequency at which it occurs is one of the limiting factors to the SSET cycle.

1.2 CANDU Reactor

The CANada Deuterium Uranium (CANDU) reactor is Canada's nuclear flagship. A typical 600 MWe CANDU reactor consists of 380 horizontal fuel channels, each containing twelve 37-element fuel bundles. The separate coolant and moderator are both comprised of heavy water, which is highly efficient at moderating neutrons. Online refuelling provides a way to micro-manage the reactivity of the core through the use of fresh and spent fuel bundles. The combination of effective moderation and micro-managed reactivity makes CANDU an excellent system for the use of thorium.

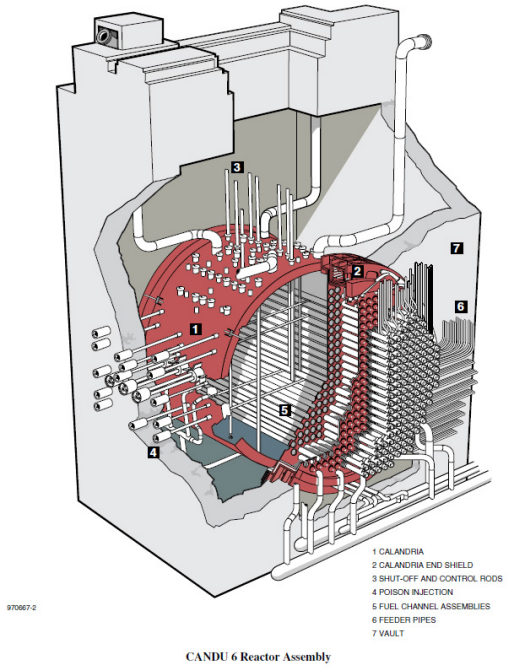

Figure 1.1: The CANDU-6 Assembly [6]

Employment of thorium fuel to the CANDU system requires extensive development and analysis to determine how to properly utilize the element. Due to the 27-day half-life of Pa-233, the flux history of the fuel is important since it dictates the amount of neutrons lost to the absorption from Pa-233 (further discussed in Chapter 2) [7]. Given the CANDU's efficient moderation and ability to control flux, it is possible to shape the breeding behaviour of the thorium fuel.

The investigation of this thesis is to assess a partially fuelled thorium CANDU system for the intent of breeding U-233. To begin, a review of the relevant literature is performed in Chapter 2. Chapter 3 will discuss the theory and tools used in this investigation. Then the assessment will undergo a two phase procedure:

1. A 2D neutron transport code will be used to model the breeding behaviour of a 37-element CANDU thorium bundle surrounded by a blanket of uranium bundle drivers in a 3x3 multi-cell [8]. This first step will be performed in Chapter 4. Properties such as burnup, fissile content, and reactivity will be examined. The results from the code will create homogenized cross-sections that are fed to the full core reactor code and modelled.

2. The second phase will involve conducting simulations on a full-core scale using a two-group 3D diffusion code. A dual fuel mode will require an investigation on different channel and core configurations that will produce time-average and instantaneous models that operate within the safety margins of the CANDU design. The results will be discussed in Chapter 5.

The objective of this thesis is to present the behaviour of the thorium bundle in the aforementioned arrangement and then to determine a possible core configuration that can utilize both uranium and thorium bundles without requiring drastic change to the CANDU platform while preserving sound engineering principles. This will be done by comparing the power distributions and operating parameters from the dual fuel analysis to current licensing standards and the NU-CANDU core. The conclusion of this thesis will hopefully help close gaps in the thorium fuel cycle by providing a means to deploying thorium fuel for the intent of breeding and possibly offer new insight for thorium utilization in CANDU reactors.

Chapter 2

Literature Review

Utilizing thorium fuel in commercial reactors has many challenges; however, finding an efficient method to breed U-233 will provide the benefits of using thorium and the possibility of closing the thorium fuel cycle. This chapter will discuss the challenges and the research done so far in implementing thorium into CANDU reactors.

2.1 Physics Challenge of Thorium

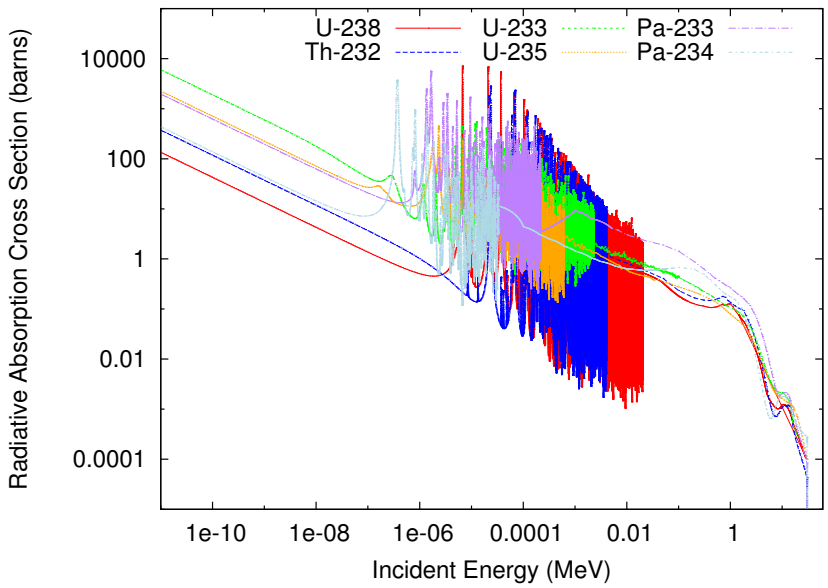

Figure 2.1: Absorption cross-sections of important actinides in Thorium cycle

The benefits of using thorium as a reactor fuel stems from its ability to produce its own fissile material to prolong fuel burnup. Being a fertile material, thorium must

absorb a neutron in order to become fissile, and thus its implementation into a reactor core must involve accounting for the lowered neutron flux and multiplication factor. As well, the transmutation process requires an external source of neutrons such as other fissile elements like U-235 or Pu-239. Consequently, the external source always comes in a mixture containing some other fertile elements for proliferative reasons, such as U-238 with U-235.; handling of purely U-235 is dangerous in terms of criticality and weaponization. As a result, the absorptive nature of fertile elements will compete with thorium, thereby lowering its breeding capability. Deploying a capable breeding reactor requires a careful design to accommodate both the external fissile component and thorium.

Equation 1.1 and 1.2 show that an absorption of a neutron by thorium will create the intermediate product Pa-233, which has a half-life of roughly 27 days. A similar intermediate step is also seen in the uranium fuel cycle with the creation of Np-239 from the absorption of U-238. However, the half-life of Np-239 is only 2.35 days, which is much shorter than that Pa-233. In addition, the thermal neutron capture cross-section of Pa-233, as shown in Figure 2.1 [9], is over five times greater than that of Th-232, which creates another sink for the neutron flux [10]. The neutron absorption chain of thorium is shown in Figure 2.2 [3]. The higher sink in neutron economy is due to the two extra neutrons required to produce a fissile isotope if Pa-233 is to absorb one. Furthermore, the resulting isotope is U-235, rather than U-233.

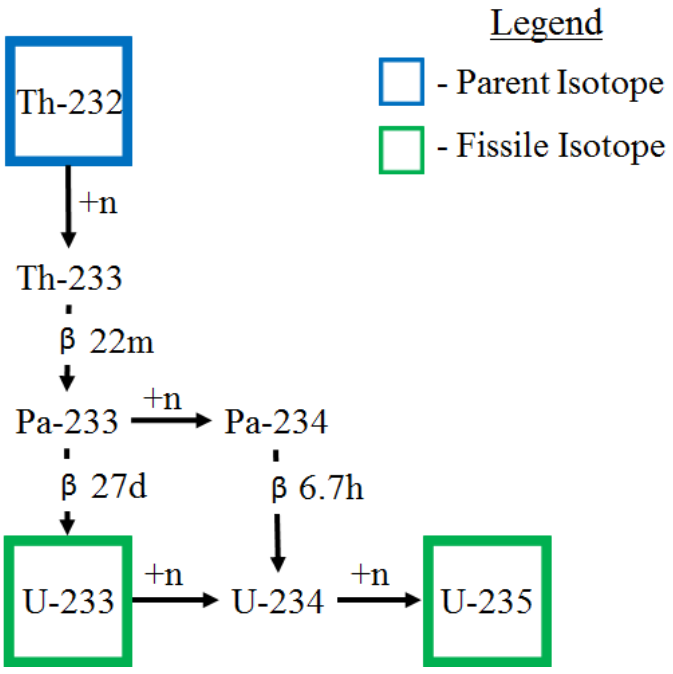

Figure 2.2: Transmutaton chain of Th-232

A longer half-life and higher neutron absorption cross-section in the thorium fuel will result in a slower onset of equilibrium from the time of startup or shutdown as compared to the uranium cycle [7]. At shutdown, an insertion of reactivity will occur from the decay of Pa-233 to U-233. It will be interesting to note how this occurrence will affect the xenon build up due to the different half-lives in each fuel cycle. Therefore, in order to be able to operate a reactor core with thorium, proper evaluation of the physics and design of the core is necessary to effectively breed U-233 while maintaining safety margins.

2.2 Fuel Cycles

There are two approaches in applying the thorium concept: an open cycle and a closed cycle. The open cycle is currently the most widely used method, and it involves a near-term means of implementing fuel cycles using the once-through-method where spent fuel is placed in long-term storage. Unfortunately, this approach results in an increasing amount of spent fuel, which is a cause for concern in the general population. On the other hand, a closed fuel cycle deals with the spent fuel by reprocessing and claiming materials still deemed valuable for power generation. This approach is the least used method due to the high cost in developing an infrastructure and performing the actual task of reprocessing. With the increasing need to develop a reprocessing industry and the increasing popularity of thorium and MOX fuels, a closed fuel cycle is highly desired [5].

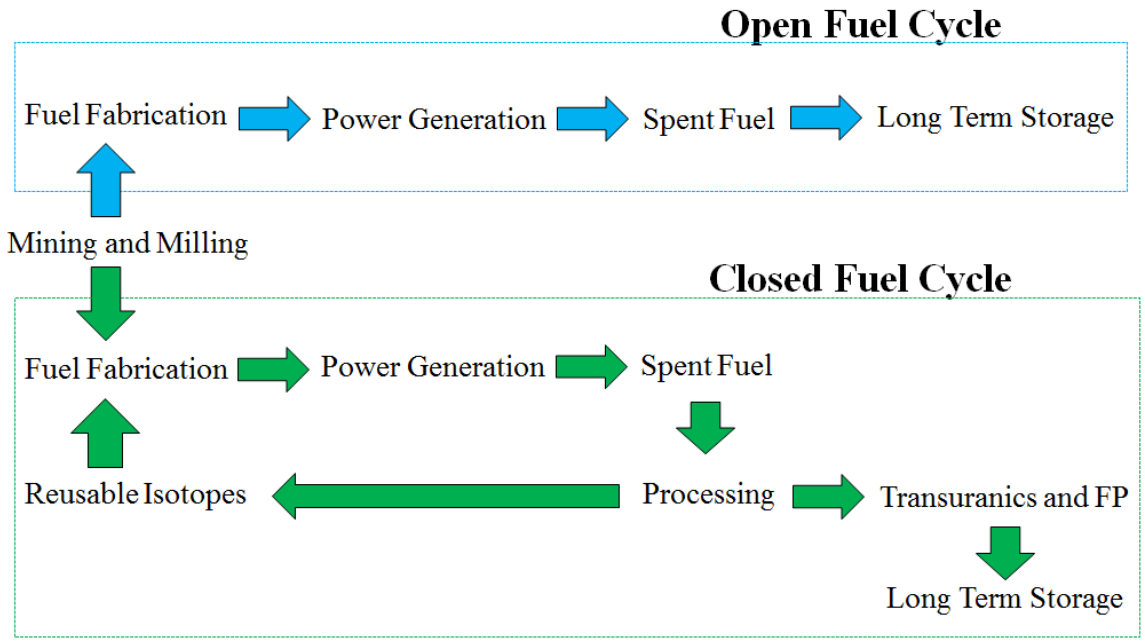

Figure 2.3: The nuclear fuel cycle

Implementing a closed fuel cycle is a difficult and expensive task, mainly due to the cost of reprocessing. Currently, it is more economical to continue with the mining and milling uranium to fabricate the fuel than to reprocess the spent bundles. There is currently momentum in the population to press for the need to reprocess spent fuel and to increase the efficiency of the nuclear fuel cycle. The last factor to consider is to improve the economics to favour the closed fuel cycle, and only then can the proper reprocessing industry be developed to help sustain the nuclear industry.

2.3 Reprocessing Spent Bundles

Reprocessing spent nuclear fuel is the last step to closing the fuel cycle. Unused fertile and fissile materials are extracted for further use, and the residual actinides and fission products can be sent to long-term storage or can be further reprocessed for MOX fuels [11]. Therefore, benefits of reprocessing spent fuel include a higher energy yield from uranium and plutonium and a decrease in overall waste volume [12].

2.3.1 PUREX

The most widely used technique for reprocessing spent nuclear fuel is the aqueous method which uses water and organic solvents to extract components from spent fuel. This route of reprocessing has the potential to be optimized for major and minor actinides and fission products [13]. PUREX is able to reprocess a variety of spent fuels and thus is the most common form of aqueous extraction due to its proven success in the industry.

There are three main steps to the PUREX technique. The first step is to remove the cladding and dissolve the fuel. The process begins with the cutting of spent fuel rods into three cm pieces and bathing the pieces in a dilute solution of nitric acid to separate the fuel from the cladding and to form an aqueous solution of uranium and plutonium. At this stage, fission products and other heavy actinides are in non-extractable states and will not affect plutonium and uranium extraction. Otherwise, the spent fuel solution would have to be preconditioned such that those elements would not contaminate the plutonium and uranium. The second step of the process involves separating the plutonium and uranium. Tributyl phosphate (TBP), due to its different affinities for plutonium and uranium, is the main chemical to be added next to form a two-phase solution: aqueous and organic. Specifically, TBP forms soluble complexes with $UO_2(NO_3)_2$ and $Pu(NO_3)_4$ at states of VI and IV, respectively. This means that by adjusting the acidity of the spent fuel solution, Pu and U can be separated into either the aqueous or organic phase of the solution. The first step involves increasing the acidity to bring the FP and MA out into the aqueous phase for extraction. Then, a low acidic solution of nitric acid is added to shift Pu and U into the aqueous phase. Lastly, a reactant is added to change the state of Pu(IV) to Pu(III) to make it insoluble

in the organic phase, thereby leaving U(VI) in the organic phase. Once the Pu, U,FP, and MA are separated, each solution is converted into a solid for storage or reuse [14].

2.3.2 THOREX

In order to reprocess thorium and U-233 using the aqueous method, the THOREX technique is employed. Due to thorium's relatively inert chemical structure, it does not dissolve readily in HNO_3 solution as compared to UO_2 in the PUREX process. The flowsheet involves other reagents in addition to nitric acid including hydrofluoric acid to enhance the dissolution process, aluminum nitrate to mitigate the corrosiveness of HF on steel components, and the use of an organic solvent, Tri-n-butyl phosphate, to extract the target components (Th, U, and Pa) [3]. The difference is in the employment of ion exchange to extract the U-233. Unfortunately, the THOREX process produces variable extraction results due to a higher difficulty in separating Th-232 from other actinides of similar atomic weights, such as U-232 [2].

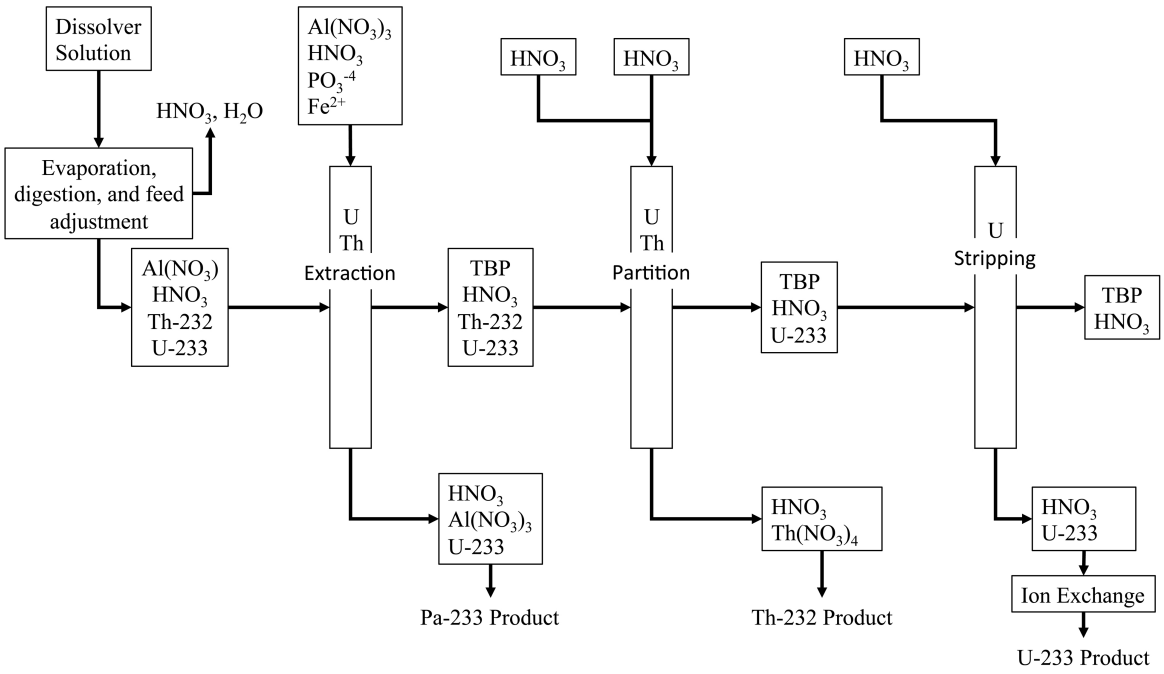

Figure 2.4: The THOREX technique (Adapted from [3] and [2])

The pyrometallurgical or "dry" method has increasingly become more important for reprocessing spent nuclear fuel. During the early stages of developing the non-aqueous method, it was found that there were inefficiencies in separating fissile material from fission products and transuranic elements, requiring further filtering to obtain desired actinides. However, this inadequacy has progressively become more desirable because of non-proliferation efforts [15]. In addition, features of the dry method such as low sensitivity to radiation and low risk to criticality due to the absence of organic solvents

and water make it an attractive option [13]. Furthermore, this allows the reprocessing of spent fuel fresh out of the core. Pyrometallurgical techniques fall short in terms of technology and deployability since aqueous processes, such as PUREX, are already well established in the field.

There are three techniques that have been investigated for dry reprocessing of spent nuclear fuel: volatilization, halide volatility and electrochemical reactions. Volatilization involves heating the spent fuel to temperatures that allow the release and separation of volatile or gaseous fission products from the desired products. Halide volatility takes advantage of the phase change from solid to gas when oxides are converted to a halide. The uranium, plutonium and some actinides are converted to halide form and separated from the rest of the spent fuel. Lastly, electrochemical or pyroprocessing utilizes molten salts and electro-refining to partition the target materials from the fission products [14]. In terms of reprocessing irradiate thorium fuel, halide volatility and pyroprocessing are the most viable techniques since volatilization would not be able to breakdown the stable matrix of thorium to remove the unwanted materials. Despite its limitations, volatilization can be a step in the two aforementioned techniques.

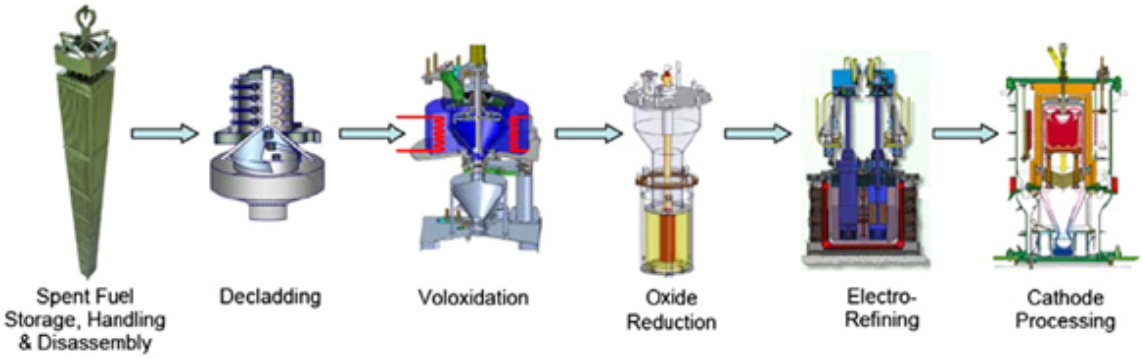

Figure 2.5: The Pyroprocess technique [16]

Halide volatility typically uses fluorine as the reactant with oxides. This technique is already being utilized in nuclear fuel enrichment and it is envisioned to help with the back-end operations of the nuclear fuel cycle. To process irradiated thorium, the stable fuel matrix must be broken down first by dissolving it in molten fluoride salts [17]. The solution is then exposed to fluorine gas where uranium oxides and some fission products will turn gaseous and are separated for further purification to yield the final product. Thorium oxide is converted to ThF_4 and sublimes at a vapour pressure lower than UF_6, thereby allowing for its extraction [3]. Utilizing fluoride volatility for the back-end of the cycle is still a novelty, but the method has proven to work for the current U-Pu cycle. Adapting it for thorium still requires further research and experimentation before it can undergo full-scale production.

The technique of pyroprocessing is when the irradiated thorium is dissolved in a molten salt bath that is typically comprised of LiCl+KCl [2]. There are several different ways to starting off the process which may include mechanically hashing the fuel to smaller pieces followed by voloxidation to remove any impurities and fission products [16] or the fuel can go straight to being dissolved in the molten salt bath. Once in the bath, electrolysis will begin and the irradiated thorium fuel will act as an anode. The cathode will be made up of different metals to attract specific elements of the fuel. Research has shown that a zinc and aluminium composite can attract thorium [17]. A combination of steel and cadmium or steel and bismuth cathode will take on uranium, plutonium, and some other actinides [15]. Once the desired amount of material is captured on the cathode, a purification procedure is performed to obtain the wanted elements. The pyroprocess technique has already been proven to work when it was first employed for the Experimental Breeder Reactor at Argonne National Laboratory in the United States; however, work still needs to be done for it to be used in the reprocessing of thorium.

2.3.3 Challenge with Reprocessing Thorium

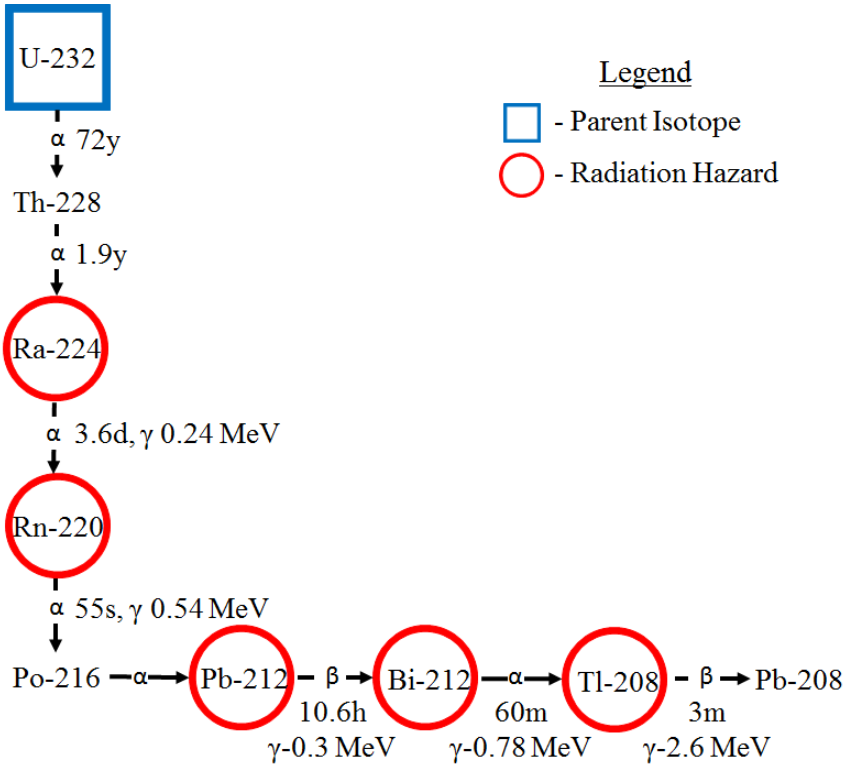

Figure 2.6: Decay chain of U-232

The main concern with reprocessing irradiated thorium is the resulting radiotoxic fission products produced. Minor actinides such as Np, Am, and Cm are not a concern since the quantity produced is small compared to what is produced from a U-Pu cycle. More specifically is the U-232 isotope generated from (n,2n) reactions with Th-232, U-233, and Pa-233. The decay of U-232 is shown in Figure 2.6 [3] and it decays down to daughter products that emit high energy gamma rays, especially thallium-208 [3]. By limiting the creation of U-232, the radiation hazard of an irradiated thorium bundle will be lowered. Therefore, the elemental composition of an irradiated thorium bundle is dependent on the intensity and duration of the neutron flux.

2.3.4 Fuel Handling System for CANDU-6

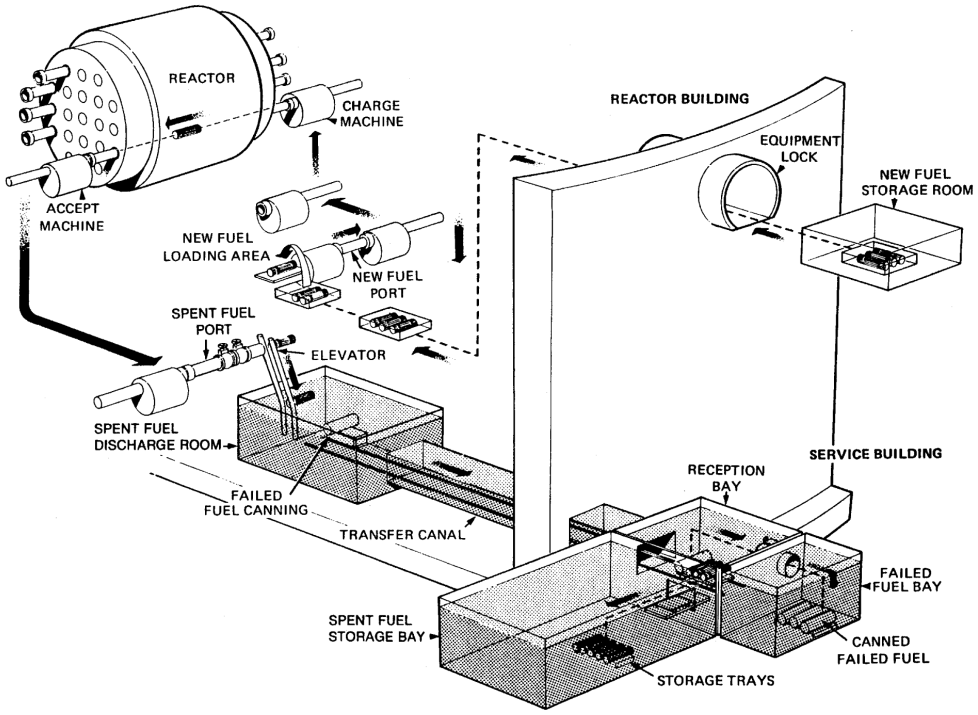

Figure 2.7: Fuel handling system of a CANDU-6 [18]

Depending on the fuel management scheme employed, the thorium bundles may have to cycle through the core several times. This can potentially be hazardous depending on the dwell time of the thorium bundles. A new bundle handling system was developed by the Korean Atomic Energy Research Institute (KAERI) for the CANDU system to address this issue. The system involves using the current spent fuel storage areas to store spent fuel and load fresh fuel simultaneously. Similarly, the conveyor belt used to move the bundles can be adapted to move the bundles to and from the refuelling machine. Furthermore, the refuelling machine would be outfitted with magazine

cartridges containing fuel bundles for a faster refuelling of channels, as seen in Figure 2.8 [18]. The entire process will be handled remotely to protect on-site workers from the radiation. Depending on the cycling scheme for a mixed core, it may be possible to change the system to handle irradiated thorium bundles.

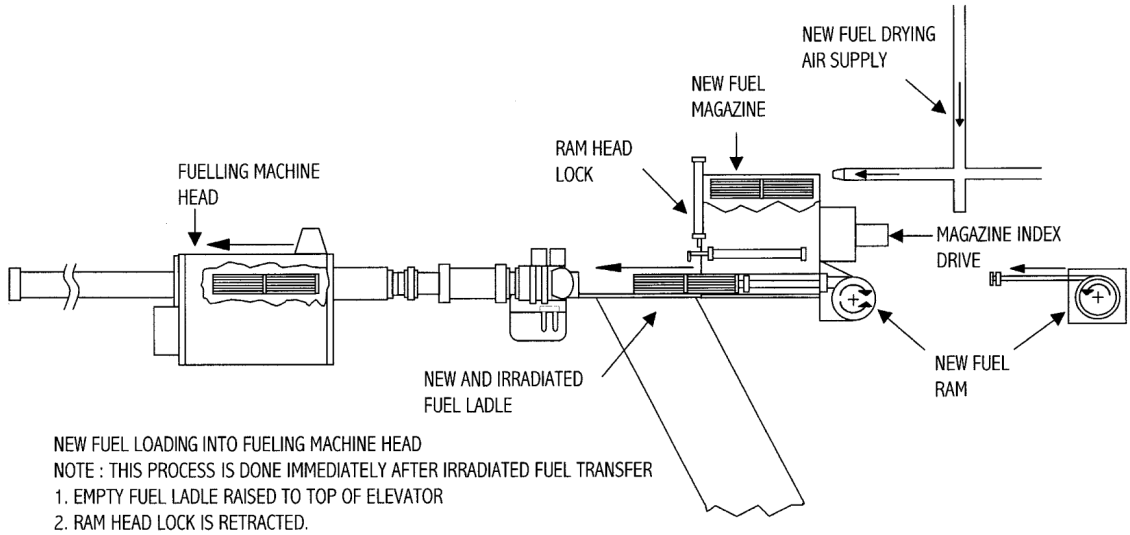

Figure 2.8: Modified refuelling machine for CANDU-6

Dismantling spent fuel bundles presents a hazard to onsite workers, therefore, proper safety measures are required in the reprocessing facility. Some safety measures may include remote fuel reprocessing where it is a guaranteed assurance to lead to lower radiation exposure. There are currently only a handful of countries that possess reprocessing plants due to the costly nature of the method itself and restrictiveness of governmental policies [19]. For example, three American civil reprocessing plants were shut down due to the staggering costs and changing governmental policies. On the other hand, countries like France and India have been able to sustain a reprocessing infrastructure because of the positive economics brought upon by reprocessing spent fuel for fast reactors [19]. In order for more countries to begin building a reprocessing infrastructure, there must be an economic incentive to reprocess spent bundle. For example, a study done by KAERI involving an economic feasibility analysis of a DUPIC fuel cycle for CANDU reactors found that implementing the proper facilities to reuse spent PWR fuel in CANDU reactors resulted in roughly the same costs as the once-through uranium fuel cycle [20]. Even though the costs are similar, the incentive for committing to the DUPIC cycle is the reuse the spent fuel and decrease the amount

of stored nuclear waste. Similarly with the thorium fuel cycle, the costs must be either on par or lower than the once-through uranium cycle. Synergizing the uranium fuel cycle with the thorium fuel cycle will accrue costs from both the front and back end operations of the uranium driver bundles and thorium bundles. To outweigh the costs, the benefits must be higher and may come in the form of credits generated from retrieving and using elements from the reprocessed spent fuel.

2.4 Prior Research

Prior work done by researchers at Atomic Energy of Canada Limited (AECL) has resulted in two methods of using thorium with CANDU reactors: mixed bundle or mixed core. The advantages and disadvantages of both approaches will be discussed in the following section.

2.4.1 Heterogeneous Bundle Approach

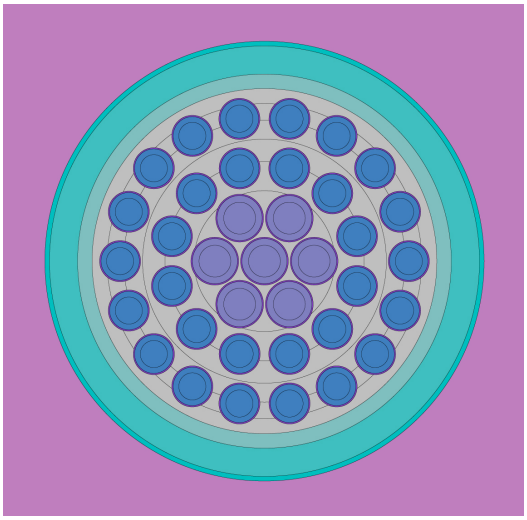

Figure 2.9: CANDU 43-element bundle

AECL has concentrated its efforts on developing a mixed (Th,U)O2 design using the newer 43-element bundle. The concept is to have a heterogeneous mixture of thorium and enriched uranium where each fuel is confined to the inner two and outer two rings, respectively.

Some time after the bundle has been incorporated into the core, the inner thorium rings can be directly recycled into a new bundle with freshly fuelled outer rings [21]. The objective of this is to maximize thorium usage without the need to dismantle the bundle and reprocess the fuel. A significant advantage of this method is the use of an

uncomplicated fuel management scheme which is unlike that seen with a mixed core. It is because of this uncomplicated fuel management scheme that there is a possibility of a near-term implementation. However, this method is dependent on a novel technology of demountable bundles to allow for the direct recycling of the thorium pins. Despite being an innovative method of recycling without the need to reprocess the fuel, the integrity of the fuel bundle may not be able to withstand the in-core conditions due to the components used to attach and detach the inner pins. Furthermore, this method does not lead to the stockpile of U-233 to envision the thorium fuel cycle, but does help prolong the in-core burnup of the fuel.

2.4.2 Homogeneous Bundle Approach

Another mixed bundle approach is the homogeneous mixture of both fertile and fissile materials in all rings of a bundle [22]. Homogeneous mixtures under consideration include (Th,U)O_2 and (Th,Pu)O_2. The mixing of both the driver and breeder element is the simplest way to transmutate thorium. However, this method is inefficient since the driver element is inherently combined with its fertile isotope for non-proliferative concerns and therefore, competes with Th-232 for neutrons. Depending on the percentage of U-235 to Th-232 desired, LEU or HEU is used to mix with thorium to produce the hybrid mixture. Similarly, the thorium plutonium hybrid fuel would utilize enriched Pu fuel with Pu-239 and Pu-241 as the fissile driver, and Pu-238 and Pu-240 as the fertile material. As a result, the burnup for these type of fuel composition will be low as shown in the results obtained by Nuttin et al [8] where a (Th,Pu)O_2 bundle obtained a burnup of 3200 MWd/t, half of NU CANDU fuel burnup since the production of U-233 was insufficient to compensate for the exhaustion of the fissile Pu elements. Another challenge to consider is the manufacturing of the thorium hybrid fuels due to the power morphology and thermo-physical properties of ThO_2 [23]. As well, thorium oxide has a plate-like powder structure compared to the granular structure of the UO_2. Thorium oxide also has a melting point of 500°C higher than that of uranium oxide, which in turn is beneficial for in-core operations, but will require higher temperatures and pressures for sintering during the fabrication process.

2.4.3 Mixed Core Approach

The last approach for using thorium is a heterogeneous core approach which involves loading CANDU reactors with both pure thorium bundles and SEU bundles [22]. Although this method is not hindered by the shortcomings mentioned in the mixed bundles approach, it does however provide a new technical challenge for fuel management as the burnup for each type of bundle will be different. Furthermore, the mixed core approach is a long-term implementation due to the need to reprocess the thorium bundle for U-233. Therefore, a reprocessing infrastructure must be put in place to

close this fuel cycle. One would must then consider the economics of stockpiling U-233 before a reprocessing infrastructure is put into place.

An investigation done by Milgram showed that such a "dual fuel" mode was possible, and depending on the set parameters, can be deemed economically competitive. However despite its positive outlook, the work did not undergo the typical methodology of lattice calculation and then full-core modelling, but rather done using an analytical approach for reactor physics calculations and cost benefit analysis, which may not be readily applied [22]. Unfortunately, the calculations required to investigate this heterogeneous core is computationally intensive and time consuming based on the time the work was completed. Also, due to the complexity of the fuel management scheme for dual fuel core loading and the need to reprocess the valuable U-233, the method has not been as popular as the mixed bundle approach and this is reflected in the lack of thorough investigation. Only recently has work been done by AECL in investigating a dual fuel loading scheme using thorium bundles and enriched uranium bundles in a heterogeneous CANDU-6 core design. The work detailed the use of Pu/Th or LEU/Th bundles that are enriched at two levels to simulate the seed and blanket concept [24]. It is assumed that the metallurgical procedure of combining the relatively inert thorium matrix with plutonium or uranium has been resolved, but will be a hurdle to over come in order to realize this method. Another approach was to burn thorium enriched U-233 bundles alongside uranium bundles. The idea suggests that the U-233/Th bundle can be produced readily, but more research is required to find ways of producing U-233 for those fuel concepts.

2.5 Benefits of SEU in CANDU

The use of thorium in the reactor will require enriched uranium fuel to provide the necessary neutron economy to account for the extensive absorption of neutrons by thorium[1]. Research has shown that an uranium enrichment between 0.9% and 1.2% is optimal is optimal for a single type fuel loading in the CANDU core. The SEU fuel can be used to uprate reactor power without the occurrence of maximum bundle and having the channel power go above the safety limits [25]. The overall increase can be completed by taking the outer channels to lower burnups, thus increasing the channel power. Furthermore, fuel management would be simplified down to a 2- or 4-bundle shift, compared to the 8-bundle shift scheme in the NU-CANDU, producing an excellent power distribution with or without the need of adjuster rods. Implementation of a SEU cycle can be easily done by simply switching the NU bundles for SEU ones during the course of refuelling with no additional changes to the reactor operations.

[1]The full-core models will be simulated with 1.2% SEU driver fuel.

2.5.1 Fuel Utilization

The use of enriched uranium bundle is beneficial in terms of uranium consumption and spent fuel production. The current NU fuel cycle in the CANDU system consumes 157 Mg U/GW(e)y and produces the same quantity of waste [2]. On the contrary, the SEU cycle has a lower quantity in both respects due to an exit burnup of up to two to three times that of the NU cycle, which translates to a fuel savings of 20% to 30%. Further cost reduction can be done if other sources of uranium are utilized, such as recycled uranium from LWR spent fuels.

By using a heterogeneous core configuration, a small proportion of uranium bundles are replaced with thorium bundles which further lowers uranium consumption. By using less uranium and more thorium, the quantity of nuclear waste produced is also reduced. Overall, the lower consumption will help conserve finite natural resource. Furthermore, thorium is capable of breeding a new source of uranium, an isotope superior to that of U-235, which can be stockpiled for future use in a heterogeneous core or for the deployment of a SSET cycle.

Table 2.1: Consumption and spent fuel arising from different fuel cycles

Fuel Cycle	Natural U Consumption Mg U/GW(e)y	Spent Fuel (Mg HE/GW(e)y
PWR with Enriched U	218	33
NU-CANDU	157	157
0.9% SEU-CANDU	119	84
1.2% SEU-CANDU	116	56

2.6 Objective

With new codes and technologies, it is possible to develop a scheme for introducing a heterogeneous CANDU model. As well, new techniques of reprocessing has also been investigated, thus prompting a renewed interested in the use of thorium. The goal of this thesis is to determine the behaviour of a heterogeneous CANDU-6 core with SEU and pure thorium bundles. This work will expand on the dual fuel core idea developed by Milgram [22] by using computational methods to quantify lattice and core operations. Based on the breeding phase of the mixed core, this thesis will also briefly evaluate a thorium equilibrium cycle on the same reactor. This thesis will hopefully shed light on utilizing a thorium fuel cycle for the intent of breeding a stockpile of U-233.

Chapter 3

Methodology

The assessment of the heterogeneous core design will begin with a multi-cell calculation which consists of a 3x3 cell of individual lattices to produce the homogenized cross-sections. These homogenized cross-sections will be subsequently fed to a full core diffusion model to simulate reactor operations and to evaluate whether it operates within the safety envelope of the design. The CANDU-6 reactor will be used as the basis for the work as its proven design allows for the comparison of the heterogeneous results with the known parameters of the CANDU core. Each phase of the assessment will be described within this chapter and the following sections.

The basis of the lattice calculation is a 2D representation of the CANDU cell that is composed of a fuel bundle enclosed within a channel surrounded by a moderator. The multi-cell will consist of nine of these cells in which the centre lattice will be the target thorium bundle surrounded by eight uranium bundles. In both cases, by solving the neutron transport equation the neutron flux distribution, power levels, and the reaction rates based on the material, geometry and nuclear data will be determined. The solutions to the equation are further used to compute the composition of the fuel over burnup. The multi-group energy macroscopic cross-sections generated from each step of the burnup calculation is then condensed and homogenized to produce a set of two-group macroscopic cross-sections for the full core diffusion code.

Homogenized cross-sections from the lattice code are used to build the 3D full core model. The diffusion code is then used to calculate the neutron flux distribution in the core. Since the CANDU model utilizes an online refuelling method, the code produces a time-average simulation of the core, which is essentially the average of the core properties over a certain time interval to generate a core profile. The results are then evaluated based on the time-averaged model of the natural uranium (NU) CANDU core for comparison, and to determine if the new core configuration operates within the designated envelope (licensing and design limits). After an equilibrium (time-average) core has been established, the next step will be to evaluate the effects

of online refuelling of the core. Instantaneous core simulations will be developed to show the effects of the ranked channel refuelling while being evaluated under the same safety envelope. Lastly, an initial core power profile will be modelled to observe the effects of fresh fuels in the core.

3.1 CANDU Lattice Description

The lattice cell used in the calculation of the neutron transport code is a single CANDU bundle contained within a single channel surrounded by a moderator. A CANDU fuel bundle consists of 37 fuel pins arranged in an annular ring formation and has a lattice pitch of 28.575 cm, as seen in Figure 3.1. Each fuel pin is composed on a zirconium sheath, which encompasses the fuel pellets. Similarly, the calandria and pressure tube is also composed of a zirconium alloy, separated by a CO_2 gas annulus. Finally, heavy water is used for both the coolant and moderator.

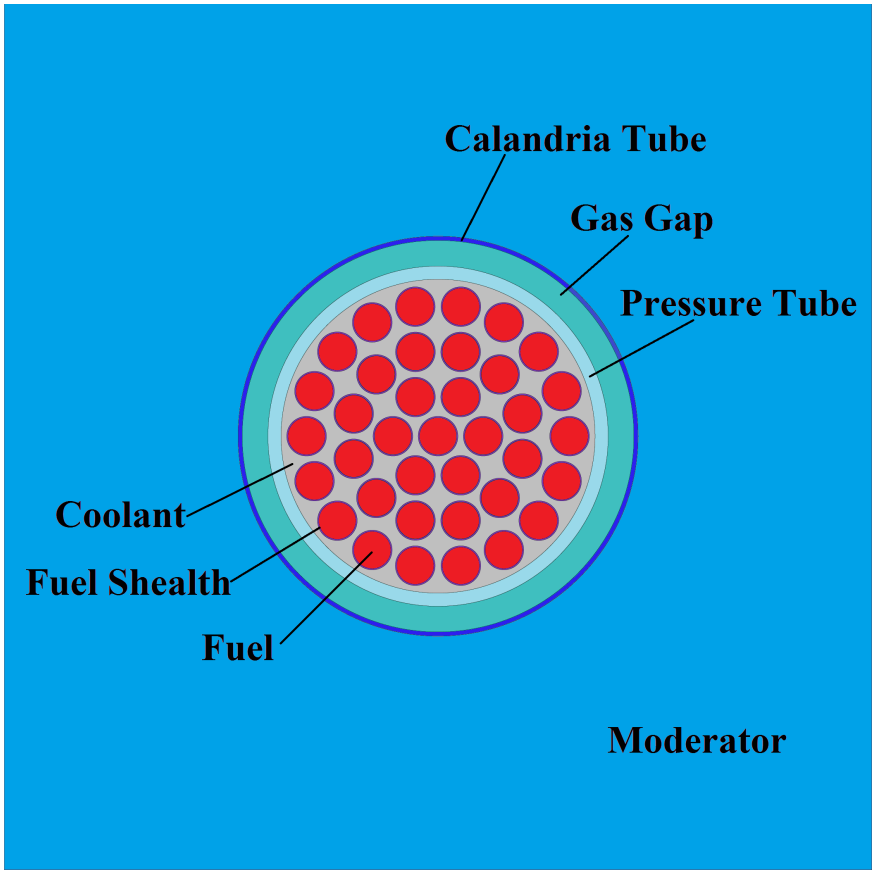

Figure 3.1: CANDU-type 37-element lattice geometry

3.2 CANDU Multi-Cell

To simulate the fuel behaviour and composition of a dual fuel core loading, a 3x3 multi-cell was developed to model the interactions between a pure thorium bundle (all fuel pins contain thorium pellets) and enriched uranium bundles. The multi-cell is depicted in Figure 3.2 where the centre cell contains the thorium bundle and the outer eight cells are uranium driver bundles.

This approach is an adaptation to performing infinite lattice cell calculations and allows for a very detailed look at the reactor physics for a dual fuel core. A disadvantage in this approach is that calculations for such a large multi-cell come with a long computational time. Overall, each lattice within the multi-cell is geometrically identical, with the exception of a different fuel type in the centre lattice.

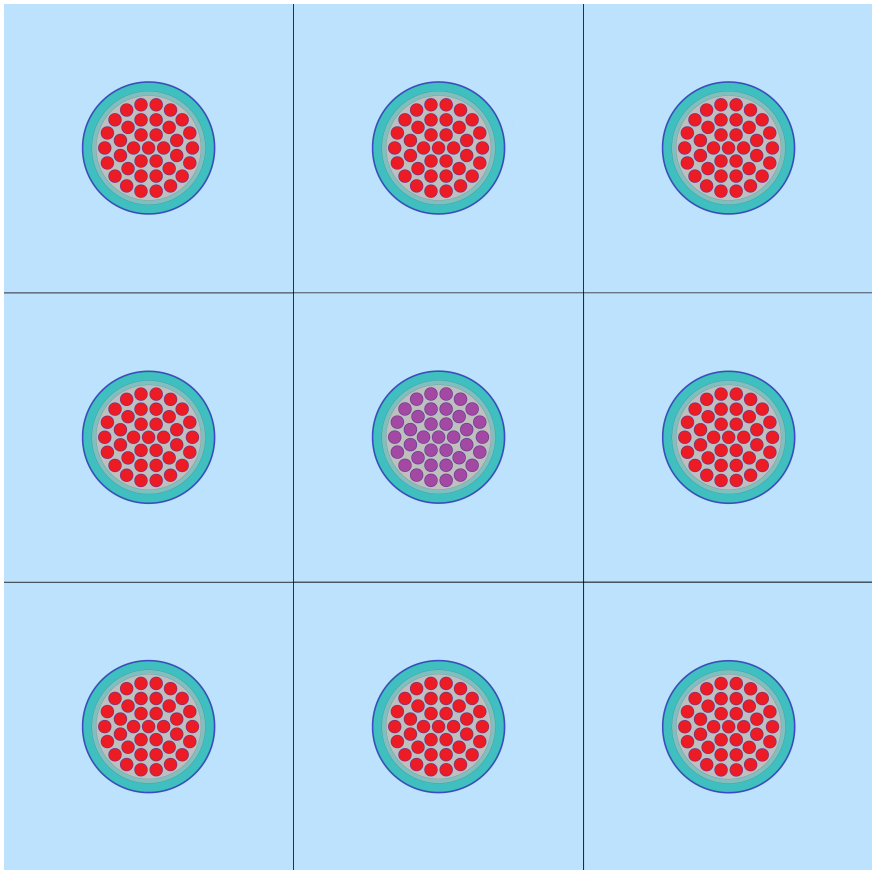

Figure 3.2: Multi-cell geometry

3.3 Solution to the Neutron Transport Equation

The start of any nuclear reactor analysis begins with solving the neutron transport equation that describes neutrons based on its energy and direction in an arbitrary volume V. The equation describes the change in neutron density based on the gain and loss mechanisms within a system as shown below.

Gain mechanisms include:

1. Neutron source.
2. Neutrons born from fission.
3. Neutrons entering the volume from a surface S.
4. Neutrons scattering from different energies and directions into values of interest.

Loss mechanisms include:

1. Neutrons leaving the volume.
2. Neutron interaction with lattice material, including scattering and absorption.

Based on the derivations found in the study done by Duderstadt [26], the final neutron transport equation can be expressed as:

$$\begin{aligned}\frac{1}{v}\frac{\partial\phi}{\partial t} + \widehat{\Omega}\cdot\nabla\phi + \Sigma_t(\overrightarrow{r},E)\phi(\overrightarrow{r},E,\widehat{\Omega},t) = \\ \int_{4\pi} d\widehat{\Omega}' \int_0^\infty dE'\Sigma_s(E'\to E,\widehat{\Omega}'\to\widehat{\Omega})\phi(\overrightarrow{r},E',\widehat{\Omega}',t) \\ + \frac{\chi(E)}{4\pi}\int_{4\pi} d\widehat{\Omega}' \int_0^\infty dE'\nu(E')\Sigma_f(E')\phi(\overrightarrow{r},E',\widehat{\Omega}',t) \\ + s(\overrightarrow{r},E',\widehat{\Omega}',t)\end{aligned} \tag{3.1}$$

v – neutron speed	ν – average number of fission neutrons produced
ϕ – angular neutron flux	Σ_s – macroscopic scattering cross-section
$\overrightarrow{r}$ – neutron position	Σ_f – macroscopic fission cross-section
E – neutron energy	$\chi(E)$ – fission energy spectrum
$\widehat{\Omega}$ – direction unit vector	s - neutron source
t – time	

The neutron transport equation cannot be solved by digital computers in its current form due to the presence of differentials and integrals. The transport equation can be readjusted to form algebraic equations for easier computation. This can be done by

discretizing the integro-differential equation in a series of algebraic equations. There are three methods to discretizing the equation: Discrete ordinates, functions expansion, and collision probability. The focus of this investigation utilizes the lattice code DRAGON, which employs the collision probability as the main method of digitally solving the neutron transport equation.

The basis of the collision probability method is that the neutron flux at point a is proportional to the neutron source at point b multiplied by an exponential attenuation factor for the neutron to go from point b to a. This is the optical path, τ, that the neutron takes:

$$\tau = \int_a^b \Sigma(R) dR \tag{3.2}$$

As the neutron travels along the optical path, there is a probability that it can be absorbed by another medium. The collision probability method calculates the probability of the neutron not being absorbed while travelling from one point of the volume to another. If the neutron survives, then it will be included in the flux calculations.

The first step is to derive the equation for the neutron flux at a point $\overrightarrow{r}$ due to neutrons created at another point $\overrightarrow{r}'$ from the neutron transport equation. To simplify the derivation, the one speed version is used and the source is isotropic $Q(\overrightarrow{r}, \overrightarrow{\Omega}) = \frac{1}{4\pi} q \overrightarrow{r}$, where the q represents the scalar source term. The final derivation in [27] shows the neutron flux to be:

$$\phi(\overrightarrow{r}, \overrightarrow{\Omega}) = e^{-\tau(R_S)} \phi(\overrightarrow{r}_S, \overrightarrow{\Omega}) + \frac{1}{4\pi} \int_0^R e^{-\tau(R')} q(\overrightarrow{r}') dR' \tag{3.3}$$

Furthermore, the scalar flux can be determined by evaluating the above equation over all angular directions to derive:

$$\phi(\overrightarrow{r}) = \int_S \frac{e^{-\tau(R_S)}}{R_N^2} (\overrightarrow{\Omega} \cdot \overrightarrow{N_-}) \phi_-(\overrightarrow{r}_S, \overrightarrow{\Omega}') d^2 r' + \int_V \frac{e^{-\tau(R)}}{4\pi R^S} q(\overrightarrow{r}') d^3 r' \tag{3.4}$$

where ϕ_- is the incoming angular flux at surface S and ϕ_+ is the outgoing flux at the same surface.

Now that the integral flux equations have been determined, the next step is to discretize the flux equations for numerical computation. To begin, the geometry is divided up into N_V regions of volumes V_i with the assumption that the cross-sections and neutron source are constant inside each region. Next, the boundary surface S is to be partitioned into the N_S surfaces with an area of S_α. Lastly, the incoming and outgoing average angular flux on these surfaces can be approximated by the limited series expansion terms of the half-range spherical harmonics:

$$\phi_{\pm}(\overrightarrow{r_S}, \overrightarrow{\Omega}) = \frac{1}{4\pi} \sum_{\nu=0}^{N_\nu} \phi_{\pm}^{\nu}(\overrightarrow{r}_S)\psi^{\nu}(\overrightarrow{\Omega}, \overrightarrow{N}_{\pm}) \tag{3.5}$$

where $\overrightarrow{N_{\pm}}$ form the three dimensional unit vector basis on the surface S_α and ψ^ν expands up to $n = 4$. Defining the average scalar flux inside each region to be:

$$\phi_i = \frac{1}{V_i} \int_{V_i} \phi(\overrightarrow{r}) d^3r \tag{3.6}$$

and the average angular flux on each surface to be:

$$\phi_{\pm.\alpha}^{\nu} = \frac{4}{S_\alpha} \int_{S_\alpha} d^2r \int_{\overrightarrow{\Omega}\cdot\overrightarrow{N}_+>0} d^2\Omega(\overrightarrow{\Omega} \cdot \overrightarrow{N}_-)\psi^{\nu}(\overrightarrow{\Omega}, \overrightarrow{N}_{\pm})\phi_{\pm}(\overrightarrow{r_S}, \overrightarrow{\Omega}) \tag{3.7}$$

then the final discretized expression for the average scalar flux is:

$$\begin{aligned} V_i\phi_i = &\sum_{\alpha=1}^{N_S} \sum_{\nu=o}^{N_\nu} \int_{V_i} \int_{\nu=0} \frac{e^{-\tau(R_S)}}{4\pi R_S^2} (\overrightarrow{\Omega} \cdot \overrightarrow{N}_-)\phi_{-,\alpha}^{\nu}\psi^{\nu}(\overrightarrow{\Omega}, \overrightarrow{N}_-)d^3rd^3r' \\ &+ \sum_{j=1}^{N_\nu} \int_{V_i} \int_{V_j} \frac{e^{-\tau(R)}}{4\pi R^2} q_j d^3rd^3r' \end{aligned} \tag{3.8}$$

and the average outgoing angular flux on the surface is:

$$\begin{aligned} &\frac{S_\alpha}{4}\phi_{+,\alpha}^{\nu} = \\ &\sum_{\beta=1}^{N_S} \sum_{\mu=0}^{N_\nu} \int_{S_\alpha} \int_{S_\beta} \frac{e^{-\tau(R_S)}}{4\pi R_S^2} (\overrightarrow{\Omega} \cdot \overrightarrow{N}_+)\psi^{\nu}(\overrightarrow{\Omega}, \overrightarrow{N}_+)(\overrightarrow{\Omega} \cdot \overrightarrow{N}_-)\psi^{\mu}(\overrightarrow{\Omega}, \overrightarrow{N}_-)\phi_{-,\beta}^{\mu} d^2rd^2r' \\ &+ \sum_{j=1}^{N_\nu} \int_{S_\alpha} \int_{V_j} \frac{e^{-\tau(R)}}{4\pi R^2} (\overrightarrow{\Omega} \cdot \overrightarrow{N}_+)\psi^{\nu}(\overrightarrow{\Omega}, \overrightarrow{N}_+)q_j d^3rd^3r' \end{aligned} \tag{3.9}$$

Using the discretized neutron flux equations, a set of collision probability expressions is derived.

$$\tilde{p}_{ij} = V_i p_{ij} = \int_{V_i} \int_{V_j} \frac{e^{-\tau(R)}}{4\pi R^2} d^3rd^3r' \tag{3.10}$$

$$\tilde{p}_{i\alpha} = V_i p_{i\alpha}^{\nu} = \int_{V_i} \int_{S_\alpha} \frac{e^{-\tau(R_S)}}{4\pi R_S^2} (\overrightarrow{\Omega} \cdot \overrightarrow{N}_-)\psi^{\mu}(\overrightarrow{\Omega}, \overrightarrow{N}_-)d^3rd^3r' \tag{3.11}$$

$$\tilde{p}_{\alpha i} = \frac{S_\alpha}{4} p_{\alpha i} = \int_{S_\alpha} \int_{V_i} \frac{e^{-\tau(R)}}{4\pi R^2} (\overrightarrow{\Omega} \cdot \overrightarrow{N}_+)d^2dr'd^3r \tag{3.12}$$

$$\tilde{p}_{\alpha\beta}^{\nu\mu} = \frac{S_\alpha}{4} p_{\alpha\beta}^{\nu\mu} = \int_{V_i}\int_{S_\alpha} \frac{e^{-\tau(R_S)}}{4\pi R_S^2} (\overrightarrow{\Omega}\cdot\overrightarrow{N}_-)\psi^\nu(\overrightarrow{\Omega},\overrightarrow{N}_-)(\overrightarrow{\Omega}\cdot\overrightarrow{N}_+)\psi^\mu(\overrightarrow{\Omega},\overrightarrow{N}_+)d^2r d^2r' \tag{3.13}$$

Each equation above describes the probability of a certain interaction between the properties of the system and the neutron. The types of interaction are as follows [28]:

- $\tilde{p}_{ij}$ - The probability that a neutron born in region i will have its first collision in region j without leaving the volume through surface S_α.
- $\tilde{p}_{i\alpha}$ - The probability that a neutron born in region i will leave the region through the surface S_α.
- $\tilde{p}_{\alpha i}$ - The probability that a neutron will enter the region through surface S_α and have its first collision in region i.
- $\tilde{p}_{\alpha\beta}^{\nu\mu}$ - The probability that a neutron entering through surface S_α will leave through another surface S_β

Each probability expression is used to describe its respective collision probability matrix. The collision probability matrices can be substituted back into the neutron transport equations 3.8 and 3.9 to yield the average flux and the average angular flux matrices in terms of the collision probability. The final matrices can now be solved iteratively to yield the flux solutions.

$$\phi_i = \sum_{\alpha=1}^{N_S}\sum_{\mu=0}^{N_\nu} p_{i\alpha}^\mu \phi_{-,\alpha}^\mu + \sum_{j=1}^{\nu} p_{ij} q_j \tag{3.14}$$

$$\phi_{+,\alpha}^\nu = \sum_{\beta=1}^{N_S}\sum_{\mu=0}^{N_\nu} p_{\alpha\beta}^{\nu\mu} \phi_{-,\beta}^\mu + \sum_{j=1}^{N_\nu} p_{\alpha j}^\nu q_j \tag{3.15}$$

DRAGON will utilize tracking modules that will process the geometry and generate integration lines based on the azimuthal angles and the number of parallel tracks per centimetre. From the tracking information and macroscopic total cross-sections, the collision probabilities are calculated using the above process. The results from the calculations will be fed forward to solve the neutron transport equation.

3.4 Burnup Calculation

Once the neutron transport equation has been solved, the flux solutions can be used to calculate the reaction rates in which the fuel undergoes fission in the lattice.. As the fuel is consumed over its life time in the core, the decreasing levels of fissile materials

and the increasing concentrations of fission products affect the flux and criticality of the reactor. The change in fissile concentration needs to be accounted for in the transport equation and can be done so with the following equation [26]:

$$\frac{\partial N_F}{\partial t} = -N_F(\overrightarrow{r}, t)\sigma_\alpha^F \phi(\overrightarrow{r}, t) \tag{3.16}$$

where N_F is the atomic number density of a fissile material and σ_a^F is the one-group absorption cross-section of the same material. The equation can be solved using the flux determined through the transport equation which would then yield the atomic number density:

$$N_F(\overrightarrow{r}, t) = N_F(\overrightarrow{r}, 0)e^{-\sigma_a^F \int_0^t \phi(\overrightarrow{r}, t')dt'} \tag{3.17}$$

Furthermore, isotopic concentration changes also stem from decay, mainly with fission products and intermediate breeding products. These concentration changes due to decay can be expressed with the Bateman equation:

$$\frac{dN_i(t)}{dt} = \lambda_i N_i(t) + \lambda_{i-1} N_{i-1}(t) \tag{3.18}$$

By combining Equations 3.16 and 3.18, a final expression can be derived for the changing isotopic concentrations due to absorption and decay for several isotopes.

$$\frac{dN_j(t)}{dt} = \gamma_j \sum_g \Sigma_{fg}\Phi_g + \sum_{i \neq j}(\lambda^{i \to j} + \sum_g \sigma_g^{i \to j}\Phi_g)N_i - (\lambda^j + \sum_g \sigma_{a,g}^j \Phi_g)N_j \tag{3.19}$$

where γ is the fraction of isotope produced from fission, $\lambda^{i \to j}$ is the decay constant, $\sigma^{i \to j}$ is the transmutation of isotope i to j, and σ_a is the is the absorption cross section [2]. Overall, the fuel composition changes with time, thus changing the macroscopic cross section of the fuel and affecting the reactivity of the core.

Lastly, the metric for following the energy released from the depletion of fissile nuclides is called burnup and is measured as MWd/t. It is used to indicate the age of the fuel and the fuel composition. Burnup is calculated based on the volume of fuel V, the amount of heavy isotopes W at $t = 0$, and the recoverable energy from neutron-induced fission H [28]. The equation for burnup is as follows:

$$B = \frac{V}{W} \int H\phi(t')dt' \tag{3.20}$$

3.5 Self-Shielding

As neutrons slow down to lower energies, the probability of it being absorbed increases. Specifically, for energies ranging from epi-thermal to fast, the absorption cross-section sharply increases for heavy nuclides like uranium and thorium. This region is called the unresolved resonance capture region due to the finely detailed resonance structure as depicted in the peaks at the respective energies in Figure 2.1 [26]. The resonance region will cause a depression in the flux for neutrons at resonance energies and the overall reduction in the number of collisions with the rest of the absorbing material.

The second type of self-shielding is due to the spatial positioning of the fuel. In the CANDU 37-element bundle, the outer rings are the first to be exposed to the incoming neutrons and therefore, will absorb the most neutrons. The inner rings would be sequentially exposed to lower neutron fluxes. Furthermore, if the neutrons are at resonance energies, then the flux is even further depressed by resonance absorption of the outer rings, which would then result in a higher concentration of thermalize neutrons in the centre of the fuel.

Self-shielding is an important parameter to account for since it is a major loss mechanism in neutron count and it influences the level of flux, and therefore affects the criticality of the reactor and its multi-group constants. Furthermore, self-shielding will also affect the breeding ratio of fertile materials and influence the fuel burnup.

3.6 Lattice Code: DRAGON

The lattice code DRAGON version 3.06 developed by École Polytechnique de Montréal will be used to create the multi-cell model. Detailed 2D calculations using the collision probability method are used to solve the neutron transport equation. The code is composed of separate modules that are tasked to complete different calculations, but compiled together to form the final solution. A list of the following modules used and its function is shown below [29]].

LIB: The LIB module is used to create a microscopic cross-section library of the materials used in defining the lattice.

GEO: The GEO module creates the geometry of the fuel bundle and defines the boundary conditions.

NXT: The NXT module is the generalized tracking option for the 2-D assembly.

SHI: The SHI module performs self-shielding calculations.

ASM: The ASM module is used to generate the collision probability matrices.

FLU: The FLU module retrieves the collision probability matrices and uses it to solve the neutron transport equation.

EDI: The EDI module is a data structure containing the stored condensed and merged microscopic cross-sections.

EVO: The EVO module performs burnup calculations and updates the new isotopic densities and macroscopic cross-sections.

CPO: The CPO module is used to store reactor diffusion coefficients and, homogenized and condensed microscopic and macroscopic cross-sections in a COMPO file to be fed forward to the diffusion code.

3.7 Solution to the Diffusion Equation

Similar to the neutron transport equation, the diffusion equation describes the rate of change in neutron population by the production, absorption and leakage of the neutrons.

$$\frac{d}{dt}\int_V N(\overrightarrow{r},t)d^3r = \int_V \frac{1}{\upsilon}\phi(\overrightarrow{r},t)d^3r \tag{3.21}$$

$$Production = \int_V S(\overrightarrow{r},t)d^3r \tag{3.22}$$

$$Absorption = \int_V \Sigma_a(\overrightarrow{r},t)\phi(\overrightarrow{r},t)d^3r \tag{3.23}$$

$$Leakage = \int_V \nabla\cdot\overrightarrow{J}(\overrightarrow{r},t)d^3r \tag{3.24}$$

Equating all of the above equations together and assuming that the neutron interactions must be true for any volume, the resulting equation is:

$$\frac{1}{\upsilon}\frac{\partial\phi}{\partial t} = -\nabla\cdot\overrightarrow{J} - \Sigma_a\phi + S \tag{3.25}$$

However, Equation 3.24 still has two unknown variables, $\overrightarrow{J}$ and ϕ. Unfortunately, there is no formal relationship between the current density and flux, and therefore one must resort to an approximation. It is known from other fields of physics that the

current density is proportional to the negative gradient of the flux. Mathematically, it is stated as:

$$\overrightarrow{J}(\overrightarrow{r},t) = -D(\overrightarrow{r})\nabla\phi(\overrightarrow{r},t) \tag{3.26}$$

where D is the diffusion coefficient which is defined by the macroscopic transport cross-section Σ_{tr}, derived from the neutron transport equation. Equation 3.26 is known as Fick's law of diffusion, which in this case postulates that the higher neutron concentration will flow to areas of lower concentration.

$$\Sigma_{tr}(\overrightarrow{r}) = \Sigma_t(\overrightarrow{r}) - \bar{\mu}_0\Sigma_S(\overrightarrow{r}) \tag{3.27}$$

where $\bar{\mu}_0$ is the average scattering angle.

By substituting equation 3.26 into 3.25, and adjusting it for multi-group energies, the final diffusion equation becomes

$$\begin{aligned}\frac{1}{\nu}\frac{\partial\phi(\overrightarrow{r},E,t)}{\partial t} - \nabla\cdot D(\overrightarrow{r},E)\nabla\phi(\overrightarrow{r},E,t) + \Sigma_t(\overrightarrow{r},E)\phi(\overrightarrow{r},E,t) = \\ \int_0^\infty \Sigma_S(E'\rightarrow E)\phi(\overrightarrow{r},E',t) + S(\overrightarrow{r},E,t)\end{aligned} \tag{3.28}$$

The main assumptions underlying the diffusion approximation is as follows: (a) angular flux is weakly dependent on angle, (b) isotropic sources, and (c) neutron density changes on a time scale slower than neutron collisions [26]. Therefore, the diffusion equation is only valid: for points that are several mean-free-paths away from boundaries, localized sources, and strong absorbing media.

Similarly, the diffusion equation can be digitally solved by first discretizing it and then applying numerical methods.

3.8 Time-Average Model

The current generation of CANDU reactors utilizes online refuelling to replenish the depleted fuel. In contrast, PWRs go through batch refuelling which requires the reactor to shutdown to replace the entire fuel assembly with a fresh one. For the CANDU reactors, new and old fuel bundles are cycled through the core to achieve the desired power distribution and maintain core criticality. As a result, the individual bundles along the channel would have experienced different irradiations. Hence, a map of the channel powers of a CANDU core at different time intervals would not be an accurate

depiction of the flux and power distributions for the core's lifetime due to the variable irradiation of the bundles. Therefore, the lattice properties are averaged over time to account for the effects of online refuelling.

To determine the time-average model of a core, the first step is to evaluated for the irradiation of the fuel at each position on the channel based on the average exit irradiation or dwell time (the average time interval between refuelling). The irradiation of the fuel at channel j and bundle position k can be defined by the dwell time T_j of the fuel experiencing a flux ϕ_{jk} at that position. Here, the flux has to be predetermined from the neutron diffusion equation. Then the irradiation experienced by the fuel can be described as:

$$\triangle \omega = \phi_{jk} T_j \tag{3.29}$$

Furthermore, for a fuel to enter a position with an initial irradiation of ω_{in}, the exit irradiation would be:

$$\omega_{out,jk} = \omega_{in,jk} + \phi_{jk} T_j \tag{3.30}$$

Each bundle position in the channel can be tabulated for its respective exit irradiation to obtain the average exit irradiation or dwell time for an N-bundle shift [30]:

$$\omega_{exit,j} = \frac{1}{N} \sum_{k=1}^{12} \phi_{jk} T_j \tag{3.31}$$

Time-averaged cross-sections of the fuel at each position along the fuel channel are averaged by the range of irradiations experienced by the fuel in that location. For the fuel to enter the position with an initial irradiation of ω_{in} and leave the position with an exit irradiation of ω_{out}, the average cross-section is:

$$\Sigma^{t,a}(r) = \frac{1}{\omega_{out} - \omega_{in}} \int_{\omega_{in}}^{\omega_{out}} \Sigma(\omega) d\omega \tag{3.32}$$

Once the average cross-sections have been determined, it can be used to calculate the global flux distribution of the core. Furthermore, from the flux distribution, the channel power distribution bundle powers can also be calculated. Then the aim of fuel management would be to determine how to achieve the target powers through average exit burnups and refuelling schemes.

Through online refuelling, the removal of spent fuel and the addition of fresh fuel will add reactivity to the core to maintain criticality. The addition in reactivity will affect the local power distribution. Instantaneous snapshot will be used to observe the power ripple effect caused by the insertion of reactivity. By specifying the average exit irradiation or dwell time of a channel for a region of the core, online refuelling gives the reactor operators the ability to micro-manage the core flux and power distribution to obtain the desired shape.

3.9 Diffusion Code: DONJON

By completing the calculations necessary to solve the multi-cell, a large model of the core can be created by using the diffusion code DONJON (version 3.02e) developed by École Polytechnique de Montréal. Version 3.02e of DONJON will be used. To create the time-averaged model of the core, the homogenized diffusion coefficients and cross-sections from the lattice calculations are fed forward to the diffusion code. Similarly, the code is composed of multiple modules to perform specific calculations used to develop the final model. The modules used and the corresponding functions are listed below [31].

GEOD: The GEOD module is used to create the core geometry.

USPLIT: The USPLIT module is used to create an index of material mixtures for the different regions in a split geometry.

INIRES: The INIRES module is used to define the fuel map information which contains bundle type and positions, burnup zones, and etc.

REFRES: The REFRES module creates cross references between geometry, index of materials, and fuel map geometry.

CRE: The CRE module creates a set of burnup interpolated nuclear properties retrieved from COMPO objects.

XSCONS: The XSCONS module creates a table for the nuclear properties from CRE.

TRIVAT: The TRIVAT module is the tracking module for DONJON.

FLXAXC: The FLXAXC module calculates the average flux over bundles and axial flux shapes.

REFUEL: This module is used to compute time-averaged burnups and to specify the refuelling scheme.

INIMAC: This module stores properties for each material region.

TRIVAA: This module computes the finite elements system matrices from the tracking information.

FLUD: The FLUD module solves for the eigenvalue solution from the system of matrices.

POWER: This module computes the bundle and channel powers from the average fluxes obtained from FLAXAXC.

Chapter 4

Lattice Calculations

The analysis of a dual fuel model in the CANDU-6 core begins with the use of the neutron transport code, DRAGON, which utilizes the probability collision method to calculate the flux and reaction rates based on tracking the neutrons and its interaction with the various cross-sections within the lattice.

4.1 Multi-Cell Analysis

The single fuel mode, such as the NU-CANDU core, can be modelled using an infinite lattice, with each lattice being the same type. In the case of simulating a dual fuel mode, a multi-cell model is required to differentiate the two types of lattices. The two types being the thorium bundle and the SEU bundle. The multi-cell in this investigation will be a 3x3 lattice, where the centre cell represents the target bundle containing thorium and the outer eight cells are the driver or blanket bundles containing SEU.

Since the thorium bundle will initially be an absorber for neutrons, the driver bundles must be enriched so that there will be excess neutrons to keep the multiplicative factor above one. The analysis will have the driver bundles at varying enrichments from 1.0% to 1.5%. The specific power densities for each bundle in all cases will be set at 32 W/g, which is the maximum value found for a NU-CANDU bundle. The specific power density is the amount of power produced from one gram of heavy metal.

Results of the simulation of the 3x3 multi-cell model with fresh SEU driver bundles and a new thorium target bundle has been completed and the results are described in the following sections.

4.1.1 Fissile Inventory

4.1.1.1 U-233 Production

Due to the difference in initial fuel type, the thorium bundle will contain a different isotopic mixture compared to the SEU bundle. The target bundle will be composed of all thorium atoms and will absorb neutrons to produce Pa-233 and subsequently U-233.

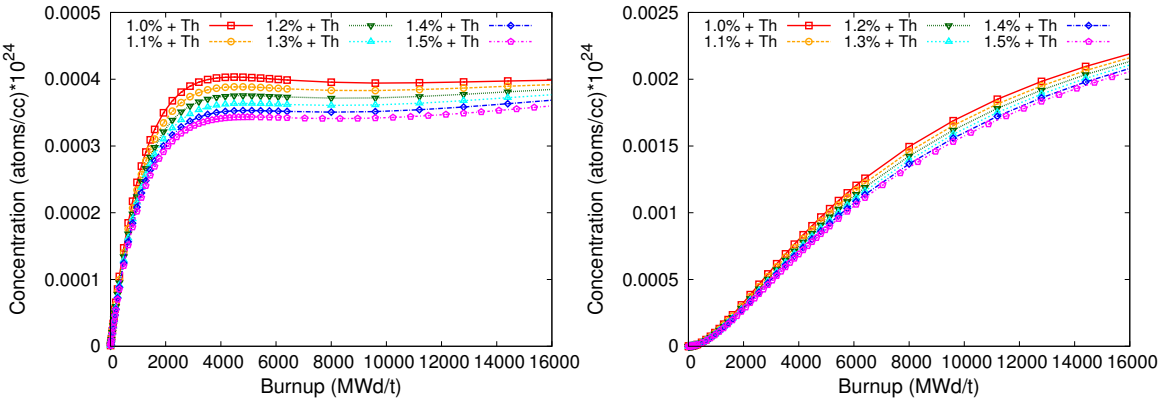

(a) Pa-233 (b) U-233

Figure 4.1: Pa-233 and U-233 concentrations throughout burnup in target bundle.

Pa-233 and U-233 levels are shown for various driver bundle enrichments in Figure 4.1. At the beginning of cycle (BOC), Pa-233 concentrations are seen to rise sharply and after about 4500 MWd/t, the levels reach equilibrium From this point on till the multi-cell reaches a multiplication factor of one, the rate of creation and loss of Pa-233 is roughly the same. U-233 concentrations (as shown in Figure 4.1b) are depicted as a continual increase over burnup. The rate at which the concentrations build up changes, with a faster rate of production over a short period during the BOC and then transitioning to a slower rate throughout the rest of the burnup. The gradual slowing of U-233 generation can be attributed to the fission and the absorption of neutrons by the isotope, which is shown to occur more readily at later stages of burnup due to a higher a concentration of the isotope.

As seen in both graphs in Figure 4.1, increasing driver enrichments result in a decrease in concentrations in both Pa-233 and U-233 as compared to the previous lower enrichment. So by increasing the driver enrichment, the thorium bundle's U-233 content would decrease for a given burnup. However, since having a higher enriched driver bundle extends burnup, the fissile content in the thorium bundle will be different at the end of the lattice cycle (EOC).

At EOC, when k_∞=1, the target bundle is assessed for the amount of U-233 that was generated. The enrichment can be calculated with the following equation:

$$\epsilon_{Th}(^{233}U + ^{233}\ Pa) = \frac{[^{233}U] + [^{233}Pa]}{[^{233}U] + [^{233}Pa] + [All - other - elements]} \tag{4.1}$$

where the square brackets denote concentrations. The calculated enrichments are shown in Table 4.1.

Table 4.1: Enrichment achieved in target bundle at end of lattice cycle (EOC).

Driver Enrichment $[\epsilon_n(\%)]$	Burnup (MWd/t)	$\epsilon_{Th}(^{233}\text{U}+^{233}\text{Pa})[\%]$	$\Delta\epsilon_{Th}$ $(^{233}\text{U}+^{233}\text{Pa})$ $[\epsilon_{n+.1} - \epsilon_n]$
1	8800	0.97750	-
1.1	10080	1.02469	4.71881
1.2	11360	1.06541	4.07287
1.3	12640	1.10103	3.56203
1.4	13760	1.12655	2.55140
1.5	14880	1.14959	2.30386
1.6	16000	1.17031	2.07177
1.7	17120	1.18930	1.89946

With increasing driver enrichment and longer burnups, the fissile content generated in the target bundle also increases; however, with each incremental increase in the enrichment of the driver bundles, the U-233 + Pa-233 content decreases. Due to the decrease in neutron flux, as described above, the amount of U-233 + Pa-233 generated decreases per increment in driver enrichment. This behaviour shows that further increases in the driver enrichment is limiting and will be counter-productive in terms of U-235 utilization and U-233 production.

The fissile content of the thorium bundle at the end of cycle described above is not indicative of the concentrations that will be found after in-core burnup. The thorium bundles will be expected to have a longer dwell time in the core as opposed to the SEU bundles. Furthermore, the adjacent driver bundles will never be the same bundles surrounding the thorium bundle due to the constant online refuelling of the core. This in turn will result in different flux levels that will affect U-233 and Pa-233 concentrations. Therefore, it can be expected that the U-233 + Pa-233 content will in fact be higher as illustrated in Figures[1] A.1 and A.2 in Appendix A.

[1]Figures are extended burnups of the multi-cell model using 1.2% SEU bundles as the driver

4.1.1.2 U-235 Consumption

The concentrations of fissile elements in the driver bundles are also an important aspect to consider. For instance, the initial concentrations of U-235 will deplete over time. Breeding can also occur in the driver bundles to produce Pu-239 from neutron absorption by U-238. The enrichment values (ϵ) are tabulated in Table 4.2.

Table 4.2: EOC fissile enrichments of driver bundle from the multi-cell lattice model

Driver Enrichment$[\epsilon_n(\%)]$	$\epsilon(^{235}U)$	$\Delta\epsilon(^{235}U)$	$\epsilon(^{239}Pu)$
1.0	0.32725	-0.67275	0.25767
1.1	0.32977	-0.77023	0.26452
1.2	0.33149	-0.86851	0.27016
1.3	0.33254	-0.96746	0.27489
1.4	0.33944	-1.06056	0.27849
1.5	0.34568	-1.15432	0.28172
1.6	0.35142	-1.24858	0.28459
1.7	0.35655	-1.34345	0.28721

Notably, the higher the initial driver enrichment is the more U-235 is consumed to reach EOC. That is, with more initial U-235, the multi-cell can have a longer burnup. The creation of plutonium in the uranium fuel cycle adds to the fissile content of the driver bundle, aiding in prolonging the burnup. By comparing $\epsilon(^{235}U)$ and $\epsilon(^{233}U)$ from Tables 4.2 and 4.1, respectively, the investment in driver enrichment for a net gain in U-233 in the target bundle can be determined. Enrichments of 1.5% or lower in the driver bundle will result in more U-233 produced and less U-235 consumed. However, this comparison is done in terms of enrichment and not in terms of weighted material. In the latter, the calculation would have to include the presence of eight driver bundles for the induction of breeding. Undoubtedly, it will take many times more the weighted amount of U-235 to produce the weighted amount of U-233 found in one target bundle at EOC.

4.1.2 Spent Fuel Characteristics

The majority of the spent fuel in the target bundle will consist of thorium. In addition, the concentrations of minor actinides (MAs) and plutonium isotopes, which result from successive neutron captures, are expected to be lower due to thorium's lower atomic number. The concentration levels of the actinides in the thorium bundle are provided in the following figures and are compared to the levels found in the driver bundles and in the NU-CANDU case. Examples of actinides under consideration are shown in the following figures and consist of isotopes of neptunium, americium, plutonium, and curium. Other actinides of interest include Pa-231 and U-232.

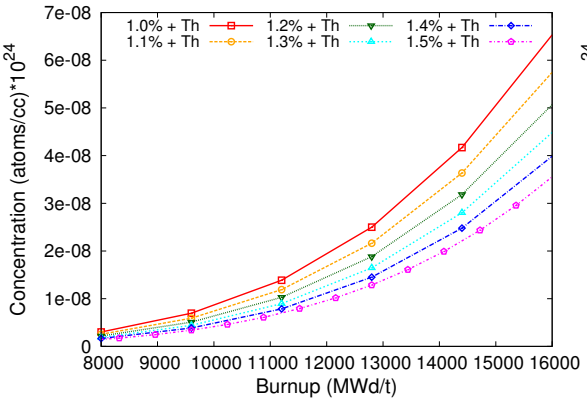

(a) Np-237 (Th Bundle)

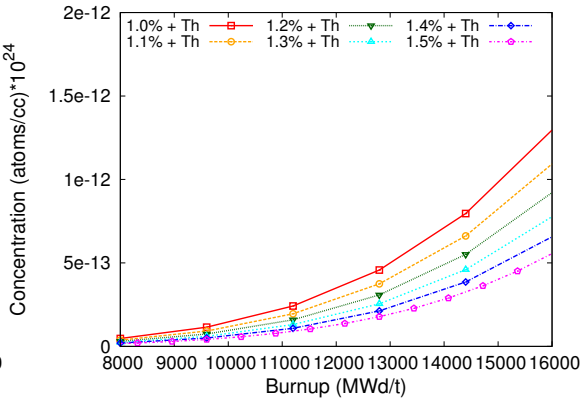

(b) Np-239 (Th Bundle)

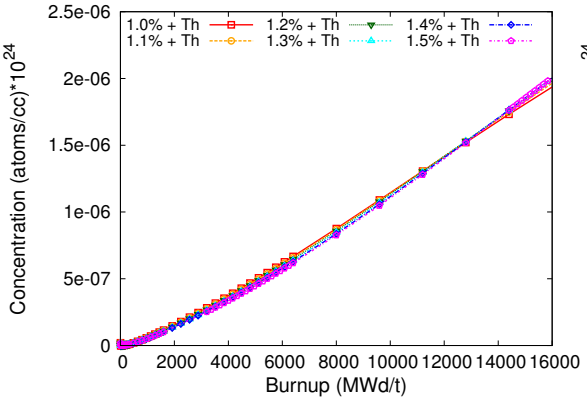

(c) Np-237 (Driver Bundle)

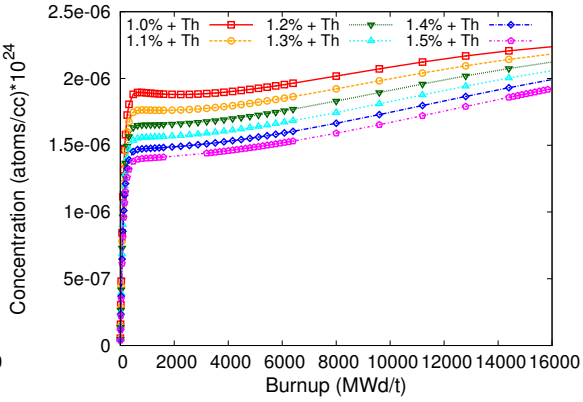

(d) Np-239 (Driver Bundle)

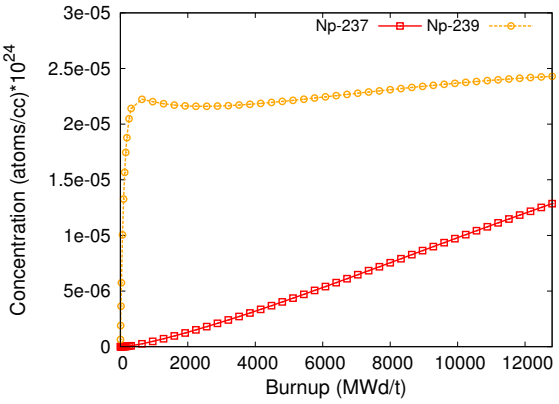

(e) NU-CANDU Case

Figure 4.2: Neptunium levels

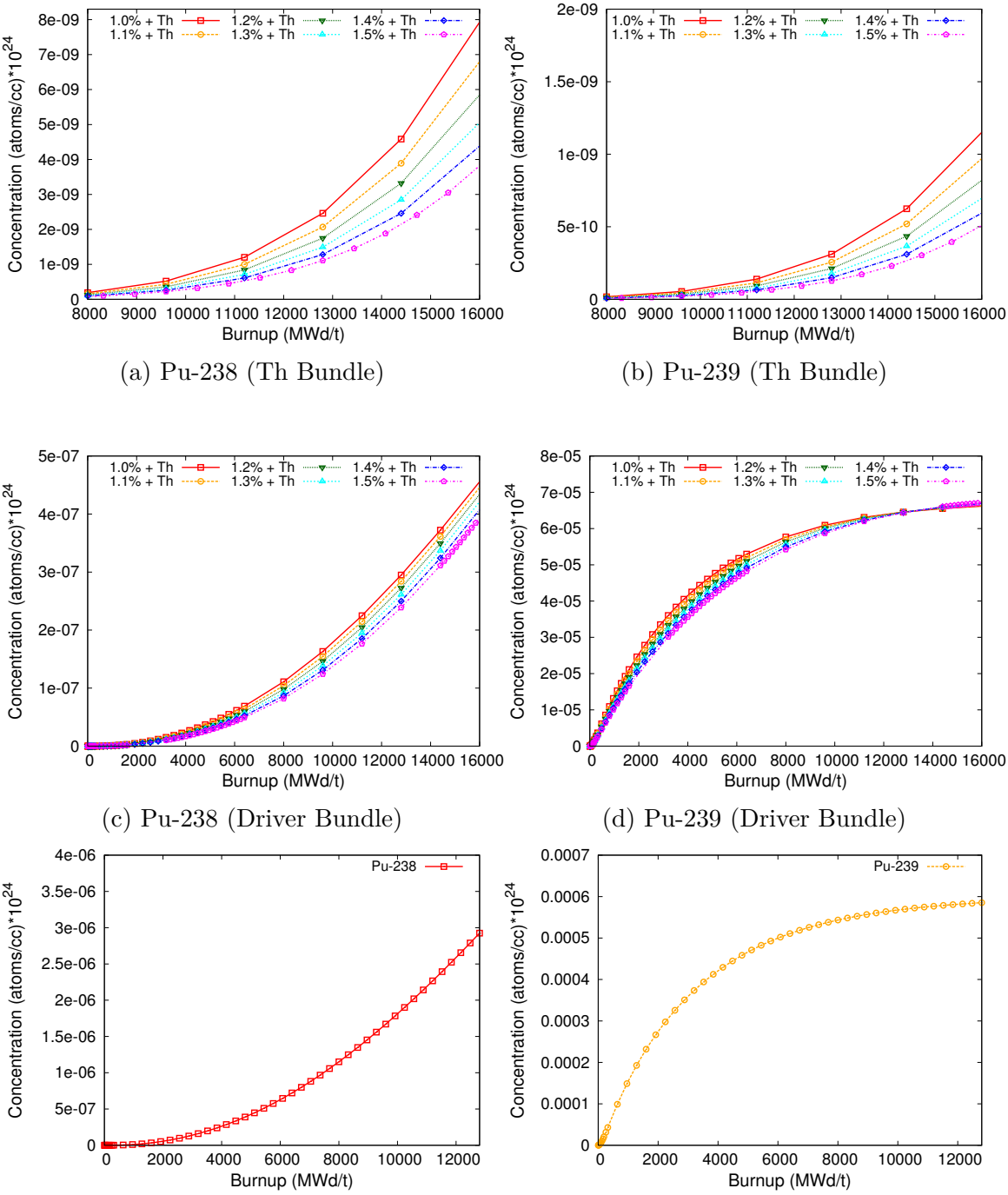

(a) Pu-238 (Th Bundle)

(b) Pu-239 (Th Bundle)

(c) Pu-238 (Driver Bundle)

(d) Pu-239 (Driver Bundle)

(e) Pu-238 (NU-CANDU Case)

(f) Pu-239 (NU-CANDU Case)

Figure 4.3: Plutonium levels

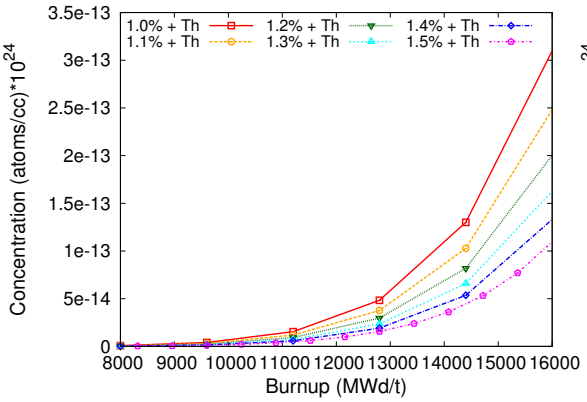

(a) Am-241 (Th Bundle)

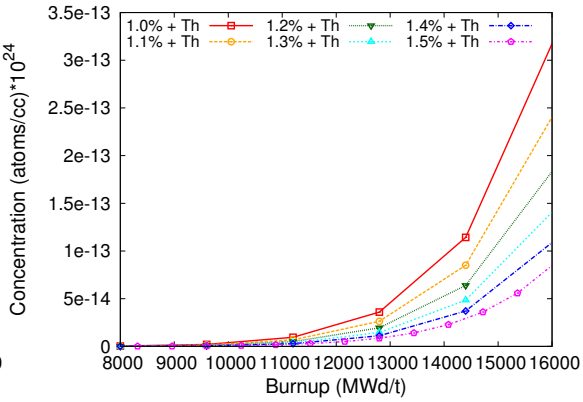

(b) Am-243 (Th Bundle)

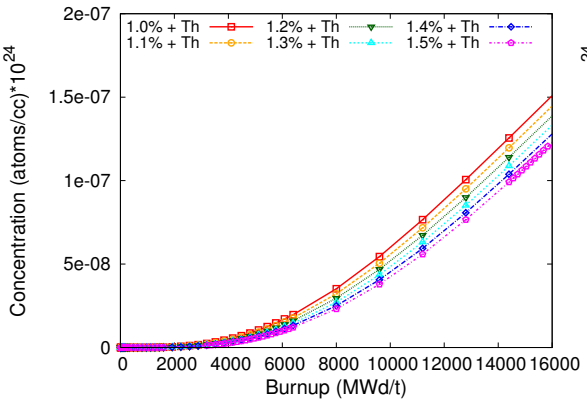

(c) Am-241 (Driver Bundle)

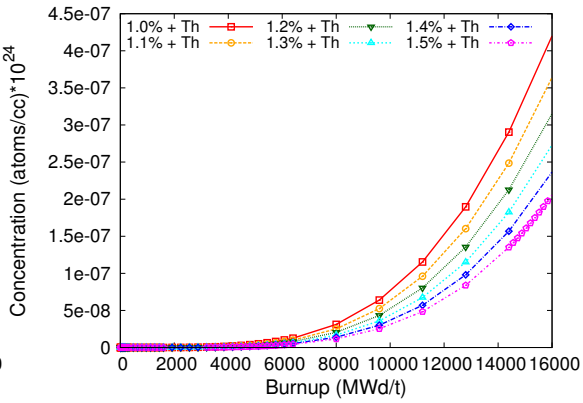

(d) Am-243 (Driver Bundle)

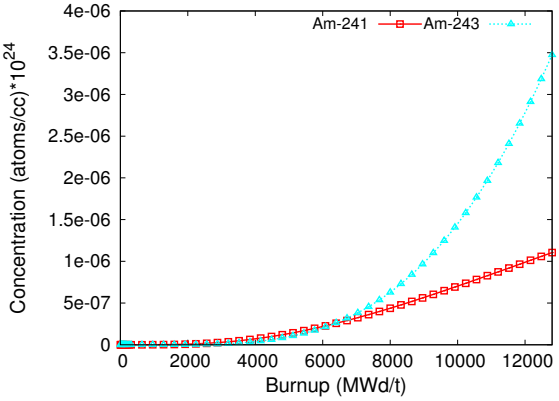

(e) NU-CANDU Case

Figure 4.4: Americium levels

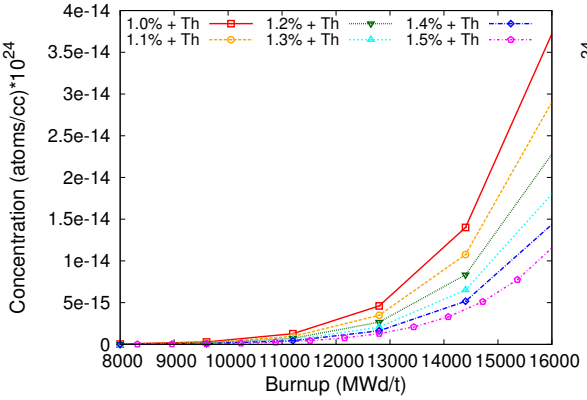

(a) Cm-242 (Th Bundle)

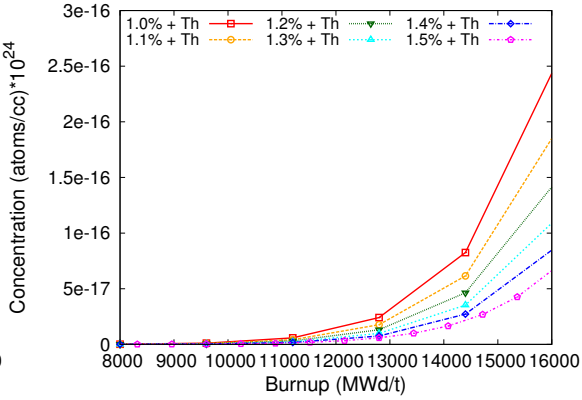

(b) Cm-243 (Th Bundle)

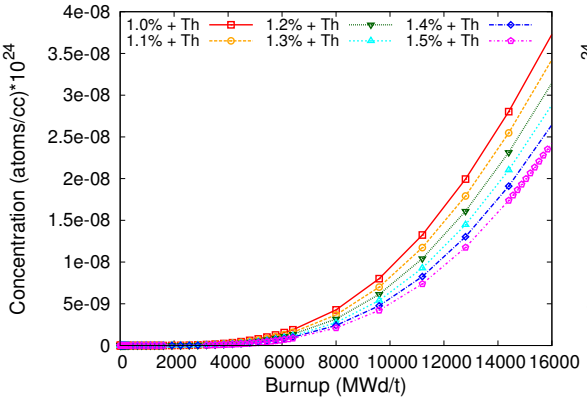

(c) Cm-242 (Driver Bundle)

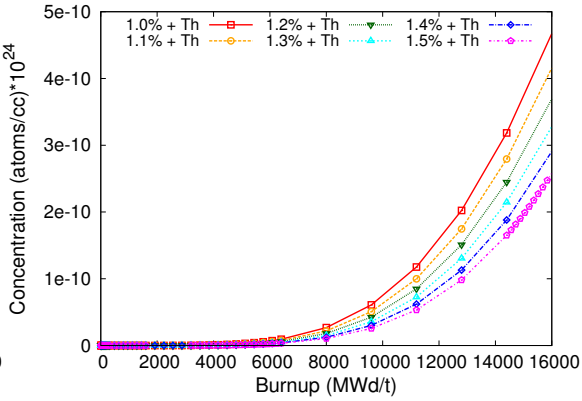

(d) Cm-243 (Driver Bundle)

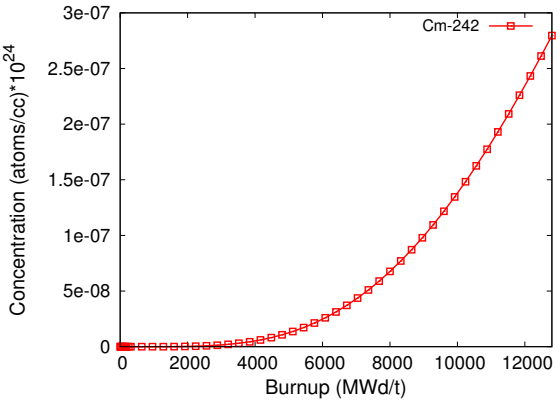

(e) Cm-242 (NU-CANDU Case)

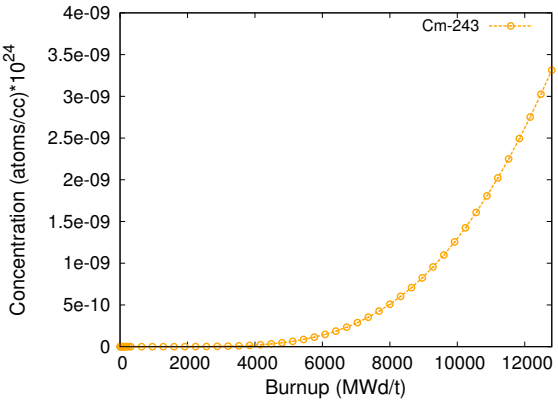

(f) Cm-243 (NU-CANDU Case)

Figure 4.5: Curium levels

The graphs from Figure 4.2 to 4.5 compares the concentration differences between the two bundle types in the multi-cell and also concentrations found in the NU-CANDU case. As expected, the select actinides in the thorium bundle show a lower concentration than that found in the driver bundles. Furthermore, these actinide levels in both the thorium and driver bundle were also lower than the concentrations found in the NU-CANDU bundle.

A similar buildup behaviour is observed between Np-239 and Pu-239 in the uranium bundle (both driver and NU cases), and Pa-233 and U-233 in the thorium bundle. This is due to the similar neutron absorption process that U-238 and Th-232 undergo. For all other actinides, the buildup behaviour between each fuel bundle type is the same as those actinides require several successive neutron absorptions in order to be produced. The concentration levels of those actinides are lower in the thorium bundle because it requires more successive neutron absorptions than the uranium bundles.

Other radionuclides generated from a thorium bundle that are of concern are Pa-231 and U-232. Pa-231 is a long-lived actinide with a half–life of over 30,000 years [32] and U-232 is radiotoxic due to the intense gamma rays emitted from its decay products. Together, these isotopes will cause difficulties in reprocessing and long-term waste disposal for thorium fuels, but will enhance proliferation resistance.

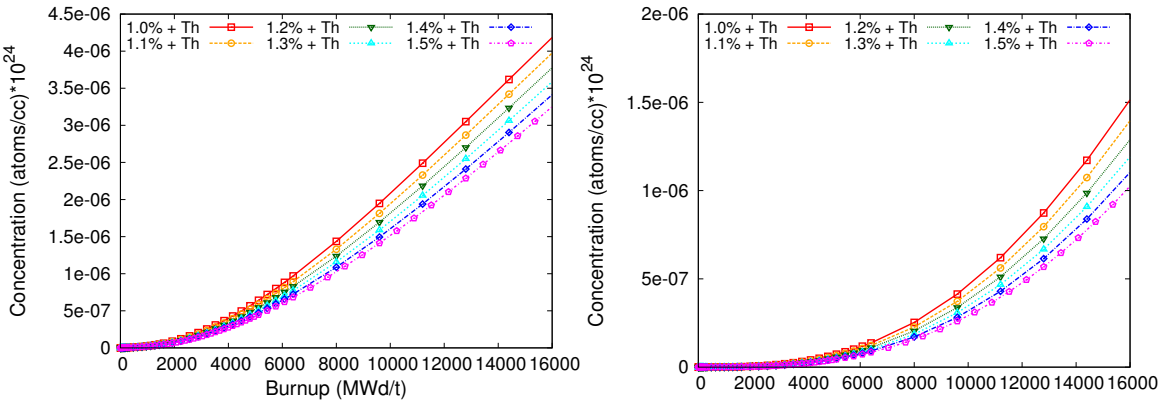

(a) Pa-231 (b) U-232

Figure 4.6: Pa-231 and U-232 concentrations in target bundle

From Figure 4.13, it can be seen that concentrations of Pa-231 and U-232 are present at higher levels than the other Mas found in the previous figures mainly because both isotopes are a product of a 2-neutron production from the absorption of a neutron by thorium and U-233 (see Figure 2.2 and 2.6), which are the dominant elements in the bundle. UOX bundles would contain minuscule levels of Pa-231 and U-232 due to the heavier isotopes of uranium that are present.

4.1.3 Neutron Spectrum

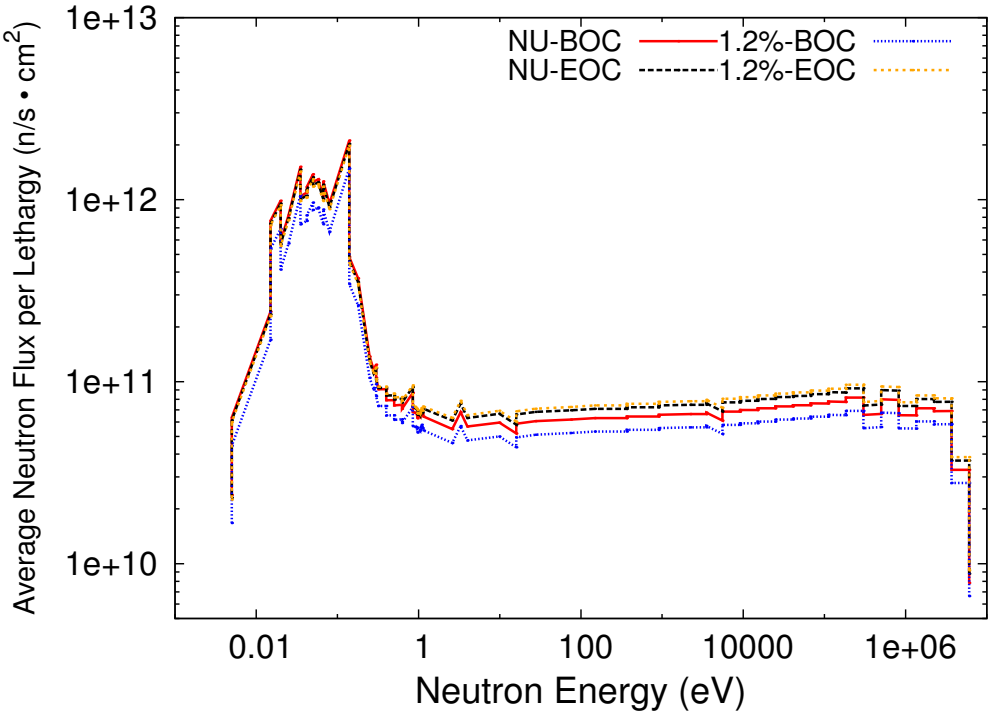

Figure 4.7: Neutron spectrum of CANDU lattice with varying enrichments

With a changing fuel composition, the neutron spectrum in the target cell will be different when compared to the beginning and end of burnup. For a base comparison, the neutron spectrum of the CANDU lattice cell is shown in Figure 4.7. Neutron flux peaks at the thermal range and decreases with increasing neutron energy due to the use of heavy water as the moderator. There is a slight increase from epi-thermal to fast energies from the fissioning of U-235 and Pu-239. With increasing U-235 enrichment, the BOC spectrum is lower compared to end of cycle (EOC) spectrum. With the depletion of U-235 at EOC, less thermal neutrons are absorbed and overall, total neutron flux increases due to less absorptive elements.

The presence of a thorium bundle will significantly lower the neutron flux in the lattice from the heavy neutron absorption properties of Th-232. The following figure shows the resulting neutron spectrum of the multi-cell for an enrichment blanket of 1.2%.

The overall neutron flux is lower by a factor of about 10. The BOC thermal neutron flux is roughly the same between the thorium and driver bundle. With increasing neutron energy, the average flux inside the target bundle decreases since there are no fissile elements to undergo fission to produce fast neutrons. By the end of burnup,

the spectrum between the two types of bundles is relatively the same magnitude throughout all energies. The Th-232 atoms are replaced with U-233, thereby creating a source of fast neutrons.

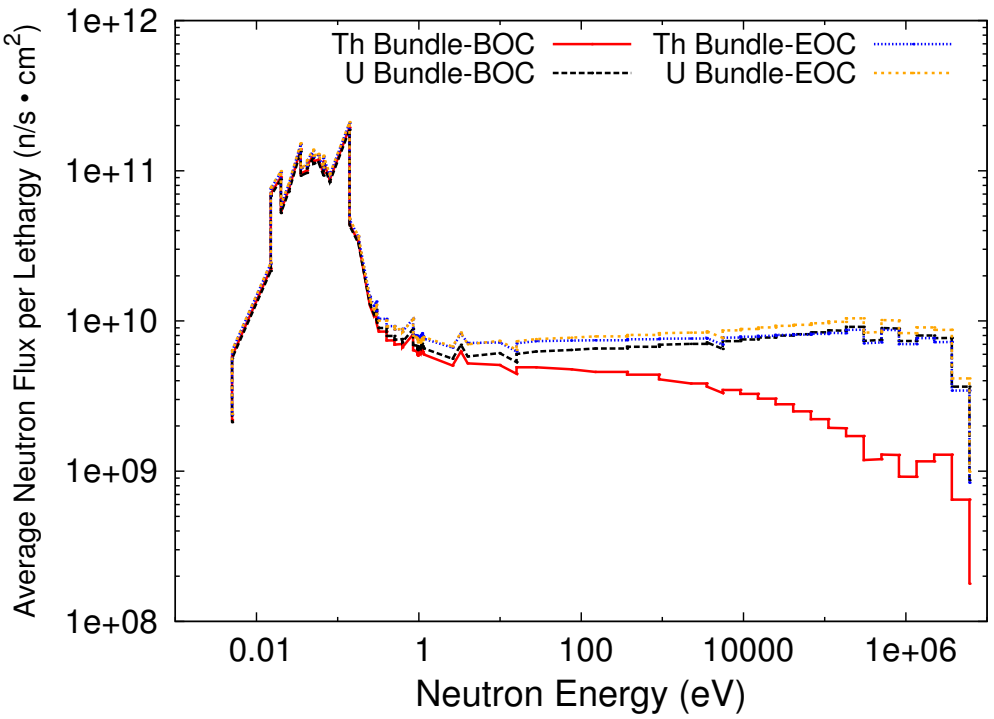

Figure 4.8: Neutron spectrum of CANDU multi-cell thorium bundle and enriched 1.2% blanket uranium bundle

4.1.4 Ring Power

Introducing an initially non-fissile target bundle will produce little power at the start of the core cycle. Over burnup, irradiation of thorium and the successful decay of Pa-233 to U-233 leads to the production of power as the newly generated fissile content undergoes fission. The normalized power in each of the rings is calculated using Equation 4.2:

$$P_i = E_{i,fiss} \times \Sigma_{f_i} \times \phi_{i,int} \tag{4.2}$$

where E_{fiss} is the energy produced per fission, Σ_f is the macroscopic fission cross-section, ϕ_{int} is the integrated flux, and i is the ring number ($i = 1$ for centre ring, $i = 2$ for intermediate ring, etc). The results are shown in Tables 4.3 and 4.4.

A bundle with no initial fissile content will experience near-zero power at BOC than that of the SEU driver bundle. Some power will be generated in the thorium bundle from gamma ray emissions as thorium absorbs neutrons. Going radially outwards from

the centre pin, the powers increase in both target and driver bundle. The difference is in the BOC and EOC powers where the target bundle increases in power at the end of burnup while the driver bundle decreases in power. This means that the target bundle is producing and using fissile content throughout burnup while the driver bundle is losing more of its fissile content than it can replace.

Table 4.3: Normalized Ring Power of target bundle 1.2% enriched driver bundle from multi-cell at BOC.

	Normalized Power (kW)			
Ring	Target	Driver	NU Case	1.2% Case
Centre	7.7E-05	0.7796	1.689	1.529
Inner	4.76E-04	4.9847	10.819	10.041
Intermediate	9.71E-04	11.7842	24.455	23.645
Outer	1.53E-03	23.6679	45.870	47.675

Table 4.4: Normalized Ring Power of target bundle 1.2% enriched driver bundle from multi-cell at EOC.

	Normalized Power (kW)			
Ring	Target	Driver	NU Case	1.2% Case
Centre	2.65E-03	0.7805	1.637	1.713
Inner	1.60E-02	4.8687	10.414	10.727
Intermediate	3.21E-02	10.6913	23.091	23.135
Outer	4.54E-02	18.4707	41.252	39.664

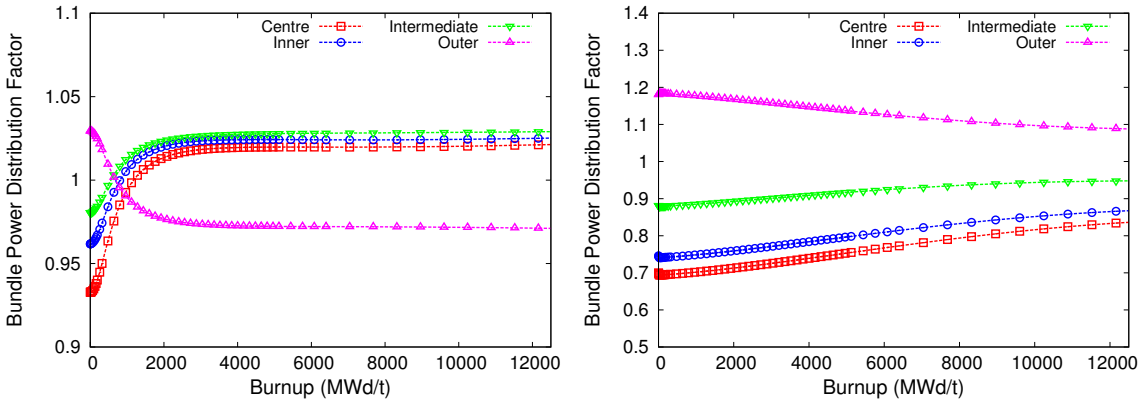

(a) Target Bundle (b) Driver Bundle

Figure 4.9: Pin power factor for target and driver bundles in the multi-cell with 1.2% enriched driver

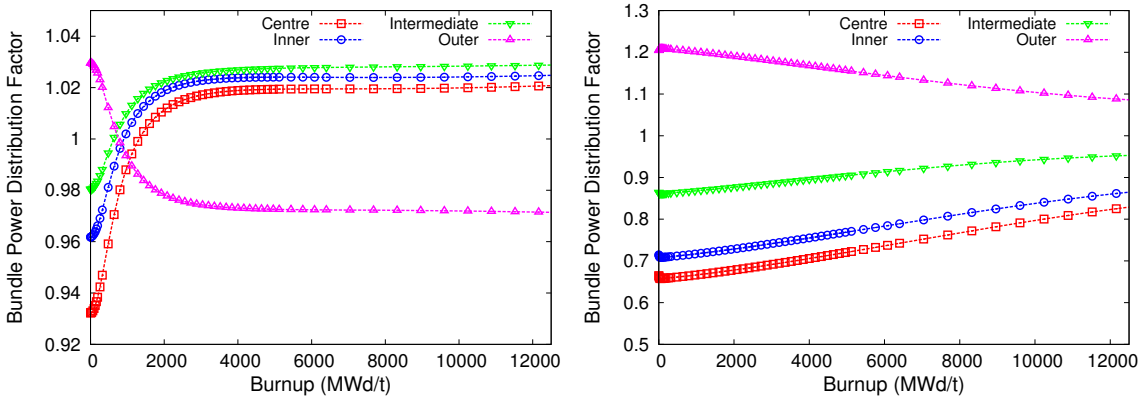

(a) Target Bundle (b) Driver Bundle

Figure 4.10: Pin power factor for target and driver bundles in the multi-cell with 1.5% enriched driver

The bundle power distribution factor is calculated for the two different bundles by the following formulation:

$$F_i = \frac{q_i}{q_{eav}} \tag{4.3}$$

where F_i is the bundle power distribution factor, q_i is the power of a single element in ring i ($i = 1$ for centre ring, $i = 2$ for intermediate ring, etc), and q_{eav} is the average pin power. The bundle power distribution factor describes the ratio of power in ring i to the average bundle power. Using DRAGON, the F_i is calculated for each ring in the thorium bundle and the uranium driver bundle. This is illustrated in Figures 4.9 and Figure 4.10.

The outer ring of a CANDU bundle is exposed to the highest thermal neutron flux compared to the other three inner rings due to spatial self-shielding. Therefore, the rate of fission is higher in this region which leads to a higher power. In addition, the centre pin would have the lowest power since it is shielded from the thermal neutrons. Overall, Figures 4.9b and 4.10b show the bundle power distribution factor of the standard NU bundle and depicts what is described. Increasing enrichment in the uranium bundle shifts the power towards the outer ring and lowers it in the centre. The increased fissile concentration enhances the spatial shielding effect of the outer ring. However, the thorium bundle is observed to have a different behaviour. Initially, the bundle power distribution factor starts with the outer ring being the highest, but over burnup, F_4 decreases while the three other rings increase in F_i and surpasses that of the outer ring. The higher exposure of the outer ring to thermal neutrons produces more Pa-233, which increases the absorption cross-section of the outer ring even further. The continued neutron exposure is preventing some of the Pa-233 from successfully decaying to U-233, as well as some neutron competition between Pa-233

and U-233 due to the similar capture cross-sections helping to lower the amount of power that can be generated in the ring. The inner three rings are exposed to the lower neutron flux, which prevents an over-breeding of Pa-233 that thus allows for less neutron competition for U-233 from the intermediary product and increases the power produced in those rings.

4.1.5 Lattice Reactivity

The multi-cell reactivity will be affected by the changing fuel composition in the target bundle and as well as in the driver bundles. In a sense, both types of bundles are breeding, but the difference is the intermediate and the subsequent products that are produced during breeding which will affect the overall reactivity. The measure of the sustainability of a nuclear reaction is the multiplication factor, k. By having a value equal to or above one means that the nuclear reaction is continuous and is termed critical or super-critical; for each fission reaction, a neutron is produced to go on and initiate another fission event. For a multi-cell analysis, the infinite multiplication factor is used since the model is the simulation of infinite lattices where there is no leakage. The multi-cell k_∞ is shown in Figure 4.11.

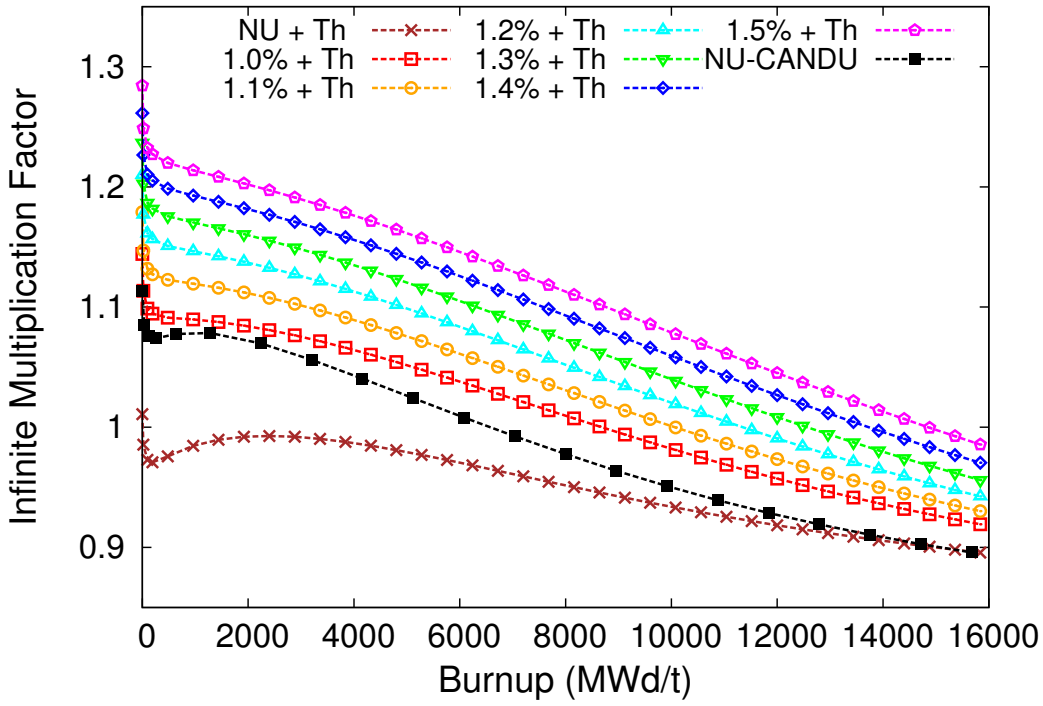

Figure 4.11: Infinite multiplication factor of multi-cell

Figure 4.11 shows that if the outer eight lattices are loaded with NU, the reactivity of the multi-cell cannot maintain criticality. Similar to the plutonium peak in the NU

case, a peak is also seen at about 2000 MWd/t and is much broader than the NU case; the slow decrease in k_∞ can be attributed to the combination of the plutonium peak and the newly formed U-233. The multi-cell k-infinity can be brought up by increasing the enrichment in the driver bundles. By enriching the driver bundles, the noticeable Pu peak diminishes as increasing driver enrichment masks it. Over burnup, reactivity decreases steadily for all cases from the creation of U-233.

4.1.6 Coolant Void Reactivity

Another variable to evaluate is the coolant void reactivity (CVR) in the CANDU system. CVR is defined as the amount of reactivity insertion or removal from a reactor system due to the absence of coolant. The multiplication formula in Equation 4.4 is composed of four factors that affect the reactivity of the core. By voiding the coolant, the neutron spectrum is shifted to the epi-thermal and fast energy range, which changes the weight of the contribution from each factor.

$$k = \eta f \rho \epsilon \tag{4.4}$$

- η is the average number of neutrons produced from thermal absorption by the fuel.
- f is the thermal utilization factor which is the probability the neutron will be absorbed into a fuel material.
- ρ is the resonance escape probability. It is the fraction of neutrons that slow and escape resonance capture.
- ϵ is the fast fission factor. Accounts for the fast neutrons born from non-thermal fission. It is calculated as the ratio between the total number of fission neutrons (thermal and fast) to the number of fission neutrons from thermal fission.

The unique design of having the coolant and moderator separate in the CANDU core affects the CVR. In the case of a voided fuel channel, there will be more fast neutrons from the lack of moderation from the coolant. A higher fast neutron flux will increase the fast fission factor, thus increasing the reactivity. Furthermore, fewer neutrons will be slowed down into the resonance region and will avoid U-238 or Th-232 resonance capture, increasing the ρ factor. Overall, the CANDU design allows for a positive reactivity insertion from voided coolant. In the event of a loss of coolant accident (LOCA), reactivity will increase, but safety systems of the CANDU reactor will react fast enough to prevent uncontrollable reactivity insertion leading to an unstable situation. Other reactors, such as the PWR, have a negative CVR. This is a result of using light water (H_2O) and the combining of coolant and moderator as one single circuit.

The CVR is calculated by subtracting the reactivity of a normal lattice to the voided lattice as shown in the equation below.

$$CVR = \left(\frac{1}{k} - \frac{1}{k_{void}}\right) * 1000 \tag{4.5}$$

Using DRAGON, a voided condition was introduced to the multi-cell by setting the density of the coolant to 0.0001 g/cm, and the resulting infinite multiplication factor was produced. Comparing the the nominal case (no voiding) to the the voided case, the CVR can be calculated, and is shown in Table 4.5 and Figure 4.12.

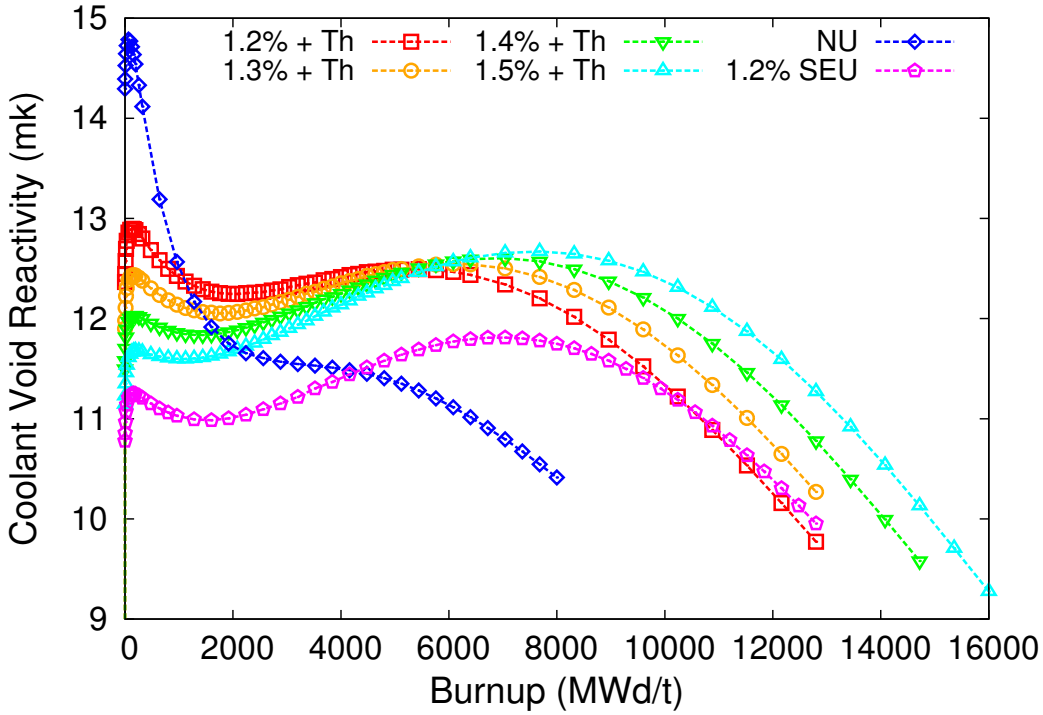

Figure 4.12: Coolant void reactivity of multi-cell

The CVR response between NU and the dual fuel configuration is different. Initially, the CVR in the NU case is 14.78 mk at around 64 MWd/t or two days in iteration time and then continually decreases until the end of burnup. The SEU case begins at a much lower CVR due to higher U-235 content displacing the U-238 atoms. By having less U-238 present for resonance capture, the reactivity impact of ρ and ϵ decreases. By introducing a thorium bundle into a 1.2% enriched lattice, the CVR increases from 10.78 mk to 12.37 mk. The presence of Th-232 increases ρ and ϵ, and thus increases the overall reactivity for a voided system. Over the course of burnup, the behaviour of the multi-cell CVR is similar to the single fuel SEU core. A dip is observed in the early stages of burnup and begins to increase to peak at mid-burnup. After, the CVR decreases until the end of burnup.

Table 4.5: Comparison between multiplication factors for normal and voided coolant conditions at initial burnup.

Lattice-Type	k-infinite		CVR	$\Delta k_{inf}(\%)$
	Nominal	Void		
NU	1.122348	1.140648	14.2946	1.617325
1.2%-SEU	1.325789	1.34011	10.77949	1.439419
1.2%+Th	1.209192	1.227546	12.3651	1.506440
1.3%+Th	1.236675	1.255146	11.89983	1.482530
1.4%+Th	1.261338	1.2799	11.49787	1.460863
1.5%+Th	1.283603	1.302234	11.14593	1.441003

4.1.7 Transient Effect of Pa-233

At reactor shutdown, transient effects occur with the decay of short lived isotopes, the most common is xenon-135 and it occurs in the NU-CANDU core. Xe-135 has a half-life of 9.2 hours and the increase in its concentration results in a substantially lowered reactivity due to its high neutron absorption. The xenon effect can seriously hamper the operations of the nuclear power plant because it would take days before xenon concentrations are low enough to restart the core. However, there is the xenon override protocol that allows the adjuster rods to be withdrawn to allow an insertion of reactivity to permit power recovery [33]. After a reactor shutdown, there is a time frame where plant operators must decide whether or not to overcome the xenon effect by using this system to bring the core back online.

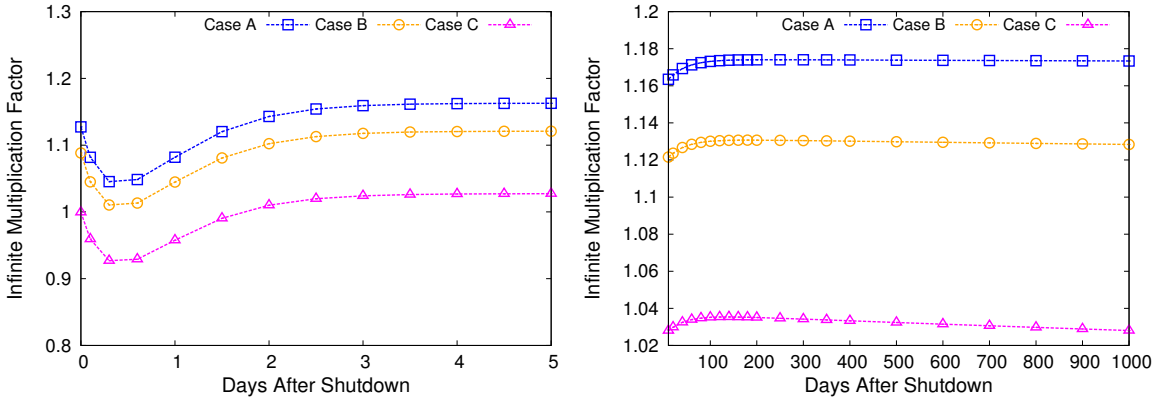

Figure 4.13: Infinite multiplication factor transient due to Pa-233

A different transient occurs in the thorium bundle due to the isotope Pa-233. During reactor shutdown, the production of Pa-233 stops and the remaining concentration begins to decay into the fissile element U-233. The result is the transient increase in reactivity in the lattice, which can cause a serious problem if the multiplicative

factor is above criticality. The above figure shows the reactivity insertion for a Pa-233 initiated transient in the multi-cell for three cases: 90 days or 2880 MWd/t (Case A), 180 days or 5760 MWd/t (Case B), and 360 days or 11520 MWd/t (Case C) of lattice burnup for 1.2% enriched driver bundles. At shutdown, k_{inf} initially decreases due to the xenon effect from the driver cells, but begins to increase after half a day.

Table 4.6: Maximum reactivity insertion for Pa-233 Transient

	Reactivity Insertion (mk)
Case A	128.715
Case B	120.266
Case C	108.342

Maximum k_{inf} for Cases A, B, and C are 1.17405, 1.13069, and 1.03534 at 250 days, 180 days, and 140 days, respectively. Accounting for the dip in reactivity for the first half of the day, Table 4.6 shows the maximum reactivity insertion due to the decay of Pa-233. With the lattice shutting down earlier in the burnup cycle, such as in Case A, there is a higher reactivity insertion than compared to the lattice at higher burnups (Cases B and C). The higher reactivity insertion can be attributed to the fissile content still available and the lower concentration of neutron absorbers produced from long burnups. Even though in Cases B and C would have more Pa-233 to decay and contribute to the increase in U-233 concentration, the increasing concentrations of parasitic neutron absorbers in the eight driver bundles over longer periods of burnup lowers the potential amount of reactivity inserted. Therefore, it is only if a shutdown occurs early in the burnup will a reactivity insertion due to the decay of Pa-233 be high enough to cause a problem, which may not be within the capacity for the reactivity control devices that is only worth about 180 mk. Depending on the placement of the thorium bundle and the configuration of the core, this transient is confined locally and not throughout the entire core. If this transient occurs in multiple areas in the core and is left unchecked, it may produce an unwanted scenario that will need to be addressed. One possible solution is to remove the thorium bundle by using the refuelling machine for a channel dump. This method is already a safety tactic used in times of emergencies and can be adapted for the target fuel channels.

4.2 Homogeneous Thorium CANDU Core

The eventual goal of a dual fuel core approach is to stockpile enough U-233 for the SSET cycle to be initiated. The SSET cycle is dependent on generating more U-233 than the initial enrichment from thorium enriched U-233 fuel such that there is no reliance on topping the reactor with fissile materials from other sources and hence a 'self-sustaining' cycle can occur. The homogeneous thorium CANDU core is fuelled with bundles of thorium enriched with U-233 oxides. This homogeneous fuel mixture is assumed to be well-developed since the current metallurgical research on mixing thorium and other fissile elements have shown that the relatively inert and stable thorium element is difficult to process during fuel fabrication [3]. The homogeneous mixture of thorium with any other elements will be a metallurgical hurdle for the future of thorium fuel fabrication and reprocessing.

In order for such a cycle to work, the EOC fissile content must be greater than the initial fissile inventory. This is calculated by using the conversion ratio (CR) in Equation 4.6, which takes the ratio of fissile content at the end of burnup to the amount initially invested [34]. For a CR>1, there is a positive gain in fissile content (breeding); a CR<1 means there is a loss in fissile content (consumption).

$$CR = \frac{(M_{U233} + M_{Pa233})_{Exit}}{(M_{U233})_{Initial}} \tag{4.6}$$

4.2.1 SSET Requirement

Using DRAGON, an infinite lattice of a CANDU-6 core will be modelled to determine the extent of U-233 enrichment required to produce a net gain in U-233. Lattice cell geometry will be the same as seen in Figure 4.1, and various enrichments of U-233 will be evaluated. Furthermore, there are three different specific power densities used to observe the effects of different neutron fluxes on the thorium fuel: a base case of 20 W/g, 25.5 W/g, or the full power of 32 W/g [34]. At higher specific power densities, the amount of fissile material burned increases compared to a lower specific power. As more burnable material is used, the neutron flux increases. The resulting increase in flux will produce more Pa-233 from neutrons being absorbed by thorium, but will also increase the chance of parasitic absorption by the intermediate product. A lower specific power density is used as a means to retarded the neutron absorption by Pa-233 while maintaining the decay process for U-233 production [34].

At full power, the CR is above 1.0 for U-233 concentrations from 1.40% to 1.45%; however, average exit burnup is less than 10 GWd/t. For lower power densities, the average exit burnup increases for the same U-233 enrichments. Furthermore, it reduces the number of times a thorium bundle has to be reprocessed, lowering the cost for

reprocessing. From Figure 4.14, the ideal enrichment is around 1.40% for the 20 W/g case and 1.44%-1.45% for the 25.5 W/g case. As for a full power core, using thorium will not be economical since average exit burnups are so low.

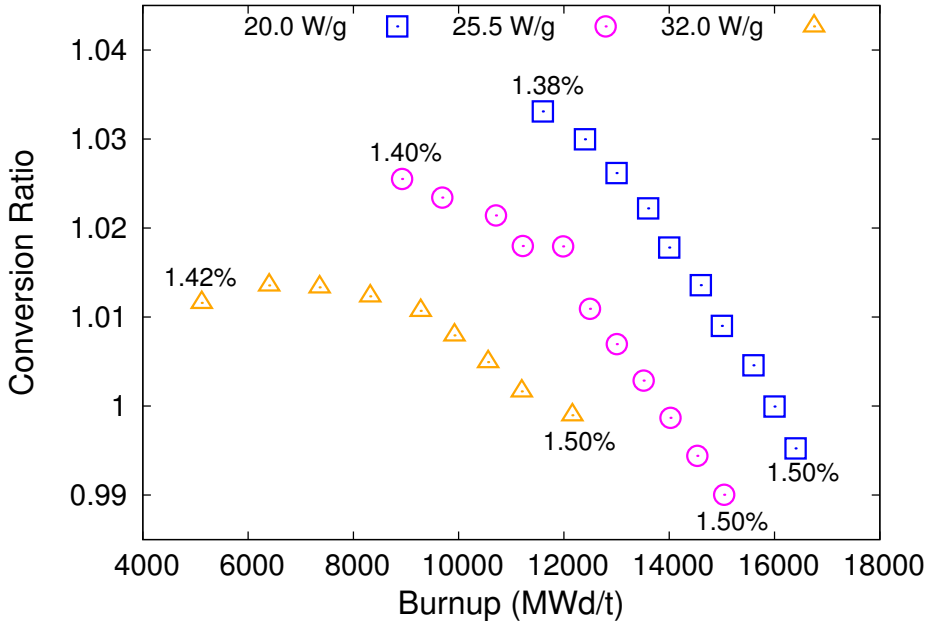

Figure 4.14: Conversion ratio for various enrichments of U-233 in a homogeneously thorium fuelled CANDU-6 core

4.2.2 Fuel Composition

An enrichment of 1.44% was chosen for the rest of the investigation. For increasing specific power densities, the neutron flux will also increase. More neutrons are available to be absorbed by thorium, creating an increase in Pa-233 concentration; however, the drawback is it allows more neutrons to be absorbed by the created Pa-233 due to its high absorption cross-section, as well as by other parasitic neutron absorbing isotopes.

The concentration level of Pa-233 throughout burnup is similar to what was found in the multi-cell calculation in Figure 4.1a. On the other hand, the concentration behaviour of U-233 is different. In this case, the homogeneously fuelled thorium core is initially in a consumption mode. After reaching 2000 MWd/t, U-233 concentrations level off due to the decay of Pa-233. The new level of U-233 results in a CR$\geq$1. For specific power densities of 25.5 W/g and 32.0 W/g, U-233 production is actually seen to increase.

The other set of important isotopes are Pa-231 and U-232, and the behaviours of these are shown in Figure 4.16. Throughout burnup, the concentration levels between the three specific power densities for each isotope are relatively equal. The effect of power densities does not have a great influence on the levels of Pa-231 and U-232. This is also evident for isotopes illustrated in Figure 4.17. Very little variance can be seen when comparing the concentrations of particular isotopes between the three different power densities. Only Am-241 and Cm-242 have deviations at different power densities.

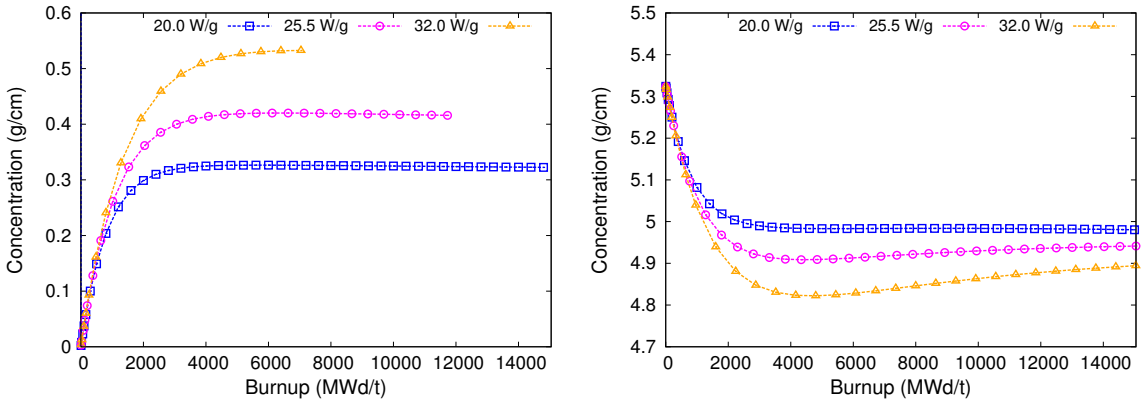

(a) Pa-233 (b) U-233

Figure 4.15: Pa-233 and U-233 levels for a homogeneously fuelled thorium CANDU core enriched at 1.44%

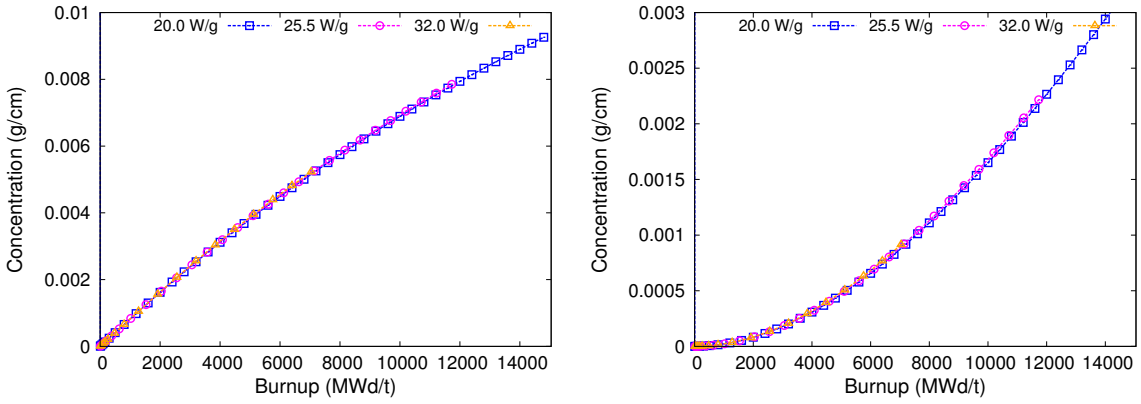

(a) Pa-231 (b) U-232

Figure 4.16: Pa-231 and U-232 levels for a homogeneously fuelled thorium CANDU core enriched at 1.44%

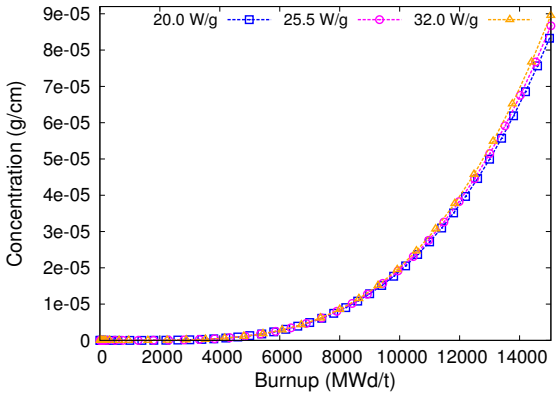

(a) Np-237

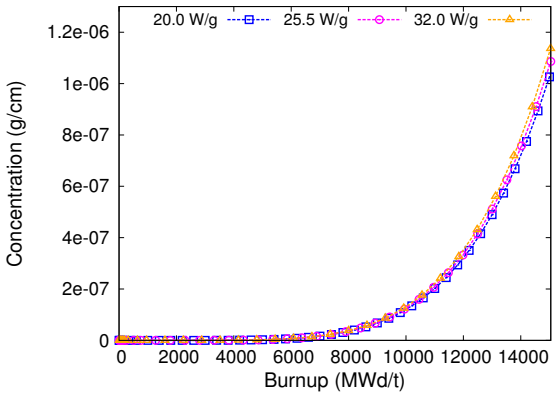

(b) Pu-239

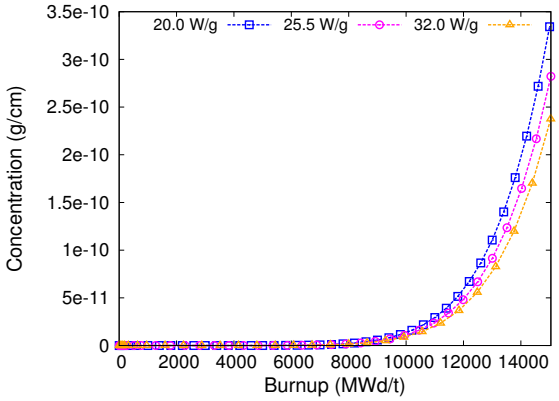

(c) Am-241

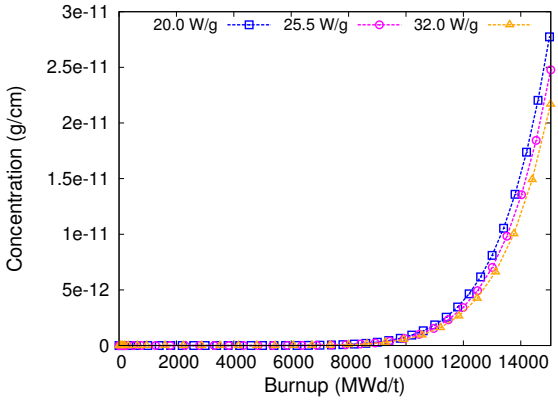

(d) Cm-242

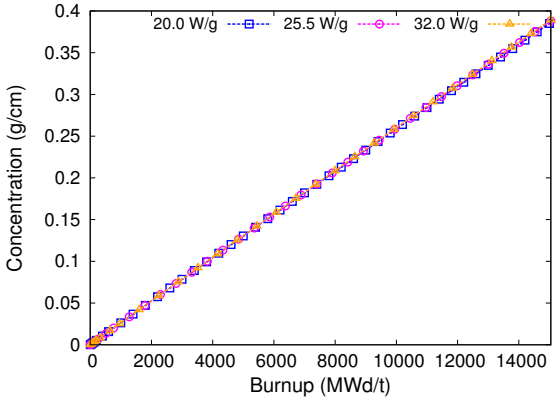

(e) Cs-137

Figure 4.17: MA concentrations in homogeneously fuelled thorium CANDU core enriched at 1.44%

4.2.3 Lattice Reactivity

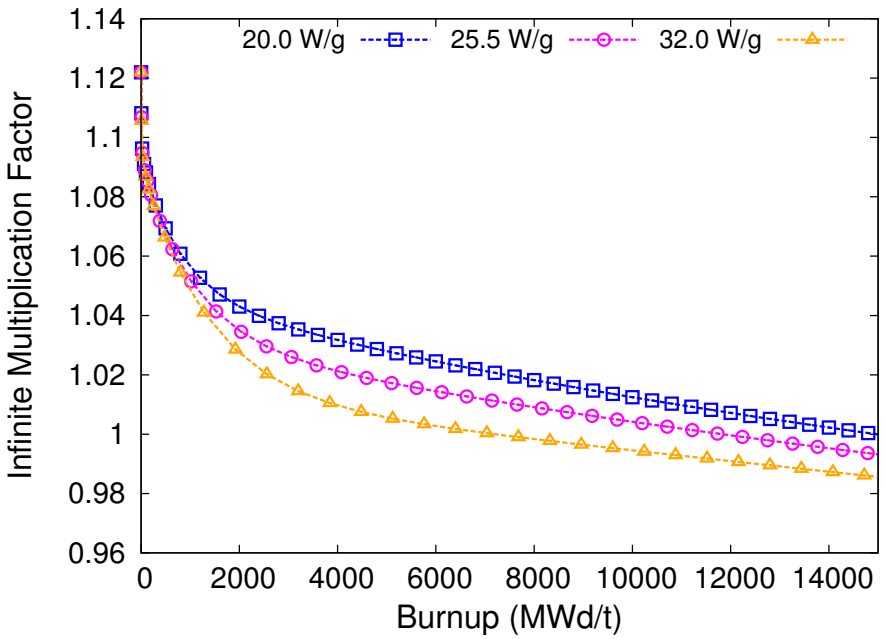

Figure 4.18: Infinite multiplication factor of a thorium bundle enriched at 1.44% U-233 in a CANDU-6 core

As such, a change in the fuel composition over burnup will cause a change in the reactivity. Figure 4.18 shows the k_∞ for the three specific power densities.

More parasitic actinides produced as a result of higher specific power density leads to a more rapid decrease in lattice reactivity. Further, the sharp decrease in reactivity is observed at the beginning of the cycle from Pa-233 production. In all cases, there is a steep initial drop in reactivity and then a gradual linear decrease. The linear behaviour is the increasing concentration of U-233 that balances the negative reactivity from Pa-233 and other MAs. Even though the CR is at 1 or higher near the end of burnup, the presence of Pa-233, other actinides, and fission products will keep the multiplicative factor from increasing.

No plutonium peak is observed, such as the one found in the NU-CANDU case. Plutonium is an extra element that adds to the reactivity due to the absorption of its neutrons by U-238 and its relatively quick decay. In the thorium case, the decay of Pa-233 to U-233 is much slower, resulting in no peak observed.

4.2.4 Transient Effect of Pa-233

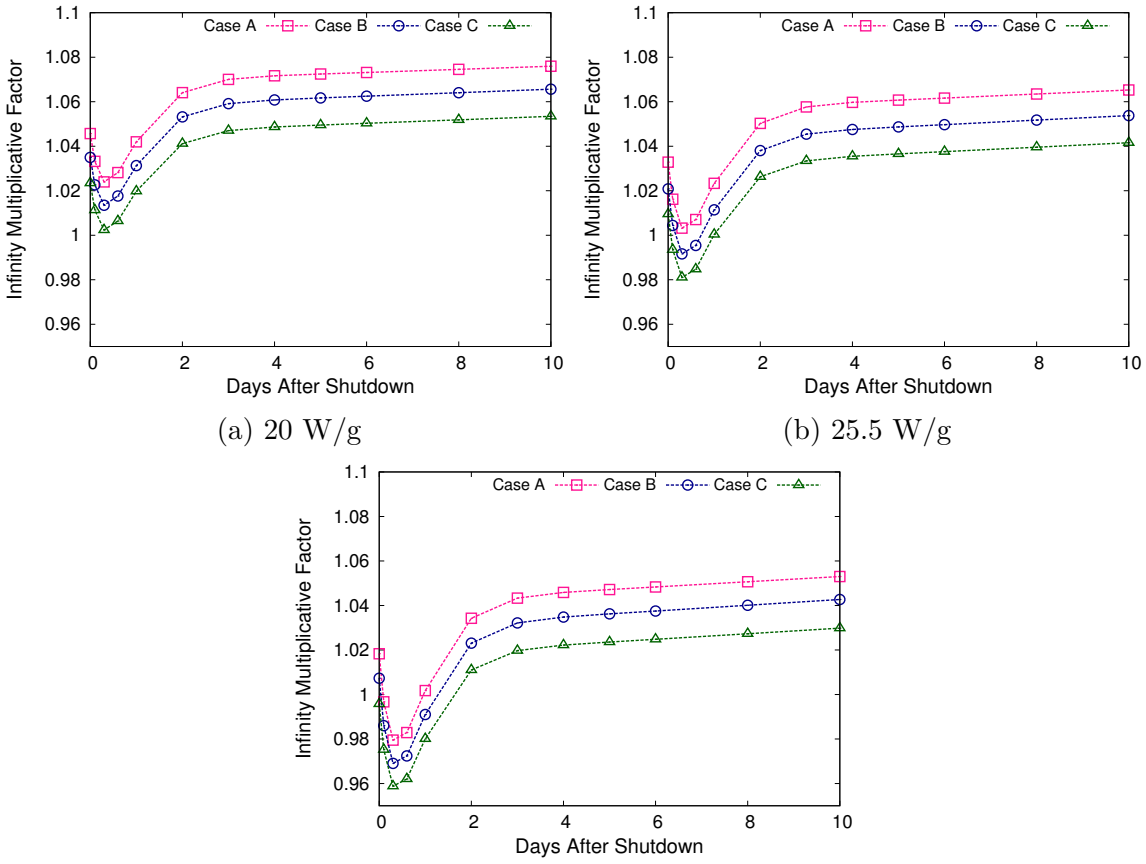

(a) 20 W/g

(b) 25.5 W/g

(c) 32 W/g

Figure 4.19: Pa-233 Transient for U-233 enrichment of 1.44% for different reactor operating conditions

Similar to the transient increase in reactivity seen in the multi-cell, a fully fuelled thorium CANDU core will experience the same effects; however, in this case, the increase in reactivity will be effective throughout the entire core rather than locally.

Evaluating the effect of the Pa-233 during a shutdown will occur for core burnups of after 90 days (2880 MWd/t), 180 days (5760 MWd/t), and 360 days (11520 MWd/t), which will be designated as Case A, B, and C, respectively. A shutdown means setting of the specific power density to 0 W/g in DRAGON to simulate zero burning of the fuel.

The graphs provided in Figure 4.19 show the Pa-233 transient over a period of 10 days. There is an initial drop in reactivity during the first half of day one due to increasing short lived FPs, followed by a rapid increase in k_∞. Reactivity continues to increase over time, but the rate of increase slows down and continues on past 600 days. Case A

Table 4.7: Maximum reactivity insertion from Pa-233 transient after 10 days

Reactor Power Density	Reactivity Insertion (mk)		
	Case A	Case B	Case C
20.0 W/g	51.96	52.128	51.07
25.5 W/g	62.06	62.152	60.537
32 W/g	73.505	73.647	71.031

has the highest infinite multiplication factor since the reactor shutdown was early on in the burnup where the concentration of FPs are low; k_∞ surpasses 1.018 after 10 days. For Case C, initial k_∞ begins fairly low and decreases to a sub-critical state, but with the decay of Pa-233 to U-233, the reactivity insertion puts the core back into a super-critical state. Table 4.7 shows that a higher specific power density increases the amount of reactivity inserted, mainly due to the higher Pa-233 created as a result of a higher power density. In all cases, the reactivity insertion is high, with Case B being the greatest. The current reactivity control system in the CANDU system would not be able to handle such an insertion if left unmanaged. Even if the reactivity systems were actuated to its maximum capacity, it may still be ineffective from the growing U-233 levels. Table 4.8 shows the total reactivity insertion after 600 days.

Table 4.8: Maximum reactivity insertion from Pa-233 transient after 600 days

Reactor Power Density	Reactivity Insertion (mk)		
	Case A	Case B	Case C
20.0 W/g	80.314	83.827	83.129
25.5 W/g	98.715	103.034	101.358
32.0 W/g	120.208	125.183	121.876

The reactivity insertion transient due to Pa-233 poses a serious concern when a core shuts down. It will require external input by the plant operators such as the use of adjuster rods and possibly ejection of bundles from the core to maintain the core in a subcritical state. Further modelling is required to evaluate the effects of adjuster rods during such a transient.

A brief analysis of a fully fuelled thorium CANDU core has been presented. Based on the findings found in Figure 4.14, a SSET cycle is possible at a chosen U-233 enrichment and specific power density; however, it has been suggested that an average exit burnup of less than 15 GWd/t will translate to more frequent reprocessing and will be uneconomical [3].

Chapter 5

Full-Core Modelling

After completing lattice calculations, a model is required to assess the use of thorium bundles on a full-core scale. Due to thorium's absorptive nature, the placement and number of thorium bundles used are important parameters to investigate in order to determine an optimal core configuration that will operate within the safety operating margins while producing the required output power and the desired levels of U-233. In particular, the model will determine the radial and axial power distributions which will be compared to the NU- and SEU CANDU core, and the operational licensing limits. The average exit burnups and full-core reactivity will also be evaluated.

CANDU reactors are refuelled online, typically every day or a few times per week. This method of refuelling allow operators to maintain an overall core multiplication factor of nearly one by removing depleted bundles and replacing it with fresh bundles, which maintains the reactivity to sustain the nuclear reaction. Therefore, the core is always in a state of quasi-equilibrium and must be simulated in a time-average model. The results of the model will show the power distribution, core reactivity, and average exit burnups, all of which can serve as a target for actual reactor operations.

By refuelling online, the added reactivity from the fresh fuel will cause a rippling effect in the power distribution. An instantaneous snapshot of the core will show the effect of the interaction between fresh fuels and other fuels at mid or high burnup. The results of the snapshot of the core will show the power tilts and core reactivity that would not normally be found in a time-average model, and can be used to determine if the outcome of the refuelling process is within the operating limits of the core.

In the startups of new CANDU reactors, the core is loaded in a dual fuel configuration with DU and NU fuel due to the large amount of excess reactivity associated with the use of NU alone, which cannot be compensated with the core control devices. Similarly, the dual fuel mode will be assessed on the power and reactivity levels at initial core startup to evaluate its status at the beginning of reactor life.

The full-core model will be developed using the diffusion code, DONJON. In order to use this code, homogenized cross-sections from the transport equation solutions are required and retrieved from the multi-cell calculations from DRAGON in the previous chapter. Dual fuel core configurations will be presented in this chapter along with the results from the diffusion calculation.

5.1 CANDU-6 Core Description

The dual fuel core will be modelled based on the CANDU-6 reactor design. A typical CANDU-6 core has 380 horizontal channels containing 12 bundles per channel and outputs a total power of 600 MW_e. The model core is outfitted with a 65 cm radial reflector to aid in radial flattening; there is no axial reflector. The horizontal geometry of the CANDU-6 core is what allows the possibility of online refuelling, compared to other reactors, such as the PWRs, that must be shutdown to refuel the entire fuel assembly. The parameters of a typical CANDU-6 core are outlined in Table 5.1.

Table 5.1: Key parameters for the CANDU-6 diffusion model

Parameters	Values
Total Thermal Power	2061.4 MW
Channels	380
Bundles/Channel	12
Bundles/Refuelling Shift	8
Bundle Length	49.53 cm
Reflector Thickness	65.375 cm

The CANDU-6 core is typically divided up into nine average exit burnup regions shown in the Figure 5.1. Each region has a predetermined average exit burnup/irradiation that helps manage the core reactivity to remain critical and to help flatten the radial power distribution. The nine regions are necessary to account for the structural differences of the core since these differences introduce a new source of parasitic neutron absorption. For example, the right region of the core contains the liquid neutron absorber injection nozzles for shutdown system 2 (SDS2); the top and bottom region of the core are structurally different where the latter contains a greater mass of steel due to the presence of guide tubes. The average exit burnups in those regions have to be adjusted to the rest of the core to achieve radial power symmetry.

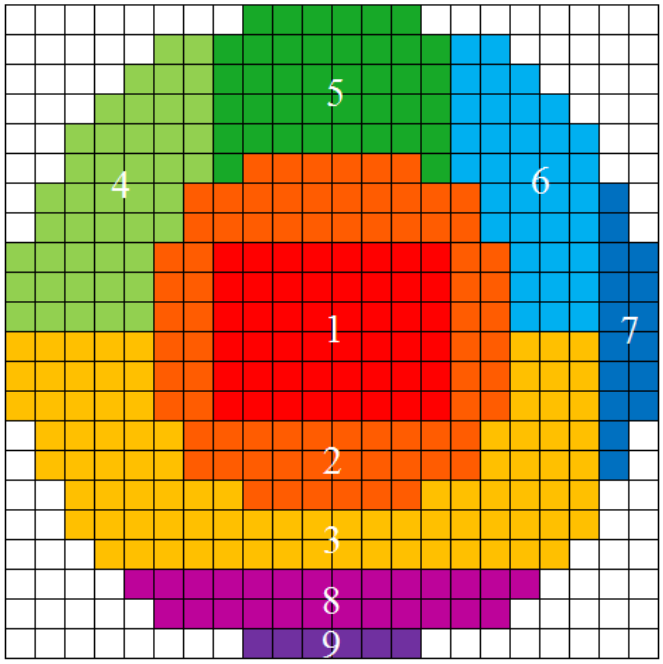

Figure 5.1: CANDU-6 burnup regions [30]

Table 5.2: average exit burnups for each region in the CANDU-6 core [30]

Core Region	1	2	3	4	5	6	7	8	9
average exit burnup (MWd/t)	8029	8029	7007	7050	7050	6904	6904	6592	6592

In most typical reactor physics analysis, cross-sections resulting from reactivity devices such as adjuster rods are retrieved from 3D multi-cell models from DRAGON and are included in the full-core model. In this analysis, a 3D model of the 3x3 multi-cell will be both incredibly computational and time intensive, therefore the following full-core models are developed without any reactivity devices. Furthermore, without the penalty of the reactivity devices, the bundle burnups would not be accurate. Therefore, the average exit burnup is adjusted such that an excess ≈20 mk is added to the core multiplicative factor, roughly estimate of the reactivity worth of the adjuster rods [35]. Region burnups from [30] were used as a baseline and subsequently adapted to include the excess reactivity required for the reactivity devices, in which the values are tabulated in Table 5.2. The iteration used to find the regional average exit burnups that satisfy the $k_{eff} \approx 1.020$, and the desired channel and bundle power are shown in Figure 5.2. This process will be used throughout this investigation. In this case, the effective multiplication factor accounts for the leakage due to the limited geometry of the core.

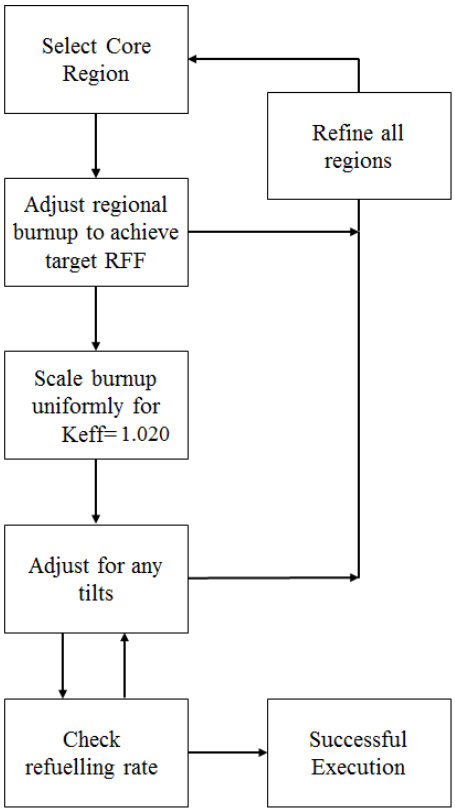

Figure 5.2: Iteration process used to determine average exit burnups

5.1.1 NU CANDU-6

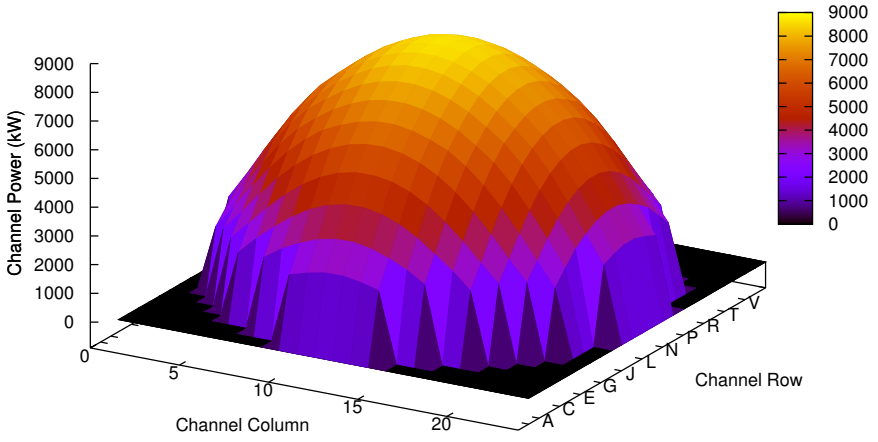

Figure 5.3: Time-average radial power distribution for the NU CANDU-6 core

By using the core description in the previous section, a model of the NU CANDU core is produced. The time-average radial power distribution for the CANDU core utilizing NU fuel and no adjuster rods is shown in Figure 5.3.

Figure 5.4 depicts the axial profile for one of the channels. The characteristic cosine shaped power is typical for a NU CANDU core without the adjuster rods inserted. This axial profile and in general any cosine power distribution is inefficient and uneconomical due to bundles at the channel ends producing less power than the ones in the core centre. The disparity in bundle power results in a decreased average neutron flux and, in turn, a lower reactor power. Flux flattening is used to increase the average neutron flux by lowering the powers in the centre and increasing it at the edges of the core [36]. This is generally achieved through the use of adjuster rods, reflectors, bi-directional refuelling, and differential burnup. All have been incorporated into the model except for the reactivity devices due to the extensive time required to compute the model.

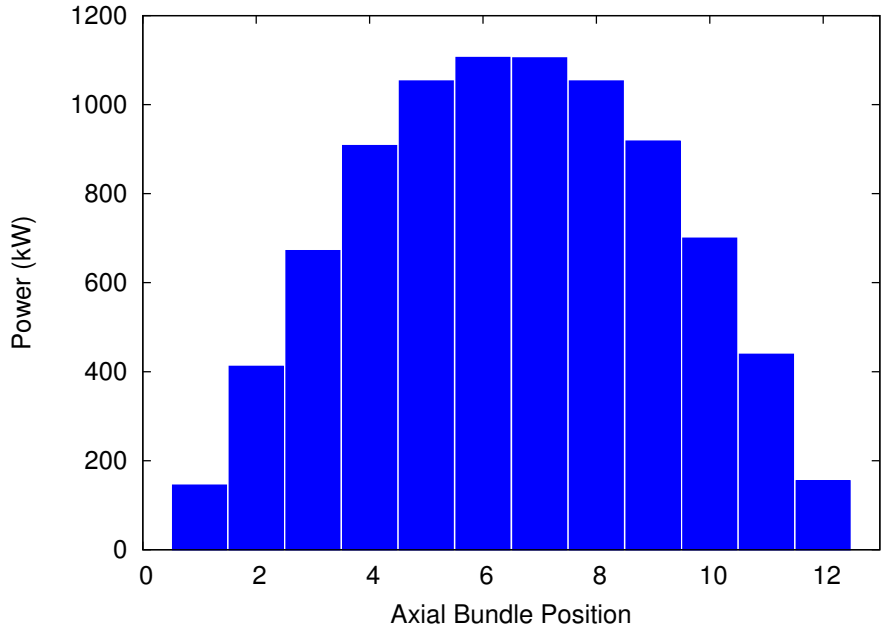

Figure 5.4: Time-average axial power distribution for channel M12 in NU CANDU core

As the core is refuelled, certain channels reach maximum power from the fresh fuel due to the reactivity insertion. This peak in power needs to be detailed so as to ensure that it is well inside safety margins outlined for the reactor. A metric for analyzing peak powers from refuelling is the Channel Peak Power Factor. It is calculated by finding the maximum ratio between the instantaneous powers, P, over the time-average powers,$\overline{P}$, of some channel, i, in the core.

$$CPPF = Max\left[\frac{P_i}{\overline{P_i}}\right] \tag{5.1}$$

The lower the CPPF value is to 1.0 the less likely that the channel will overpower from refuelling, thereby providing a margin for safety. Therefore, the number of fresh

bundles refuelled is important since it will add reactivity and result in an increase in the CPPF. For the CANDU-6 model, the CPPF value is calculated to be roughly 1.08.

Similar to the CPPF, the Bundle Power Peaking Factor (BPPF) measures the maximum ratio between the instantaneous bundle powers to the bundle power at equilibrium [37]. Again, the closer the value is to 1.0, the less likely it will overpower during refuelling.

Another evaluation variable is the radial form factor which measures the "flatness" of the core by the ratio of the channel average power to the maximum channel power. There are two other variations of the form factors which are the axial and overall form factors. The axial form factor is the ratio of maximum channel to maximum bundle multiplied by the number of bundles in a channel (12). The overall form factor is the ratio between the average bundle power to maximum bundle power.

Table 5.3: NU CANDU-6 Characteristics (with no reactor control systems)

Characteristics	Time-Average	Instantaneous
k-effective	1.01830	1.018820
CPPF	-	1.078
BPPF	-	1.101
Mean Exit Burnup	7407.49 MWd/t	-
Max. Channel Power [Location]	8.7 MW [M12]	9.0 MW [N12]
Max. Bundle Power [Location]	1.1 MW [M12-B6]	1.2 MW [N12-B7]
Radial For Factor	0.626	-
Axial Form Factor	0.653	-
Overall Form Factor	0.409	-

The results shown in the above table do not reflect the actual values for a *fully modelled* CANDU-6 core because of the absence of any reactivity control devices. In order for the core to be deemed safe to operate, the powers in Table 5.3 are required to be derated to at least the licensing limits in Table 5.4 to be within the thermal limits. By including the reactivity devices, the maximum channel and bundle powers are much lower, and the form factors are higher to obtain the desired flattened cosine distribution. For reference, the maximum channel power obtained is 6.54 MW and the RFF is 0.83 for the fully modelled CANDU-6 core.

Table 5.4: CANDU-6 power limits [38, 39]

	Licensing Power Limit(kW)	Safety Design Limits (kW)
Channel	7300	8300
Bundle	935	950

5.1.2 SEU CANDU-6

For the investigation of the dual fuel model, the driver bundles have been selected to have an enrichment of 1.2%, and were chosen because of the prior research that has been done with a CANDU core using that level of enriched fuel. The region average exit burnups for a CANDU-6 core using 1.2% SEU bundles were determined to establish a baseline for the dual fuel model. The initial region average exit burnups used were from Table 5.2 initially and then readjusted to meet the target k_{eff} and power distributions. Again, the model does not use any adjuster rods.

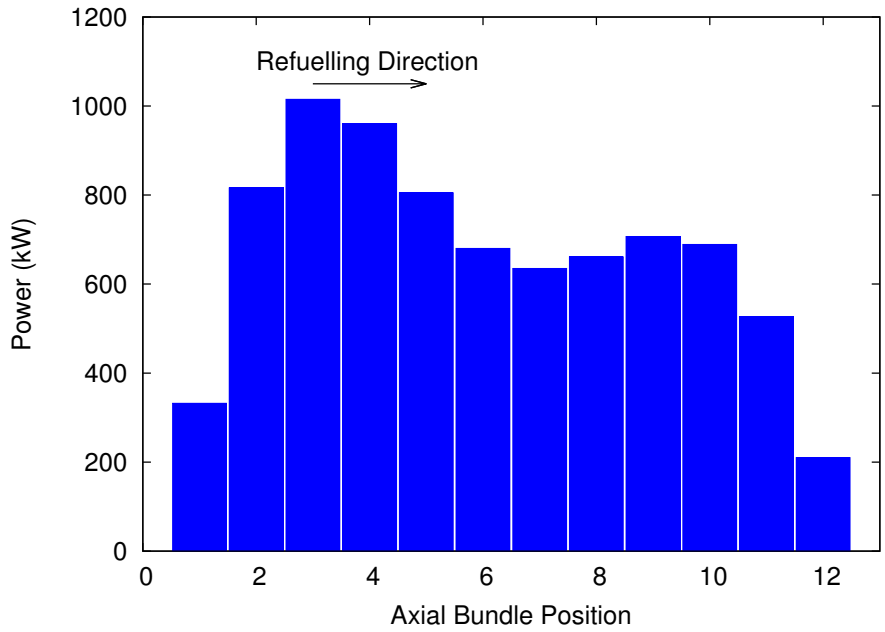

Figure 5.5: Time-average axial power distribution for 1.2% SEU in the CANDU-6 for channel L12

The refuelling scheme will be a 2-bundle shift and is based on core simulations using SEU bundles performed by Younis and Boczar [40]. Their investigation focused on the refuelling schemes that can be employed with the 1.2% SEU CANDU core. The three main schemes are the 2-bundle shift, with or without adjuster rods, and axial shuffling. The last technique involves removing some or all of the fuel bundles to

reorder and reinsert it into the channel with fresh fuel. For this thesis, the axial shuffling technique will not be utilized in order to keep the fuel management simple. The resulting time-average axial power distribution for the 2-bundle shift scheme is shown in Figure 5.5. The increase in bundle power at positions 9 and 10 is caused by the fresh fuel in the adjacent channels. The highest bundle power is located in position 3 where the refuelling is located to that of where the fresher bundles are located. This occurrence has the added advantage in that it increases the margin for dry-out for coolant flowing in the direction of refuelling since coolant enthalpy is the lowest at the inlet.

Table 5.5: Regional average exit burnups for 1.2% SEU fuelled CANDU-6 core

Core Region	1	2	3	4	5	6	7	8	9
average exit burnup (GWd/t)	2.26	2.26	2.10	2.09	2.09	2.07	2.11	2.06	2.06

The average exit burnup for each region in the 1.2% SEU CANDU-6 is shown in Table 5.5. The power distributions for the SEU core are shown in Figure 5.6. From the distribution calculations, the CPPF value calculated by DONJON was 1.118 and is comparable to the 1.11 determined by Younis and Boczar [40]. Furthermore, the axial profile calculated by DONJON also matches the profile documented in [39]. Based on the full-core results, the chosen parameters reflect the literature and validate the chosen average exit burnups and refuelling rate used in the model, which serves as a good starting point for the dual fuel model.

Table 5.6: 1.2% SEU CANDU-6 Characteristics

Characteristics	Time-Average Values	Instantaneous Values
k-effective	1.0199	1.0147
CPPF	-	1.118
BPPF	-	1.156
Mean Exit Burnup	21574.95 MWd/t	-
Max. Channel Power [Location]	8.1 MW [L12]	8.3 MW [L10]
Max. Bundle Power [Location]	1.0 MW [L12-B3]	1.1 MW [L10-B3]
Radial For Factor	0.672	-
Axial Form Factor	0.652	-
Overall Form Factor	0.438	-

	1	2	3	4	5	6	7	8	9	10	11	12	13	14	15	16	17	18	19	20	21	22
A									2835	2979	3120	3123	2986	2848								
B						2496	2940	3492	3761	4041	4163	4166	4052	3778	3517	2969	2534					
C					2775	3260	3897	4373	4803	5049	5198	5204	5061	4827	4403	3939	3309	2843				
D				2776	3405	4170	4743	5303	5661	5940	6063	6068	5956	5686	5341	4791	4235	3485	2896			
E			2533	3318	4197	4886	5532	5999	6371	6590	6719	6725	6606	6400	6039	5588	4954	4288	3434	2719		
F			3122	4006	4816	5552	6086	6554	6720	6930	7032	7037	6948	6747	6596	6139	5622	4899	4113	3253		
G		2770	3648	4555	5387	6019	6434	6796	7086	7267	7371	7377	7282	7112	6832	6484	6079	5462	4638	3739	2855	
H		3208	4109	5036	5794	6405	6736	7099	7362	7554	7648	7652	7568	7385	7132	6778	6458	5852	5100	4169	3256	
J	2599	3494	4493	5372	6111	6549	6978	7315	7587	7765	7861	7866	7777	7607	7342	7013	6589	6157	5417	4533	3516	2616
K	2753	3748	4731	5613	6305	6724	7128	7470	7729	7911	8002	8005	7921	7745	7493	7155	6755	6338	5645	4754	3756	2755
L	2881	3866	4860	5724	6410	6806	7207	7541	7800	7977	8069	8071	7985	7814	7558	7229	6828	6433	5743	4873	3863	2876
M	2881	3864	4858	5718	6404	6800	7202	7532	7792	7967	8058	8060	7973	7802	7546	7217	6817	6419	5730	4863	3857	2872
N	2755	3750	4728	5607	6293	6711	7109	7448	7701	7880	7968	7970	7885	7709	7457	7120	6722	6303	5613	4729	3740	2745
O	2611	3503	4499	5368	6098	6528	6949	7276	7541	7713	7805	7806	7716	7547	7283	6957	6536	6104	5371	4497	3492	2600
P		3237	4128	5043	5782	6378	6695	7046	7296	7481	7568	7568	7483	7300	7051	6701	6383	5785	5044	4125	3226	
Q		2831	3695	4576	5384	5988	6385	6724	7001	7170	7267	7268	7172	7004	6727	6389	5991	5386	4576	3692	2823	
R			3209	4052	4821	5526	6025	6449	6613	6811	6903	6903	6813	6615	6452	6027	5528	4822	4052	3208		
S			2679	3381	4217	4864	5475	5889	6234	6434	6552	6552	6435	6236	5891	5477	4866	4218	3381	2678		
T				2852	3430	4164	4699	5212	5538	5798	5908	5909	5799	5539	5213	4700	4165	3431	2853			
U					2815	3277	3891	4327	4734	4962	5102	5102	4962	4735	4328	3892	3277	2816				
V						2514	2941	3467	3718	3986	4099	4099	3986	3718	3468	2942	2515					
W									2808	2944	3079	3080	2944	2808								

(a) Time-average radial power distribution of 1.2% SEU CANDU core

	1	2	3	4	5	6	7	8	9	10	11	12	13	14	15	16	17	18	19	20	21	22
A									2672	3120	3329	3361	3124	2892								
B						2362	2988	3323	3779	4004	4095	4174	4282	3811	3621	3029	2472					
C					2806	3418	3803	4213	5001	5099	5459	5610	5193	4927	4779	4050	3563	3051				
D				2634	3308	4166	4633	5340	5759	5845	5985	6289	5985	5948	5575	4871	4238	3687	2886			
E			2356	3470	4128	5021	5142	6039	6103	6974	6768	7043	6322	6576	5955	6070	5137	4559	3352	2783		
F			3064	3975	4693	5380	5822	6561	6690	6972	6905	6908	6688	6863	6665	6325	5647	4981	4065	3386		
G		2611	3366	4608	5492	6142	6287	6542	6593	7389	7581	7548	7180	6890	6448	6693	6429	5773	4770	3747	2756	
H		2960	3988	4829	5474	6091	6727	6661	7169	7260	7212	7282	7575	6986	7009	6651	6271	5822	5335	4142	3311	
J	2437	3257	4564	5257	6193	6762	6757	6861	7735	7591	7985	8106	7566	7171	7592	6991	6923	6632	5575	4499	3810	2697
K	2595	3710	4710	5408	6052	6724	6854	7432	7690	7613	7662	8022	7646	7784	7563	7074	6711	6717	5779	5059	3980	2846
L	2631	3840	4627	5975	6350	6958	6668	7486	7374	8324	7992	8273	7458	7857	7309	7769	7107	7023	5751	5193	3932	3215
M	2720	3892	4851	5788	6270	6611	6820	7510	7676	7968	7848	7914	7687	7978	7679	7559	7048	7121	5914	5264	4103	3093
N	2707	3630	4485	5743	6512	6843	6963	7124	7155	7966	8212	8221	7897	7598	7198	7546	7359	6930	5995	4932	3764	2995
O	2594	3351	4429	5245	5791	6233	6908	6831	7289	7414	7363	7536	7859	7312	7330	7009	6508	6245	5790	4594	3679	2695
P		3054	4275	4942	5921	6557	6505	6553	7415	7234	7709	7883	7434	7023	7458	6787	6822	6332	5281	4184	3560	
Q		2850	3647	4395	5113	6017	6099	6683	6827	6789	6871	7362	7013	7155	6815	6287	5936	5698	4712	3967	3036	
R			3015	3722	4743	5596	5621	6343	6161	6224	6759	7084	6433	6682	6194	5727	5591	5150	3995	3418		
S			2596	3373	4040	4778	5202	5937	6093	6403	6353	6470	6221	6368	5889	5533	4838	4270	3406	2850		
T				2867	3575	4247	4702	5044	5258	5909	6186	6130	5848	5463	4978	4866	4388	3650	2925			
U					2640	3203	3922	4195	4683	4926	4935	5026	5108	4613	4342	3857	3207	2748				
V						2593	2950	3306	3944	3996	4326	4363	4037	3630	3659	2989	2617					
W									2842	2944	3033	3220	2965	2916								

(b) Instantaneous radial power distribution of 1.2% SEU CANDU core

	1	2	3	4	5	6	7	8	9	10	11	12	13	14	15	16	17	18	19	20	21	22
A									2339	2487	2593	2595	2492	2349								
B						2083	2510	2927	3194	3409	3526	3529	3417	3207	2946	2534	2113					
C					2334	2825	3343	3795	4151	4398	4526	4529	4409	4169	3820	3376	2867	2388				
D				2362	2988	3639	4222	4713	5097	5362	5498	5502	5374	5119	4744	4263	3691	3057	2461			
E			2184	2932	3710	4427	5056	5581	5989	6269	6414	6419	6284	6013	5615	5102	4486	3786	3035	2344		
F			2757	3567	4398	5156	5820	6374	6803	7098	7250	7254	7113	6828	6409	5867	5216	4473	3660	2877		
G		2441	3251	4150	5015	5803	6494	7071	7518	7825	7983	7988	7840	7544	7106	6540	5860	5083	4229	3338	2530	
H		2835	3713	4649	5537	6348	7060	7655	8116	8432	8595	8600	8447	8140	7688	7103	6400	5596	4714	3779	2897	
J	2278	3126	4085	5041	5946	6774	7501	8109	8581	8904	9070	9074	8917	8603	8140	7540	6819	5997	5094	4138	3173	2315
K	2441	3356	4344	5312	6229	7067	7805	8421	8899	9226	9394	9398	9239	8919	8448	7839	7107	6272	5356	4386	3393	2470
L	2553	3480	4478	5453	6376	7219	7961	8581	9062	9392	9560	9564	9402	9080	8605	7991	7253	6412	5490	4512	3510	2577
M	2558	3486	4485	5460	6382	7225	7967	8586	9066	9395	9563	9566	9404	9081	8606	7992	7254	6412	5490	4513	3510	2577
N	2455	3374	4364	5333	6249	7085	7820	8434	8910	9236	9402	9405	9244	8924	8452	7842	7109	6273	5358	4387	3393	2470
O	2304	3158	4121	5077	5979	6803	7527	8131	8599	8919	9083	9085	8926	8610	8146	7545	6823	6000	5097	4140	3174	2316
P		2886	3767	4701	5584	6389	7095	7684	8141	8453	8612	8614	8458	8150	7696	7109	6405	5600	4717	3781	2898	
Q		2522	3329	4220	5074	5853	6536	7106	7547	7849	8003	8004	7854	7555	7116	6548	5866	5087	4232	3340	2532	
R			2871	3654	4468	5213	5866	6411	6834	7124	7271	7272	7128	6840	6419	5875	5223	4478	3664	2879		
S			2340	3031	3783	4485	5102	5619	6021	6296	6436	6437	6299	6025	5625	5110	4493	3791	3038	2346		
T				2459	3055	3691	4265	4749	5127	5386	5519	5520	5389	5130	4753	4271	3697	3061	2464			
U					2388	2867	3378	3825	4177	4420	4544	4545	4422	4179	3828	3382	2871	2392				
V						2114	2537	2950	3214	3427	3541	3542	3428	3216	2953	2539	2117					
W									2354	2500	2604	2604	2501	2355								

(c) Initial core start-up radial power distribution of 1.2% SEU CANDU core

Figure 5.6: Different core power maps for 1.2% SEU CANDU core

5.2 Two Fuel Model

Due to the lack of fissile elements and the absorptive nature of the thorium bundle, the neutron flux would be lower for a dual fuel mode. Employing this mode using thorium requires attention to placement and frequency in the core since a grouping of thorium bundles will cause a significant decrease and possibly a tilt in power. An excess of thorium bundles would lower the overall reactivity of the core to a point where average exit burnups are unpractical and uneconomical.

The first step is to determine which channels will be selected for thorium bundle loading. The simplest method is to mimic the multi-cell array used in the DRAGON calculations. Recall that the array is composed of 3x3 individual lattices where the centre is the thorium bundle and the eight outer lattices contain driver bundles. The core will be configured with multiple arrays spread evenly amongst each other. Each thorium bundle will be enveloped with its own eight driver bundles. For instance, all thorium channels will be radially separated by two driver channels between one another.

Therefore, the criteria for developing a core configuration were to ensure that each thorium bundle was surrounded by SEU bundles. Secondly, the core must have been radially symmetric with the thorium bundles in place; this ensures that the radial power distribution is balanced. The parameters used to evaluate the configuration's viability are channel configurations, bundle shifts, and average exit burnups that will shape the radial and axial powers and the effective core multiplication factor.

5.3 Core Configuration A

Core Configuration A is the product of the design method outlined in the previous section and is displayed in Figure 5.7. This configuration was designed to maximize the number of channels designated for thorium bundle loading. As a result, thorium channels at the outer periphery are not completely surrounded by driver channels, but partially with reflectors. Furthermore, some thorium channels will have a mix of driver channels with different average exit burnups. The effects from the placement of thorium bundles using this configuration on core and channel power profiles will be presented throughout this chapter. From herein, thorium bundles and thorium channels are referred to as targets bundles and target channels.

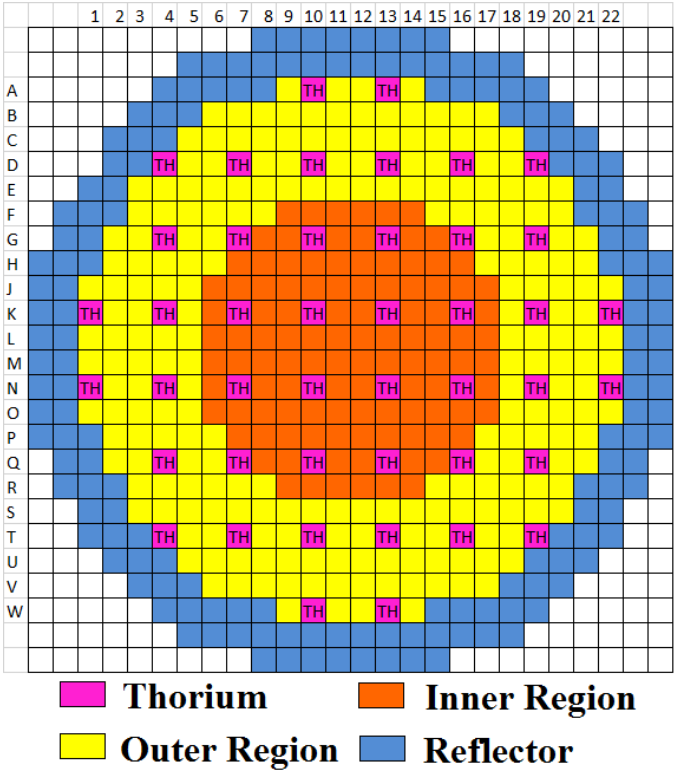

Figure 5.7: Core A configuration

Table 5.7: Key parameters for Core A diffusion model

Parameters	Values
Total Thermal Power	2061.4 MW
SEU Channels	336
Target Channels	44
SEU Bundles/Refuelling Shift	2

5.3.1 Sensitivity Analysis

Before embarking on producing the full-core power distributions, a sensitivity analysis of the parameters governing the use of thorium bundles will be conducted. More specifically, the parameters under investigation are the average exit burnups of those channels containing thorium bundles (target channels), bundle shift scheme employed, and the optimal number of thorium bundles used within the target channels. The three parameters will be evaluated on how they affect the power profiles and core reactivity. Then, based on the results, a combination of the three parameters is used to produce the full-core power distributions.

Average exit burnup for target channels is an important parameter to consider. The target bundles require additional time to convert the thorium nuclei to fissile U-233 in order to produce power. Since the average exit burnup is an average, it should be carefully chosen since each channel will have one bundle that has the highest burnup value. The upper limit for the average exit burnup of a bundle should be no more than 40 GWd/t, this is the maximum burnup that LWR fuel cladding composed of Zircaloy-4 can sustain before structural integrity of the fuel bundle degrades and becomes unsuitable for in-core use [41]. Since the maximum burnup limit of a CANDU bundle is not exactly known and that the typical CANDU bundle is also composed of Zr-4 cladding [35], the LWR limit will be used as a metric for this study. Furthermore, the bundle with the upper boundary burnup value should be the target bundle so that the thorium fuel can be fully utilized.

The bundle shift schemes employed in the NU CANDU and SEU CANDU are eight and two, respectively. Meaning, that eight or two fresh bundles were inserted and the corresponding number of depleted bundles are removed at the other end of the channel with each visit by the fuelling machine. Those schemes have been chosen based on axial power considerations to maintain the lowest possible peak bundle power and proper axial distributions to maintain thermal margins for critical heat flux in the coolant. As well as considerations for the effects of reactivity insertion to the total core reactivity and power ripples. Difference schemes will be investigated for the target channels for the same considerations.

Lastly, applying all 12 positions in a channel with thorium bundles would be ideal in terms of thorium utilization and the amount of U-233 produced. Consequently, the lack of fissile content within the thorium bundles may cause unwanted power differences between target and driver channels. Therefore, a third parameter to investigate in the full-core analysis is configuring target channels to use both SEU and thorium bundles.

5.3.1.1 Variation in Target Channel average exit burnup

To begin, the target channels' average exit burnups were evaluated on its effect to core and channel operations. Since thorium bundles require time to breed a sufficient amount of U-233 in order to begin generating power, the target channels were modelled for different average exit burnups. The average exit burnup of the target channels and its corresponding bundle shift scheme varied to observe the effect on the power and multiplication factor. For this variable analysis, a target channel loading of 12 thorium bundles was used. The effect of target channel average exit burnup on a loading with a combination of SEU and thorium bundles will be examined in section 5.3.1.3.

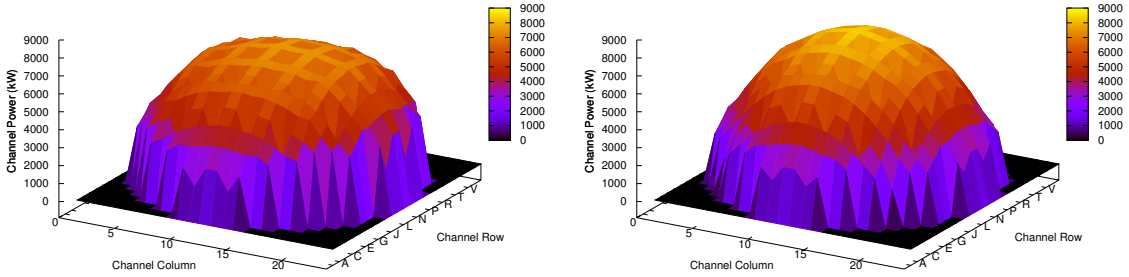

(a) 22 GWd/t (b) 37 GW/dt

Figure 5.8: 3D time-average radial power distribution of Core A with target channel at two different average exit burnups

Figure 5.8 shows the power increase in the target channels as a result of increasing the average exit burnups of the target channels since more U-233 is produced in the target bundles. With a lower average exit burnup in the thorium channels, the radial power distribution of the core is flattened; the thorium bundles act like a control rod. By increasing the average exit burnup in the target channels to 37 GWd/t, the target channels increase in power and neutron flux from the fission of U-233 as well as furthering the powers produced in the driver channels, raising the overall radial distribution.

In Figure 5.15, the effect of changing average exit burnups for the target channels on the effective multiplication factor is shown. By increasing the average exit burnup, the duration at which the thorium bundles stay in the channel also increases, allowing for more U-233 to be bred, and subsequently providing more fissile material to contribute to the core reactivity.

Figure 5.9: Resulting k_{eff} for varying average exit burnups in target channels

Table 5.8: Individual bundle burnups for varying target channel average exit burnups.

	Average Channel Exit Burnup (MWD/t)				
Bundle	20000	25000	30000	35000	37000
Position	Bundle Burnup (MWD/t)				
1	7.68	9.06	12.01	24.38	36.97
2	4688.31	8108.41	11596.81	15059.54	16438.70
3	17207.22	22406.11	27541.47	32647.83	34683.71
4	27073.44	33484.79	39872.04	46258.42	48811.64
5	33801.69	41065.45	48331.55	55616.05	58532.29
6	37221.65	44926.19	52646.12	60393.80	63496.68
7	37221.65	44926.19	52646.12	60393.80	63496.68
8	33801.70	41065.46	48331.56	55616.06	58532.30
9	27073.44	33484.79	39872.04	46258.42	48811.64
10	17207.24	22406.11	27541.48	32647.83	34683.71
11	4688.30	8108.40	11596.80	15059.53	16438.69
12	7.68	9.06	12.01	24.38	36.97

The average exit burnup is calculated from the burnups of each thorium bundle in the channel. Of the 12 bundles, there exists one or two bundles with the highest burnup value and similarly with the lowest value; these are the upper and lower limits of the mean. From Table 5.8, the highest burnup in one of the exiting bundles can be mapped for various average exit burnups and is graphed in Figure 5.10. Increasing the average

exit burnups will increase the maximum bundle burnup found in the target channel. With a target channel loading of 12 thorium bundles and using a 12-bundle shift, an average exit burnup is required to be roughly 20 GWd/t; otherwise, the central bundles will go beyond the 40 GWd/t burnup limit. Furthermore, the bundle burnups in positions 1, 2, 11, and, 12 are significantly low, which represents an inefficient loading scheme being utilized.

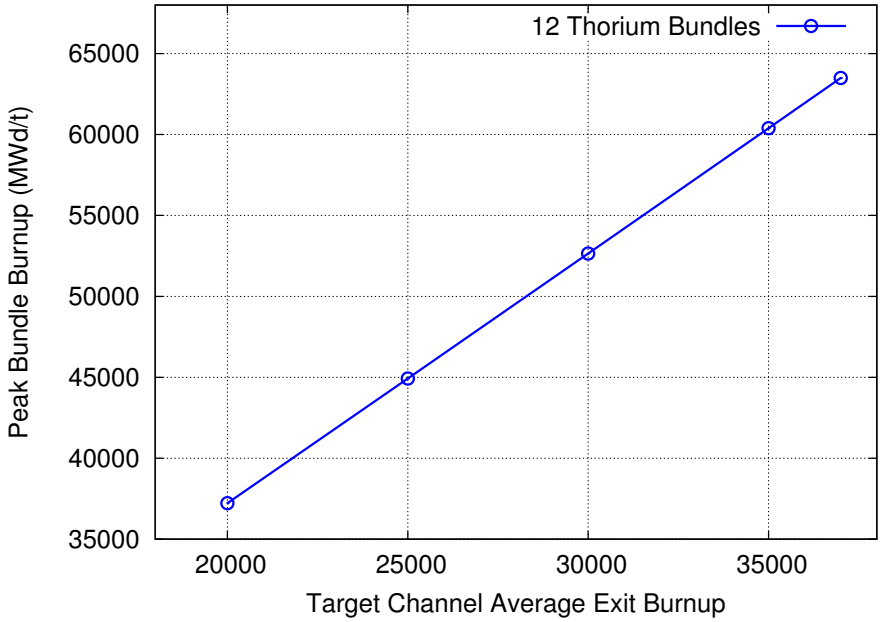

Figure 5.10: Maximum bundle burnup for varying channel average exit burnups

5.3.1.2 Variation in Bundle Shift

The next parameter to analyze is the different bundle shift schemes that can be employed. Continuing with the 12 thorium bundle loading in the target channels, bundle shift schemes of 2, 4, 6, 8, 10, and 12 were applied to examine the effects on axial power profile, bundle burnups, and core k-effective.

For a target channel to utilize 12 thorium bundles, a 12-bundle shift is required because bundle shift schemes of less than 12 will cause a tilt in power distribution along the axial direction. The first half of the channel will contain fresher bundles while the latter half will have bundles with longer dwell times, with the latter producing more power as a result of higher concentration of U-233. The shift in bundle powers due to changing bundle shift schemes is illustrated in Figures 5.11 and 5.12.

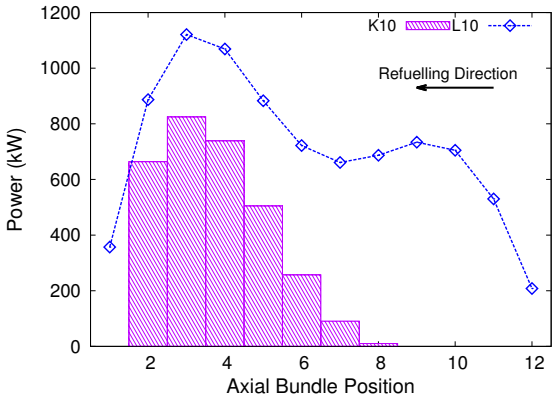

(a) 2-Bundle Shift

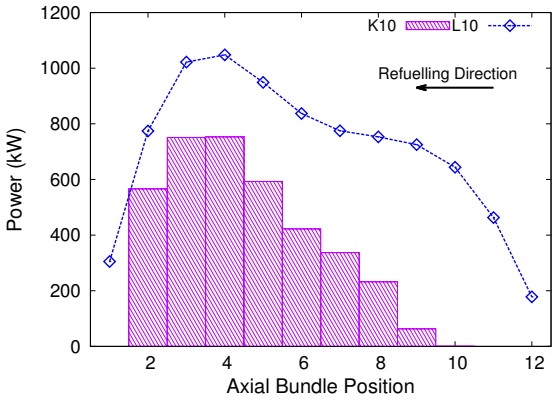

(b) 4-Bundle Shift

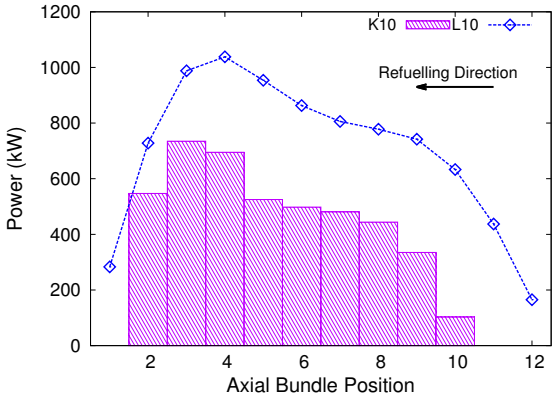

(c) 6-Bundle Shift

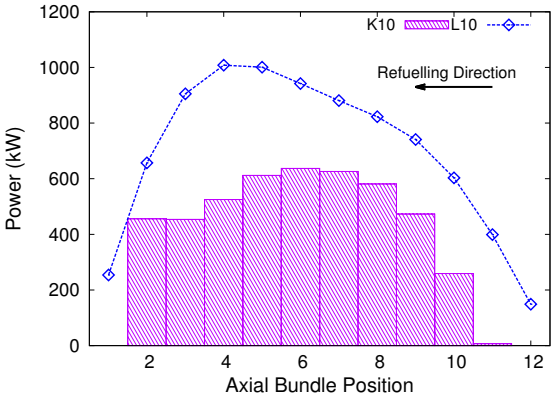

(d) 8-Bundle Shift

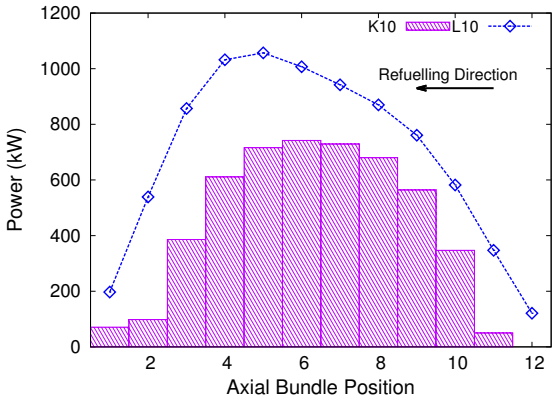

(e) 10-Bundle Shift

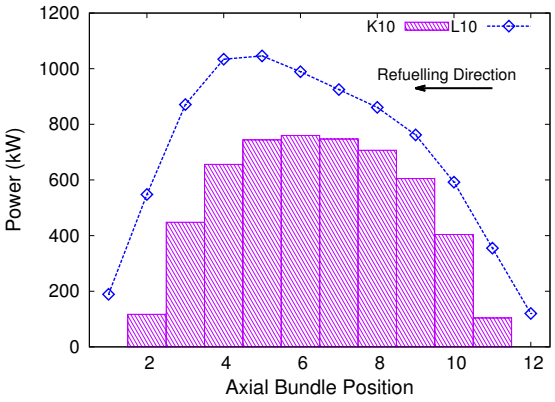

(f) 12-Bundle Shift

Figure 5.11: Time-average target channel K10 powers with varying bundle shift schemes and adjacent channel L10 powers

The 12-bundle shift produces a nearly symmetrical axial power distribution in the target channel. By changing the refuelling scheme, the peak bundle power shifts

towards the exit end of the channel. Since the exiting end of the target channel would be the refuelling end for the adjacent driver channels, having fresh fuel at those positions will cause increased bundle powers at those parts of the channel. The core is refuelled in a checkered pattern to prevent accumulation of peak bundle powers at one end of the core; hence a flattening effect on the overall core axial profile. Furthermore, coolant flows in the direction of refuelling to lower the margin to CHF; this method works since the entering coolant is colder and flows over the fresher and hotter bundles. On the other hand, when the entering coolant flows through the more burned up bundles (lower heat), the coolant temperature would gradually rise as it approaches the fresher and hotter bundles, which lowers the margin to CHF. So, if peak bundle powers shift towards the exiting end of the channel, it poses a risk to losing the heat sink.

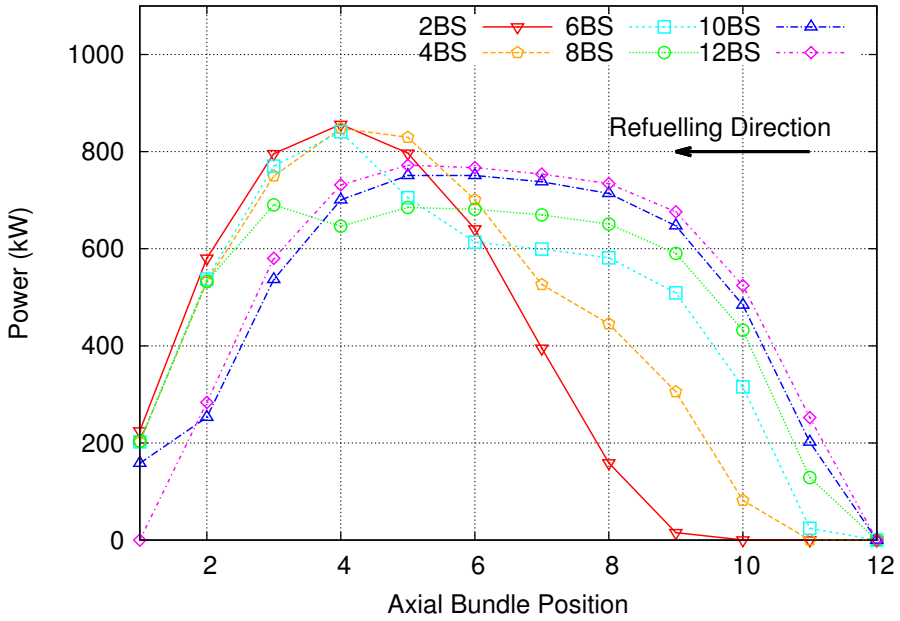

Figure 5.12: Time-average axial power profile of target channel K10 using different bundle-shifts

At the refuelling end, it does show that some bundles produce very little or no power; these positions contain, on a time-average basis, fresher thorium bundles. The corresponding burnups and powers for the target channel are shown in Figure 5.13.

Beginning with the 12-bundle shift in Figure 5.13, the burnup and power curve are symmetrical and is typical for a channel to be refuelled with all 12 bundle at the same time since each half of the channel are irradiated for the same period of time. In this case, burnup is the amount of fissile elements burned. The periphery channel positions will have a lower power and burnup due to the decrease in neutron flux levels

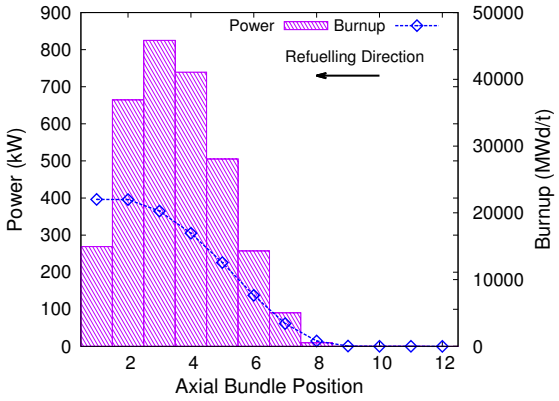

(a) 2-Bundle Shift

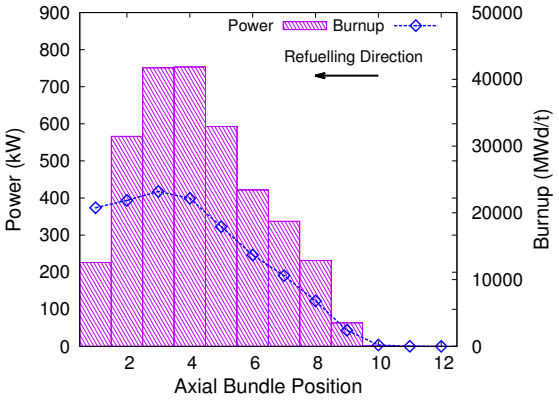

(b) 4-Bundle Shift

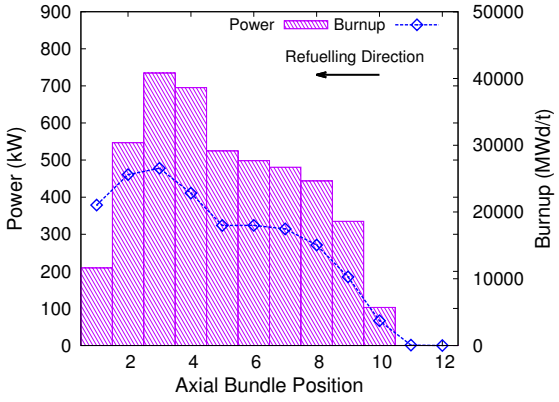

(c) 6-Bundle Shift

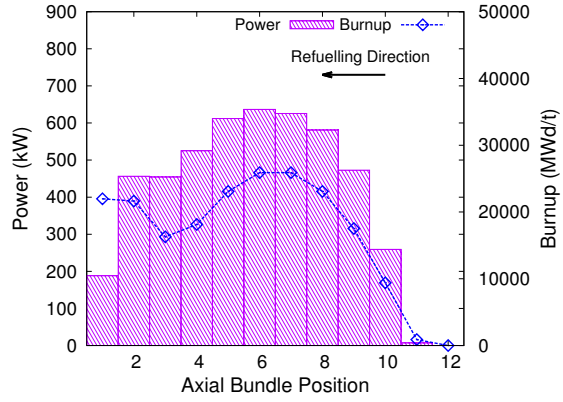

(d) 8-Bundle Shift

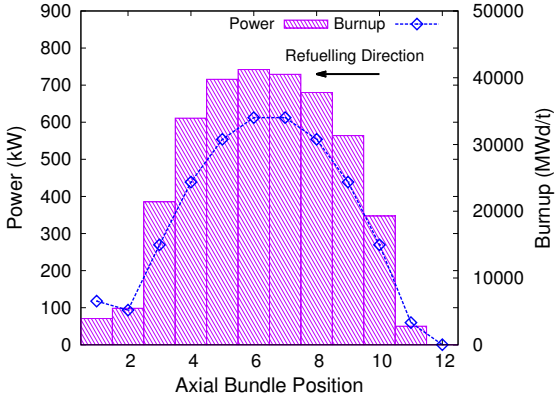

(e) 10-Bundle Shift

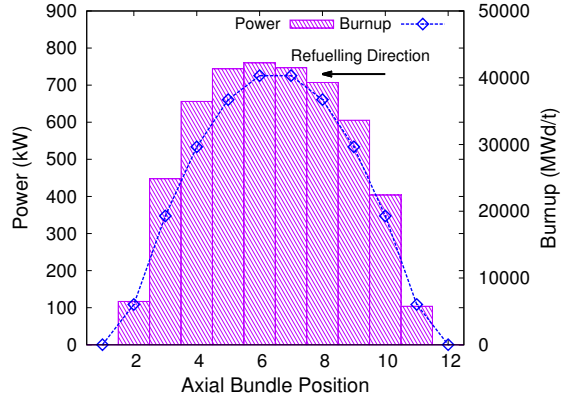

(f) 12-Bundle Shift

Figure 5.13: Time-average bundle burnups and powers with different bundle-shift schemes for channel K10

at those locations. For example, at positions one and 12, the burnup and power are 2.7 MWd/t and 50 W, respectively, showing that the lowered flux has a large impact on the thorium bundles at those positions. The power curve does have a slight tilt towards the latter half of the channel due to the higher flux from the fresh fuel bundles in the adjacent channels that are inserted in the opposite direction.

Figure 5.13e shows the time-average burnups of the newly inserted bundles for a 10-bundle shift scheme. In positions one and two, the burnups are higher for periphery positions eleven and twelve since those were the bundles that did not leave the channel from the previous refuelling process. The powers in the first ten positions reflect the typical burnup behaviour where higher burnup results in higher power, but the last two positions show opposite of what was expected. Position two has a lower burnup value than position one, but has a higher bundle power. This reflects the effect of the periphery position on the thorium bundles; with a lower neutron flux, the power generated will be lower compared to position two, which will result in a slightly higher neutron flux. Bundle shift schemes of six and eight reflect the same behaviour.

The burnup and power levels for bundle-shift schemes two and four show a similar behaviour. The refuelled half of the channel (positions 7-12) show a lower burnup compared to the other half. This indicates that these bundles in positions one through six have been in the channel for a shorter period of time, with positions one and two having the smallest dwell times. The other half of the channel has bundles with burnups of 20 GWd/t and higher, meaning those bundles have a higher dwell time, with bundle at position one being the oldest bundle. The bundle powers reflect the behaviour found in the other bundle shift schemes where the outer peripheral positions will have lower power due to the lower neutron flux. Maximum bundle power is seen to occur at around position nine due to a higher U-233 content from the longer dwell time and the higher neutron flux the bundle is exposed to due to its closer proximity to the inner core.

A twelve bundle-shift scheme will result in the highest channel power attainable; however, with an average exit burnup of 37 GWd/t for the target channel, some bundles will have a final burnup of over 60 GWd/t. Achieving high burnups for thorium bundles is desired, but a proper average exit burnup and bundle shift scheme should be chosen to avoid having bundles surpassing the limits of structural integrity.

With a smaller bundle shift scheme, the maximum bundle burnup is closer to the channel average exit burnup value since the variation in individual bundle burnup values is lower. Increasing the bundle shift scheme will increase the maximum bundle burnup value because there are more variations due to differences in neutron fluxes that affect the burnup rate. Since the maximum burnup for a CANDU bundle is rated to be around 40 GWd/t, it can be clearly seen in Figure 5.14 where average exit burnups and bundle-shift schemes are feasible. Achieving the highest overall

possible burnup can be accomplished with an average exit burnup of 37 GWd/t with an eight bundle-shift scheme; however, the reactivity would be lowered compared to a 12 bundle-shift scheme, as shown in Figure 5.15.

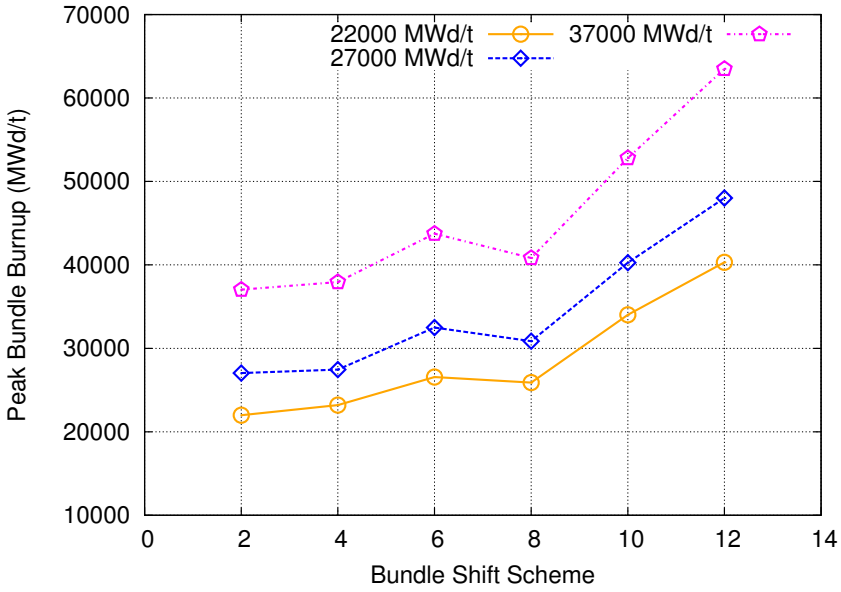

Figure 5.14: Maximum bundle burnups from varying bundle shift schemes with different average exit burnups

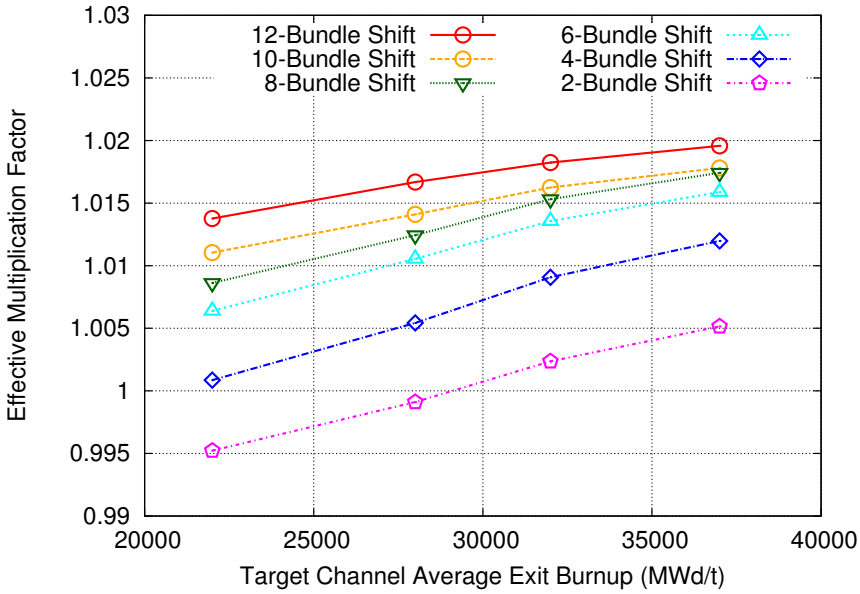

Figure 5.15: Resulting k_{eff} for varying average exit burnups in target channels

By lowering the number of thorium bundles inserted with each refuelling pass in the target channels, the core effective multiplication factor drops. The drop in reactivity can be explained by to the data in Table A.3, which shows the burnups associated for each bundle for the different schemes implemented. With a two bundle-shift, refuelling occurs when the total average exit burnup of the two exiting bundles is averaged at 37 GWd/t. The rest of the bundles are seen to have a lower burnup. By increasing the bundle-shift scheme, more bundles are exiting, and together are required to reach the target average exit burnup, thereby requiring higher levels of burnup to satisfy this condition. Therefore, the increased frequency in refuelling for fewer bundle-shift schemes results in the target channels containing more thorium bundles with low fissile content, which contributed to a lower core reactivity.

5.3.1.3 Channel Configuration

The time-average power of a target channel will be lower compared to the driver channel due to the lack of initial fissile elements. As a result, the local power drops from the thorium fuelled channels will result in a jagged radial power profile along a channel row with target channels as shown in Figure 5.16. The highest disparity is seen between channel columns at and around the inner core. To offset the local power dips, SEU bundles could be inserted along with the thorium bundles. A sample of three types of arrangements, as shown in Figure 5.17, is used to increase the maximum power in the target channels. Using other arrangements of SEU and thorium bundles, different bundle positions were investigated and the results are shown later in this section.

Another factor to account for when deciding the channel configuration is the periphery position bundles. From Figure 5.13f, bundle positions one and twelve in the thorium channels produce very little power due to the lower neutron flux from leakage at the peripheral position in the core, resulting in the lack of fissile material. The lower power generated by the thorium bundle at those positions is undesirable since it would mean an insufficient amount of U-233 breeding for such a dwell time, and thus is considered inefficient and uneconomical. Conversely, Figure 5.13 shows that the position one bundle does produce some power for bundle shifts other than twelve as its burnup value increases. However, the total power output of the channel for those bundle shifts reduces and more bundles closer to the refuelling end produce lower power. The goal is to produce power at the periphery positions and also to increase total channel power to offset the power disparity seen in Figure 5.17. A solution is to replace the thorium bundles in positions one and twelve with SEU bundles. Therefore, any thorium bundle arrangement for a channel should avoid having any fresh thorium bundles in positions one and twelve.

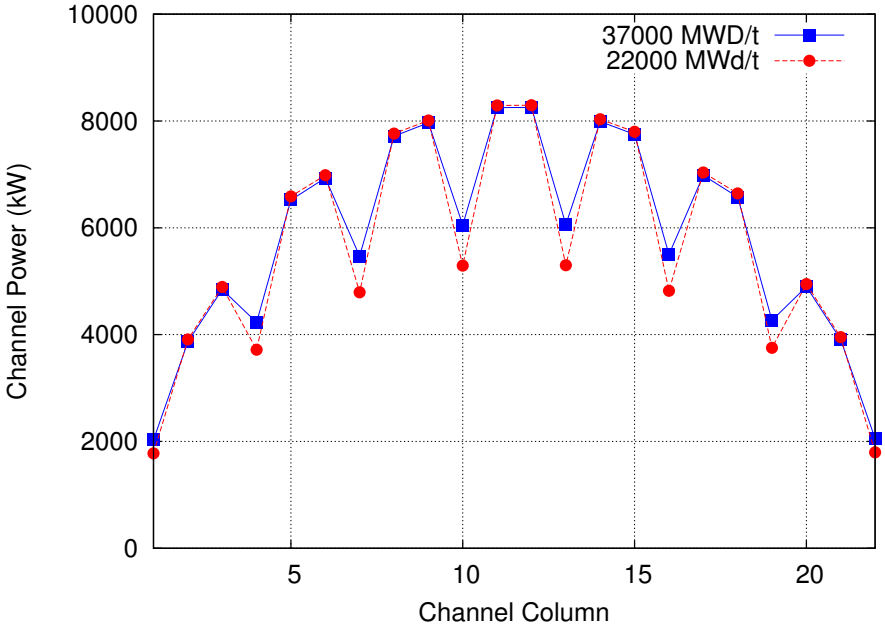

Figure 5.16: Power distribution for channel row K at different average exit burnups for thorium bundles

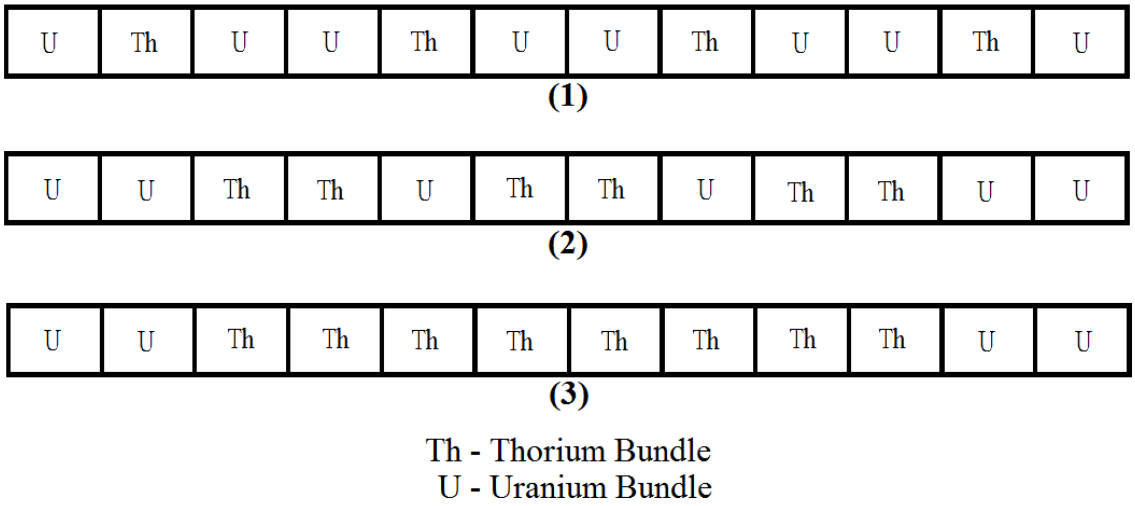

Figure 5.17: Bundle arrangments

The analysis begins with using one thorium bundle and placing it at positions two through eleven along the channel. Figure 5.18 shows an example of the different axial power distributions along the target channel for a thorium bundle occupying positions 2, 6, 8, and 11. A 12-bundle shift scheme will be used to view the effect of the single thorium bundle on the freshly loaded SEU bundles. The thorium bundle does not

initially contain any fissile content so its time-average power will be significantly lower than the uranium bundles. From Figure 5.18, the placement of the thorium bundle anywhere along the channel will result in a sink in power at that position as well as in the surrounding bundles.

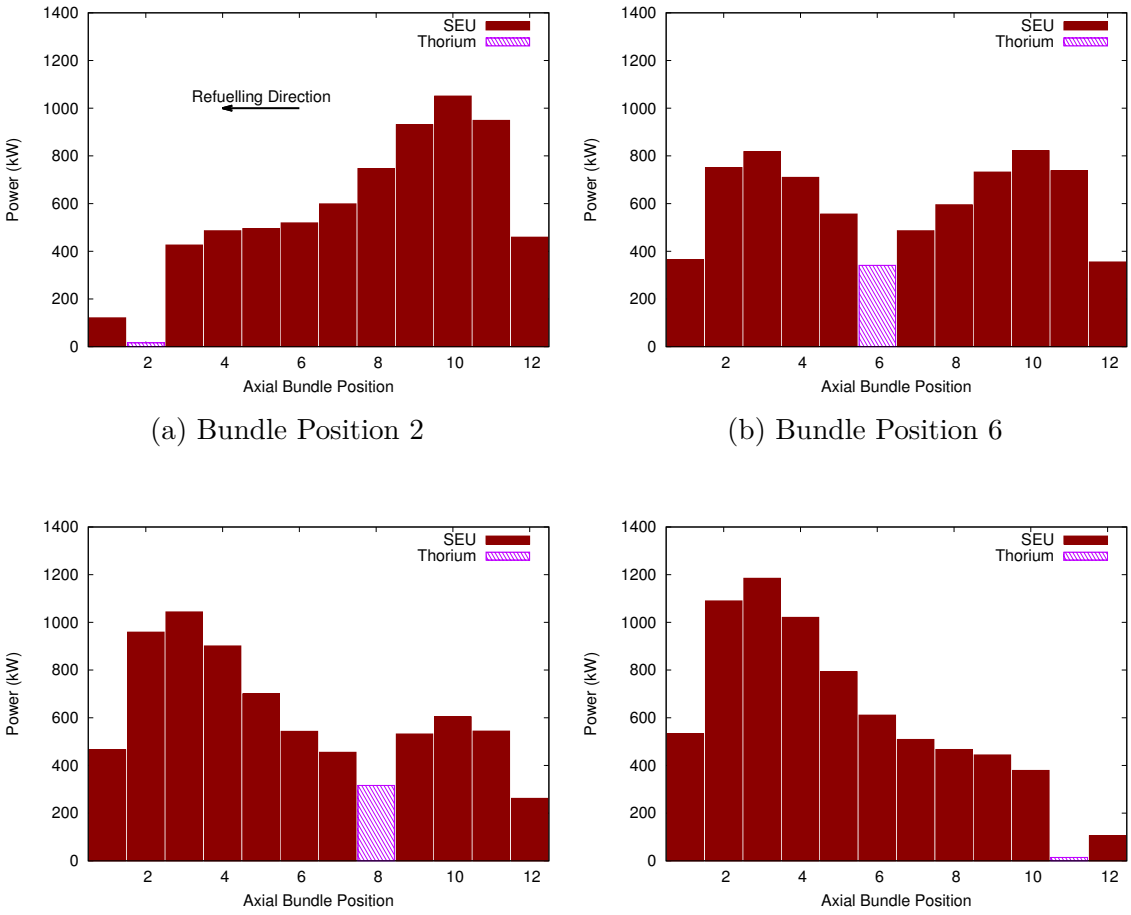

(a) Bundle Position 2

(b) Bundle Position 6

(c) Bundle Position 8

(d) Bundle Position 11

Figure 5.18: Axial power distribution for different thorium bundle positions

By shifting the thorium bundle closer to the centre of the channel, the total power increases. The higher flux at the inner channel puts the thorium bundle at a higher burnup and power than at the outer periphery. Moreover, placing the thorium bundle at the outer periphery reduces the power of the neighbouring SEU bundles, lowering the overall total channel power. It would have been expected that Figure 5.19 be symmetrical; however the flux from the adjacent channels do influence the total power of the target channel. Bundles at positions 1-4 will have a higher exposure to the neutron flux from the fresh SEU bundles in the adjacent channel. For the SEU bundles at those positions, the added neutron flux will further increase the bundle powers as seen in Figure 5.18d, but a thorium bundle occupying one of those positions will hinder

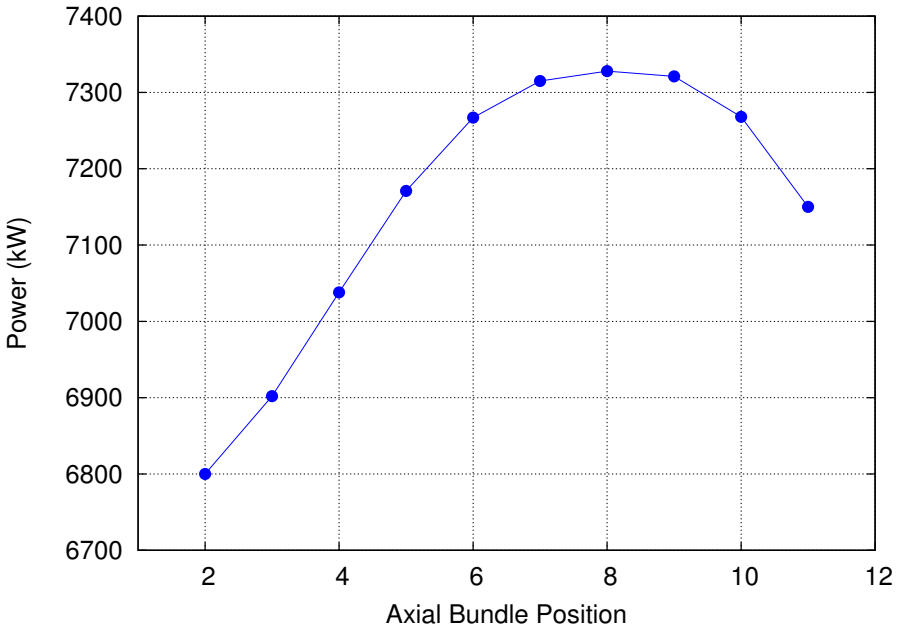

Figure 5.19: Total channel power for varying position of a single thorium bundle

the effect, as seen in Figure 5.18a. Therefore, the goal is to place the thorium bundles in positions that produces an axial tilt towards the refuelling end or in positions that help flatten the power level without sacrificing a large portion of the total channel power.

To further the investigation, the Figures 5.20 to 5.22 shows the time-average axial power distribution for 4, 6 and 8 thorium bundles with different combinations of positions. In all cases, a 12 bundle-shift is used. This bundle shift scheme may be the easiest way to handle a dual fuel loading, but it may not be ideal for some channel configurations due to resulting power profiles.

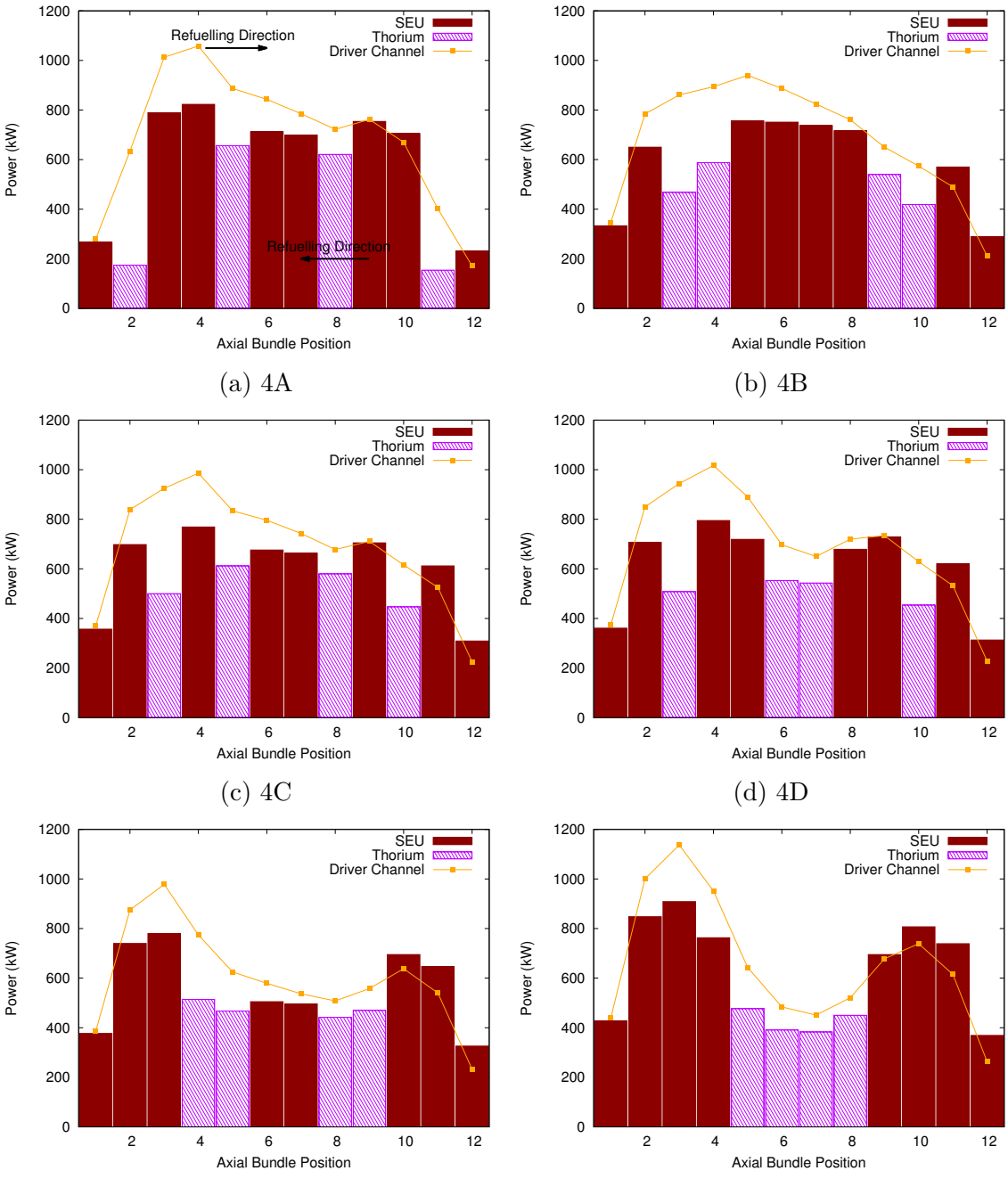

(a) 4A (b) 4B

(c) 4C (d) 4D

(e) 4E (f) 4F

Figure 5.20: Four thorium bundle combination

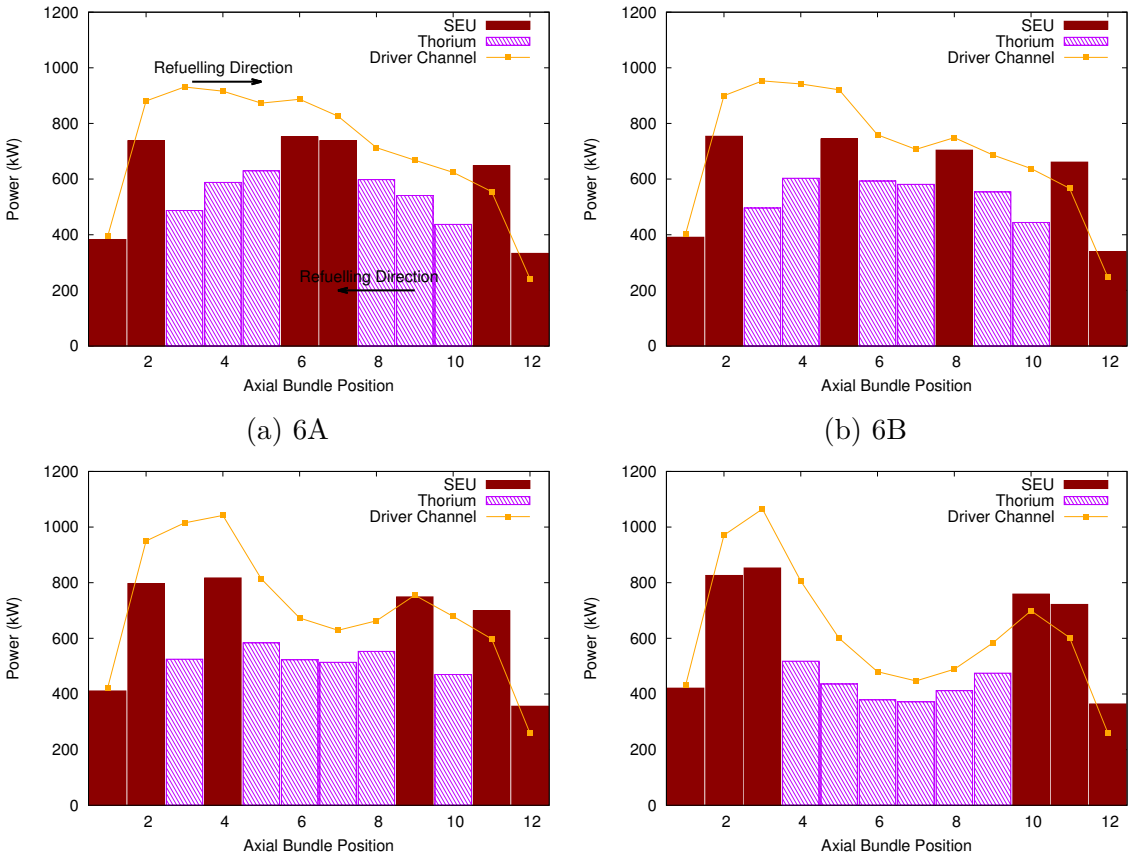

(a) 6A (b) 6B

(c) 6C (d) 6D

Figure 5.21: Six thorium bundle combination

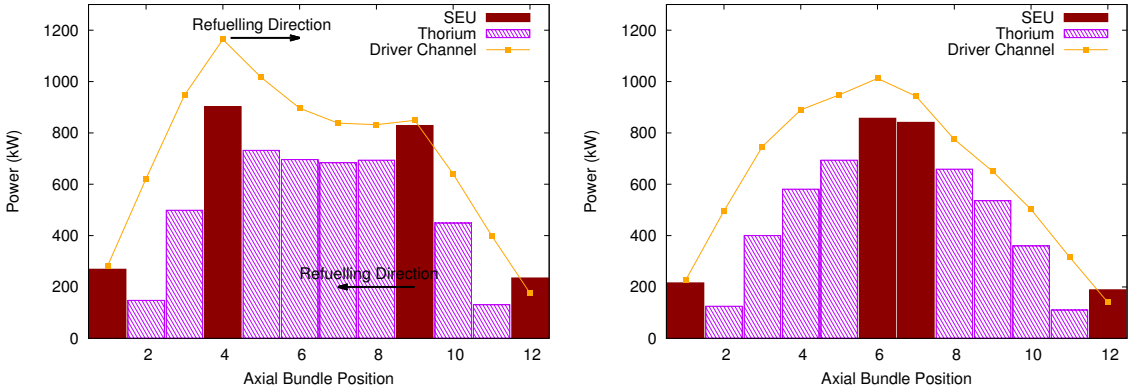

(a) 8A (b) 8B

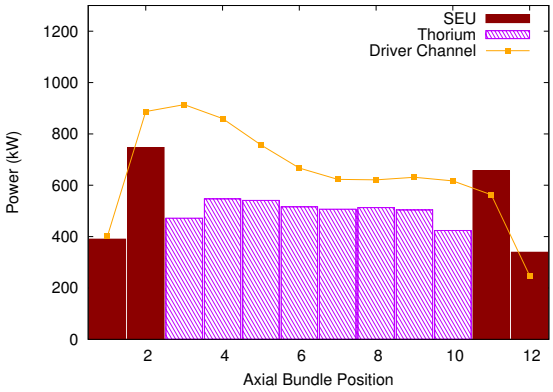

(c) 8C

Figure 5.22: Eight thorium bundle combination

Table 5.9: Total power channels for each channel configuration type at K10

	Total Channel Powers (kW)		
Target Channel Configuration	4 Thorium Bundles	6 Thorium Bundles	8 Thorium Bundles
A	6584	6873	6268
B	6817	6864	6213
C	6928	6998	6848
D	6981	7423	-
E	7242	-	-
F	7259	-	-

Changing the number of thorium bundles used and varying the placement of those bundles within the channel will change the channel power distribution. Placing SEU bundles in between thorium bundles helps flatten the profile while placing all the thorium bundles in the centre will produce a dip in the centre as seen in Figure 5.20f and Figure 5.21d. In all cases, a slight power tilt towards the exiting end of the channel is observed, which is likely due to the fresher SEU bundles in the adjacent channels. The thorium bundles also affect the adjacent channels' bundles powers; the driver bundles directly adjacent to a thorium bundle have their power lowered.

Total channel power for each configuration is tabulated in Table 5.9. The amount of power produced is dependent on the arrangement of thorium and SEU bundles. To maximize total channel power, SEU bundles need to be strategically placed to synergize between the adjacent driver bundles and the thorium bundles. For example, the 4F configuration produces the highest channel power for that category by having an equal number of SEU bundles on either side of the channel. Using the same arrangement seen in 6D, but with two less SEU bundles, the power produced is not the highest; rather, a slight rearrangement to produce the 6C scheme produces higher power.

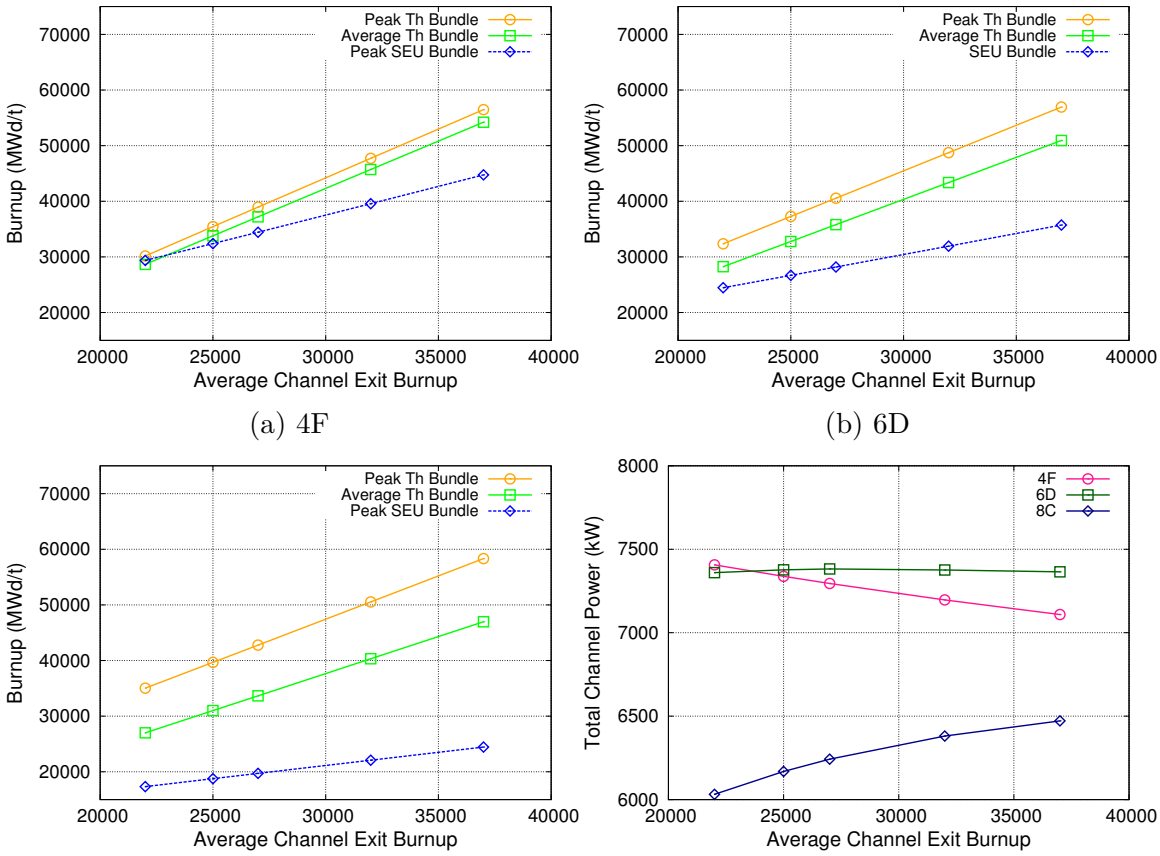

(a) 4F

(b) 6D

(c) 8C

(d) Total Channel Power

Figure 5.23: Bundle burnups and total channel power for different channel average exit burnups using a 12-bundle shift

Three of the channel configurations from above were chosen based on the double hump axial profile produced. Those configurations were then evaluated for different target channel average exit burnup where the upper limit of a bundle burnup was 40 GWd/t with varying bundle shift schemes; the results are shown in Figure 5.23.

By varying the average exit burnup of the target channel, the upper limit of the burnup is shown in Figure 5.23. Using four thorium bundles (4F channel configuration) would yield the lowest maximum thorium bundle burnup while the 8C-10BS configuration will have the highest individual burnup in a thorium bundle. This is caused by the difference between the individual burnups in the SEU and thorium bundles. By replacing the thorium bundles closer to the inner core with SEU bundles, the burnups of the thorium bundles need to change in order to satisfy the average exit burnup. For example, by reconfiguring the 8C channel to a 4F channel, four SEU bundles replace must replace four thorium bundles. Since the newly placed SEU bundles achieve higher

burnups than the replaced thorium bundles, all other bundles in the channel have to lower its individual burnup to satisfy the average exit burnup.

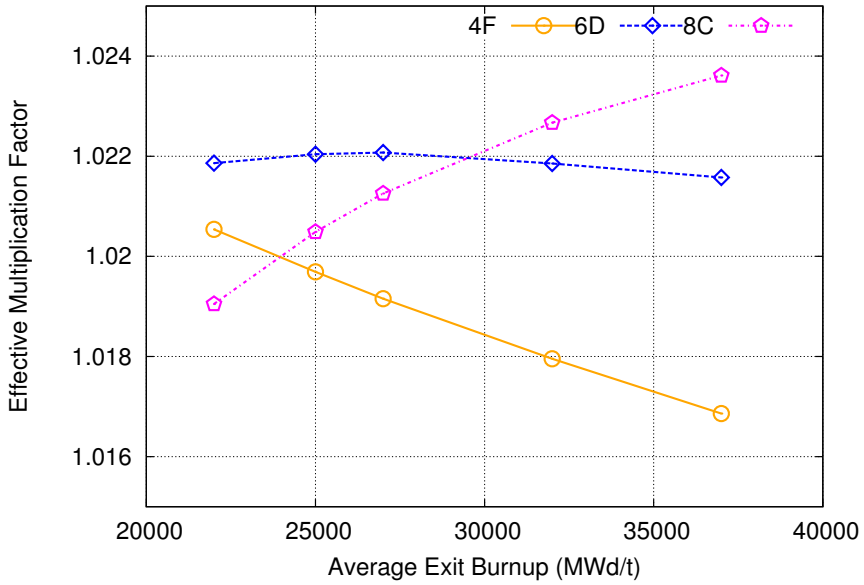

Figure 5.24: Core k_{eff} for varying target channel average exit burnup using a 12-bundle shift scheme

Changing the target channel exit burnup will also affect the core k_{eff} since increasing the dwell time for thorium bundles will increase the fissile content and thus the reactivity of the core. Figure 5.24 shows that each of the three channel configurations yield different core reactivity behaviours. Increasing the burnup for the 4F case will lower the k_{eff} while the 8C configuration displays the opposite behaviour. The 6D configuration shows a peak at 27 GWd/t. Using the data above, a realistic average exit burnup for the target channel can be determined and used in the time-average calculation.

For a channel loading of two fuel types, a bundle scheme other than a full channel shift can be possible. It was previously not possible with the 12 thorium bundle loading because it would slightly shift the peak bundle power of the target channel towards the exiting end of the channel, which is undesirable because it would lower the margin to critical heat flux in the coolant. For channel configurations 4F, 6D, 8C, the bundle shift employed will be eight, nine, and ten, respectively. These three channel configurations were chosen because of the simplicity in refuelling with the respective bundle shift schemes; the thorium bundles and SEU bundles at one channel end would be shifted out, while the remaining SEU bundles will be shifted downwards. An example of the refuelling scheme is illustrated in Figure 5.25.

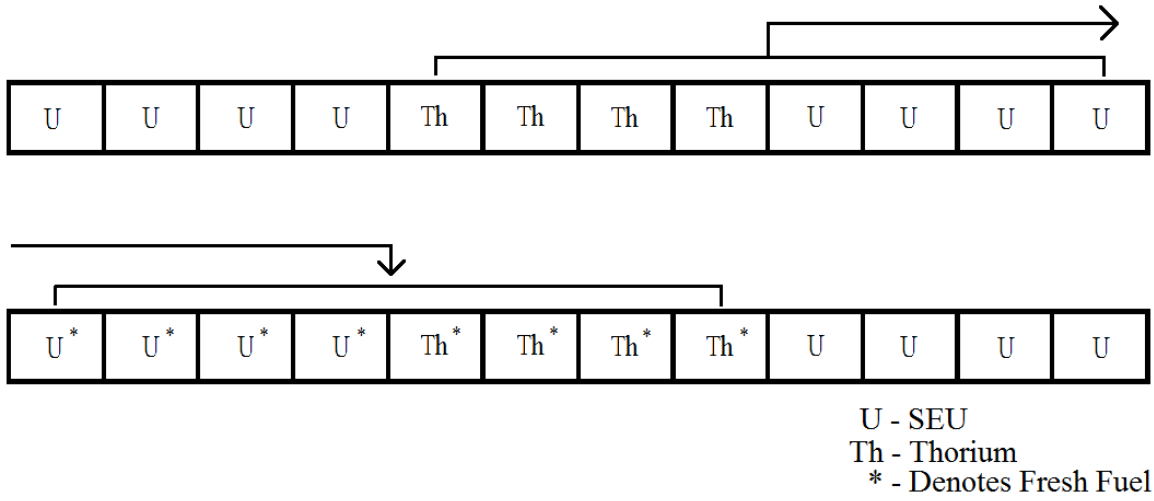

Figure 5.25: Example of the eight bundle shift of a the 4F channel configuration

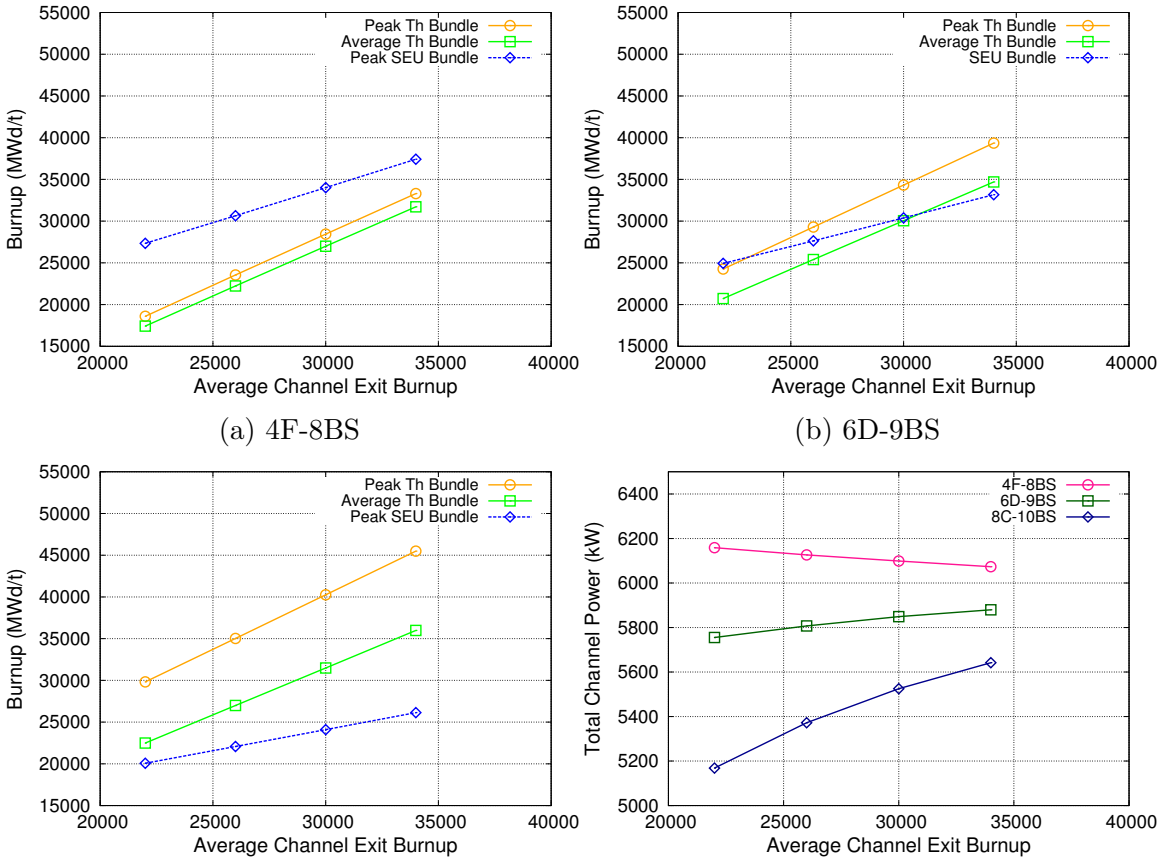

(a) 4F-8BS (b) 6D-9BS

(c) 8C-10BS (d) Total Channel Power

Figure 5.26: Upper bundle burnup of the mean channel burnup for Core A for different refuelling schemes

By using a different bundle shift scheme, the individual burnups of the bundles changes and must be evaluated to determine the average exit channel burnup that will not go beyond the 40 GWd/t limit. Figure 5.26 shows the thorium and uranium bundle with the highest burnup with varying average exit burnup for the channel it resides in. With increasing mean exit channel burnup, the burnup of bundles also increases. In the 6D and 8C configuration, the thorium bundle will have the highest burnup because it is located at the centre of the channel where the neutron flux would be the highest. In the 4F case, the SEU bundle has the highest burnup since these bundles would not have be shuffled out during refuelling, prompting a longer dwell time.

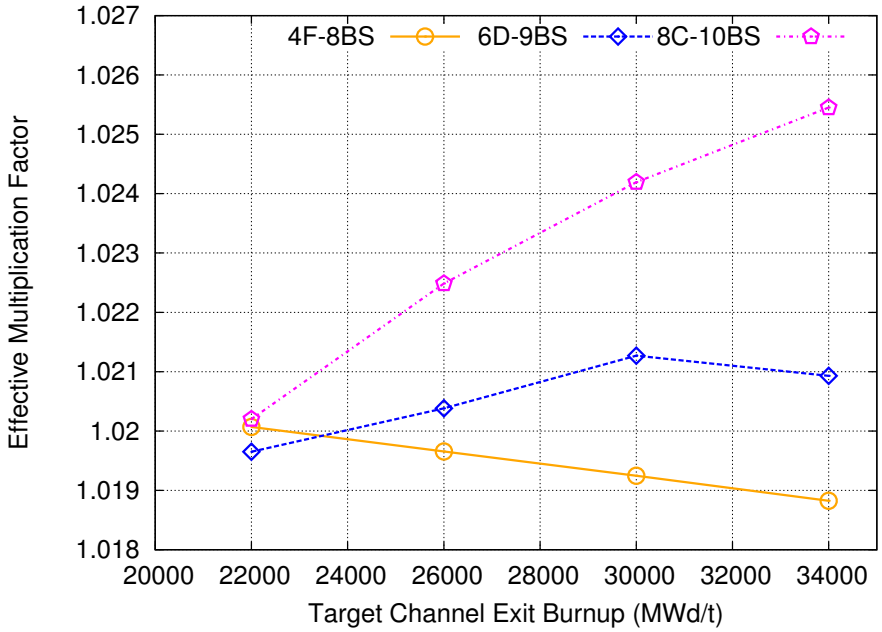

Figure 5.27: Core k_{eff} due to changing average exit burnup of target channels for different bundle shift schemes

Core k_{eff} also changes as seen in Figure 5.27. By increasing the average exit burnup of the target channel, the 4F configuration decreases in reactivity due to the depletion in fissile content in the SEU bundles. Configuration 8C displays the opposite effect as there is a continued increase in the fissile content in the thorium bundles, while the depleting SEU bundles have little effect on the k_{eff}. The 6D case is different from the other two configurations as it shows that the 30 GWd/t channel average exit burnup yields the highest core k_{eff} and by increasing U-233 content with further burnup in the thorium bundles, it cannot compensate for the loss in the SEU bundles and results in the drop in the multiplication factor.

Based on the highest burnup for the individual SEU and thorium bundles and the reactivity change, an average exit burnup of 30 GWd/t is ideal for the 6D and 8C

configuration. The 4F configuration should have a burnup of around 22 GWd/t or lower since core reactivity will lower as a result of having SEU bundles burn upto 30 GWd/t. The burnup values can be found in Table A.7.

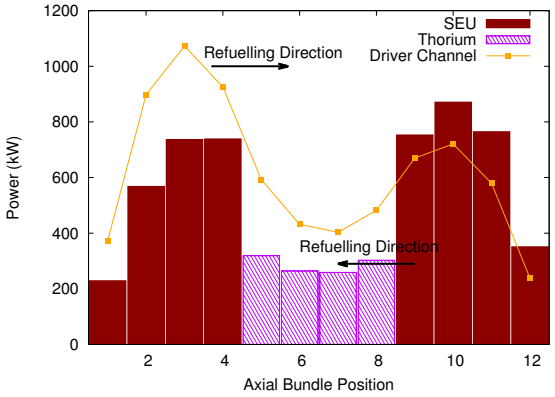

(a) 4F-8BS

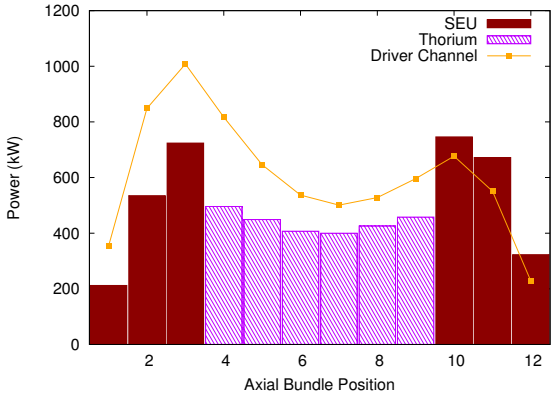

(b) 6D-9BS

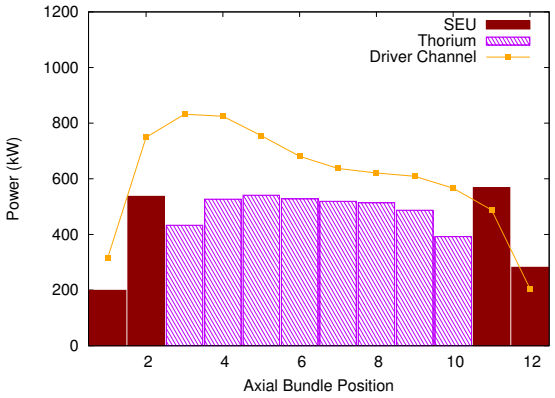

(c) 8C-10BS

Configuration	Power (kW)
4F-8BS	6159
6D-9BS	5849
8C-10BS	5525

Figure 5.28: Bundle powers for 4F, 6D, and 8C configurations with different bundle shift schemes

Figure 5.43 illustrates the resulting bundle powers with the new bundle shift scheme employed. As compared to Figures 5.20f, 5.21d, and 5.22c, the axial profile changes. The peak bundle in the target channel shifts towards the refuelling end, and the peak power in the adjacent driver channel decreases. The effect is less noticeable for the 8C configuration since its profile is flatter, but it did indeed flatten the adjacent channel profile as compared to the other two configurations. Overall, the combined power profiles of the channels balance out by having the peak powers at opposite sides of the channel. However, the total power for these three cases decreased as a result of having some SEU bundles remain after refuelling. Those SEU bundles can achieve higher burnups, but since the fissile materials have diminished, there will be less power generated. In addition, the thorium bundles will also achieved a lower burnup, which

will contribute to the lower channel power. Please refer to Appendix A and compare the burnup values of one channel configuration using the two different bundle shift schemes.

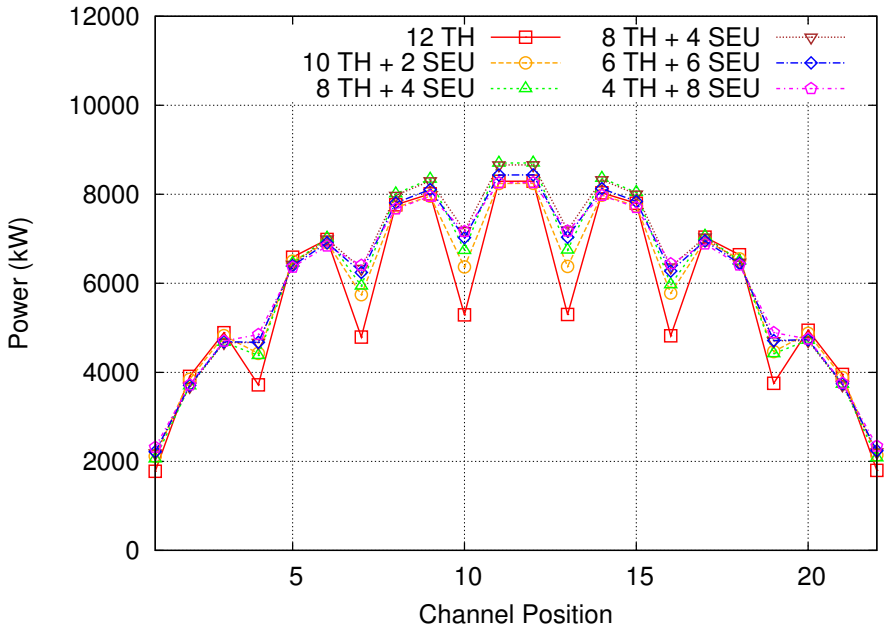

Figure 5.29: New radial profile with changing number of thorium fuel bundles in target channel

By introducing thorium bundles into the core, there will a drop in total channel power because of the lack of fissile material in the target bundles. Introducing SEU bundles into the target channels will offset the drop in power and the results as shown in Figure 5.29 for configurations using a 12-bundle shift. The drop in channel power along the rows reduces with more SEU bundles. The dips at the target channels seem to have roughly the same total power when using four, six, or eight thorium bundles, mainly due to the different average exit burnups that allow the different channel configurations to produce roughly the same power. The biggest drop is seen with the 10 thorium and 12 thorium bundle channel configuration. The use of bundle shift schemes of less than 12 was not used since it would create greater disparity between the driver and target channels.

5.3.2 Time-Average Results

The sensitivity analysis shows the effect that the three parameters have on the axial power profile, bundle burnups, and the core effective multiplication factor. Using the selected values for each parameter, the time-average radial power distribution of Core A can be produced to visualize the effect of these three parameters on the full-core scale.

After the three parameters have been supplied to DONJON, the average exit burnups in the driver channels need to be determined in order to produce the desired power profiles, peak power levels, and core reactivity levels. The process to develop the core model Figure 5.2. Numerous iterations were required to find the burnup which bares the lowest possible peak powers and a flatten radial profile. Once that is achieved, the core k-effective is brought to a value of around 1.020 by modifying each burnup region proportionally, excluding the target channels. The results are shown in Table 5.10 and depicted in the four maps in Figure 5.30.

Table 5.10: Time-average results for Core A

Target Channel Configuration	Burnups (GWd/t)		Peak Power (kW)		
	Average	Target Channels	Channel	Bundle	RFF
12Th-12BS	17.21	22	8435 [M12]	1060 [M12-B8]	0.643
(10Th+2SEU)-12BS	17.24	23.5	7514 [M12]	905 [N12-B5]	0.722
8C-12BS	18.13	25	7445 [M12]	875 [N12-B3]	0.729
6D-12BS	19.48	27	7470 [M12]	1069 [N12-B3]	0.726
4F-12BS	20.37	28	7441 [M12]	1067 [N12-B3]	0.729
8C-10BS	18.01	30	7413 [M12]	853 [N12-B3]	0.732
6D-9BS	18.76	30	7404 [M12]	1017 [N12-B3]	0.733
4F-8BS	19.29	22	7467 [M12]	1075 [N12-B3]	0.726

By implementing thorium bundles into a SEU fuelled core, the average exit burnup decreases as a result of diverting some of the burnup to creating U-233. For a 12 thorium bundle loading scheme, a 20% drop in the mean burnup for the driver channels is seen. To include SEU bundles with the target bundles, the mean driver channel burnups do not decrease as greatly. For example, only a 5-10% drop is seen for the 4F configuration. The drop in average exit burnups for the driver channels will affect the amount of enriched uranium required for this reactor, and ultimately the economics to operate it.

Peak channel power for the core for all target channel configurations implemented is roughly around 7400 kW, except for the 12Th case. Loading the target channel with 12 thorium bundles produces powers and a RFF value closely to that of the single fuel NU

and SEU core. Core flattening does occur with the other channel configurations, with RFF values between 0.72-0.73. In all cases, peak powers produced is over the licensing limit and will require external intervention to derate it through adjusters or poisons.

The time-average radial power profile is depicted in the maps in Figure 5.30 for the selected channel configurations to illustrate the effect of the thorium bundles. The lower channel powers are shaded lighter than for the higher power channels. It can be seen that the thorium fuelled channels have lower powers than its surrounding driver channels. For the 12 thorium bundle configuration (Figure 5.30a), the maximum difference between target and driver channels is around 3000 MW at the centre of the core. The difference is less substantial when approaching the periphery channels. The use of other channel configurations, which contain a combination of SEU and thorium bundles, lower the power difference between the target and driver channels. Conversely, a significant power difference is still observed in the periphery channels. This is the result in the lower neutron flux at the outer most region of the core where neutron leakage inhibits power production.

	1	2	3	4	5	6	7	8	9	10	11	12	13	14	15	16	17	18	19	20	21	22
A									2811	1816	2975	2978	1822	2826								
B						2803	3300	3843	3841	4004	4128	4131	4017	3861	3873	3335	2845					
C					2828	3393	4023	4509	4844	4977	5156	5161	4992	4870	4544	4068	3446	2894				
D				1707	3494	4254	3098	5387	5679	3749	6022	6027	3760	5709	5430	3133	4322	3577	1781			
E			2570	3403	4371	5083	5686	6183	6499	6638	6814	6820	6657	6533	6229	5748	5161	4469	3529	2767		
F			3247	4116	5036	5759	6256	6748	6889	7019	7180	7186	7039	6922	6797	6318	5840	5134	4236	3398		
G		3139	3829	3019	5616	6231	4272	6991	7245	4781	7522	7528	4793	7278	7036	4310	6306	5705	3083	3941	3256	
H		3659	4376	5280	6126	6716	6978	7392	7639	7759	7919	7925	7777	7669	7434	7032	6784	6203	5364	4461	3739	
J	2703	3735	4735	5604	6443	6854	7223	7630	7883	7992	8160	8165	8009	7911	7668	7272	6912	6509	5673	4802	3790	2746
K	1772	3922	4904	3707	6594	6981	4766	7746	7987	5253	8263	8268	5263	8011	7779	4792	7030	6648	3742	4954	3961	1792
L	2918	4064	5091	5969	6771	7144	7496	7904	8152	8261	8426	8431	8273	8173	7932	7531	7185	6816	6012	5131	4093	2939
M	2921	4068	5095	5972	6775	7150	7503	7910	8158	8266	8431	8435	8277	8176	7934	7532	7184	6812	6008	5127	4091	2938
N	1781	3940	4922	3720	6611	7001	4778	7765	8005	5264	8278	8281	5270	8020	7785	4794	7029	6641	3738	4947	3958	1790
O	2733	3771	4773	5640	6477	6888	7257	7662	7913	8020	8185	8188	8028	7926	7679	7277	6911	6501	5663	4793	3784	2743
P		3723	4437	5336	6176	6762	7022	7436	7680	7798	7955	7957	7804	7690	7450	7039	6782	6196	5355	4452	3734	
Q		3242	3922	3070	5684	6291	4309	7045	7298	4813	7567	7569	4816	7307	7057	4318	6306	5699	3079	3934	3251	
R			3383	4220	5119	5831	6321	6818	6952	7078	7235	7237	7083	6959	6827	6332	5844	5131	4231	3392		
S			2756	3519	4461	5158	5756	6257	6573	6707	6881	6882	6711	6579	6265	5765	5168	4470	3527	2763		
T				1778	3574	4326	3143	5461	5752	3793	6090	6091	3795	5756	5467	3147	4333	3581	1782			
U					2896	3454	4086	4577	4914	5045	5222	5223	5047	4918	4581	4091	3459	2901				
V						2855	3353	3905	3900	4063	4185	4185	4065	3902	3908	3357	2858					
W									2855	1843	3018	3018	1844	2857								

(a) 12Th-12BS

	1	2	3	4	5	6	7	8	9	10	11	12	13	14	15	16	17	18	19	20	21	22
A									2983	2363	3187	3192	2371	3002								
B						2874	3364	3953	4008	4230	4342	4346	4247	4033	3990	3406	2924					
C					2968	3529	4223	4675	5048	5221	5370	5377	5239	5081	4718	4280	3593	3047				
D				2197	3648	4463	3929	5576	5853	4705	6182	6188	4722	5890	5631	3982	4548	3745	2298			
E			2692	3549	4526	5217	5830	6236	6513	6646	6767	6776	6669	6556	6293	5909	5311	4644	3693	2907		
F			3366	4301	5159	5862	6314	6672	6652	6782	6851	6857	6808	6693	6734	6392	5963	5276	4443	3536		
G		3180	3988	3803	5730	6275	5167	6702	6869	5578	7035	7044	5597	6911	6758	5226	6369	5843	3900	4124	3318	
H		3721	4494	5412	6134	6605	6677	6889	7027	7132	7193	7199	7157	7065	6944	6745	6694	6234	5523	4604	3828	
J	2832	3853	4876	5719	6400	6583	6826	7011	7154	7248	7308	7316	7268	7191	7059	6890	6658	6491	5813	4970	3934	2898
K	2275	4088	5084	4606	6543	6703	5537	7104	7237	5873	7387	7392	5888	7268	7149	5582	6772	6619	4668	5161	4158	2315
L	3084	4220	5238	6062	6663	6773	6980	7159	7290	7381	7435	7442	7397	7319	7197	7031	6831	6731	6130	5305	4277	3129
M	3092	4229	5250	6071	6674	6781	6990	7165	7297	7384	7441	7445	7401	7321	7200	7032	6833	6732	6132	5306	4278	3129
N	2292	4119	5116	4632	6574	6733	5557	7126	7253	5884	7399	7404	5895	7276	7155	5587	6776	6624	4671	5164	4159	2316
O	2874	3904	4935	5776	6456	6628	6867	7043	7185	7272	7330	7333	7284	7203	7070	6899	6666	6497	5818	4974	3938	2900
P		3804	4576	5495	6207	6672	6729	6936	7065	7166	7219	7223	7176	7082	6958	6758	6705	6244	5530	4609	3832	
Q		3300	4104	3884	5824	6354	5219	6756	6917	5610	7070	7072	5616	6931	6776	5238	6383	5853	3906	4129	3322	
R			3523	4430	5264	5954	6389	6738	6704	6828	6888	6891	6835	6717	6755	6410	5977	5288	4451	3542		
S			2898	3685	4637	5308	5910	6302	6572	6694	6810	6811	6701	6582	6316	5927	5326	4655	3702	2912		
T				2295	3743	4548	3986	5641	5908	4742	6222	6224	4746	5917	5652	3996	4561	3756	2304			
U					3047	3596	4286	4729	5098	5263	5408	5409	5268	5105	4738	4295	3606	3056				
V						2928	3412	4001	4048	4267	4373	4375	4270	4053	4008	3420	2935					
W									3014	2383	3212	3212	2385	3017								

(b) 8C-12BS

	1	2	3	4	5	6	7	8	9	10	11	12	13	14	15	16	17	18	19	20	21	22
A									2879	2548	3096	3100	2557	2896								
B						2715	3153	3728	3830	4079	4178	4182	4094	3851	3761	3190	2761					
C					2881	3390	4081	4478	4864	5058	5185	5192	5073	4894	4516	4133	3448	2955				
D				2395	3537	4350	4236	5409	5679	5082	6009	6014	5099	5711	5458	4289	4428	3627	2501			
E			2633	3456	4401	5063	5687	6047	6331	6483	6583	6591	6503	6370	6097	5757	5146	4508	3588	2835		
F			3271	4216	5021	5725	6186	6517	6512	6677	6717	6723	6701	6547	6572	6254	5815	5125	4345	3425		
G		3031	3897	4134	5617	6166	5652	6611	6795	6133	6967	6975	6151	6832	6659	5709	6247	5717	4228	4017	3147	
H		3563	4368	5307	6000	6489	6603	6806	6954	7095	7130	7135	7116	6985	6854	6661	6566	6084	5401	4458	3648	
J	2780	3744	4768	5622	6285	6491	6782	6952	7111	7241	7275	7282	7258	7142	6992	6837	6553	6360	5698	4843	3804	2829
K	2495	4008	5004	5041	6459	6657	6126	7095	7245	6540	7408	7412	6554	7270	7133	6168	6714	6520	5095	5062	4057	2527
L	3048	4132	5141	5981	6565	6710	6967	7139	7286	7417	7447	7453	7430	7311	7170	7009	6755	6619	6032	5190	4169	3078
M	3056	4139	5153	5990	6581	6724	6988	7156	7307	7435	7467	7470	7448	7326	7184	7021	6765	6624	6035	5193	4172	3080
N	2516	4042	5039	5079	6503	6713	6176	7155	7301	6592	7465	7470	6602	7320	7177	6201	6745	6541	5111	5073	4068	2534
O	2826	3799	4838	5696	6370	6577	6878	7046	7211	7338	7374	7376	7348	7225	7066	6901	6606	6400	5727	4865	3821	2842
P		3655	4466	5421	6115	6616	6729	6942	7088	7235	7265	7268	7242	7102	6958	6751	6639	6142	5445	4489	3673	
Q		3161	4040	4261	5773	6323	5798	6781	6975	6291	7146	7148	6297	6985	6796	5813	6343	5793	4278	4057	3175	
R			3456	4397	5198	5918	6384	6737	6727	6900	6936	6938	6905	6737	6749	6400	5934	5215	4412	3470		
S			2874	3647	4599	5267	5917	6292	6594	6748	6852	6853	6754	6601	6303	5928	5280	4612	3659	2884		
T				2559	3725	4568	4444	5682	5964	5335	6309	6311	5339	5971	5689	4452	4577	3735	2566			
U					3070	3601	4337	4764	5179	5384	5521	5522	5387	5184	4771	4344	3609	3077				
V						2903	3373	3995	4106	4375	4480	4481	4377	4110	4000	3378	2907					
W									3097	2730	3332	3333	2731	3099								

(c) 6D-12BS

	1	2	3	4	5	6	7	8	9	10	11	12	13	14	15	16	17	18	19	20	21	22
A									2928	2715	3164	3168	2725	2947								
B						2706	3137	3728	3873	4141	4244	4248	4157	3895	3762	3175	2754					
C					2910	3410	4115	4516	4923	5131	5261	5268	5148	4955	4557	4170	3472	2989				
D				2535	3562	4389	4456	5463	5744	5363	6087	6093	5382	5778	5516	4514	4472	3658	2652			
E			2658	3478	4427	5090	5729	6093	6389	6549	6649	6658	6571	6431	6148	5804	5180	4541	3617	2868		
F			3285	4244	5041	5757	6225	6563	6557	6733	6768	6775	6758	6595	6622	6299	5853	5152	4381	3447		
G		3002	3911	4328	5638	6193	5923	6645	6836	6432	7010	7020	6453	6876	6698	5988	6282	5747	4435	4040	3128	
H		3531	4369	5319	6008	6505	6624	6827	6976	7125	7155	7161	7148	7011	6879	6689	6590	6102	5425	4470	3629	
J	2797	3745	4776	5632	6292	6499	6798	6961	7124	7259	7289	7297	7278	7159	7007	6860	6570	6377	5720	4863	3820	2858
K	2627	4019	5018	5266	6463	6665	6392	7100	7249	6821	7413	7418	6837	7279	7143	6441	6730	6534	5334	5090	4084	2671
L	3074	4142	5150	5987	6561	6704	6964	7126	7274	7408	7433	7439	7423	7301	7163	7012	6758	6625	6051	5212	4195	3116
M	3082	4149	5161	5996	6573	6711	6973	7132	7280	7411	7437	7441	7427	7303	7165	7013	6759	6626	6052	5213	4195	3117
N	2646	4048	5047	5295	6492	6694	6414	7122	7265	6834	7424	7429	6846	7287	7149	6446	6735	6539	5337	5092	4086	2672
O	2836	3791	4831	5685	6345	6542	6838	6993	7153	7281	7309	7313	7293	7170	7017	6868	6578	6383	5725	4867	3822	2860
P		3607	4445	5399	6077	6569	6674	6872	7011	7158	7181	7184	7167	7027	6893	6701	6600	6111	5431	4475	3633	
Q		3112	4022	4419	5730	6268	5981	6697	6882	6467	7044	7046	6475	6895	6715	6001	6294	5757	4442	4045	3132	
R			3434	4369	5141	5846	6297	6626	6607	6777	6804	6806	6784	6618	6642	6316	5867	5163	4389	3453		
S			2860	3610	4535	5177	5806	6155	6445	6594	6690	6692	6600	6455	6169	5821	5194	4552	3625	2873		
T				2648	3655	4472	4518	5526	5795	5404	6126	6127	5408	5803	5536	4529	4485	3668	2658			
U					2989	3474	4176	4568	4971	5172	5297	5299	5176	4977	4575	4185	3483	2998				
V						2757	3182	3772	3910	4176	4274	4275	4179	3914	3778	3188	2763					
W									2958	2738	3187	3188	2740	2961								

(d) 4F-12BS

Figure 5.30: Examples of time-average radial power distributions of Core A for different target channel configurations. Values shown are depicted in kW.

5.3.3 Instantaneous Results

The CANDU core is maintained with a multiplication factor of slightly above one with very little excess reactivity. As fissile isotopes begin to deplete, the k_{eff} decreases below one, and thus requires refuelling to bring the core back up to criticality to sustain the nuclear chain reaction. The act of refuelling will cause a ripple effect in the channels surrounding the one being refuelled, which can potentially cause overpowering in some of the channels and/or bundles. Instantaneous snapshots can be developed for observing these refuelling affects on the power distribution of the core. Based on the ranking, each channel will be at different stages of burnup to simulate a refuelling sequence. Simply, a typical age pattern is developed using a random number generator to pick and choose the order of refuelling. For this study, the age pattern is taken from [42] and is shown in Figure 5.31.

The values in the age pattern distribution indicate the sequence for when the channel is refuelled. As such, the channel labelled with one is to be refuelled first and the channel labelled 380 would be the last to be refuelled. This pattern allows DONJON to produce a burnup distribution that is a more realistic representation of a core with channels at various stages of burnup at a particular instant in time, hence the power distribution to be called an instantaneous snapshot.

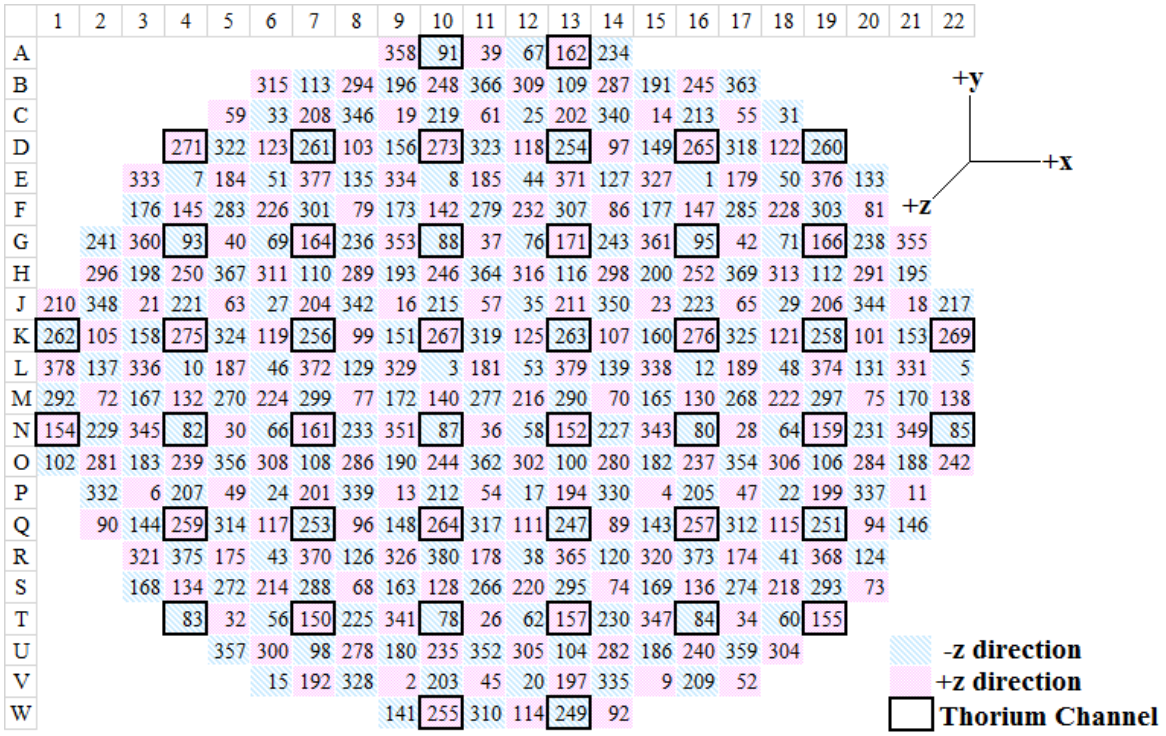

	1	2	3	4	5	6	7	8	9	10	11	12	13	14	15	16	17	18	19	20	21	22
A									358	91	39	67	162	234								
B						315	113	294	196	248	366	309	109	287	191	245	363					
C					59	33	208	346	19	219	61	25	202	340	14	213	55	31				
D				271	322	123	261	103	156	273	323	118	254	97	149	265	318	122	260			
E			333	7	184	51	377	135	334	8	185	44	371	127	327	1	179	50	376	133		
F			176	145	283	226	301	79	173	142	279	232	307	86	177	147	285	228	303	81		
G		241	360	93	40	69	164	236	353	88	37	76	171	243	361	95	42	71	166	238	355	
H		296	198	250	367	311	110	289	193	246	364	316	116	298	200	252	369	313	112	291	195	
J	210	348	21	221	63	27	204	342	16	215	57	35	211	350	23	223	65	29	206	344	18	217
K	262	105	158	275	324	119	256	99	151	267	319	125	263	107	160	276	325	121	258	101	153	269
L	378	137	336	10	187	46	372	129	329	3	181	53	379	139	338	12	189	48	374	131	331	5
M	292	72	167	132	270	224	299	77	172	140	277	216	290	70	165	130	268	222	297	75	170	138
N	154	229	345	82	30	66	161	233	351	87	36	58	152	227	343	80	28	64	159	231	349	85
O	102	281	183	239	356	308	108	286	190	244	362	302	100	280	182	237	354	306	106	284	188	242
P		332	6	207	49	24	201	339	13	212	54	17	194	330	4	205	47	22	199	337	11	
Q		90	144	259	314	117	253	96	148	264	317	111	247	89	143	257	312	115	251	94	146	
R			321	375	175	43	370	126	326	380	178	38	365	120	320	373	174	41	368	124		
S			168	134	272	214	288	68	163	128	266	220	295	74	169	136	274	218	293	73		
T				83	32	56	150	225	341	78	26	62	157	230	347	84	34	60	155			
U					357	300	98	278	180	235	352	305	104	282	186	240	359	304				
V						15	192	328	2	203	45	20	197	335	9	209	52					
W									141	255	310	114	249	92								

Figure 5.31: Age pattern distribution map for Core A

The age pattern map in Figure 5.31 also illustrates the direction of refuelling that occurs for each channel. The CANDU core utilizes a checker refuelling pattern where if one channel inserts in the –z direction, the adjacent channels are refuelled in the opposite direction. This method prevents power tilts from occurring axially in the core by balancing the powers between channels and help flatten the radial distribution. The resulting instantaneous profiles are shown in Table 5.11 and in power maps in Figure 5.34.

The following four figures depict the radial power distribution for an instantaneous modelling.

	1	2	3	4	5	6	7	8	9	10	11	12	13	14	15	16	17	18	19	20	21	22
A									2732	1560	3271	3367	2220	3079								
B						2899	3582	3906	4045	4173	4283	4424	4547	4184	4286	3683	3041					
C					3163	3856	4307	4682	5436	5420	5846	5995	5576	5252	5327	4581	4050	3434				
D				2292	3656	4639	4136	5879	6207	5142	6427	6777	5162	6462	6114	4391	4711	4100	2503			
E			2490	3667	4528	5496	5675	6553	6583	7364	7268	7579	6854	7130	6487	6537	5615	5020	3681	3047		
F			3147	4084	4978	5817	6239	7023	6998	7183	7248	7404	7158	7380	7055	6593	5989	5378	4387	3703		
G		2923	3465	2462	5757	6506	4774	6915	6820	3842	7844	7983	5541	7332	6753	3700	6660	6141	3603	4101	3270	
H		3392	4223	5078	5880	6630	7241	7216	7600	7595	7682	7895	8175	7585	7493	6980	6686	6304	5778	4588	3929	
J	2624	3550	4909	5641	6766	7386	7414	7527	8423	8200	8715	8880	8303	7873	8261	7528	7468	7192	6045	4947	4231	2962
K	2179	3973	5001	4759	6583	7344	6124	8147	8368	6873	8371	8788	6875	8485	8191	6354	7191	7183	4966	5406	4301	2445
L	2708	4017	4847	6229	6799	7484	7225	8093	7951	8845	8605	8921	8047	8423	7775	8092	7403	7318	5999	5440	4137	3258
M	2700	3943	4844	5763	6460	6942	7169	7917	7950	8114	8131	8303	8014	8288	7812	7461	7008	6801	5945	5331	4144	2976
N	1779	3580	4304	2665	6460	6963	5049	7302	7164	3982	8188	8344	5525	7654	7058	3455	7023	6769	4069	4864	3700	1369
O	2554	3361	4349	5106	5854	6402	7087	7044	7379	7358	7452	7710	7971	7419	7284	6764	6376	6216	5737	4607	3681	2574
P		3304	4326	5012	6090	6802	6754	6831	7629	7403	7921	8128	7640	7218	7562	6809	6857	6412	5354	4294	3832	
Q		3077	3723	3606	5291	6204	5152	6891	7014	5714	7055	7537	5827	7297	6937	5198	6014	5780	3834	4056	3303	
R			3022	3738	4818	5706	5719	6449	6193	6213	6768	7135	6474	6734	6236	5711	5583	5175	4013	3458		
S			2465	3199	3976	4719	5133	5808	5855	5996	6094	6289	6063	6217	5711	5248	4659	4174	3322	2787		
T				1217	3299	4003	2992	4735	4749	2439	5551	5671	3740	5116	4602	2164	3966	3390	1814			
U					2407	2986	3649	3878	4195	4256	4401	4565	4642	4256	3985	3443	2897	2500				
V						2585	2933	3263	3578	3574	3880	3968	3695	3385	3573	2919	2546					
W									2583	2081	2704	2869	2125	2668								

(a) 12Th-12BS

	1	2	3	4	5	6	7	8	9	10	11	12	13	14	15	16	17	18	19	20	21	22
A									2992	2195	3599	3701	2803	3391								
B						3012	3735	4110	4334	4520	4651	4806	4949	4575	4606	3952	3255					
C					3306	4039	4526	4945	5712	5747	6176	6353	5993	5809	5732	4950	4376	3703				
D				2622	3852	4838	4665	6084	6427	5733	6677	7033	5866	6823	6499	5090	5098	4446	2973			
E			2639	3848	4713	5664	5846	6656	6678	7391	7304	7602	7003	7314	6793	6902	6016	5390	4035	3318		
F			3330	4308	5169	5947	6325	6956	6805	6978	6978	7122	6975	7255	7193	6916	6376	5787	4788	4036		
G		3028	3677	3273	5867	6508	5358	6593	6473	4752	7294	7399	5976	7003	6645	4806	6967	6501	4435	4473	3536	
H		3492	4376	5217	5896	6470	6789	6627	6887	6881	6894	7085	7395	6993	7056	6840	6827	6600	6150	4975	4218	
J	2732	3679	5009	5679	6593	6904	6775	6729	7387	7166	7555	7702	7330	7068	7560	7138	7322	7345	6402	5342	4586	3238
K	2475	4098	5100	5113	6391	6796	6034	7150	7242	6434	7177	7542	6522	7500	7407	6472	7005	7344	5682	5833	4690	2918
L	2857	4155	4975	6194	6568	6874	6493	7058	6871	7544	7328	7587	6990	7397	7046	7547	7233	7493	6418	5883	4569	3605
M	2867	4111	5002	5833	6302	6443	6475	6945	6901	7034	6982	7140	6994	7328	7108	7109	6934	7412	6414	5823	4589	3359
N	2189	3779	4546	3606	6354	6520	5341	6512	6366	4643	7124	7233	5699	6873	6574	4526	7042	7071	5039	5366	4162	2026
O	2695	3542	4534	5261	5816	6071	6510	6341	6540	6535	6536	6769	7058	6715	6752	6576	6388	6525	6157	5067	4077	2908
P		3413	4470	5114	6043	6553	6296	6210	6814	6568	6979	7153	6853	6585	7055	6587	6944	6661	5742	4683	4147	
Q		3162	3857	4013	5340	6126	5385	6412	6411	5667	6378	6826	5862	6798	6604	5618	6204	6078	4466	4401	3553	
R			3174	3898	4933	5722	5712	6256	5895	5859	6337	6646	6159	6451	6238	5875	5852	5476	4360	3750		
S			2603	3382	4141	4871	5247	5838	5846	5996	6039	6235	6065	6261	5866	5543	4985	4509	3632	3038		
T				1721	3496	4201	3633	4931	4995	3434	5741	5819	4461	5357	4927	3086	4336	3700	2309			
U					2578	3186	3861	4121	4452	4576	4677	4841	4915	4556	4285	3790	3197	2764				
V						2689	3075	3426	3808	3820	4133	4207	3959	3637	3796	3126	2738					
W									2748	2429	2910	3083	2490	2867								

(b) 8C-12BS

	1	2	3	4	5	6	7	8	9	10	11	12	13	14	15	16	17	18	19	20	21	22
A									2790	2433	3361	3379	2635	3023								
B						2711	3357	3709	3968	4169	4237	4364	4436	4096	4037	3484	2844					
C					3048	3695	4117	4489	5218	5205	5621	5725	5389	5180	5138	4386	3933	3310				
D				2404	3580	4476	4180	5581	5863	5077	6044	6390	5174	6169	5832	4475	4588	4054	2648			
E			2555	3692	4484	5326	5448	6191	6224	6848	6775	6971	6404	6676	6258	6346	5590	4960	3727	3043		
F			3291	4261	5008	5703	5992	6620	6479	6709	6589	6688	6453	6795	6740	6603	6010	5461	4448	3775		
G		2954	3675	3824	5788	6293	5314	6318	6300	5510	7079	6996	5759	6579	6374	5403	6741	6146	4305	4163	3264	
H		3405	4326	5180	5760	6285	6531	6404	6663	6724	6619	6770	6979	6656	6723	6619	6515	6294	5780	4682	3877	
J	2678	3600	4940	5539	6449	6676	6535	6457	7156	6862	7282	7326	6971	6684	7243	6766	7020	6957	6065	5005	4316	3007
K	2386	4053	5009	4866	6220	6628	5688	6937	6971	6011	6869	7261	6052	7202	7058	5993	6664	7046	5275	5558	4421	2695
L	2862	4160	5009	6181	6563	6778	6382	6920	6785	7397	7228	7396	6808	7192	6914	7355	7104	7270	6216	5668	4425	3480
M	2916	4234	5150	6065	6414	6527	6463	7013	6963	7204	7028	7179	6941	7367	7143	7265	6952	7414	6305	5767	4530	3385
N	2382	3919	4819	4635	6669	6665	5631	6623	6614	5783	7426	7361	6051	6975	6818	5763	7314	7136	5255	5353	4212	2509
O	2791	3711	4757	5585	6037	6286	6656	6551	6764	6867	6750	6988	7207	6920	6965	6887	6560	6660	6198	5117	4116	3001
P		3487	4678	5282	6292	6732	6494	6366	7093	6758	7262	7345	7056	6734	7305	6736	7146	6751	5805	4693	4157	
Q		3266	3970	4048	5487	6362	5434	6682	6622	5714	6583	7111	5918	7051	6780	5624	6320	6213	4421	4443	3534	
R			3341	4054	5200	5982	6011	6583	6286	6184	6770	7004	6487	6758	6568	6112	6123	5646	4465	3807		
S			2789	3681	4428	5251	5610	6369	6388	6685	6601	6799	6508	6777	6320	6041	5332	4787	3785	3159		
T				2346	3895	4595	4211	5455	5693	4853	6559	6460	5138	5887	5503	4174	4845	4013	2602			
U					2887	3586	4317	4696	5103	5360	5359	5519	5521	5147	4841	4349	3606	3084				
V						2977	3453	3830	4389	4367	4764	4770	4491	4094	4280	3504	3079					
W									3103	2698	3293	3513	2754	3248								

(c) 6D-12BS

	1	2	3	4	5	6	7	8	9	10	11	12	13	14	15	16	17	18	19	20	21	22
A									2743	2711	3317	3272	2598	2864								
B						2557	3168	3529	3833	4058	4088	4195	4217	3880	3753	3233	2621					
C					2925	3525	3920	4283	5023	4980	5405	5462	5121	4886	4855	4094	3698	3102				
D				2264	3443	4302	3892	5363	5621	4719	5772	6118	4793	5870	5511	4108	4317	3842	2438			
E			2533	3636	4393	5177	5268	6003	6058	6649	6584	6716	6145	6395	6024	6085	5385	4740	3556	2896		
F			3309	4293	4967	5621	5861	6524	6396	6681	6473	6537	6236	6621	6571	6508	5854	5307	4269	3639		
G		2928	3719	4327	5816	6232	5376	6237	6301	6245	7082	6862	5733	6411	6300	5983	6688	5982	4262	3995	3110	
H		3367	4332	5209	5726	6227	6437	6339	6616	6730	6542	6661	6807	6524	6597	6559	6380	6146	5583	4520	3683	
J	2658	3566	4930	5482	6405	6584	6434	6341	7088	6743	7192	7166	6810	6503	7115	6589	6885	6757	5878	4815	4177	2885
K	2312	4045	4975	4681	6140	6561	5458	6850	6852	5748	6726	7138	5756	7065	6887	5681	6488	6892	4990	5411	4282	2545
L	2883	4192	5066	6222	6603	6761	6341	6873	6772	7359	7213	7323	6728	7107	6876	7293	7074	7176	6118	5568	4375	3446
M	2978	4362	5308	6294	6547	6624	6486	7096	7048	7372	7102	7241	6940	7439	7221	7440	7025	7482	6281	5787	4548	3463
N	2550	4054	5063	5542	6947	6797	5875	6712	6801	6745	7659	7463	6349	7062	7017	6826	7561	7233	5456	5392	4298	2955
O	2885	3856	4950	5847	6210	6430	6742	6669	6897	7074	6869	7102	7279	7035	7105	7111	6690	6771	6252	5182	4182	3111
P		3546	4836	5399	6450	6822	6570	6407	7212	6811	7371	7392	7110	6764	7420	6795	7260	6802	5842	4704	4183	
Q		3333	4040	4006	5539	6450	5337	6753	6647	5590	6591	7165	5799	7099	6792	5505	6333	6256	4317	4459	3516	
R			3437	4122	5315	6062	6088	6658	6398	6246	6886	7062	6531	6800	6649	6157	6215	5693	4488	3821		
S			2907	3851	4551	5393	5708	6551	6572	6960	6771	6952	6583	6915	6453	6244	5462	4895	3833	3214		
T				2843	4086	4726	4479	5598	5948	5833	6851	6604	5388	5991	5686	4931	5068	4130	2764			
U					2982	3676	4387	4802	5234	5566	5468	5605	5562	5213	4929	4502	3709	3176				
V						2992	3468	3815	4466	4401	4826	4776	4494	4082	4300	3520	3129					
W									3093	2635	3263	3503	2677	3244								

(d) 4F-12BS

Figure 5.32: Examples of instantaneous radial power distributions for core A for different target channel configurations. Values are in kW

Table 5.11: Core A Instantaneous results

Target Channel Configuration	k-effective	Peak Power (kW) Channel	Bundle	CPPF	BPPF
12Th-12BS	1.0240784	8921 [L12]	1161 [L10-B5]	1.405	1.816
(10Th+2SEU)-12BS	1.0237289	8046 [J12]	988 [J12-B5]	1.428	2.189
8C-12BS	1.0182974	7702 [J12]	896[L10-B3]	1.294	1.689
6D-12BS	1.0111979	7426 [N11]	1071 [N11-B10]	1.141	1.461
4F-12BS	1.0094795	7659 [N11]	1135 [N11-B10]	1.151	1.436
8C-10BS	1.0198963	7766 [J12]	909 [L10-B03]	1.316	1.696
6D-9BS	1.0147340	7557 [L10]	1061 [L10-B03]	1.169	1.560
4F-8BS	1.0077654	7796 [L10]	1315 [L10-B03]	1.118	1.459

With the 12 thorium bundle configuration, a large disparity is seen between the target and driver channels. For example, in Figure 5.32a, the target channel G10 and its adjacent driver channel, G11, have a difference of 4000 kW because of the burnup ranking assigned in the age pattern distribution map. Furthermore, the channel powers between each target channel vary due to the age pattern imposed. As a result of these differences, there is a tilt in the radial profile. The imbalance is less pronounce with the 4F, 6D, 8C configurations since the addition of SEU bundles shifts the power distributions closer to a pure SEU core. Nonetheless, these differences can result in radial power tilts in reactor scenarios that deviate from the norm. Since the instantaneous power maps are more representative of the core at an instant, additional proper measures would be required to rebalance the radial form, such as through the use of zone controllers and/or adjusters.

Generally, the real instantaneous channel powers are higher than the time-average powers [33]. The CPPF measures this difference, which is significantly higher for larger thorium bundle allotments. The CPPF values produced increase dramatically from the 1.12 value found in an all SEU fuelled core because the difference in the target channel powers between the time-averages and the instantaneous snapshots are very large. As for the peak powers during refuelling, it does not deviate from the centre of the core; however, there is still a tilt in the radial power distribution as seen in Figures 5.32a and 5.32b. The most ideal is the 6 Th + 6 SEU (6A) configuration.

The lowering of the k-effective value to increase SEU bundle implementation in the target channel is due to the longer dwell time assigned to those configurations. As a result, the thorium bundles benefit from the increase in U-233 and will continue to contribute neutrons from the fissioning, but the SEU bundles would have burned up most of their fissile uranium and become a net absorber for neutrons.

5.3.4 Target Channel Refuelling

The refuelling of the target channel will cause an immediate effect on the radial power distribution and reactivity of the core. The instantaneous snapshot of the core is developed based on the age pattern distribution specified to closely depict a true power distribution of the core at a specific instant in time. A brief look into the event of refuelling the target channels with fresh thorium bundles will be performed on the instantaneous model in this section.

Table 5.12: Instantaneous Core A characteristics after refuelling channel N16

Target Channel Configuration	k_{eff}	$\Delta\rho$	Peak Power (kW)		CPPF	BPPF
			Channel	Bundle		
12Th-12BS	1.0232209	-1.038	9051 [L10]	1188 [L10-B5]	1.468	1.895
8C-12BS	1.0176693	-0.6281	7864 [E12]	919[L10-B03]	1.298	1.723
6D-12BS	1.0111843	-0.0136	7450 [N11]	1363 [N16-B10]	1.141	1.461
4F-12BS	1.0100574	0.578	8672 [N16]	1659 [N16-B10]	1.151	1.436
8C-10BS	1.0192516	-0.645	7942 [E12]	930[L10-B3]	1.332	1.726
6D-9BS	1.0147251	-0.00892	7546 [L10]	1109 [N16-B3]	1.169	1.560
4F-8BS	1.0085523	0.79	8516 [N17]	1465 [N16-B3]	1.439	2.069

	1	2	3	4	5	6	7	8	9	10	11	12	13	14	15	16	17	18	19	20	21	22
A									3183	2219	3783	3885	2853	3511								
B						3276	4058	4429	4652	4791	4921	5035	5149	4714	4749	4053	3339					
C					3600	4399	4893	5339	6113	6125	6517	6673	6204	5853	5864	5064	4447	3762				
D				2831	4199	5246	5004	6539	6890	6040	7051	7343	6022	6991	6646	5125	5160	4461	2944			
E			2871	4200	5118	6157	6298	7164	7111	7842	7659	7942	7214	7502	6885	6974	6014	5385	3984	3273		
F			3635	4658	5617	6423	6812	7433	7240	7304	7298	7358	7160	7355	7256	6865	6325	5683	4689	3923		
G		3322	3980	3383	6333	7036	5615	7035	6800	4705	7523	7617	5942	7049	6570	4509	6766	6321	4185	4304	3387	
H		3814	4783	5643	6401	6970	7289	7033	7274	7128	7123	7211	7464	6935	6941	6590	6575	6292	5860	4712	4010	
J	2984	4035	5456	6191	7136	7470	7237	7161	7753	7467	7739	7830	7294	6955	7290	6823	6893	6917	5978	5007	4284	3036
K	2684	4470	5575	5513	6934	7298	6396	7552	7611	6606	7338	7555	6376	7223	7034	5973	6469	6714	5159	5350	4335	2669
L	3111	4546	5398	6734	7077	7403	6894	7467	7146	7785	7399	7570	6776	7025	6476	6812	6420	6684	5731	5329	4143	3294
M	3125	4459	5433	6260	6791	6871	6875	7274	7174	7137	7026	7013	6718	6783	6344	6061	5944	6129	5632	5172	4128	3011
N	2313	4102	4872	3653	6771	6960	5502	6818	6525	4446	7064	7087	5275	6302	5677	1946	5836	6047	4281	4742	3687	1716
O	2930	3824	4902	5613	6234	6438	6879	6598	6756	6579	6524	6593	6726	6159	5964	5552	5449	5624	5391	4465	3630	2575
P		3710	4810	5507	6449	6990	6616	6496	7004	6687	6947	7031	6537	6146	6367	5835	6077	5873	5060	4167	3692	
Q		3415	4169	4268	5717	6487	5617	6663	6628	5712	6395	6691	5591	6391	6116	5043	5581	5422	3947	3928	3194	
R			3403	4182	5245	6082	5985	6534	6049	5965	6326	6582	5956	6168	5834	5434	5330	4980	3929	3389		
S			2796	3589	4410	5133	5507	6050	6021	6044	6063	6152	5921	6002	5566	5144	4610	4124	3313	2754		
T				1729	3683	4429	3691	5115	5083	3256	5716	5780	4255	5183	4672	2736	4012	3424	2066			
U					2726	3338	4035	4252	4574	4603	4704	4802	4844	4420	4129	3574	3008	2569				
V						2837	3207	3565	3898	3895	4153	4216	3903	3566	3670	3006	2592					
W									2835	2451	2946	3077	2443	2806								

Figure 5.33: 8C-10BS radial power profile from refuelling N16. Values are in kW.

The effect of refuelling one target channel is shown in Table 5.12 and an example of the radial power profile is illustrated in Figure 5.48. This is done by calling the

REFUEL module in DONJON and specifying the channel and the number of bundles to be refuelled. In this case, channel N16 was refuelled. An example of the refuelling process that was being performed is illustrated in Figure 5.25.

The change in reactivity is highest for the 12 thorium bundle reloading, with a drop of 1.038mk. By changing the target channel configuration to include SEU bundles, the drop in reactivity decreases from the presence of U-235 that adds to the core reactivity. Similarly results are seen for different refuelling schemes used on the same channel configurations. The change in reactivity may not be the same for each target channel since the burnup in the adjacent driver channels will be different.

The number of fresh thorium bundles refuelled affects the radial profile of the core. With the 8C channel configuration, the peak channel power is shifted towards the upper left corner of the core as shown in Figure 5.48. Conversely, the 4F channel configuration will produce peak powers at or around the refuelled channel since there are less thorium bundles involved and four fresh SEU bundles fuelled in.

Peak bundle powers are generally located in the refuelled target channel due to the fresh SEU bundles. Only the 8C configuration has peak bundle powers remaining near the centre of the core as the insertion of the fresh SEU bundles do not produce peaking powers. This is due to the periphery positioning of the fresh SEU bundles.

Change in k_{eff} by refuelling all target channels is shown below in Table 5.13. Similarly, the same DONJON module will be called to refuel all target channels at the same time. The insertion of 12 thorium bundles in all the target channels simultaneously lowered the k_{eff} factor to sub-critical levels. Combining thorium and SEU bundles through the different channel configurations increased the k_{eff} factor. The 6D configuration is slightly above the capacity of the reactivity devices, but 4F is extremely super-critical, mainly due to the insertion of eight SEU bundles for each target channel to be refuelled.

Table 5.13: k-effective after refuelling all target channels for Core A

Target Channel Configuration	k_{eff}	$\Delta\rho$
12Th	0.9737558	-50.5031
8C-12BS	0.9991593	-19.0265
6D-12BS	1.0229341	11.8665
4F-12BS	1.0350726	25.9226
8C-10BS	0.9956251	-24.2712
6D-9BS	1.0167806	2.0466
4F-8BS	1.0260881	18.3227

Refuelling with 12 fresh thorium bundles lowers the power of those channels to nearly zero as shown in Figure 5.34a. By replacing some of the thorium bundles with SEU bundles as seen in the 4F, 6D, and 8C configurations in the other power maps of Figure 5.34, the channel powers increase as a result. For the 4F case, there are more SEU bundles than thorium bundles, which causes the channel power to be higher than the surrounding driver channels.

By comparing the radial power profiles of the refuelled target channel model to the instantaneous model, it can be seen that large power differences is no longer present as a result of refuelling the target channels simultaneously. Therefore, the tilt and power differences seen in the instantaneous models is due to the different levels of burnup in the target thorium channels, resulting in varying amounts of fissile content in the target channels; some target channels will contain more U-233, which produce more power and flux while some will have less. As a result, a different age pattern distribution needs to be developed to account for the thorium bundles.

Table 5.14: Core A characteristics after refuelling all target channels

Target Channel Configuration	Peak Power (kW) Channel	Bundle	CPPF	BPPF
12Th	9518 [L12]	1143 [L12-B4]	1.252	1.775
8C-12BS	8302 [L10]	1904[K10-B2]	1.125	2.658
6D-12BS	8090 [L10]	1748 [K10-B2]	1.155	2.164
4F-12BS	8583 [K10]	1532 [K10-B3]	1.280	1.914
8C-10BS	7740 [N11]	1647[N11-B11]	1.428	3.777
6D-9BS	8744 [N11]	2111 [N13-B10]	1.189	3.784
4F-8BS	8746 [N11]	1968 [N13-B10]	1.317	2.889

The core characteristics after refuelling the target channels are shown Table 5.14. Peak powers in a 12 thorium bundle refuelling scheme (12Th configuration) is located in the driver channels at the centre of the core. The higher channel power is due to the zero power produced in the target channels, which requires all the driver channels to increase power to maintain the target core power produced. By adjusting the channel configurations to use SEU bundles, bundle powers increases tremendously beyond the safety limits. The peak bundle power occurs in the fresh SEU bundles located at the channel exit side; the adjacent channels are refuelled from the same reactor end and the fresh SEU bundles from these channels exacerbated the power of the SEU bundles in the target channel. Therefore, the refuelling scheme is required to be modified such that the SEU bundles do not become over-powered. This is observed by changing the bundle shift schemes. The peak bundle powers are now shifted to the refuelling side of the channel, which increases the safety margins to CHF.

	1	2	3	4	5	6	7	8	9	10	11	12	13	14	15	16	17	18	19	20	21	22
A									2827	1	3172	3179	1	2997								
B						3197	3956	4334	4323	4268	4416	4502	4473	4315	4582	3948	3243					
C					3213	3983	4376	4927	5609	5313	5901	5995	5368	5301	5446	4523	4069	3365				
D				1	3689	4627	2	5937	6187	2	6341	6637	2	6312	6038	2	4588	3994	1			
E			2584	3770	4855	5789	5810	6930	6966	7482	7600	7825	6840	7337	6768	6580	5822	5181	3606	2952		
F			3434	4328	5429	6208	6408	7503	7539	7527	7751	7789	7197	7695	7459	6800	6331	5647	4336	3731		
G		3377	3789	1	6174	6755	2	7221	7240	2	8235	8169	2	7455	7040	2	6914	6307	2	4104	3507	
H		3914	4723	5490	6479	7148	7483	7768	8223	8019	8278	8381	8275	7993	7976	7276	7144	6714	5855	4807	4232	
J	2695	3914	5311	5894	7299	7845	7583	7995	8922	8391	9200	9281	8352	8212	8655	7631	7840	7529	6063	5096	4405	2874
K	1	4192	5170	2	6889	7557	2	8351	8544	3	8550	8927	3	8568	8312	2	7308	7332	2	5351	4317	1
L	2743	4423	5338	6629	7497	8107	7552	8731	8619	9224	9296	9541	8321	8993	8407	8424	8000	7854	6172	5692	4373	3158
M	2804	4476	5523	6428	7357	7741	7662	8769	8879	8851	9080	9166	8496	9121	8731	8178	7857	7552	6268	5743	4514	3041
N	1	4072	4917	2	7308	7606	2	7971	7972	3	9073	9048	3	8314	7900	2	7844	7415	2	5173	4080	1
O	2840	4028	5152	5878	6840	7308	7711	8003	8440	8241	8539	8732	8633	8404	8368	7640	7361	7111	6225	5186	4253	2866
P		4057	5107	5663	7043	7691	7371	7730	8640	8125	8975	9121	8292	8130	8597	7509	7803	7276	5858	4877	4554	
Q		3731	4165	1	5884	6769	2	7540	7652	2	7722	8209	2	7924	7581	2	6558	6344	2	4399	3871	
R			3469	4142	5575	6509	6339	7426	7189	6952	7829	8154	7150	7682	7205	6345	6400	5891	4342	3818		
S			2839	3693	4764	5588	5913	6970	7080	7088	7334	7465	6911	7350	6852	6164	5563	4939	3682	3059		
T				1	3923	4673	2	5684	5791	2	6659	6612	2	5979	5580	2	4747	3947	1			
U					2972	3721	4452	4940	5316	5211	5450	5548	5384	5242	5068	4348	3676	3047				
V						3422	3901	4324	4561	4329	4750	4782	4365	4226	4725	3923	3419					
W									3044	1	2997	3159	1	3109								

(a) 12Th-12BS

	1	2	3	4	5	6	7	8	9	10	11	12	13	14	15	16	17	18	19	20	21	22
A									2736	1770	3170	3243	1823	2957								
B						2730	3386	3774	4018	4131	4281	4293	4382	3996	4070	3397	2867					
C					2967	3660	4148	4616	5228	5322	5581	5744	5291	5112	4991	4419	3751	3205				
D				1669	3581	4471	3056	5659	6064	3833	6281	6403	3822	6091	5918	3237	4614	3827	1767			
E			2508	3657	4520	5433	5619	6471	6490	7167	6999	7264	6581	6903	6337	6460	5475	4909	3538	2890		
F			3295	4247	5166	5854	6314	6884	6947	7029	7104	7034	6921	6987	7020	6573	6102	5321	4384	3521		
G		3013	3715	2944	5869	6566	4237	6844	6759	4674	7481	7580	4723	7084	6621	4282	6626	6122	3076	4067	3108	
H		3473	4452	5295	6097	6608	7035	6922	7356	7286	7368	7352	7625	7107	7207	6789	6721	6237	5698	4501	3791	
J	2627	3693	4980	5789	6675	7132	7004	7173	7750	7694	7915	8086	7543	7346	7573	7179	7054	6960	5864	4908	4046	2841
K	1678	4038	5162	3722	6637	7010	4661	7516	7809	5152	7766	7917	5075	7696	7626	4759	6941	6895	3762	5247	4223	1777
L	2801	4232	5117	6434	6860	7306	6941	7683	7506	8302	7958	8221	7465	7867	7361	7729	7155	7201	6009	5456	4176	3207
M	2892	4220	5313	6185	6838	6946	7130	7596	7781	7861	7888	7853	7701	7847	7674	7429	7117	6915	6150	5431	4318	3059
N	1698	4000	4890	3685	6850	7148	4655	7330	7234	5041	8000	8093	5094	7592	7182	4705	7232	7011	3766	5157	3970	1736
O	2779	3738	4908	5691	6405	6634	7187	7071	7455	7428	7482	7563	7815	7364	7404	7044	6724	6553	6017	4893	3933	2761
P		3615	4685	5482	6422	7052	6819	6932	7521	7399	7723	7905	7466	7219	7518	6982	7069	6649	5582	4545	3927	
Q		3231	4048	2984	5708	6468	4212	6944	7108	4631	7113	7429	4697	7255	7037	4266	6361	6008	3054	4180	3346	
R			3294	4151	5211	6111	6149	6846	6544	6592	7005	7284	6699	6957	6650	6200	5996	5468	4266	3561		
S			2748	3562	4498	5222	5735	6376	6561	6696	6776	6835	6605	6713	6329	5883	5228	4591	3567	2881		
T				1690	3722	4555	3045	5489	5629	3708	6358	6356	3732	5799	5366	3046	4570	3751	1713			
U					2828	3442	4242	4552	5006	5115	5216	5267	5269	4915	4647	4122	3410	2858				
V						2922	3311	3784	4137	4169	4422	4467	4170	3878	4030	3323	2886					
W									2916	1774	3023	3134	1774	2935								

(b) 8C-12BS

	1	2	3	4	5	6	7	8	9	10	11	12	13	14	15	16	17	18	19	20	21	22
A									2612	2724	3136	3220	2816	2845								
B						2440	3034	3367	3728	3922	4021	4037	4190	3696	3653	3037	2567					
C					2833	3448	3910	4269	4908	5116	5280	5448	5076	4767	4641	4178	3530	3073				
D				2596	3441	4297	4548	5374	5808	5690	5996	6137	5668	5821	5627	4807	4419	3693	2754			
E			2431	3564	4256	5141	5320	6068	6061	6880	6571	6847	6239	6481	5904	6183	5160	4645	3416	2822		
F			3165	4127	4883	5533	6056	6487	6556	6748	6685	6618	6608	6588	6605	6315	5761	5028	4246	3384		
G		2772	3565	4417	5648	6366	6264	6567	6456	6853	7217	7317	6916	6792	6311	6315	6405	5901	4623	3925	2849	
H		3176	4208	5079	5739	6244	6804	6526	6968	7000	6944	6938	7365	6701	6810	6517	6337	5875	5501	4241	3483	
J	2580	3486	4764	5610	6350	6818	6767	6787	7398	7439	7548	7722	7285	6948	7219	6934	6725	6632	5678	4665	3842	2802
K	2620	3925	5059	5597	6397	6805	6897	7291	7585	7574	7492	7681	7462	7473	7395	7044	6698	6677	5660	5140	4113	2797
L	2793	4067	4895	6283	6528	6990	6682	7332	7132	8090	7591	7869	7191	7515	6988	7539	6823	6879	5807	5252	3997	3245
M	2892	4052	5102	6017	6495	6612	6885	7256	7427	7644	7513	7492	7452	7513	7327	7226	6778	6577	5959	5224	4149	3078
N	2651	3870	4749	5536	6649	6966	6890	7097	6990	7430	7816	7908	7520	7373	6937	6980	7059	6813	5669	5036	3830	2721
O	2738	3524	4674	5506	6059	6312	7001	6733	7121	7217	7122	7227	7640	7030	7072	6835	6389	6221	5857	4656	3721	2707
P		3307	4443	5279	6113	6750	6626	6589	7231	7187	7429	7611	7286	6886	7216	6773	6769	6340	5397	4292	3621	
Q		2987	3919	4502	5491	6316	6314	6786	6931	6881	6905	7287	7020	7115	6858	6377	6166	5835	4644	4069	3096	
R			3169	4033	4984	5876	5976	6566	6266	6396	6747	7038	6532	6700	6354	6011	5755	5246	4166	3449		
S			2698	3504	4287	5009	5555	6123	6300	6575	6517	6597	6451	6476	6056	5732	5000	4394	3496	2845		
T				2678	3674	4493	4643	5352	5525	5667	6332	6319	5713	5707	5221	4645	4517	3699	2720			
U					2766	3340	4169	4394	4890	5140	5139	5207	5311	4803	4489	4041	3302	2808				
V						2737	3100	3549	4051	4181	4419	4462	4199	3779	3810	3108	2708					
W									2962	2875	3149	3292	2892	2999								

(c) 6D-12BS

	1	2	3	4	5	6	7	8	9	10	11	12	13	14	15	16	17	18	19	20	21	22
A									2690	3353	3290	3350	3456	2908								
B						2415	2997	3334	3743	4001	4052	4098	4254	3724	3592	3005	2514					
C					2889	3474	3945	4247	4956	5169	5349	5488	5171	4754	4668	4175	3569	3110				
D				3165	3473	4353	5403	5414	5824	6727	5998	6210	6719	5888	5620	5685	4422	3767	3366			
E			2473	3615	4254	5114	5306	5995	6006	6859	6528	6774	6227	6401	5854	6154	5157	4626	3471	2870		
F			3177	4173	4831	5493	5992	6421	6420	6704	6528	6508	6487	6509	6489	6322	5688	5018	4258	3436		
G		2723	3576	5219	5652	6316	7266	6433	6350	7902	7133	7163	7949	6640	6227	7357	6423	5876	5468	3933	2831	
H		3120	4158	5064	5612	6131	6671	6353	6737	6851	6686	6729	7170	6517	6604	6437	6198	5807	5484	4231	3429	
J	2635	3451	4760	5562	6269	6661	6653	6541	7202	7201	7326	7448	7113	6687	7057	6777	6632	6538	5699	4634	3878	2864
K	3176	3960	5052	6544	6281	6715	7917	7134	7338	8583	7210	7478	8487	7305	7185	8086	6556	6656	6670	5211	4156	3419
L	2861	4048	4863	6238	6410	6792	6514	7046	6860	7804	7303	7538	6957	7214	6755	7364	6683	6760	5797	5240	4027	3360
M	2945	4063	5050	6002	6326	6438	6654	7013	7098	7406	7154	7189	7150	7256	7042	7088	6581	6477	5915	5244	4164	3199
N	3199	3861	4751	6470	6591	6795	7843	6830	6749	8389	7576	7602	8479	7092	6733	7997	6978	6734	6646	5044	3869	3326
O	2768	3498	4607	5471	5885	6134	6784	6474	6792	6966	6763	6914	7345	6751	6786	6680	6192	6112	5827	4638	3709	2778
P		3210	4407	5194	6002	6561	6467	6292	6970	6882	7134	7268	7044	6571	6988	6575	6641	6221	5382	4240	3586	
Q		2943	3883	5255	5367	6229	7241	6610	6662	7759	6599	7052	7955	6916	6633	7309	6035	5794	5475	4098	3055	
R			3155	3974	4892	5716	5834	6309	6008	6114	6467	6725	6302	6421	6132	5841	5638	5160	4163	3453		
S			2692	3507	4163	4882	5367	5914	6021	6371	6211	6331	6197	6248	5816	5608	4860	4320	3488	2885		
T				3195	3651	4382	5316	5138	5337	6446	6149	6092	6495	5496	5048	5348	4461	3671	3265			
U					2677	3218	3988	4176	4634	4950	4870	4970	5102	4580	4265	3898	3179	2755				
V						2570	2909	3287	3861	3988	4239	4259	4043	3575	3592	2915	2574					
W									2851	3330	3056	3237	3372	2929								

(d) 4F-12BS

Figure 5.34: Examples of power distributions after refuelling of target channels for Core A. Values are in kW

5.3.5 Initial Core Powers

In the NU CANDU system, initial start-up of the core results in a reactivity level that is beyond the capabilities of the core control devices to handle. To counter the excess reactivity, bundles of depleted uranium (DU) are used as part of the initial core start up. After a certain level of burnup, the DU bundles are shuffled out and replaced with NU bundles. The dual fuel core utilizes driver uranium bundles with an enrichment of 1.2% for an even higher reactivity level at core start-up. Since thorium bundles are used, the initial core power distribution is mapped to determine if the thorium bundles are sufficient at reducing the initial core reactivity. The core configurations evaluated will be the same ones evaluated in the time-average calculation.

Table 5.15: Initial core start-up k_{eff} and peak powers

Target Channel Configuration	k_{eff}	Peak Powers (kW)	
		Channel	Bundle
12 Th	1.193227	10990 [M12]	1413 [M12-B7]
8 Th + 4 SEU (8C)	1.207267	10610 [M12]	1077 [M12-B2]
6 Th + 6 SEU (6D)	1.235509	10230 [M12]	1323 [M12-B3]
4 Th + 8 SEU (4F)	1.257724	9988 [M12]	1233 [M12-B3]

In all cases, the initial core k-effective is well beyond the capacity of the combined effect of the reactivity control systems. Core reactivity increases as the target channel configurations change for more inclusion of SEU bundles. Therefore, at the start of core life, DU or NU bundles will be required to lower the reactivity of the core.

	1	2	3	4	5	6	7	8	9	10	11	12	13	14	15	16	17	18	19	20	21	22
A									2560	0.495	2640	2640	0.496	2570								
B						2750	3340	3850	3820	3790	4030	4030	3800	3840	3870	3370	2790					
C					2640	3300	3810	4530	4810	4750	5130	5130	4760	4830	4560	3840	3340	2690				
D					3290	3980	1.094	5320	5640	1.368	6050	6050	1.371	5660	5350	1.104	4030	3350				
E			2360	3180	4320	5110	5650	6550	6970	6980	7450	7460	6990	7000	6590	5700	5170	4390	3280	2530		
F			3070	3820	5050	5850	6330	7350	7790	7730	8310	8320	7740	7820	7390	6380	5920	5130	3920	3210		
G		3070	3560	1.054	5570	6290	1.649	7810	8220	1.987	8770	8770	1.99	8250	7850	1.66	6360	5640	1.074	3660	3180	
H		3600	4320	5160	6450	7280	7780	8870	9340	9290	9920	9930	9300	9370	8900	7830	7340	6510	5230	4400	3680	
J	2420	3640	4640	5500	6860	7710	8180	9330	9810	9710	10400	10410	9730	9840	9360	8220	7770	6920	5560	4700	3700	2460
K	0.475	3660	4610	1.339	6880	7650	1.975	9260	9700	2.336	10290	10290	2.339	9720	9290	1.983	7700	6920	1.351	4660	3700	0.481
L	2550	3910	5000	5930	7350	8230	8710	9890	10390	10280	10990	10990	10290	10410	9910	8740	8270	7390	5970	5040	3950	2580
M	2560	3920	5010	5940	7360	8240	8720	9890	10390	10290	10990	10990	10300	10410	9910	8740	8270	7390	5970	5040	3950	2580
N	0.479	3680	4640	1.345	6900	7670	1.979	9280	9710	2.339	10300	10300	2.341	9730	9290	1.984	7700	6930	1.351	4660	3710	0.482
O	2450	3690	4680	5540	6900	7750	8210	9350	9840	9730	10420	10420	9740	9850	9370	8230	7770	6920	5560	4700	3700	2460
P		3670	4390	5220	6500	7330	7820	8900	9370	9310	9940	9940	9320	9380	8910	7830	7350	6520	5240	4400	3680	
Q		3170	3650	1.071	5630	6350	1.659	7840	8250	1.992	8790	8790	1.993	8260	7860	1.662	6360	5640	1.074	3660	3190	
R			3200	3920	5120	5910	6380	7390	7820	7760	8340	8340	7760	7830	7400	6390	5920	5140	3930	3210		
S			2520	3280	4390	5170	5700	6590	7000	7000	7470	7480	7010	7010	6600	5710	5180	4400	3280	2530		
T					3350	4030	1.104	5350	5670	1.374	6070	6070	1.374	5670	5360	1.105	4040	3360				
U					2690	3340	3840	4570	4840	4770	5150	5150	4770	4840	4570	3850	3340	2690				
V						2790	3370	3880	3840	3810	4050	4050	3810	3850	3880	3370	2790					
W									2580	0.497	2650	2650	0.497	2580								

(a) 12Th

	1	2	3	4	5	6	7	8	9	10	11	12	13	14	15	16	17	18	19	20	21	22
A									2430	730	2570	2570	730	2440								
B						2490	3020	3500	3580	3630	3830	3840	3640	3590	3520	3050	2520					
C					2490	3110	3630	4270	4570	4620	4920	4920	4630	4590	4290	3660	3150	2540				
D				700	3160	3850	1340	5120	5460	1710	5870	5880	1710	5480	5140	1350	3900	3220	720			
E			2260	3070	4100	4880	5460	6250	6670	6770	7140	7140	6780	6690	6280	5510	4940	4170	3160	2420		
F			2930	3720	4830	5630	6180	7060	7500	7560	8010	8010	7570	7530	7090	6230	5690	4900	3810	3060		
G		2820	3430	1310	5390	6150	2080	7610	8040	2520	8570	8570	2530	8060	7640	2100	6210	5460	1330	3520	2920	
H		3310	4100	4990	6160	7000	7590	8520	9000	9080	9560	9560	9090	9030	8560	7630	7060	6220	5060	4170	3380	
J	2320	3440	4440	5350	6580	7440	8010	8990	9480	9530	10050	10050	9540	9510	9020	8040	7490	6630	5410	4500	3490	2360
K	710	3530	4510	1680	6690	7500	2510	9050	9520	2980	10080	10090	2980	9540	9080	2520	7540	6730	1700	4550	3570	720
L	2500	3740	4820	5780	7060	7940	8520	9530	10030	10080	10610	10620	10090	10050	9560	8550	7980	7090	5820	4860	3770	2520
M	2510	3750	4830	5790	7060	7950	8530	9540	10040	10080	10620	10620	10090	10050	9560	8550	7980	7100	5820	4860	3770	2520
N	710	3550	4530	1690	6710	7520	2510	9070	9530	2980	10090	10090	2980	9540	9080	2520	7540	6730	1700	4550	3570	720
O	2350	3480	4480	5390	6620	7470	8030	9010	9500	9540	10060	10060	9550	9510	9030	8050	7490	6640	5410	4500	3490	2360
P		3370	4160	5040	6210	7040	7620	8550	9030	9090	9580	9580	9100	9040	8560	7630	7060	6230	5060	4170	3380	
Q		2910	3510	1320	5450	6200	2090	7640	8070	2530	8590	8590	2530	8070	7650	2100	6210	5460	1330	3520	2920	
R			3050	3810	4900	5690	6230	7090	7530	7590	8030	8030	7590	7540	7100	6240	5700	4910	3810	3060		
S			2410	3160	4170	4940	5510	6280	6700	6790	7160	7160	6800	6700	6290	5510	4940	4180	3170	2420		
T				720	3220	3900	1350	5150	5490	1720	5890	5890	1720	5490	5150	1350	3900	3220	720			
U					2540	3150	3660	4300	4600	4640	4940	4940	4640	4600	4300	3660	3150	2540				
V						2520	3050	3530	3600	3650	3850	3850	3650	3600	3530	3050	2520					
W									2450	740	2580	2580	740	2450								

(b) 8C

	1	2	3	4	5	6	7	8	9	10	11	12	13	14	15	16	17	18	19	20	21	22
A									2350	1420	2540	2550	1420	2360								
B						2270	2760	3210	3380	3510	3670	3670	3510	3390	3230	2780	2300					
C					2390	2960	3480	4040	4370	4510	4730	4740	4520	4390	4060	3510	2990	2430				
D				1350	3060	3740	2550	4930	5300	3260	5710	5720	3270	5320	4960	2570	3790	3120	1400			
E			2200	2990	3910	4670	5290	5960	6380	6570	6840	6840	6580	6400	5990	5330	4730	3980	3080	2350		
F			2830	3640	4630	5430	6040	6780	7220	7390	7710	7710	7410	7240	6810	6080	5480	4700	3720	2950		
G		2620	3330	2500	5230	6010	3980	7410	7860	4810	8360	8370	4820	7880	7440	4000	6070	5290	2540	3420	2710	
H		3070	3910	4840	5900	6740	7390	8190	8670	8860	9200	9200	8870	8690	8220	7430	6790	5950	4900	3980	3130	
J	2270	3280	4270	5220	6320	7180	7830	8660	9150	9330	9690	9700	9340	9170	8690	7870	7220	6360	5270	4320	3320	2300
K	1390	3430	4430	3220	6510	7350	4800	8840	9320	5690	9860	9870	5700	9340	8860	4810	7380	6550	3240	4470	3460	1400
L	2490	3600	4660	5650	6780	7660	8330	9180	9680	9860	10230	10240	9870	9700	9200	8360	7690	6810	5680	4690	3630	2510
M	2490	3610	4670	5650	6790	7670	8340	9180	9680	9860	10240	10240	9870	9700	9200	8360	7700	6810	5680	4690	3630	2510
N	1400	3450	4450	3230	6530	7360	4810	8850	9330	5700	9870	9870	5700	9340	8870	4820	7390	6550	3240	4470	3470	1400
O	2290	3310	4310	5250	6350	7210	7850	8680	9170	9340	9700	9710	9350	9180	8690	7870	7220	6370	5270	4320	3320	2300
P		3120	3970	4890	5940	6780	7420	8210	8690	8870	9210	9210	8880	8700	8220	7440	6790	5950	4900	3980	3130	
Q		2700	3410	2530	5280	6060	4000	7440	7880	4830	8380	8380	4830	7890	7450	4000	6070	5290	2540	3420	2710	
R			2940	3720	4700	5480	6080	6810	7250	7420	7730	7730	7420	7260	6820	6090	5490	4710	3730	2950		
S			2350	3070	3980	4730	5330	5990	6410	6590	6860	6860	6590	6410	6000	5330	4730	3980	3080	2350		
T				1400	3120	3790	2570	4960	5330	3270	5730	5730	3270	5330	4970	2570	3790	3120	1400			
U					2430	2990	3510	4060	4390	4530	4750	4750	4530	4390	4070	3510	3000	2440				
V						2300	2790	3230	3400	3520	3690	3690	3520	3400	3240	2790	2300					
W									2360	1430	2550	2550	1430	2370								

(c) 6D

	1	2	3	4	5	6	7	8	9	10	11	12	13	14	15	16	17	18	19	20	21	22
A									2336	1822	2555	2557	1826	2345								
B						2189	2650	3087	3294	3461	3607	3609	3468	3307	3105	2673	2216					
C					2360	2897	3417	3933	4277	4463	4648	4651	4472	4293	3957	3447	2935	2407				
D				1735	3026	3696	3206	4842	5218	4089	5629	5632	4097	5238	4869	3233	3743	3087	1800			
E			2188	2959	3827	4573	5194	5808	6225	6452	6671	6675	6465	6248	5840	5236	4628	3897	3054	2340		
F			2797	3608	4538	5319	5956	6619	7060	7284	7533	7537	7298	7084	6653	5999	5375	4608	3695	2912		
G		2542	3297	3144	5144	5935	4976	7283	7732	6015	8224	8229	6025	7755	7315	5007	5988	5207	3196	3379	2630	
H		2968	3828	4761	5753	6587	7269	7983	8459	8702	8970	8974	8715	8482	8014	7309	6636	5809	4822	3892	3029	
J	2262	3209	4193	5148	6171	7023	7711	8450	8936	9175	9459	9463	9188	8957	8479	7747	7066	6219	5198	4243	3254	2297
K	1783	3395	4394	4044	6402	7246	5996	8688	9169	7109	9697	9701	7118	9188	8713	6020	7282	6442	4074	4434	3429	1802
L	2508	3549	4587	5572	6622	7494	8197	8953	9450	9694	9983	9986	9704	9466	8975	8224	7526	6656	5606	4619	3577	2529
M	2512	3555	4593	5579	6629	7500	8202	8957	9453	9696	9985	9988	9705	9468	8976	8225	7526	6657	5607	4620	3577	2529
N	1792	3412	4414	4058	6420	7262	6007	8700	9180	7116	9704	9707	7122	9192	8717	6022	7285	6443	4075	4435	3430	1802
O	2287	3241	4228	5182	6203	7051	7735	8471	8954	9190	9471	9473	9196	8964	8484	7751	7069	6222	5200	4245	3255	2298
P		3019	3880	4810	5797	6625	7301	8010	8482	8721	8986	8987	8726	8490	8022	7315	6640	5812	4825	3894	3031	
Q		2623	3371	3190	5199	5981	5004	7315	7759	6031	8242	8244	6035	7766	7324	5012	5993	5211	3199	3381	2632	
R			2906	3689	4603	5371	5998	6654	7089	7308	7553	7554	7311	7095	6662	6006	5381	4612	3698	2914		
S			2336	3051	3894	4626	5236	5843	6254	6476	6691	6692	6479	6259	5849	5243	4633	3901	3057	2342		
T				1798	3085	3743	3234	4874	5245	4105	5647	5648	4107	5249	4878	3238	3748	3090	1802			
U					2407	2935	3449	3961	4300	4482	4664	4665	4484	4303	3964	3453	2939	2411				
V						2217	2675	3109	3313	3477	3620	3621	3478	3315	3112	2678	2220					
W									2350	1830	2565	2565	1831	2351								

(d) 4F

Figure 5.35: Initial radial distribution powers for Core A at start-up. Values are in kW.

From the four figures, it can be seen that the target channels will have a lower power due to the lack of fissile elements in the target bundles. For example, the twelve bundle loading in the target channel will generate a power of only 2.3 kW from gamma ray emissions when thorium absorbs a neutron. By loading SEU bundles along with the thorium bundles, the power increases, but is still lower than the driver channels.

Maximum channel power occurs at the centre of the core, and in all cases, the power generated is above 10000 kW, which is far beyond the imposed safety design limits. All channels in the inner region also surpass the set channel power safety limits. Powers rapidly decrease as channel location is further away from the centre with a larger disparity in power generated between the centre channels and peripheral channels. Comparing to the SEU model, it also has maximum channel powers at the centre of the core, but at a lower power of 9566 kW as shown in Figure 5.6c. Intuitively, it was thought that the inclusion of thorium bundles would decrease the powers in the surrounding driver channels. On the contrary, the powers increased and can be attributed to the microscopic cross-sections in the different bundles; the microscopic absorption cross-section for thorium is lower than that of U-235. Therefore, from the SEU model to the core A model, the addition of thorium bundles shifts some of the neutron flux from the target channels into the driver channels, thereby causing the SEU bundles to generate more power. As burnup progresses, U-233 content increases, which then increases the macroscopic cross-section of the thorium bundle. At the same time, the SEU bundles burn some of the U-235, lowering its macroscopic cross-section,

leading to a balancing effect in the powers seen in the time-average power distributions. Also, as a consequence of the thorium bundles producing nearly zero power, the driver channels must produce more energy in order to compensate for the missing power in the target channels so that the total thermal output of the core is still achieved.

The powers generated in the initial startup of a dual fuel mode core warrants a serious consideration to implement solutions to counteract these levels of power. The use of DU is one possible way of derating the channel powers, as it is done in the startup of a NU CANDU core.

5.4 Core Configuration B

From the results of Core A, the heterogeneous design can be refined to produce a more optimized power profile. In Core A, the most outer periphery target channels sees the lowest neutron flux due to leakage, and by having target channels located there will only further lower the surrounding channel powers. The result will force the rest of the non-periphery channels to ramp up in order to produce more power to compensate for the loss as well as to create a more significant power difference between the inner and outer region channels. Then, to improve the core radial power profile, the periphery target channels are replaced with SEU channels; this will increase the power produced in the outer region and flatten the inner region of the core. This new configuration will be Core B which is shown in Figure 5.36.

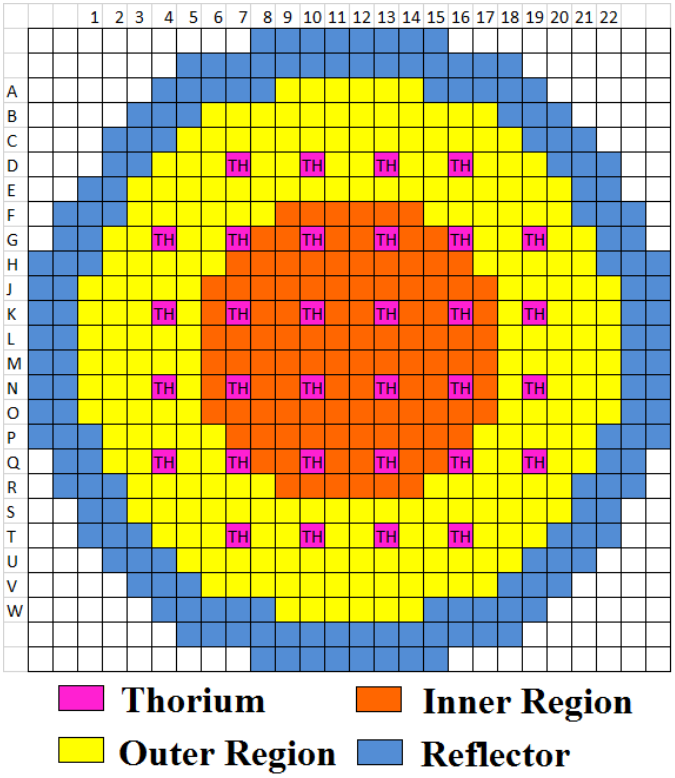

Figure 5.36: Core B configuration

Table 5.16: Key parameters for Core B diffusion model

Parameters	Values
Total Thermal Power	2061.4 MW
SEU Channels	348
Target Channels	32
SEU Bundle/Refuelling Shift	2

5.4.1 Time-Average Results

The target channel configuration for Core B will be the same as the ones used in the time-average models for Core A: 12Th, 8C, 6D, and 4F. Following a similar procedure, Core B will be modelled using the three different channel configurations with either the 12-bundle shift or the respective bundle shift schemes for each case to evaluate the effect on axial power profiles, bundle burnup, and core k-effective.

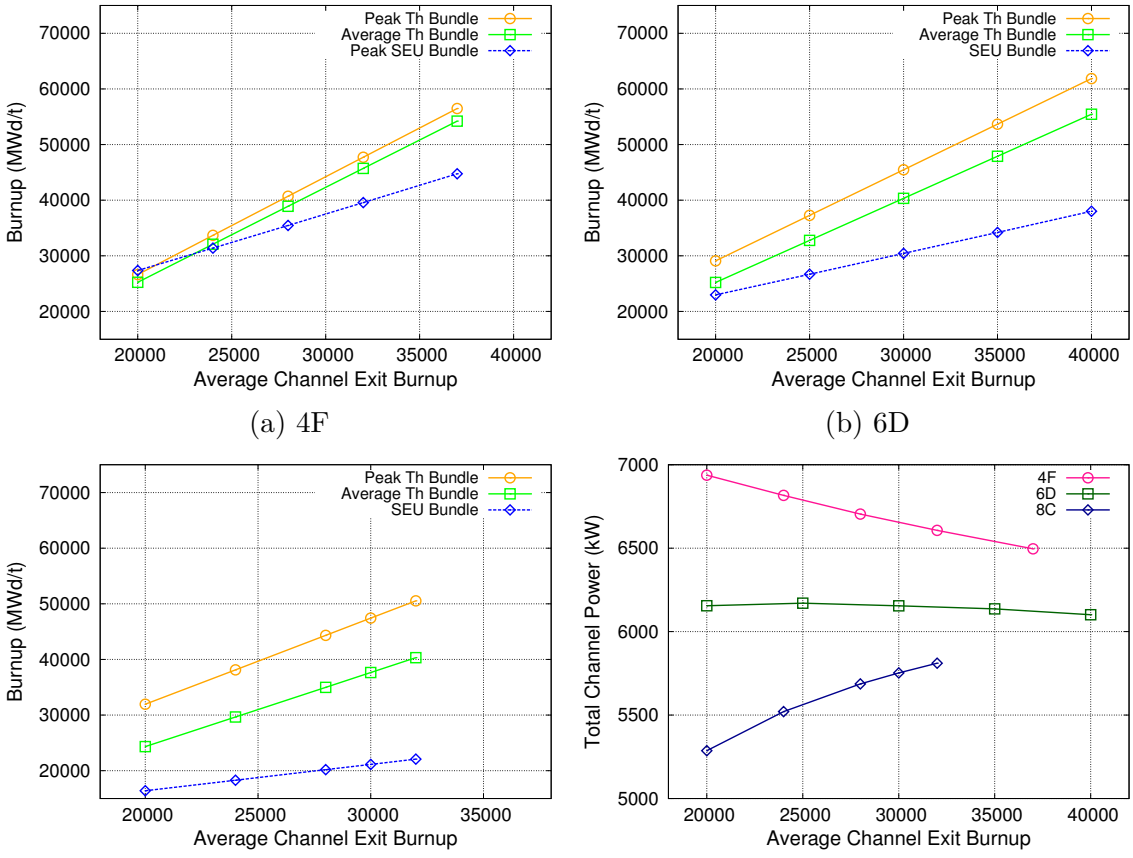

(a) 4F (b) 6D

(c) 8C (d) Total Channel Power

Figure 5.37: Highest individual bundle burnup and total channel powers for Core B using a 12-bundle shift

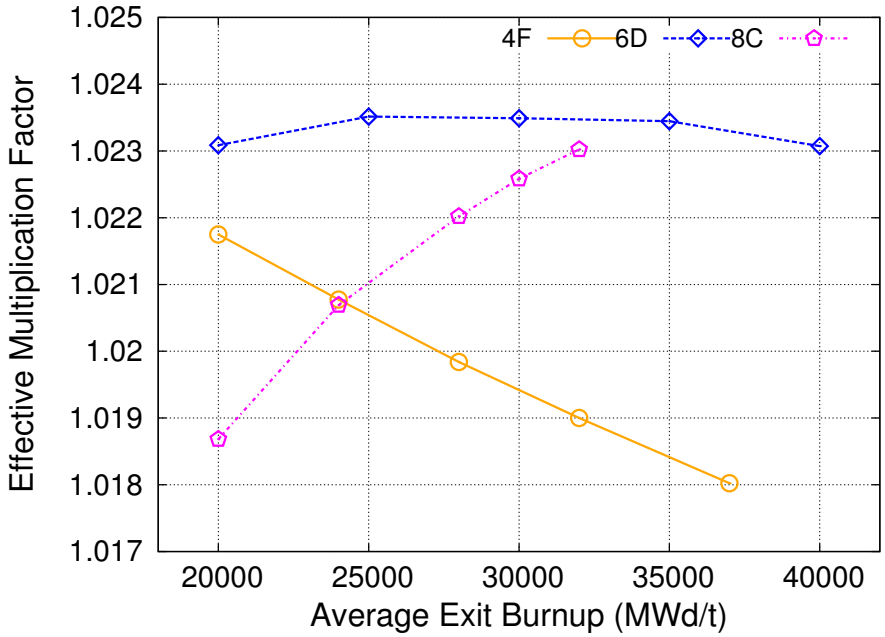

Figure 5.38: k_{eff} for varying average exit burnup in target channels using a 12-bundle shift

Figure 5.37 shows the highest individual burnup found for each type of fuel bundle in the channel. At a specified channel average exit burnup, the highest individual burnup for a thorium bundle is found in the 8C configuration, followed by the 6D and 4F case. It is the reverse for the highest burnups for SEU bundles. The highest bundle burnup is directly related to the number of SEU and thorium bundles present in the channel. The 4F configuration is closer to a "burning" stage where the neutron flux is directed more towards the SEU bundle due to the higher macroscopic cross-section of U-235. As the more SEU bundles are replaced with thorium bundles, the neutron flux is directed more towards the latter, resulting in increased breeding and subsequent burnup of U-233.

A similar core k_{eff} behaviour found in the modelling of Core A is also seen in Figure 5.38 for Core B. The 8C configuration shows an increase in reactivity with higher target channel average exit burnups. In the 6D case, a maximum k-effective is found for an average exit burnup of 25 GWd/t. Lastly, the 4F case has a continued decrease in reactivity for higher burnups. The result is due to the number of thorium and SEU bundles used. Thorium bundles contribute to the increase core k-effective for higher average exit burnups in the target channel because of the breeding of more fissile elements. The opposite is observed for SEU bundles since it is mainly a consumer of fissile elements. In the 6D case, since there are an equal number of thorium and SEU bundles used, a high or low average exit burnup will favor the one type of bundle and so a maximum is observed.

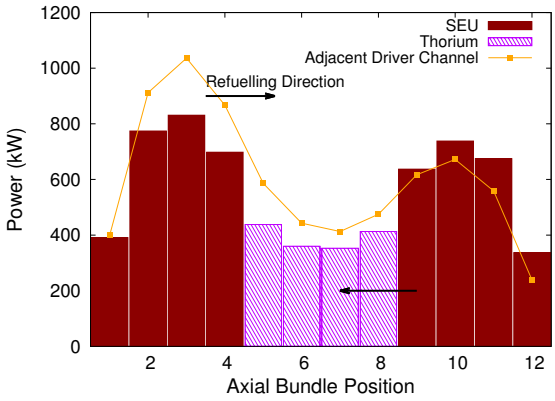

(a) 4F

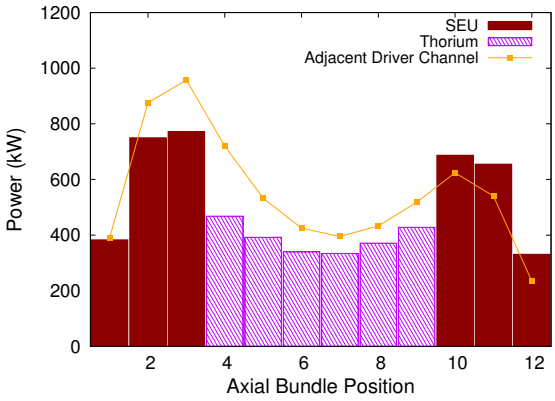

(b) 6D

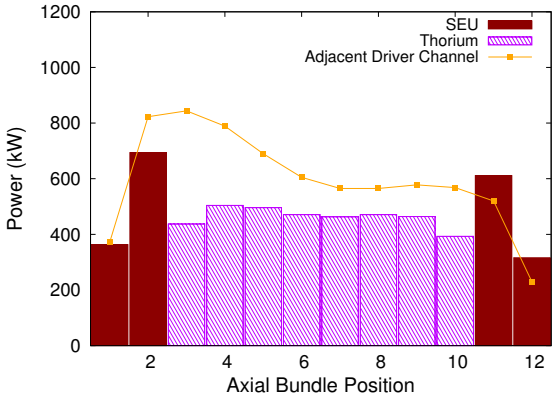

(c) 8C

Configuration	Power (kW)
4F	6185
6D	5911
8C	5682

Figure 5.39: Bundle powers for 4F, 6D, and 8C configurations with a 12-bundle shift scheme

In Figure 5.39, the axial power profiles are shown for the three channel configurations using a 12-bundle shift. As previously seen, the thorium bundles are generally producing lower levels of power compared to the SEU bundles. A 12-bundle shift will cause a slight power tilt in the axial direction when looking at the target channel and its adjacent driver channels. The fresh SEU bundles at each end of the channel will result in higher bundle powers at those positions, especially at positions 1-3 with the adjacent channels since those positions are also occupied by fresh SEU bundles. To avoid overpowering, a bundle shift scheme of eight, nine, and ten will be used for 4F, 6D, and 8C, respectively. This shifting scheme will allow the remaining SEU bundles, after a refuelling event, to shift downwards to the end of the refuelling channel, therefore lowering the bundle powers by balancing the axial powers amongst the adjacent channels and also utilizing the SEU bundles to its potential.

Using a bundle shift scheme of less than 12 bundles lowers the individual burnups of each bundle, especially the thorium bundles (refer to A). The target channel is evaluated for various average exit burnups for the specific channel configuration to determine what value maximizes the burnup of the thorium bundles and to see that no bundles exceed the 40 GWd/t burnup limit.

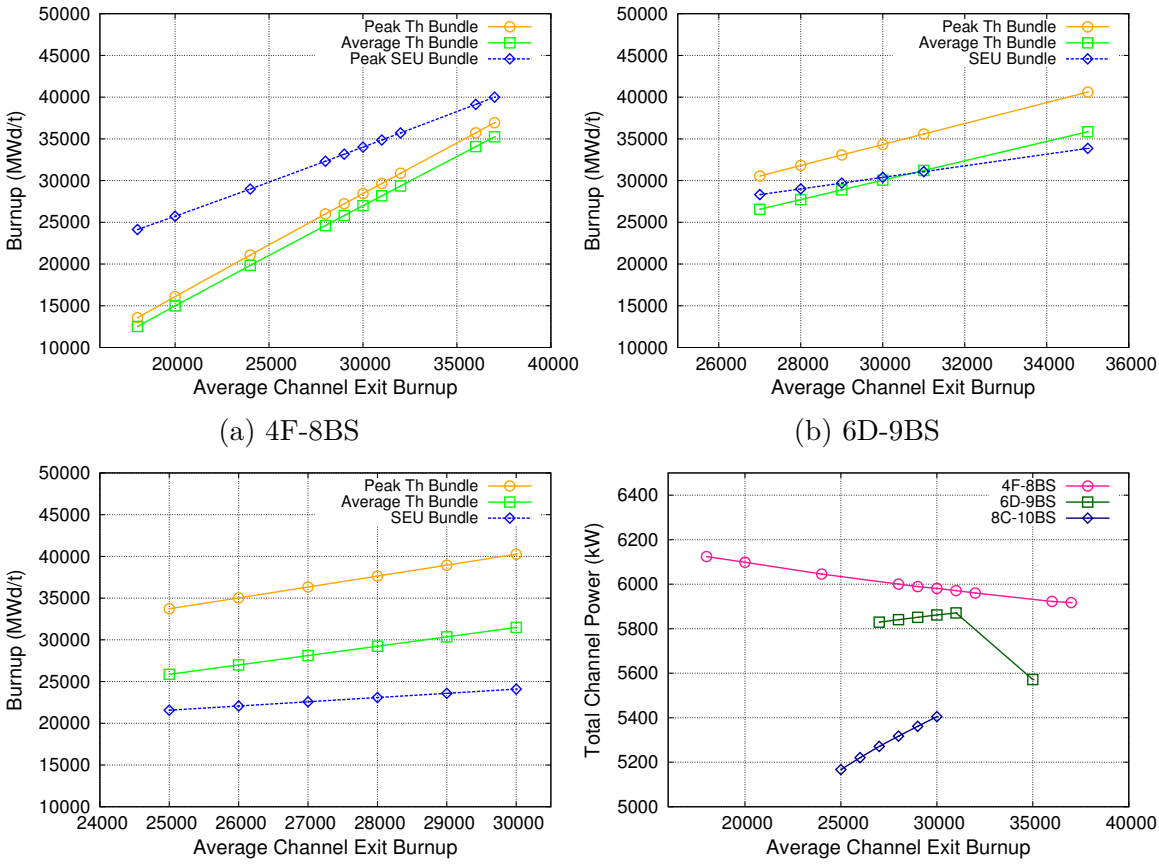

(a) 4F-8BS (b) 6D-9BS

(c) 8C-10BS (d) Total Channel Power

Figure 5.40: Highest individual bundle burnup and total channel powers for Core B using a different refuelling schemes

With increasingly more thorium bundles in the configuration, the average exit burnup of the target channel can be higher. Figures 5.40b and 5.40c show that a thorium bundle will attain the highest individual burnup. However, at a specific channel average exit burnup, the individual burnup of the thorium bundles decrease with more SEU bundles in the mix. Adding more SEU bundles into the configuration increases the overall macroscopic cross-section and diverts neutrons from being absorbed by thorium, and thus lowering the breeding and burnup. Furthermore, the SEU bundles will begin burning immediately, but the rate of the burnup increments is dependent on the location of the bundle. In the case of configurations 6D and 8C, the thorium

bundle increases in burnup faster than the SEU bundle because the latter is located further away from the centre of the channel. However, for the 4F case, it is the SEU bundle that burns up faster because it has replaced the thorium bundle at position four in the channel. Refer to Tables A.10 to A.15.

The average exit burnups for the 6D and 8C configuration can be chosen to be 30 GWd/t and 35 GWd/t, respecitvely; however, the 4F configuration will require a lower average exit burnup. By setting a high channel average exit burnup, the exiting SEU bundles will have dwell times far beyond its capacity to keep the core critical and will prove more of a neutron absorber. However, it is desirable to have higher burnups to benefit the thorium bundles. Looking at Table A.13 for bundle burnups from varying average exit burnups, the thorium bundle will have burnups lower than the exit channel burnup. A target channel average exit burnup was chosen to be 28 GWd/t to have thorium bundles with a longer burnup, but the problem would be the SEU bundles reaching a burnup of 30 GWd/t.

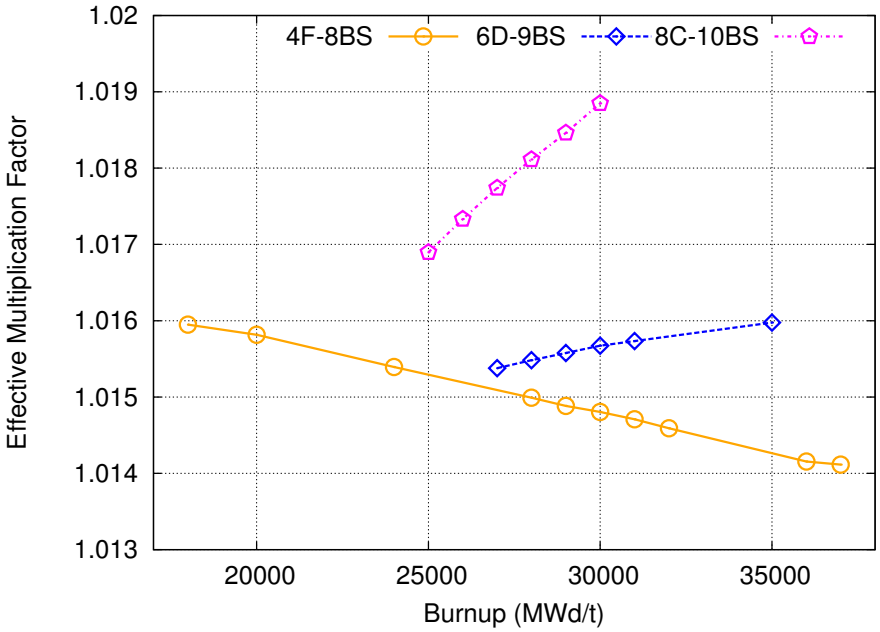

Figure 5.41: Core k_{eff} for varying average exit burnup in target channels for different refuelling schemes

Figure 5.41 shows the effective multiplication factor for varying average exit burnups for the target channels. For the 6D and 8C channel configuration, the core reactivity increases, mainly due to the high U-233 content produced as a result of a higher burnup. However, the 4F configuration's k-effective decreases with increasing average exit burnup because the majority of the bundles in the target channels are composed of SEU bundles located at the ends of the channel. Neutron leakage prevails at those loca-

tions and the thorium bundles are inadequate at compensating for the loss in neutron population. The higher burnup results in an increasingly depleted SEU bundle. Furthermore, in Figure 5.41, the bundle with the highest burnup of above 30 GWd/t is an SEU bundle. A typical SEU bundle would be discharged with a burnup of around 21.5 GWD/t based on the SEU core model in Section 5.1.2. A burnup discharge of over 30 GWd/t would suggest the bundle is strong neutron absorber due to large a build of FPs.

The resulting axial power distribution for one of the target channels (K10) is shown in the Figures 5.42a-5.42c. Compared to the 12 bundle-shift figures in Section 5.3.1.3, the power tilt is seen to occur at opposite ends for the target channel and the adjacent channel. The SEU bundles left over from a refuelling shift would have a lower fissile content, allowing for a lower bundle power profile at those positions after refuelling. As a result, the larger peak power from the compounding effect of fresh bundles in both target and driver channels is avoided.

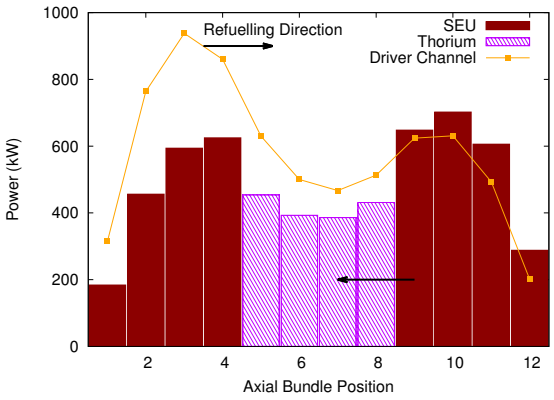

(a) 4F-8BS

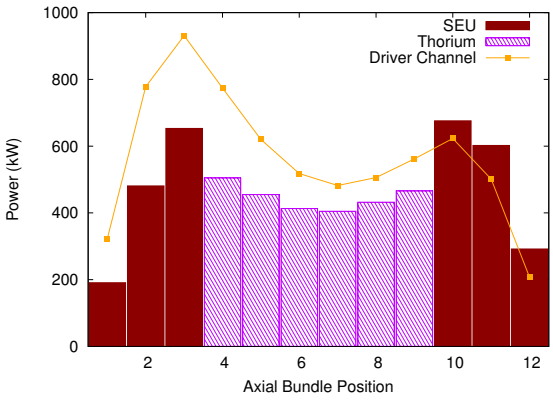

(b) 6D-9BS

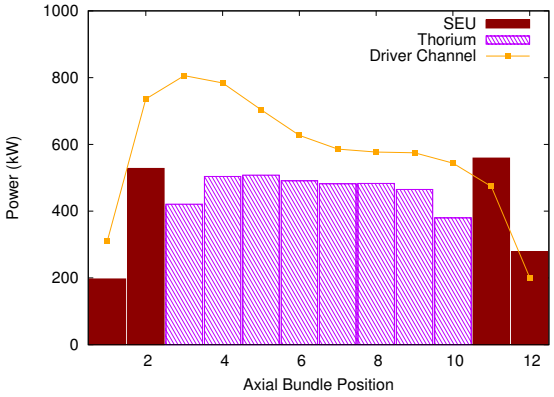

(c) 8C-10BS

Table 5.17: Channel Powers

Configuration	Power (kW)
4F-8BS	5767
6D-9BS	5571
8C-10BS	5297

Figure 5.43: Bundle powers for 4F, 6D, and 8C configurations with different bundle shift schemes

Total channel power drops for the different bundle shift schemes used. A 12-bundle shift produces more power because of more fresh SEU bundles present. For the channel configurations using 8, 9, or a 10-bundle shift schemes, the total channel power drops. That is less fresher bundles contribute to the channel power. The same conclusion can be used for the drop in power for varying channel configuration.

Table 5.18: Time-averaged results for Core B

Target Channel Configuration	Burnup (GWd/t)		Peak Power (kW)		
	Average	Target Channel	Channel	Bundle	RFF
12 Th	17.48	22	6961 [M12]	870 [N12-B5]	0.779
8C-12BS	18.32	25	6647 [M12]	788 [N12-B3]	0.816
6D-12BS	19.52	26	7197 [M12]	1029 [N12-B3]	0.753
4F-12BS	20.38	28	7249 [M12]	1039 [N12-B3]	0.748
8C-10BS	18.38	30	6650 [M12]	774 [N12-B3]	0.815
6D-9BS	19.28	35	6897 [M12]	935 [N12-B3]	0.787
4F-8BS	19.61	28	7094 [M12]	985 [N12-B3]	0.765

The resulting time-average peak powers are shown in Table 5.18. The peak powers are below the licensing limits of 8.3 MW for channel power with about a 15% margin. In contrast, the peak bundle powers come too close to the safety limit of 950 kW, with the 8C-12BS configuration with the lowest value of 788 kW [39]. Bundle powers are seen to increase because of more SEU bundles used in the configuration. Radial form factor is the ratio between the average channel power and the peak channel power which describes the flatness of the core. In all configurations, the RFF values are similar. Comparing the RFF values of Core A, the RFF value of Core B is higher and flatter as a result of increasing channel powers in the outer region of the core. Also, when compared with the NU- and SEU CANDU core, the RFF of Core B is higher, meaning a flatter core is produced even without adjuster rods.

With the new core configuration, the overall radial power distribution flattens out with the outer fuel channels having an increased in power while the central channels have lowered. Target channel powers still remain lower than driver channel powers. Overall, the time averaged model for Core B shows a flatter and centred power distribution. Furthermore, the jagged radial power seen has lessened when compared to Core A.

A jagged power form is still observed across a row of channels as seen in Figure 5.45. The change in core configuration did not affect this profile, but applying bundle shift schemes of 8, 9, and 10 for the respective channel configurations will increase these drops.

	1	2	3	4	5	6	7	8	9	10	11	12	13	14	15	16	17	18	19	20	21	22
A									3840	4101	4314	4322	4119	3872								
B						3198	3710	4426	4800	5153	5364	5371	5179	4840	4483	3775	3280					
C					3538	3772	4367	4870	5316	5558	5771	5781	5585	5366	4934	4453	3873	3675				
D				3576	4195	4621	3206	5511	5791	3827	6176	6184	3847	5845	5589	3270	4752	4357	3794			
E			3203	4075	4998	5232	5663	6018	6279	6383	6551	6563	6417	6340	6101	5775	5372	5185	4296	3510		
F			3572	4438	5166	5711	5986	6338	6364	6449	6573	6583	6485	6422	6424	6096	5855	5334	4640	3803		
G		3476	4096	3089	5551	5941	3962	6322	6471	4243	6632	6643	4265	6529	6400	4029	6072	5708	3199	4282	3665	
H		4140	4649	5322	5898	6260	6291	6520	6631	6677	6781	6791	6710	6684	6596	6386	6383	6036	5474	4802	4295	
J	3630	4582	5103	5626	6146	6279	6420	6611	6728	6751	6857	6867	6780	6778	6679	6509	6385	6271	5758	5239	4712	3739
K	3929	4947	5375	3726	6258	6354	4204	6643	6737	4397	6859	6867	4414	6781	6705	4254	6450	6365	3799	5492	5064	4023
L	4147	5177	5593	6022	6423	6477	6565	6741	6835	6851	6948	6956	6874	6875	6795	6635	6560	6519	6122	5697	5278	4233
M	4160	5190	5608	6035	6437	6488	6577	6749	6843	6857	6954	6961	6879	6879	6798	6638	6562	6521	6124	5698	5280	4234
N	3962	4992	5419	3754	6299	6394	4225	6673	6761	4411	6877	6883	4423	6793	6715	4260	6457	6371	3802	5496	5067	4026
O	3691	4655	5182	5701	6220	6342	6477	6658	6770	6785	6887	6892	6802	6797	6695	6523	6397	6282	5766	5246	4718	3743
P		4251	4757	5431	5997	6351	6364	6585	6685	6724	6821	6826	6739	6710	6618	6405	6400	6050	5485	4811	4302	
Q		3634	4251	3179	5681	6051	4022	6399	6540	4280	6681	6685	4288	6560	6427	4044	6092	5725	3207	4292	3672	
R			3781	4619	5316	5844	6093	6432	6441	6516	6629	6633	6527	6459	6457	6124	5879	5353	4655	3814		
S			3495	4282	5175	5368	5779	6115	6365	6455	6615	6618	6464	6381	6136	5805	5397	5207	4311	3522		
T				3786	4353	4753	3275	5607	5874	3873	6239	6242	3878	5887	5624	3288	4776	4377	3810			
U					3675	3878	4465	4955	5397	5628	5835	5837	5634	5407	4969	4481	3894	3693				
V						3287	3789	4505	4871	5221	5424	5426	5226	4879	4516	3801	3299					
W									3899	4154	4365	4366	4158	3905								

(a) 12Th-12BS

	1	2	3	4	5	6	7	8	9	10	11	12	13	14	15	16	17	18	19	20	21	22
A									3638	3866	4060	4068	3883	3669								
B						3108	3587	4278	4613	4946	5134	5140	4973	4651	4336	3650	3187					
C					3450	3737	4398	4843	5284	5539	5704	5716	5565	5335	4906	4485	3835	3581				
D				3476	4091	4670	3986	5585	5850	4731	6211	6218	4756	5902	5665	4065	4801	4245	3684			
E			3128	3978	4935	5253	5757	6053	6304	6421	6538	6552	6454	6366	6134	5872	5389	5117	4187	3422		
F			3551	4488	5188	5777	6072	6356	6295	6407	6462	6471	6445	6351	6444	6181	5922	5352	4687	3773		
G		3375	4132	3842	5642	6028	4911	6273	6395	5184	6507	6520	5212	6454	6349	4994	6157	5801	3976	4315	3554	
H		4007	4633	5395	5936	6278	6243	6374	6442	6513	6550	6557	6547	6493	6450	6336	6403	6072	5549	4782	4156	
J	3442	4412	5078	5690	6171	6213	6344	6422	6503	6550	6586	6598	6577	6554	6488	6434	6317	6298	5820	5213	4535	3545
K	3710	4754	5365	4609	6298	6314	5136	6479	6537	5293	6615	6621	5313	6578	6542	5199	6410	6404	4699	5479	4866	3797
L	3907	4961	5534	6061	6412	6369	6441	6510	6565	6607	6634	6643	6629	6606	6562	6512	6450	6510	6161	5637	5057	3989
M	3920	4972	5550	6072	6428	6379	6455	6517	6575	6612	6641	6647	6635	6608	6567	6514	6453	6511	6163	5638	5059	3989
N	3740	4798	5406	4643	6337	6355	5163	6510	6559	5309	6631	6639	5324	6591	6551	5206	6417	6412	4703	5483	4869	3800
O	3500	4480	5156	5763	6246	6274	6402	6467	6546	6582	6617	6622	6600	6572	6505	6447	6330	6308	5829	5219	4541	3548
P		4114	4738	5507	6032	6371	6314	6440	6494	6562	6588	6593	6575	6519	6471	6356	6419	6087	5560	4791	4162	
Q		3524	4284	3952	5774	6136	4984	6348	6465	5231	6558	6561	5241	6484	6377	5013	6179	5818	3986	4325	3561	
R			3751	4667	5334	5910	6178	6452	6370	6476	6518	6522	6486	6389	6476	6210	5945	5372	4702	3784		
S			3407	4173	5107	5385	5875	6149	6391	6493	6604	6607	6503	6407	6171	5901	5414	5138	4203	3433		
T				3677	4241	4802	4072	5684	5932	4788	6274	6278	4795	5946	5701	4087	4825	4264	3699			
U					3581	3840	4497	4927	5365	5608	5769	5771	5615	5375	4941	4512	3856	3598				
V						3194	3663	4356	4681	5012	5191	5193	5017	4690	4367	3674	3206					
W									3694	3916	4109	4110	3920	3700								

(b) 8C-12BS

	1	2	3	4	5	6	7	8	9	10	11	12	13	14	15	16	17	18	19	20	21	22
A									3256	3441	3606	3613	3453	3281								
B						2856	3282	3917	4203	4500	4660	4664	4521	4231	3963	3331	2920					
C					3187	3507	4187	4588	5013	5267	5400	5410	5287	5055	4637	4259	3586	3295				
D				3210	3797	4483	4271	5439	5713	5120	6074	6079	5142	5754	5506	4342	4592	3921	3386			
E			2904	3702	4663	5084	5669	5983	6272	6428	6531	6544	6453	6324	6048	5765	5194	4813	3875	3158		
F			3361	4324	5030	5694	6077	6405	6408	6580	6622	6628	6612	6453	6479	6165	5814	5164	4493	3548		
G		3121	3961	4137	5571	6041	5528	6467	6655	5991	6822	6835	6016	6706	6529	5603	6146	5704	4259	4115	3268	
H		3694	4420	5280	5888	6340	6443	6643	6774	6914	6947	6952	6944	6815	6707	6519	6444	5998	5408	4540	3814	
J	3100	4048	4846	5587	6163	6342	6613	6758	6909	7028	7060	7071	7049	6952	6811	6689	6426	6267	5690	4954	4143	3181
K	3323	4352	5133	5014	6330	6504	5948	6886	7017	6319	7168	7172	6338	7050	6940	6005	6584	6415	5092	5221	4438	3389
L	3492	4532	5269	5958	6431	6548	6769	6915	7043	7162	7186	7195	7178	7078	6957	6829	6612	6510	6035	5349	4603	3552
M	3503	4540	5284	5966	6446	6555	6783	6919	7053	7164	7193	7197	7184	7079	6961	6829	6616	6510	6038	5350	4604	3552
N	3348	4389	5166	5045	6362	6540	5974	6914	7034	6334	7180	7187	6348	7062	6946	6011	6588	6421	5096	5225	4439	3391
O	3149	4103	4913	5646	6228	6392	6663	6794	6946	7053	7087	7090	7069	6966	6825	6698	6436	6274	5698	4959	4147	3183
P		3785	4508	5376	5968	6419	6502	6699	6816	6956	6977	6982	6965	6837	6723	6535	6455	6010	5415	4547	3818	
Q		3247	4093	4239	5683	6129	5595	6528	6714	6033	6865	6867	6042	6729	6552	5619	6163	5715	4267	4122	3274	
R			3532	4477	5150	5805	6162	6484	6468	6637	6665	6669	6644	6483	6502	6187	5831	5178	4503	3556		
S			3148	3865	4805	5191	5768	6059	6343	6483	6584	6585	6492	6354	6076	5786	5213	4826	3886	3166		
T				3380	3918	4592	4348	5520	5777	5169	6122	6125	5175	5788	5532	4361	4608	3935	3396			
U					3295	3589	4268	4653	5076	5319	5449	5450	5324	5083	4663	4278	3601	3307				
V						2925	3340	3977	4253	4549	4701	4703	4552	4259	3984	3349	2933					
W									3298	3476	3641	3642	3479	3302								

(c) 6D-12BS

	1	2	3	4	5	6	7	8	9	10	11	12	13	14	15	16	17	18	19	20	21	22
A									3130	3297	3451	3457	3307	3153								
B						2782	3193	3805	4072	4354	4503	4507	4374	4098	3848	3239	2842					
C					3110	3463	4151	4540	4959	5208	5332	5342	5227	4999	4588	4220	3537	3212				
D				3129	3713	4456	4450	5429	5704	5336	6059	6063	5358	5743	5494	4521	4559	3829	3296			
E			2841	3624	4587	5070	5678	5994	6287	6445	6544	6556	6469	6337	6057	5770	5174	4728	3787	3084		
F			3331	4305	5019	5707	6108	6437	6432	6608	6645	6650	6640	6475	6507	6192	5822	5147	4467	3511		
G		3051	3939	4318	5584	6074	5806	6503	6694	6291	6861	6873	6317	6743	6562	5881	6175	5712	4441	4087	3191	
H		3600	4386	5280	5907	6376	6481	6680	6814	6960	6988	6993	6989	6853	6742	6553	6475	6012	5403	4501	3712	
J	2988	3933	4805	5588	6186	6372	6655	6799	6954	7080	7108	7118	7100	6996	6850	6728	6452	6286	5687	4908	4021	3062
K	3192	4221	5087	5234	6355	6538	6249	6934	7070	6646	7224	7228	6664	7102	6985	6307	6615	6436	5312	5170	4300	3252
L	3350	4389	5214	5953	6452	6577	6812	6958	7092	7218	7239	7247	7234	7125	6999	6869	6638	6527	6026	5289	4454	3405
M	3360	4397	5228	5961	6467	6584	6825	6963	7101	7221	7246	7249	7240	7127	7002	6869	6641	6528	6028	5289	4455	3405
N	3215	4255	5119	5266	6386	6573	6275	6961	7086	6660	7235	7242	6675	7113	6991	6312	6619	6442	5316	5174	4302	3254
O	3034	3985	4869	5645	6248	6419	6703	6833	6989	7104	7133	7136	7119	7009	6863	6736	6462	6292	5694	4912	4025	3064
P		3686	4471	5373	5984	6452	6537	6734	6854	7000	7017	7022	7009	6873	6757	6569	6487	6023	5410	4507	3716	
Q		3171	4066	4421	5692	6159	5873	6561	6750	6333	6902	6903	6342	6764	6584	5897	6191	5723	4449	4093	3196	
R			3496	4452	5134	5814	6189	6512	6489	6663	6686	6689	6670	6504	6530	6213	5838	5160	4476	3518		
S			3075	3778	4721	5171	5772	6067	6355	6497	6594	6595	6506	6366	6083	5790	5192	4741	3797	3091		
T				3291	3826	4560	4526	5506	5765	5384	6104	6107	5390	5775	5518	4539	4575	3842	3305			
U					3212	3540	4227	4602	5019	5256	5378	5379	5262	5026	4611	4237	3551	3222				
V						2846	3247	3861	4118	4399	4540	4542	4402	4124	3867	3255	2853					
W									3168	3329	3483	3483	3331	3172								

(d) 4F-12BS

Figure 5.44: Examples of time-average power distributions for Core B. Values are in kW

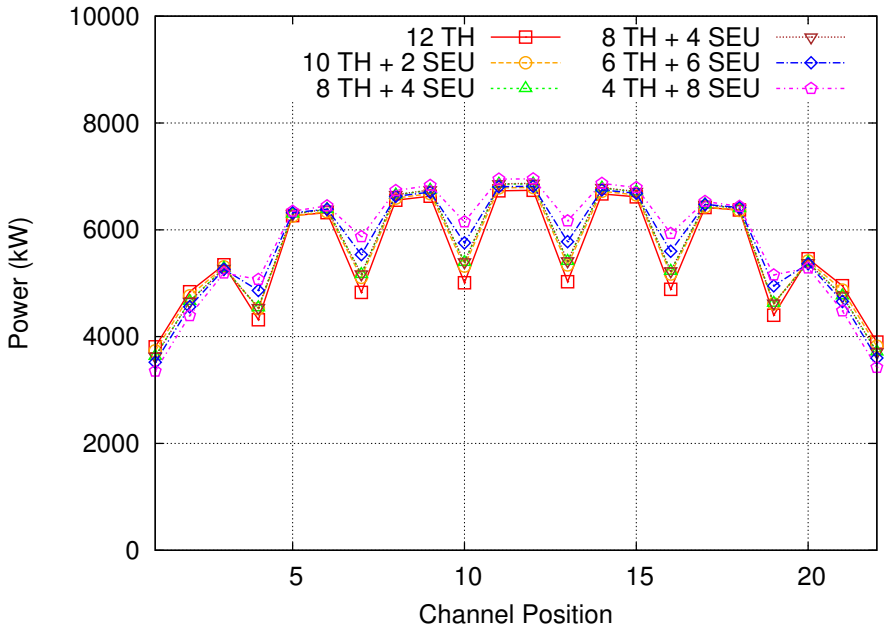

Figure 5.45: Radial power distribution for channel row K in Core B

5.4.2 Instantaneous Results

The age pattern distribution in the modelling of Core A produced a radial tilt, and thus a modified distribution was developed to address the issue. The age pattern map has been described and can be found in Chapter 5.3.3. This modified age map shows all the target channels to have the same rank for refuelling since the instantaneous power maps from Core A show that thorium channels having various burnups amongst each other can cause a tilt in the radial power distribution. Moreover, the different rankings between the all target channels cause different power variances and differences between its adjacent driver channels. The age pattern was developed by redirecting the refuelling of a target channel to the channel after the target channel with all the latter refuelled at the end. For example, if the refuelling sequence was E16-V9-L10 and the target channel was V9, then the sequence would be E16-L10-P15 where P15 is after L10; V9 would be refuelled last along with the other target channels. This method only approximates the radial power distribution for target channels aged simultaneously and may not be a true representative of a real age map for a dual fuel core and requires further development.

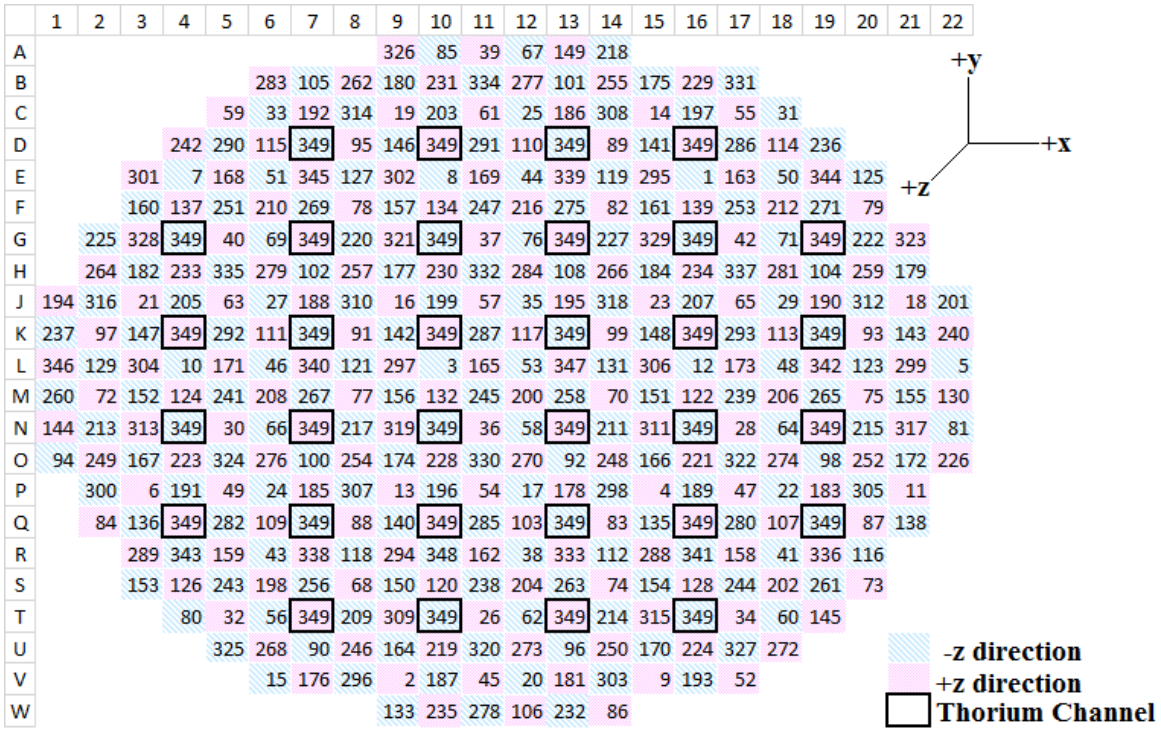

Figure 5.46: Modified age pattern distribution map for Core B

Table 5.19: Instantaneous results for Core B

Target Channel Configuration	k-effective	Peak Power (kW) Channel	Bundle	CPPF	BPPF
12 Th	1.0322182	7623 [L10]	968 [L10-B4]	1.458	2.371
8C-12BS	1.0257607	6880 [P12]	804 [L10-B4]	1.161	1.507
6D-12BS	1.0148542	7013 [P12]	841 [L10-B3]	1.166	1.710
4F-12BS	1.0008592	6999 [P12]	852 [L10-B3]	1.223	1.746
8C-10BS	1.0269308	6965 [P12]	827 [L10-B4]	1.192	1.523
6D-9BS	1.014985	6932 [P12]	815 [L10-B4]	1.108	1.537
4F-8BS	1.0147436	6977 [P12]	841 [P15-B9]	1.144	1.599

With the new age pattern distribution, the radial profile of Core B is more balanced than compared to the age map used for Core A. The target channel power differences are not as wide compared to the age pattern used for Core A, meaning that a tilt in the radial power is less likely thereby improving safety. Total power values are lower than that of Core A by at 8-15%. Similarly are the peak bundle powers by 12-36

.

The k_{eff} decreases as the number of SEU bundles used increases. This is due to the higher average exit burnup of the target channels compared to the driver channels. The

SEU bundles in the target channel stay in the core longer, resulting in the depletion of the majority of the fissile content which causes it to become a net absorber for neutrons.

The CPPF and BPPF is the highest for the 12 thorium bundle configuration since there is a higher channel and bundle power disparity when comparing the time-average to instantaneous models where the latter has an increase in channel and bundle powers. As such, the powers come from the aged target channels that contain enough U-233 to affect the adjacent channels by increasing its powers. The lowest CPPF is seen in the 6D configuration.

Powers in the target channel is seen to decrease as a result of lowering the number of thorium bundles used. Again, the higher average exit burnup in the target channels lowers the effectiveness of the SEU bundles to provide reactivity due to the lack of fissile content. With a lowered U-235 content, the power produced in the SEU bundles lowers.

	1	2	3	4	5	6	7	8	9	10	11	12	13	14	15	16	17	18	19	20	21	22
A									3281	3772	4036	4037	3774	3452								
B						2820	3459	3908	4381	4657	4770	4864	4876	4391	4127	3477	2893					
C					3301	3683	4070	4455	5219	5292	5671	5765	5361	4966	4927	4238	3813	3521				
D				3160	3815	4420	3988	5408	5717	4902	5947	6211	4922	5863	5533	4170	4459	4196	3408			
E			2785	3932	4653	5159	5239	5940	6008	6658	6556	6743	6138	6343	5873	5968	5273	5036	3858	3233		
F			3287	4186	4863	5453	5738	6355	6362	6574	6531	6553	6336	6529	6386	6132	5649	5129	4292	3642		
G		3038	3608	3790	5528	6005	5094	6222	6244	5593	7018	6964	5616	6458	6142	5211	6239	5743	4014	3984	3249	
H		3552	4266	4982	5529	6046	6430	6389	6707	6745	6709	6807	6994	6591	6606	6334	6131	5839	5424	4462	3936	
J	3084	3935	4906	5396	6203	6559	6497	6523	7218	7015	7374	7448	7021	6719	7113	6617	6656	6518	5672	4851	4543	3386
K	3322	4480	5077	4709	6080	6548	5592	7009	7133	6059	7093	7392	6038	7219	7050	5751	6452	6570	4902	5400	4767	3637
L	3414	4658	5077	6108	6390	6749	6429	7041	6934	7623	7402	7592	6941	7270	6877	7238	6776	6803	5840	5548	4786	4057
M	3516	4731	5258	5942	6298	6468	6538	7078	7139	7334	7260	7327	7114	7388	7139	7043	6679	6566	5950	5604	4944	3936
N	3471	4405	4883	4715	6469	6622	5573	6729	6716	6001	7548	7545	6099	7058	6763	5760	6933	6674	4923	5252	4559	3781
O	3285	4098	4818	5434	5895	6191	6659	6590	6891	6944	6932	7129	7358	6969	6948	6672	6318	6227	5861	4966	4422	3403
P		3721	4652	5202	6060	6554	6401	6409	7094	6890	7324	7489	7315	6795	7177	6585	6726	6354	5470	4549	4234	
Q		3400	4007	3928	5377	6109	5208	6564	6634	5622	6673	7105	5817	6952	6656	5313	6008	5847	4145	4289	3578	
R			3408	4127	5095	5817	5761	6373	6147	6161	6655	6932	6368	6596	6255	5825	5787	5422	4352	3761		
S			3161	4005	4722	5105	5432	6046	6158	6381	6397	6503	6261	6408	5997	5682	5135	4905	4017	3390		
T				3498	4197	4583	4034	5251	5423	4823	6264	6224	4878	5605	5187	4073	4678	4238	3534			
U					3194	3548	4214	4523	4996	5214	5284	5384	5400	4947	4636	4123	3518	3285				
V						3072	3464	3929	4616	4710	5089	5134	4757	4306	4265	3484	3073					
W									3486	3648	3788	3976	3672	3559								

(a) 12Th-12BS

	1	2	3	4	5	6	7	8	9	10	11	12	13	14	15	16	17	18	19	20	21	22
A									3397	3904	4171	4176	3911	3580								
B						2924	3606	4057	4551	4832	4948	5045	5061	4573	4293	3641	3014					
C					3408	3871	4266	4683	5441	5525	5898	5998	5604	5210	5175	4461	4025	3651				
D				3258	3969	4610	4463	5606	5922	5416	6136	6394	5450	6085	5762	4684	4683	4377	3533			
E			2880	4076	4796	5360	5416	6084	6109	6713	6599	6780	6234	6455	6056	6177	5514	5214	4034	3357		
F			3454	4361	5060	5611	5862	6362	6254	6400	6342	6366	6194	6434	6435	6282	5849	5363	4505	3841		
G		3162	3783	4232	5671	6102	5445	6053	5988	5730	6614	6574	5765	6209	6008	5604	6371	5930	4505	4191	3398	
H		3676	4458	5156	5655	6052	6234	6069	6284	6262	6204	6296	6497	6203	6296	6180	6177	5999	5631	4688	4087	
J	3178	4072	5091	5563	6249	6404	6200	6112	6638	6410	6686	6754	6428	6221	6667	6344	6535	6596	5874	5075	4706	3501
K	3424	4619	5266	5171	6117	6340	5703	6480	6507	5897	6384	6645	5890	6603	6545	5886	6286	6620	5408	5621	4934	3760
L	3518	4796	5266	6235	6392	6501	6059	6478	6297	6833	6611	6774	6261	6608	6361	6815	6558	6813	6014	5764	4952	4183
M	3620	4869	5444	6076	6307	6245	6159	6510	6474	6585	6489	6550	6407	6706	6588	6640	6466	6593	6119	5817	5108	4061
N	3576	4548	5081	5183	6486	6412	5690	6235	6145	5844	6768	6767	5941	6455	6286	5892	6726	6709	5426	5471	4724	3903
O	3381	4240	5010	5608	5968	6068	6353	6177	6350	6347	6298	6476	6710	6433	6508	6386	6205	6315	6049	5184	4581	3515
P		3849	4850	5378	6171	6534	6213	6087	6630	6380	6736	6880	6766	6367	6798	6391	6721	6481	5667	4768	4378	
Q		3530	4186	4386	5535	6211	5561	6368	6333	5746	6287	6683	5934	6635	6455	5681	6132	6016	4629	4485	3720	
R			3587	4310	5295	5963	5887	6374	6044	5998	6440	6685	6198	6462	6278	5957	5958	5630	4552	3951		
S			3263	4156	4866	5313	5600	6181	6238	6437	6427	6532	6320	6481	6138	5858	5353	5064	4178	3504		
T				3597	4352	4767	4510	5446	5629	5328	6425	6379	5383	5803	5394	4560	4875	4400	3645			
U					3300	3737	4405	4748	5212	5441	5503	5606	5618	5170	4860	4325	3711	3400				
V						3174	3610	4073	4784	4876	5258	5298	4927	4469	4416	3633	3183					
W									3598	3774	3912	4105	3795	3676								

(b) 8C-12BS

	1	2	3	4	5	6	7	8	9	10	11	12	13	14	15	16	17	18	19	20	21	22
A									3345	3858	4124	4129	3864	3530								
B						2877	3568	4001	4501	4777	4890	4989	5009	4521	4240	3600	2965					
C					3362	3862	4231	4670	5432	5499	5896	5997	5578	5194	5171	4427	4016	3605				
D				3208	3928	4580	4289	5589	5915	5216	6126	6394	5249	6080	5747	4504	4649	4339	3481			
E			2836	4042	4746	5365	5393	6108	6127	6739	6638	6824	6241	6484	6074	6173	5519	5167	3991	3313		
F			3443	4333	5059	5613	5863	6400	6316	6446	6413	6437	6232	6498	6471	6291	5853	5364	4472	3830		
G		3124	3748	4067	5664	6114	5259	6099	6036	5558	6694	6652	5592	6261	6049	5414	6385	5924	4332	4159	3358	
H		3627	4448	5136	5669	6083	6288	6148	6383	6345	6310	6406	6587	6297	6379	6228	6206	6019	5619	4678	4040	
J	3134	4022	5086	5553	6282	6473	6259	6207	6761	6510	6826	6894	6529	6327	6779	6402	6607	6633	5868	5063	4665	3458
K	3378	4572	5244	4981	6130	6392	5535	6575	6612	5751	6496	6770	5744	6712	6638	5713	6330	6648	5212	5603	4888	3715
L	3469	4746	5258	6238	6434	6582	6125	6598	6422	6962	6762	6930	6367	6743	6474	6902	6641	6863	6006	5764	4899	4142
M	3572	4822	5440	6078	6344	6320	6227	6632	6605	6709	6633	6698	6519	6846	6710	6724	6545	6636	6113	5817	5061	4016
N	3533	4497	5054	4994	6514	6463	5521	6318	6238	5700	6900	6895	5795	6556	6370	5720	6786	6739	5230	5449	4672	3862
O	3339	4193	4999	5601	5988	6131	6415	6276	6461	6449	6421	6610	6823	6550	6614	6449	6267	6345	6048	5175	4536	3472
P		3799	4849	5361	6205	6580	6270	6167	6747	6467	6870	7012	6874	6470	6902	6446	6774	6516	5658	4761	4338	
Q		3498	4157	4218	5520	6229	5376	6430	6392	5577	6356	6774	5762	6709	6511	5490	6136	6017	4456	4464	3687	
R			3575	4273	5302	5973	5890	6413	6105	6032	6520	6767	6242	6529	6312	5953	5969	5638	4523	3945		
S			3217	4121	4812	5318	5582	6211	6261	6461	6460	6573	6331	6516	6159	5850	5352	5016	4139	3465		
T				3548	4318	4738	4335	5423	5616	5132	6431	6378	5184	5789	5371	4383	4851	4363	3599			
U					3246	3725	4372	4739	5197	5418	5489	5599	5594	5157	4849	4292	3696	3351				
V						3131	3573	4017	4744	4821	5212	5247	4878	4417	4373	3593	3143					
W									3550	3729	3860	4061	3746	3635								

(c) 6D-12BS

	1	2	3	4	5	6	7	8	9	10	11	12	13	14	15	16	17	18	19	20	21	22
A									3354	3876	4145	4151	3881	3547								
B						2888	3584	4016	4521	4796	4910	5010	5037	4541	4265	3618	2980					
C					3381	3911	4267	4723	5501	5547	5970	6077	5627	5257	5243	4473	4071	3633				
D				3220	3943	4623	4138	5639	5965	5027	6170	6446	5060	6134	5805	4353	4696	4364	3501			
E			2843	4062	4768	5431	5428	6174	6178	6786	6695	6889	6268	6551	6138	6242	5590	5205	4007	3332		
F			3479	4369	5115	5670	5894	6449	6348	6451	6434	6457	6232	6534	6527	6337	5922	5430	4513	3877		
G		3130	3770	3919	5710	6155	5048	6095	6013	5309	6677	6636	5343	6248	6042	5202	6434	5981	4181	4195	3367	
H		3633	4493	5170	5718	6122	6290	6143	6372	6303	6285	6382	6554	6284	6382	6226	6251	6081	5671	4731	4057	
J	3139	4029	5141	5590	6338	6509	6243	6192	6745	6460	6798	6869	6479	6301	6779	6391	6647	6704	5914	5118	4688	3472
K	3381	4584	5281	4794	6153	6393	5285	6539	6565	5463	6432	6711	5457	6666	6605	5461	6331	6688	5022	5651	4910	3727
L	3470	4759	5306	6285	6480	6605	6091	6578	6384	6909	6718	6890	6299	6713	6452	6892	6667	6926	6042	5832	4916	4164
M	3575	4836	5494	6117	6388	6334	6195	6611	6571	6648	6586	6653	6454	6818	6693	6708	6567	6691	6154	5885	5083	4032
N	3539	4505	5082	4805	6549	6467	5271	6274	6179	5412	6844	6838	5505	6505	6329	5467	6802	6781	5039	5492	4686	3879
O	3347	4203	5049	5636	6032	6153	6402	6260	6434	6396	6381	6577	6778	6529	6607	6439	6294	6404	6100	5233	4556	3484
P		3807	4907	5399	6271	6633	6267	6159	6743	6423	6856	6999	6846	6458	6919	6446	6838	6594	5710	4816	4364	
Q		3511	4188	4065	5555	6269	5159	6431	6374	5322	6322	6756	5504	6705	6511	5272	6170	6075	4302	4510	3705	
R			3610	4300	5361	6037	5916	6455	6123	6014	6538	6787	6234	6557	6355	5979	6038	5710	4562	3994		
S			3227	4136	4828	5375	5616	6272	6307	6490	6499	6620	6350	6575	6215	5899	5410	5044	4155	3486		
T				3563	4337	4779	4178	5457	5647	4936	6478	6418	4988	5823	5407	4227	4902	4383	3620			
U					3254	3763	4407	4786	5247	5455	5537	5655	5633	5210	4899	4328	3733	3366				
V						3145	3584	4025	4764	4831	5233	5265	4894	4425	4396	3603	3161					
W									3559	3738	3865	4076	3753	3651								

(d) 4F-12BS

Figure 5.47: Examples of instantaneous radial power distributions for Core B. Values are in kW

5.4.3 Target Channel Refuelling

Similarly to the Core A in Chapter 5.3.4, a refuelling of the target channels was performed on different channel configurations. The model to be refuelled is the instantaneous power map.

Table 5.20: Instantaneous Core B characteristics after refuelling channel N16

Target Channel Configuration	k_{eff}	$\Delta\rho$	Peak Power (kW) Channel	Bundle	CPPF	BPPF
12Th-12BS	1.0151736	-17.045	8054 [E12]	1019 [L10-B4]	1.527	2.406
8C-12BS	1.0247066	-1.054	7242 [E10]	847 [E10-B4]	1.251	1.641
6D-12BS	1.0145190	-0.335	7020 [L10]	1119 [N16-B10]	1.169	1.711
4F-12BS	1.0093047	-0.00071	8274 [N17]	1485 [N16-B10]	1.302	1.985
8C-10BS	1.0257890	-1.142	7281 [E10]	861 [E10-B4]	1.297	1.659
6D-9BS	1.0142798	-0.0007	7468 [L10]	952 [N16-B3]	1.135	1.608
4F-8BS	1.0147417	-2E-06	7044 [L16]	1149 [N16-B3]	1.155	1.763

Firstly, one channel was chosen to be refuelled to examine the effect on the effective multiplication factor and is shown in the above table. Channel N16 was chosen to be refuelled. The resulting k_{eff} is compared to the k_{eff} of the instantaneous core in Table 5.19; the difference in reactivity is computed and shown in Table 5.20. The refuelling of

12 thorium bundles produced a lowered k_{eff} factor with a decrease of -8.1772 mk. By incorporating SEU bundles along with the thorium bundles, the change in reactivity increases, with the highest increase seen with the 4F channel configuration with the most SEU bundles.

	1	2	3	4	5	6	7	8	9	10	11	12	13	14	15	16	17	18	19	20	21	22
A									3593	4108	4359	4337	4027	3658								
B						3150	3864	4329	4831	5095	5184	5242	5217	4663	4340	3632	2981					
C					3697	4179	4594	5018	5806	5858	6204	6260	5781	5316	5214	4444	3947	3556				
D				3549	4311	5007	4821	6055	6368	5769	6501	6706	5630	6212	5808	4630	4578	4211	3373			
E			3148	4450	5241	5851	5907	6630	6632	7254	7058	7179	6490	6620	6083	6107	5336	4991	3791	3133		
F			3778	4781	5549	6166	6449	7008	6917	7030	6905	6832	6543	6643	6473	6157	5627	5052	4196	3511		
G		3463	4149	4642	6262	6760	6040	6784	6693	6309	7249	7106	6053	6424	6043	5441	6038	5528	4105	3782	3018	
H		4031	4900	5689	6271	6753	7038	6863	7083	6985	6834	6798	6863	6359	6287	5963	5777	5464	5058	4131	3581	
J	3481	4467	5604	6154	6963	7232	7038	6947	7499	7170	7342	7272	6710	6305	6509	6016	5985	5897	5136	4399	4032	2995
K	3748	5065	5798	5709	6825	7174	6440	7367	7357	6527	6987	7070	6013	6511	6223	5317	5588	5706	4594	4747	4164	3150
L	3844	5257	5786	6903	7126	7359	6886	7359	7090	7589	7165	7141	6311	6351	5749	5896	5507	5683	4971	4783	4090	3469
M	3952	5325	5975	6703	7016	7042	6980	7354	7259	7246	6985	6800	6360	6200	5641	5220	5122	5244	4955	4716	4175	3311
N	3893	4960	5551	5679	7178	7194	6353	7004	6824	6333	7192	6968	5747	5870	5094	1349	4997	5228	4280	4400	3801	3166
O	3675	4606	5456	6124	6558	6741	7088	6861	6998	6858	6652	6592	6531	5832	5447	4901	4793	4912	4800	4127	3682	2823
P		4169	5253	5843	6718	7150	6837	6696	7211	6842	7033	6982	6560	5883	5886	5287	5362	5181	4515	3822	3507	
Q		3802	4514	4713	5972	6696	5985	6884	6810	6031	6516	6719	5715	6168	5771	4812	5081	4898	3733	3617	3005	
R			3833	4610	5646	6364	6247	6756	6380	6258	6574	6685	6000	6063	5636	5186	5037	4691	3742	3230		
S			3480	4406	5158	5596	5886	6442	6454	6557	6448	6410	6064	6036	5568	5155	4608	4279	3490	2898		
T				3804	4568	4994	4672	5616	5730	5342	6362	6224	5120	5416	4906	4042	4243	3771	3082			
U					3451	3868	4542	4834	5264	5415	5411	5421	5354	4819	4453	3877	3265	2945				
V						3281	3685	4129	4791	4834	5140	5121	4679	4184	4060	3285	2827					
W									3595	3720	3818	3952	3613	3443								

Figure 5.48: 8C-10BS radial power profile from refuelling N16. Values are in kW.

By refuelling one thorium bundle at channel N16, the effect on the radial power distribution is significant. With 12Th-12BS and 8C-12/10BS, the radial power profile shifts towards the top of the core at channel E12/10, respectively. The 6D configuration produces a balance peak channel power, but the presence of more SEU bundles generates a larger power in the channel that was refuelled. Lastly, the 4F configuration has the most insertion of fresh SEU bundles and as such, the peak powers produced is also tilted towards the refuelled channel's region.

In the second part, the simulations deals with refuelling all 32 target channels at the same time. Firstly, the insertion of 12 fresh thorium bundles would result in a dramatic decrease in both channel powers surrounding the target channels and the target channels themselves, therefore causing peak powers to occur in the periphery channels where there are no thorium bundles. Core reactivity also decreases as a result.

The other channel configurations that include SEU bundles help produce power in the target channels and also limit the decrease in power in the driver channels. In most cases, channel and bundle power go beyond the safety and design limits of the core, except for the channel power of the 8C configuration. Location of the peak powers is close to the centre of the core and no major tilts in the radial power distribution are observed. The occurrence of the peak bundle powers in all cases are located at

the refuelling end of the target channel, which contain SEU bundles. Thus, it is the fresh SEU bundles that accompany the thorium bundles that are causing the spike in powers, which can only be addressed by reactivity control devices or neutron poison.

Table 5.21: k-effective of Core B after refuelling all target channels

Target Channel Configuration	k_{eff}	$\Delta\rho$ (mk)
12Th-12BS	0.9836655	-48.5527
8C-12BS	1.0018177	-25.2899
6D-12BS	1.0240412	4.5182
4F-12BS	1.0358926	21.0762
8C-10BS	0.994807	-32.1238
6D-9BS	1.0117015	-7.8215
4F-8BS	1.0222667	7.4503

Table 5.22: Core B characteristics after refuelling all target channels

	Peak Power (kW)			
Target Channel Configuration	Channel	Bundle	CPPF	BPPF
12Th-12BS	8551 [V12]	1025 [V11-B9]	1.681	1.991
8C-12BS	7013 [L10]	1564[K10-B2]	1.171	2.406
6D-12BS	8137 [L10]	1714 [K10-B2]	1.204	2.149
4F-12BS	8957 [K10]	1579 [K10-B3]	1.348	1.899
8C-10BS	6942 [E12]	1174[K13-B2]	1.308	2.335
6D-9BS	7371 [L10]	1363 [K13-B3]	1.085	2.153
4F-8BS	7573 [L10]	1335 [N13-B10]	1.098	1.892

The refuelling of all target channels may not be realistic since the general operations for the CANDU core performs refuelling only a handful of times per day. However, it was observed that refuelling one thorium channel generated significant power tilts. Further work is required to generate the proper refuelling technique for this type of dual fuel loading in order to avoid any radial power tilts.

	1	2	3	4	5	6	7	8	9	10	11	12	13	14	15	16	17	18	19	20	21	22
A									5518	6537	7113	7140	6591	5892								
B						4052	4990	5857	6746	7345	7670	7841	7771	6875	6324	5161	4319					
C					4564	4777	5075	5764	6860	6898	7702	7861	7069	6669	6521	5464	5161	5129				
D				4318	4964	5178	2	5985	6287	2	6700	7015	2	6588	6312	2	5500	5776	4969			
E			3647	4993	5694	5744	5383	6143	6148	6547	6738	6962	6136	6657	6289	6411	6202	6563	5260	4578		
F			3944	4689	5324	5635	5442	6071	5977	5935	6122	6164	5819	6295	6345	6101	6202	5994	5188	4756		
G		3937	4095	1	5463	5573	2	5329	5243	2	5815	5802	2	5584	5470	2	6166	6095	2	4960	4639	
H		4792	5014	5112	5426	5573	5401	5361	5475	5238	5398	5501	5523	5548	5774	5616	6042	6170	6059	5775	5887	
J	4649	5452	5836	5464	5944	5864	5295	5269	5655	5225	5662	5752	5323	5449	5972	5695	6363	6747	6268	6398	6988	5684
K	5147	6326	5963	2	5583	5584	2	5321	5255	2	5116	5350	2	5489	5587	2	5896	6500	2	7020	7502	6275
L	5378	6697	6214	6258	6091	5938	5107	5494	5245	5444	5454	5619	5062	5671	5607	6056	6368	6986	6546	7509	7652	7116
M	5560	6828	6457	6109	6026	5716	5208	5537	5411	5254	5367	5441	5191	5767	5823	5905	6291	6751	6675	7573	7912	6898
N	5435	6305	5809	2	5991	5708	2	5166	5002	2	5474	5492	2	5403	5399	2	6345	6625	2	6844	7180	6537
O	5035	5784	5855	5614	5770	5651	5521	5410	5494	5251	5405	5584	5634	5708	5900	5798	6100	6497	6511	6559	6826	5716
P		5144	5609	5479	6083	6178	5502	5490	5895	5443	5972	6117	5848	5784	6336	5897	6678	6762	6156	5933	6350	
Q		4542	4710	2	5487	5839	2	5743	5679	2	5632	6003	2	6064	5972	2	6013	6272	2	5393	5152	
R			4267	4814	5776	6210	5632	6250	5918	5686	6352	6606	5922	6422	6277	5861	6430	6411	5332	4983		
S			4328	5312	6019	5905	5768	6439	6474	6443	6729	6855	6358	6820	6501	6196	6144	6500	5562	4872		
T				4988	5688	5588	2	6016	6177	2	7247	7197	2	6430	6047	2	5885	5943	5243			
U					4610	4804	5466	6093	6844	7067	7433	7593	7321	6840	6317	5471	4887	4897				
V						4602	5216	6141	7416	7721	8484	8551	7840	6960	6757	5337	4721					
W									6095	6566	6913	7277	6624	6281								

(a) 12Th

	1	2	3	4	5	6	7	8	9	10	11	12	13	14	15	16	17	18	19	20	21	22
A									3768	4371	4665	4712	4363	4012								
B						3094	3781	4356	4937	5270	5484	5543	5553	4958	4671	3843	3266					
C					3573	3962	4401	4888	5653	5820	6190	6339	5857	5535	5344	4700	4152	3923				
D				3438	4108	4702	2786	5646	6009	3474	6316	6480	3487	6129	5919	2978	4921	4541	3820			
E			2999	4170	4940	5402	5456	6129	6180	6738	6668	6882	6288	6579	6133	6313	5605	5471	4203	3559		
F			3504	4417	5126	5653	5887	6364	6353	6448	6506	6474	6364	6484	6557	6265	6007	5444	4680	3907		
G		3265	3854	2650	5622	6061	3679	6127	6078	4028	6659	6705	4081	6371	6075	3789	6309	5982	2832	4335	3535	
H		3876	4574	5170	5703	6070	6261	6160	6422	6369	6410	6448	6651	6330	6446	6211	6285	6034	5702	4840	4373	
J	3452	4361	5216	5599	6218	6420	6235	6261	6712	6586	6801	6916	6552	6426	6714	6458	6544	6628	5903	5327	5023	3865
K	3779	4933	5455	3314	6142	6339	3989	6533	6663	4313	6605	6771	4289	6695	6676	4127	6398	6582	3447	5821	5359	4172
L	3900	5191	5497	6278	6407	6556	6149	6618	6466	7013	6784	6959	6438	6782	6503	6884	6626	6856	6121	6059	5411	4671
M	4025	5237	5686	6100	6374	6306	6285	6597	6659	6723	6718	6730	6611	6824	6733	6694	6577	6644	6240	6076	5583	4520
N	3921	4906	5267	3312	6410	6452	3999	6377	6297	4264	6879	6916	4327	6615	6412	4120	6728	6681	3462	5713	5129	4324
O	3683	4518	5191	5620	6031	6117	6415	6286	6506	6488	6503	6648	6832	6583	6617	6458	6291	6359	6067	5392	4915	3851
P		4082	4928	5414	6124	6521	6216	6215	6686	6510	6837	6977	6840	6501	6855	6417	6706	6446	5694	4917	4613	
Q		3611	4266	2731	5570	6143	3727	6363	6418	4043	6422	6761	4148	6689	6475	3818	6126	6004	2859	4556	3829	
R			3653	4435	5340	6011	5900	6423	6154	6138	6562	6766	6321	6525	6366	5988	6039	5657	4670	4001		
S			3420	4274	5076	5385	5677	6207	6331	6478	6554	6649	6384	6551	6190	5920	5448	5276	4319	3655		
T				3824	4483	4914	2831	5572	5760	3436	6551	6502	3459	5909	5541	2873	5031	4546	3883			
U					3533	3878	4592	4974	5514	5759	5882	5984	5904	5481	5075	4538	3868	3642				
V						3388	3819	4438	5212	5373	5804	5834	5426	4887	4780	3845	3406					
W									4023	4265	4447	4650	4278	4107								

(b) 8C

	1	2	3	4	5	6	7	8	9	10	11	12	13	14	15	16	17	18	19	20	21	22
A									2786	3194	3373	3406	3172	2953								
B						2481	3053	3450	3880	4094	4219	4259	4300	3860	3673	3063	2580					
C					2914	3415	3900	4262	4922	5130	5330	5452	5129	4761	4626	4116	3517	3141				
D				2798	3460	4269	4344	5321	5723	5468	5960	6123	5459	5783	5515	4570	4373	3746	3039			
E			2499	3555	4302	5029	5265	5955	6034	6770	6553	6760	6232	6382	5864	6037	5111	4668	3481	2892		
F			3120	4082	4794	5456	5951	6424	6506	6760	6690	6651	6602	6584	6519	6244	5676	4980	4204	3378		
G		2753	3530	4196	5535	6199	6098	6512	6517	6815	7264	7294	6863	6780	6355	6182	6321	5758	4395	3866	2885	
H		3195	4132	4986	5615	6181	6716	6583	6981	7087	7013	7059	7383	6807	6810	6534	6260	5820	5379	4240	3493	
J	2663	3556	4702	5470	6230	6696	6778	6815	7462	7485	7649	7764	7414	7027	7275	6908	6697	6498	5627	4639	3970	2882
K	2875	3993	4986	5329	6273	6769	6831	7351	7610	7605	7599	7823	7533	7596	7417	6983	6679	6618	5439	5164	4192	3066
L	2934	4164	4892	6136	6447	6897	6743	7342	7265	8137	7751	7951	7378	7586	7119	7518	6854	6779	5805	5246	4194	3406
M	3025	4191	5061	5944	6396	6604	6893	7318	7491	7786	7649	7669	7589	7649	7389	7301	6786	6559	5923	5269	4331	3296
N	2966	3940	4767	5304	6557	6867	6813	7116	7134	7502	7968	7994	7603	7473	7091	6969	7081	6718	5461	5056	4009	3179
O	2820	3652	4627	5443	5965	6310	6948	6819	7166	7348	7243	7427	7751	7221	7138	6913	6396	6216	5789	4709	3880	2876
P		3326	4410	5170	6012	6617	6616	6595	7269	7216	7528	7679	7628	6997	7290	6758	6738	6243	5375	4303	3699	
Q		3009	3863	4286	5395	6222	6157	6757	6876	6814	6938	7370	7028	7187	6825	6255	6106	5793	4465	4080	3130	
R			3188	4012	4936	5750	5904	6431	6249	6355	6747	6968	6573	6638	6339	5943	5729	5185	4199	3456		
S			2798	3575	4344	4940	5428	5982	6141	6455	6391	6504	6331	6370	5932	5659	4952	4496	3577	2976		
T				3063	3720	4399	4367	5177	5406	5354	6174	6116	5395	5545	5131	4410	4489	3743	3094			
U					2822	3284	4020	4280	4722	5013	4994	5093	5145	4693	4356	3952	3253	2902				
V						2682	3035	3460	4040	4119	4429	4446	4166	3772	3736	3041	2688					
W									2939	3077	3177	3331	3081	3005								

(c) 6D

	1	2	3	4	5	6	7	8	9	10	11	12	13	14	15	16	17	18	19	20	21	22
A									2527	2878	3040	3056	2863	2665								
B						2325	2873	3216	3595	3789	3868	3921	3966	3577	3402	2875	2390					
C					2745	3304	3810	4114	4774	4973	5145	5244	4989	4568	4487	3981	3391	2924				
D				2619	3279	4190	5165	5279	5668	6476	5868	6073	6467	5746	5422	5395	4233	3546	2809			
E			2363	3390	4121	4942	5227	5892	5976	6763	6499	6687	6209	6297	5790	5964	5005	4431	3290	2709		
F			3038	4025	4704	5409	5951	6412	6455	6783	6618	6605	6562	6554	6451	6263	5576	4880	4090	3282		
G		2617	3473	5003	5543	6230	7236	6510	6528	8050	7313	7295	8079	6754	6355	7325	6362	5711	5213	3770	2731	
H		3008	4024	4960	5558	6166	6738	6556	6940	7115	6950	7026	7385	6773	6747	6553	6197	5766	5318	4116	3259	
J	2443	3318	4595	5440	6221	6684	6822	6770	7479	7497	7657	7741	7457	6968	7281	6903	6689	6448	5600	4472	3709	2618
K	2609	3736	4872	6336	6266	6819	8090	7412	7635	8957	7599	7884	8883	7657	7426	8247	6660	6640	6462	5048	3882	2775
L	2657	3861	4738	6105	6422	6872	6764	7311	7246	8173	7746	7928	7402	7552	7091	7544	6829	6726	5747	5053	3871	3068
M	2732	3901	4894	5927	6340	6583	6889	7319	7455	7844	7604	7658	7592	7654	7350	7348	6730	6515	5849	5096	3992	2976
N	2701	3660	4659	6311	6601	6886	8048	7117	7161	8845	8043	8030	8956	7482	7111	8245	7134	6722	6481	4913	3716	2876
O	2576	3413	4486	5426	5904	6286	6965	6797	7126	7386	7190	7408	7782	7201	7100	6942	6341	6172	5753	4565	3609	2626
P		3113	4313	5118	5993	6601	6654	6538	7277	7215	7528	7661	7689	6950	7288	6763	6737	6202	5342	4172	3483	
Q		2871	3785	5099	5348	6269	7319	6802	6876	8035	6921	7416	8317	7236	6834	7420	6105	5784	5330	4020	2973	
R			3095	3909	4851	5685	5914	6385	6202	6316	6705	6922	6570	6594	6298	5927	5669	5094	4115	3359		
S			2627	3396	4123	4842	5362	5933	6060	6451	6302	6439	6293	6320	5856	5623	4837	4289	3388	2815		
T				2845	3530	4283	5167	5088	5341	6330	6121	6040	6378	5472	5053	5226	4393	3544	2888			
U					2621	3156	3897	4127	4532	4859	4773	4885	4983	4515	4197	3840	3118	2710				
V						2498	2846	3196	3744	3786	4078	4084	3844	3477	3480	2846	2515					
W									2651	2767	2836	2990	2764	2724								

(d) 4F

Figure 5.49: Examples of power distributions for Core B after refuelling target channels. Values are in kW

5.4.4 Initial Core Powers

Following similar steps as with Core A in Chapter 5.3.5, the radial power distributions for Core B at initial start-up was determined and shown in the following figures.

The multiplication factor for each of the configurations at start-up is at least 200 mk above critical, making any reactivity devices barely able to prevent super-criticality. The lowest is seen with the 12 thorium bundle channel configuration. Adding SEU bundles into the target channel loading will increase in the k_{eff}. In order to lower the reactivity, DU will be required to be fuelled in the initial core stage.

The behaviour of the thorium bundles acting like adjuster rods are seen again here in Figure 5.50a. Radial distribution for the 12 thorium bundle loading scheme is flatter compared to the three other configurations with the maximum channel power at 7543 kW. Starting with configuration 8C, the peak channel power is just within the design limit of 8300 kW and the peak bundle power has a 14% margin to the same limit. Adding more SEU bundles into the target channel increases both the peak channel and peak bundle powers, pushing it towards the power profile of that of a pure SEU core.

Comparing Core B radial power distributions to Core A, the maximum powers drop in Core B by removing the target channels in the periphery of Core A. The cause is due to the thorium bundles lowering the local neutron flux and thus the bundle power in the periphery region, resulting in the inner core bundles to burnup higher to generate the missing power to achieve the target power rating of the core.

Table 5.23: Initial core results for core configuration B

Target Channel Configuration	k_{eff}	Peak Powers (kW)	
		Channel	Bundle
12 Th	1.202626	7549 [M12]	970 [M12-B6]
8 Th + 4 SEU (8C)	1.221350	8255 [M12]	819 [M12-B7]
6 Th + 6 SEU (6D)	1.238025	9116 [M12]	1172 [M12-B3]
4 Th + 8 SEU (4F)	1.259051	9397 [M12]	1157 [M12-B3]

	1	2	3	4	5	6	7	8	9	10	11	12	13	14	15	16	17	18	19	20	21	22
A									4822	5312	5633	5642	5338	4863								
B						3575	4292	5180	5817	6305	6663	6674	6337	5870	5252	4379	3678					
C					3872	4122	4516	5352	5881	6075	6562	6573	6109	5940	5432	4616	4255	4044				
D				3929	4627	4641	1.166	5498	5835	1.426	6345	6356	1.435	5899	5584	1.194	4801	4844	4199			
E			3463	4461	5276	5384	5483	6100	6378	6329	6776	6789	6368	6449	6198	5613	5563	5513	4745	3830		
F			3791	4416	5293	5665	5744	6355	6594	6481	6920	6932	6521	6666	6455	5874	5839	5505	4656	4079		
G		3879	4148	1.106	5347	5679	1.394	6320	6506	1.545	6778	6789	1.554	6573	6411	1.423	5834	5526	1.152	4370	4120	
H		4752	4993	5242	5922	6244	6272	6836	7020	6850	7263	7274	6887	7087	6927	6385	6390	6089	5418	5191	4957	
J	4477	5432	5546	5581	6186	6460	6432	6990	7159	6961	7378	7390	6996	7222	7075	6537	6593	6337	5741	5725	5618	4634
K	4986	5941	5763	1.368	6140	6338	1.524	6802	6939	1.635	7137	7146	1.642	6994	6875	1.546	6453	6269	1.401	5919	6112	5132
L	5313	6308	6249	6098	6574	6764	6676	7199	7343	7124	7533	7543	7153	7395	7268	6760	6871	6694	6226	6395	6464	5449
M	5328	6326	6266	6113	6589	6778	6687	7209	7352	7131	7540	7549	7158	7399	7272	6763	6874	6697	6227	6396	6466	5450
N	5031	5997	5816	1.38	6187	6381	1.533	6835	6968	1.641	7159	7166	1.646	7009	6887	1.548	6461	6276	1.403	5924	6116	5135
O	4554	5527	5640	5669	6270	6536	6497	7049	7210	7004	7417	7423	7024	7246	7096	6555	6608	6350	5751	5733	5625	4639
P		4888	5125	5360	6037	6348	6357	6913	7088	6905	7313	7319	6923	7120	6955	6407	6410	6106	5431	5201	4966	
Q		4072	4325	1.143	5492	5807	1.419	6411	6586	1.561	6837	6842	1.565	6612	6445	1.429	5857	5546	1.156	4382	4130	
R			4047	4630	5482	5825	5871	6466	6691	6562	6993	6997	6575	6714	6497	5907	5869	5530	4675	4093		
S			3808	4726	5499	5557	5618	6218	6482	6416	6856	6859	6427	6502	6244	5649	5595	5542	4768	3846		
T				4188	4838	4802	1.197	5611	5937	1.447	6426	6429	1.45	5952	5631	1.203	4832	4872	4222			
U					4045	4263	4634	5464	5987	6169	6651	6654	6177	6000	5481	4653	4286	4071				
V						3690	4401	5288	5921	6404	6757	6759	6411	5933	5303	4417	3707					
W									4909	5396	5714	5715	5402	4917								

(a) 12Th

	1	2	3	4	5	6	7	8	9	10	11	12	13	14	15	16	17	18	19	20	21	22
A									3997	4374	4623	4629	4392	4026								
B						3091	3715	4450	4967	5363	5643	5650	5386	5005	4502	3778	3167					
C					3387	3719	4150	4868	5339	5541	5918	5926	5567	5383	4928	4226	3818	3515				
D				3443	4133	4349	1261	5283	5632	1583	6106	6114	1590	5681	5349	1282	4470	4294	3650			
E			3063	4002	4823	5126	5395	5993	6312	6360	6720	6730	6391	6367	6069	5495	5262	5000	4219	3354		
F			3470	4173	5055	5550	5808	6420	6715	6713	7080	7090	6744	6771	6497	5909	5684	5217	4359	3696		
G		3418	3873	1219	5289	5759	1759	6610	6869	2041	7203	7213	2049	6923	6682	1783	5879	5428	1254	4045	3601	
H		4144	4606	5092	5861	6338	6574	7170	7437	7399	7757	7766	7429	7489	7241	6663	6450	5989	5227	4754	4293	
J	3762	4703	5102	5447	6172	6618	6815	7415	7673	7611	7979	7988	7639	7722	7481	6897	6719	6286	5568	5232	4832	3869
K	4160	5121	5326	1543	6223	6609	2024	7363	7595	2284	7887	7895	2291	7638	7420	2044	6696	6320	1568	5437	5236	4257
L	4417	5411	5707	5933	6577	6970	7129	7710	7953	7877	8242	8250	7900	7993	7763	7194	7049	6665	6025	5808	5514	4505
M	4429	5425	5720	5945	6589	6981	7138	7718	7961	7883	8248	8255	7904	7996	7766	7196	7051	6667	6027	5809	5515	4506
N	4194	5163	5368	1552	6261	6643	2032	7389	7618	2289	7904	7909	2294	7649	7429	2046	6702	6325	1570	5441	5239	4259
O	3820	4774	5176	5517	6238	6678	6867	7461	7713	7644	8008	8013	7660	7740	7497	6909	6730	6295	5575	5237	4837	3872
P		4249	4711	5187	5952	6420	6642	7231	7490	7442	7795	7799	7456	7514	7262	6679	6464	6000	5236	4761	4298	
Q		3570	4016	1248	5404	5860	1781	6681	6932	2055	7248	7252	2059	6951	6706	1789	5896	5442	1257	4053	3607	
R			3676	4341	5201	5673	5906	6504	6788	6773	7134	7137	6783	6805	6526	5932	5703	5233	4372	3705		
S			3340	4207	4991	5258	5498	6082	6389	6424	6777	6780	6432	6403	6100	5520	5283	5019	4233	3364		
T				3642	4290	4471	1284	5366	5706	1600	6163	6165	1601	5717	5380	1288	4490	4312	3663			
U					3515	3822	4237	4948	5412	5606	5977	5979	5611	5421	4959	4250	3837	3531				
V						3173	3791	4524	5036	5427	5702	5703	5432	5043	4533	3801	3184					
W									4053	4427	4673	4674	4431	4058								

(b) 8C

	1	2	3	4	5	6	7	8	9	10	11	12	13	14	15	16	17	18	19	20	21	22
A									3134	3392	3567	3570	3403	3151								
B						2573	3094	3669	4058	4358	4556	4560	4371	4080	3700	3133	2620					
C					2859	3260	3726	4319	4729	4942	5203	5208	4958	4757	4357	3775	3324	2942				
D				2910	3576	3994	2473	5006	5371	3133	5811	5817	3143	5403	5050	2502	4073	3682	3053			
E			2625	3485	4301	4806	5255	5838	6207	6363	6631	6638	6383	6242	5888	5321	4894	4417	3634	2840		
F			3105	3873	4757	5392	5852	6470	6839	6969	7257	7263	6990	6875	6521	5919	5480	4865	4003	3267		
G		2919	3549	2413	5185	5822	3676	6925	7283	4368	7698	7704	4380	7318	6973	3709	5902	5279	2465	3668	3045	
H		3484	4159	4887	5757	6421	6904	7545	7922	8046	8340	8346	8066	7955	7592	6963	6494	5841	4977	4255	3578	
J	3002	3910	4593	5262	6124	6782	7251	7908	8286	8397	8705	8711	8415	8317	7951	7304	6847	6197	5339	4673	3987	3065
K	3281	4231	4823	3084	6283	6909	4348	8024	8387	5052	8803	8808	5061	8415	8062	4373	6964	6344	3117	4890	4295	3334
L	3464	4439	5092	5716	6551	7195	7655	8313	8690	8798	9108	9112	8813	8715	8347	7696	7244	6605	5771	5149	4494	3510
M	3472	4448	5101	5724	6560	7202	7662	8319	8695	8802	9111	9116	8815	8717	8349	7698	7245	6606	5771	5149	4494	3510
N	3303	4259	4852	3098	6309	6933	4359	8042	8403	5059	8814	8818	5066	8422	8067	4376	6968	6347	3119	4891	4297	3335
O	3041	3958	4644	5310	6170	6823	7286	7938	8312	8418	8723	8726	8428	8328	7960	7312	6853	6202	5343	4676	3989	3066
P		3557	4233	4956	5820	6477	6950	7585	7956	8074	8364	8367	8082	7970	7604	6972	6502	5847	4982	4259	3581	
Q		3030	3653	2457	5265	5891	3705	6972	7324	4387	7726	7728	4391	7335	6987	3715	5911	5286	2468	3672	3048	
R			3257	3993	4857	5474	5918	6524	6885	7006	7289	7291	7012	6894	6536	5932	5490	4874	4009	3272		
S			2833	3628	4412	4892	5322	5894	6254	6402	6665	6666	6406	6262	5904	5334	4905	4426	3641	2844		
T				3050	3680	4073	2504	5058	5416	3153	5843	5845	3155	5422	5066	2509	4083	3690	3059			
U					2942	3326	3780	4366	4771	4978	5234	5235	4980	4776	4372	3787	3333	2949				
V						2623	3139	3710	4095	4391	4585	4586	4393	4098	3714	3144	2628					
W									3163	3418	3590	3591	3420	3165								

(c) 6D

	1	2	3	4	5	6	7	8	9	10	11	12	13	14	15	16	17	18	19	20	21	22
A									2757	2962	3104	3106	2970	2770								
B						2344	2820	3321	3653	3911	4072	4075	3922	3670	3346	2851	2382					
C					2617	3057	3544	4075	4459	4683	4886	4890	4696	4481	4106	3584	3109	2686				
D				2661	3312	3832	3170	4877	5250	4021	5673	5678	4032	5276	4913	3203	3897	3398	2782			
E			2424	3237	4042	4643	5176	5741	6130	6340	6558	6563	6357	6159	5782	5231	4716	4137	3363	2610		
F			2943	3734	4604	5299	5854	6454	6854	7054	7290	7295	7072	6884	6497	5910	5372	4694	3844	3083		
G		2696	3408	3103	5120	5830	4789	7025	7426	5729	7869	7875	5742	7456	7066	4827	5897	5200	3165	3510	2803	
H		3183	3954	4785	5678	6417	7009	7645	8065	8272	8518	8523	8289	8094	7685	7059	6479	5749	4861	4034	3260	
J	2662	3547	4359	5168	6067	6811	7401	8055	8480	8681	8939	8944	8697	8506	8091	7447	6865	6128	5232	4424	3607	2711
K	2885	3823	4598	3971	6280	7009	5708	8256	8674	6688	9134	9139	6699	8698	8288	5737	7056	6331	4008	4651	3873	2925
L	3035	3993	4808	5604	6499	7244	7837	8498	8927	9130	9390	9394	9143	8949	8526	7872	7284	6543	5648	4852	4034	3069
M	3041	4000	4816	5611	6507	7251	7843	8503	8932	9134	9393	9397	9145	8951	8528	7873	7285	6544	5649	4853	4034	3069
N	2903	3846	4622	3987	6303	7030	5721	8271	8688	6697	9144	9147	6704	8704	8292	5740	7059	6334	4009	4652	3874	2926
O	2694	3586	4402	5209	6106	6846	7431	8080	8502	8700	8954	8957	8708	8515	8098	7453	6870	6132	5235	4426	3608	2712
P		3245	4017	4844	5733	6465	7049	7679	8094	8296	8538	8540	8303	8105	7694	7067	6485	5754	4865	4036	3262	
Q		2792	3498	3156	5189	5888	4823	7065	7460	5750	7893	7895	5754	7469	7077	4834	5904	5206	3168	3513	2805	
R			3075	3837	4687	5367	5908	6500	6892	7085	7316	7317	7090	6899	6510	5920	5380	4701	3849	3086		
S			2605	3358	4133	4714	5232	5787	6169	6372	6585	6586	6376	6175	5795	5241	4724	4144	3367	2614		
T				2779	3396	3897	3205	4919	5286	4043	5699	5700	4045	5291	4925	3210	3904	3404	2786			
U					2685	3110	3588	4113	4492	4711	4910	4911	4713	4495	4117	3593	3115	2691				
V						2384	2855	3353	3680	3936	4093	4093	3937	3683	3356	2859	2387					
W									2778	2981	3120	3121	2982	2780								

(d) 4F

Figure 5.50: Instantaneous radial power distribution for Core B. Values are in kW

Chapter 6

Summary and Conclusions

The work in this thesis presents a new method of utilizing pure thorium bundles in a dual fuel core loading with SEU driver bundles in the CANDU-6 system. The first step was to perform a multi-cell calculation by developing a 3x3 lattice configuration that has the eight outer lattices containing SEU bundles and the central lattice containing a thorium bundle. This multi-cell is meant to depict a local area containing nine channels in the core. From the multi-cell calculation, the thorium bundle was evaluated for its breeding dynamics, its effect on the SEU bundles and the overall multi-cell performance.

The multi-cell calculations show the effect that a thorium bundle has on a local region of the core. The reactivity of the multi-cell decreases sharply at the BOC and decreases linearly over burnup. Overall, the k_{inf} increases by increasing the enrichment in the driver fuel. Furthermore, the burnup, in which the multi-cell reaches $k_{inf} = 1$, also increases with higher driver enrichment. Throughout burnup, the U-233 concentration increases, but Pa-233 comes to equilibrium early in. In terms of safety, the CVR was calculated and it suggests that the multi-cell model operates with a CVR at a level between a NU- and SEU CANDU core during a coolant void scenario.

A preliminary infinite lattice calculation for a homogeneous thorium CANDU core was also presented in this thesis. Firstly, the thorium bundle was evaluated for the enrichment required to produce a conversion ratio of one in order to satisfy the SSET requirement. It was shown that the specific power density must be around 25.5 W/g to allow for a CR of above one and a burnup of greater than 11 GWd/t; the enrichment for this case is between 1.44% and 1.47%. The specific power rating of 32 W/g for the typical NU 37-element bundle results in a CR of one, but exit burnups of less than 10 GWd/t.

In a homogeneous thorium CANDU core, the decay of Pa-233 introduces another safety variable in managing transients. The decay produces a continued increase in concentrations of U-233, which increases the multiplication factor and can push to the

core into a critical or super-critical state. The highest insertion of reactivity occurs when the lattice has operated for only 90 days, compared to 180 days and 360 days, due to the lack of parasitic absorption from FPs.

Once the multi-cell calculation was completed, the macroscopic cross-sections from the multi-cell were passed through a 3D diffusion code to evaluate a dual fuel loading on a full core scale. Three factors were evaluated when using thorium bundles: the number of channels to be loaded with thorium bundles, the number and combination of thorium bundles to be used in those channels and the exit burnups of those channels. Time-average, instantaneous and initial start-up power maps were produced to show the power distributions for the varying configurations in terms of the number of target channels and thorium bundles used per target channel.

Core Configuration A shows the maximum number of channels designated for thorium loading. Multiple channel configurations were developed with different combinations of SEU and thorium bundles. Three channel configurations were chosen where either eight, six, or four thorium bundles, along with the remaining being SEU bundles, are loaded into the target channel. Based on the results in Core A, a modified model using the same channel configurations, Core B, was produced to show that a flattened core was possible as a result of the use of thorium bundles. All three types of channel configuration produced time-average and instantaneous channel and bundle powers to be slightly below or at the set licensing limits without the need of reactivity devices. The time-average powers for Core B are about 10% lower than that of Core A. The best time-average characteristics of Core B is shown in the following table.

At core start-up in either core configurations, the initial reactivity was at least 200 mk above critical, well beyond the safety design limit. Both core configurations also had maximum initial channel powers of at least 9000 kW, which is well above the safety design limit and the core would not be allowed to operate at such level.

Manual refuelling of the target channels was performed on the instantaneous models. Firstly, one target channel was refuelled to observe the effect on the multiplication factor. Refuelling a target channel with 12 thorium bundles decreased the k_{eff} by -8.17 mk for Core B. When the target channel was loaded with a combination of SEU and thorium bundles, the reactivity change increased as more SEU bundles replace the thorium bundles. Lastly, all target channels were then refuelled. Again, when the channel was loaded with 12 thorium bundles, the reactivity had the highest decrease of -48.55 mk, while a combination of SEU and thorium bundles did not have such large decrease in reactivity. On the contrary, the 4F configuration had an increase in k_{eff} of 7.45 mk.

Table 6.1: Best time-average characteristics of the dual fuel CANDU-6 core

Core	B	B	NU	Licensing Limits
# Target Channels (Thorium)	32	32	-	-
# Thorium Bundles per Target Channel	8	8	-	-
# 1.2% SEU Bundles per Target Channel	4	4	-	-
Arrangement	2U-8TH-2U	2U-8TH-2U	-	-
Bundles per Shift	12	10	-	-
# Driver Channels (1.2% SEU)	348	348	-	-
Bundles per Shift	2	2	8	-
Direction	Bi-directional	Bi-directional	Bi-directional	-
Adjuster Rods	No	No	No	-
Reactor Power (MW_{th})	2061.4	2061.4	2061.4	-
Max. Channel Power (MW)	6647	6650	8666	7300
Max. Bundle Power (MW)	788	774	1106	935
Max. Channel	M12	M12	M12	-
Max. Bundle	N12-B3	N12-B3	M12-B6	-
Radial Form Factor	0.816	0.815	0.626	-
k-effective	1.020234	1.019779	1.01830	-
Core-Average Burnup (MWd/t)	18315.57	18377.80	7407.49	-
Inner Region Burnup (MWd/t)	19556.23	19406.23	-	-
Outer Region Burnup (MWd/t)	17108.74	17058.74	-	-
Target Channel Exit Burnup (MWd/t)	25000	30000	-	-
Average Thorium Burnup (MWd/t)	2966.53	31448.46	-	-

Based on the models developed, it can be conclude that:

- It is feasible to implement pure thorium bundles into the current CANDU-6 core without drastic deviation from core operations. Time-average and instantaneous models show the core to operate within limits with proper placement of the thorium bundles.
- Channel configurations of thorium and SEU bundles are important in controlling axial power profiles.
  - 4F, 6D, and 8C channel configurations can be used to mimic the double-peaked hump as seen in the NU CANDU core and also to produce higher burnups in the thorium bundles.
- Core A with the 8C channel configuration can operate around the licensing limits and will require control devices to prevent overpowering.
- Core B operates with a flatter radial distribution and lower peak powers
  - Channel configuration 8C with a 12-bundle shift generates power profiles well within safety and licensing limits in both time-average and instantaneous models. This configuration would be the ideal configuration to use based on this study.
- The use of control devices and poisons will be required during refuelling target channels to prevent overpowering in the driver bundles.
- Powers and k_{eff} at initial startup are beyond safety limits and require a combination of control devices, poison, and DU or NU to lower it.

Implementing thorium bundles into the CANDU-6 core can help shape the core's power distribution. In a sense, the thorium bundles act as control rods inserted horizontally to flatten the radial form. Overall, the full core models show that it is possible to utilize a dual fuel loading in the current CANDU-6 reactors on a time-average scale. The use of thorium bundles in the configurations shown in this thesis can be a preliminary step to producing the necessary U-233 for the start of a thorium fuel cycle.

Chapter 7

Future Work

The work presented in this thesis shows the possibility of a dual fuel core loading with pure thorium and SEU bundles. Subsequently, the work has also generated many issues that require further work to fully validate this model. The core configurations for the full-core CANDU-6 using thorium bundles in this thesis did not include the reactivity devices, such as the control rods and the zone controllers, which are normally present. This is due to the intensive computational time required to perform the necessary calculations. To do so would require the use of the lattice code to calculate a 3D 3x3 multi-cell to include control rods to model the interaction between the two types of bundles from the insertion of the rods. From this, the macroscopic cross-sections would be fed to the diffusion code for a full-core calculation and then analyzed under standard and transient operations.

The multi-cell model developed in this thesis only depicts a loading of fresh fuel bundles and these macroscopic cross-sections were utilized for the entire full-core modelling. To be more accurate, the multi-cell model should be simulated with bundles starting at different stages of burnup. More specifically, the full-core is comprised of 12 X-Y planes (the face of the core) which have bundles are different levels of burnup depending if the plane is closer to the centre of the core or closer to the periphery. Work will be required to develop twelve multi-cell simulations to mimic each plane of the core to create a more representative model of the dual-fuel core.

The bundle integrity limit of 40 GWD/t is a sensible metric for the CANDU fuel bundle utilizing enriched fuel, but a different limit must determined for a pure thorium bundle since it will initially produce insignificant amounts of power for during the time it requires to breed sufficient U-233 content. During this time, the thorium bundle would not be exposed to the same stresses as a driver bundle with enriched uranium fuel and therefore, may have a higher limit. Experimental work will be required to determine the burnup limit of a pure thorium bundle and subsequently, used to re-evaluate the full-core models.

There is also the concern of the initial start-up for the dual fuel CANDU core. The massive excess reactivity from the use of SEU driver fuel needs to be attenuated by the use of lower enriched uranium bundles such as DU used in the start-up of current NU CANDU cores. Part of the inner regions of the core will need to be fueled with DU/NU bundles to lower the initial reactivity to within effectiveness of the reactivity devices. Furthermore, once refuelling begins, an evaluation of the refuelling scheme needs to be considered to shuffle out the DU/NU bundles.

An economic evaluation is required to determine the feasibility of implementing of such a dual fuel mode with the configurations outlined in this thesis. The outcome of such analysis must be such that sacrifice of burnup of the core from the use of thorium bundles is mitigated by the credit given for the amount of U-233 produced. To do so, the refuelling rate of a driver and target channel must be determined to calculate the amount of enriched uranium and thorium will be used.

The realization of the SSET cycle in the CANDU system still requires work. Further evaluations of a fully-fuelled thorium CANDU core using 3D lattice simulations is required to observe the interactions between thorium bundles and control rods. The next step would also be to perform full-core scale calculations to produce time-average and instantaneous models. The scope is not just limited to these recommendations; extensive research is still required to fully develop the idea of a (Th,U-233) fuel cycle in the CANDU system.

Finally, the implementation of enriched uranium and thorium fuels will require an investigation into the radiological impacts it poses, specifically regarding the concentrations of Cesium, Strontium, Protactinium, and Uranium the final fuel composition contains. If the resulting radiation levels are higher, then the need to design waste fuel repositories is warranted.

Bibliography

[1] Nuclear Waster Management Organization, "Used nuclear fuel reprocessing." http://www.nwmo.ca/uploads_managed/MediaFiles/1965_backgrounder_usednuclearfuelreprocessing2012.pdf, 2010.

[2] K. D. Kok, *Nuclear engineering handbook*. Taylor and Francis Group, 2009.

[3] International Atomic Energy Agency, "Thorium fuel cycle – potential benefits and challenges," Tech. Rep. IAEA-TECDOC-1450, May 2005.

[4] World Nuclear Association, "Thorium." http://www.world-nuclear.org/info/current-and-future-generation/thorium/, July 2014.

[5] Generation IV International Forum Experts' Group, "Use of thorium in the nuclear fuel cycle," *2013 GIF Annual Report*, Decemeber 2010.

[6] CANTEACH, "CANDU6 reactor assembly." https://canteach.candu.org/Image%20Library1/00000/CANDU6_Reactor_Assembly.jpg, February 2012.

[7] J. Veeder, "Thorium fuel cycles in CANDU," Tech. Rep. AECL-6254, AECL, 1978.

[8] A. Nuttin, P. Guillemin, T. Courau, and G. Marleau, "Study of CANDU Thorium-based Fuel Cycles by Deterministic and Monte Carlo Methods," in *Advances in Nuclear Analysis and Simulation*, American Nuclear Society, September 2006.

[9] "Evaluated Nuclear Data File (ENDF) Database." https://www-nds.iaea.org/exfor/endf.htm, 2010.

[10] K.-H. Beckurts and K. Wirtz, "Table of thermal neutron cross sections of the isotopes." link.springer.com/content/pdf/bbm%3A978-3-642-87614-1%2F1.pdf, 1964.

[11] A. Morreale, *Analysis of transuranic mixed oxide fuel in CANDU nuclear reactor*. PhD thesis, Dept. Eng. Phys., McMaster University, Hamilton, Ontario, 2013.

[12] World Nuclear Association, "Processing of used nuclear fuel." http://www.world-nuclear.org/info/Nuclear-Fuel-Cycle/Fuel-Recycling/Processing-of-Used-Nuclear-Fuel/, August 2012.

[13] "Spent fuel reprocessing options," Tech. Rep. IAEA-TECDOC-1587, International Atomic Energy Agency, August 2008.

[14] T. Todd, "Dry (non-aqueous) processing of used nuclear fuel." www.wmsym.org/archives/2012/panels/017-164.pdf.

[15] K. Goff and M. F. Simpson, "Dry processing of used nuclear fuel," in *Proceedings of Global 2009*, SAS Institute Inc., September 2009.

[16] C. J. Park, K. H. Kang, J. W. Lee, and K. S. Seo, "An investigation on recycling the recovered uranium from electro-refining process in a CANDU reactor," *Annals of Nuclear Energy*, vol. 38, pp. 742–747, Decemeber 2011.

[17] W. Carter, "Thorium utilization program: A survey of processing methods for thorium reactor fuels," Tech. Rep. ORNL-TM-241, ORNL, Oak Ridge, U.S.A., July 1962.

[18] H. Choi, W. I. Ko, and M. S. Yang, "Economic analysis on direct use of spent pressurized water reactor fuel in CANDU reactors – II: DUPIC fuel-handling cost," *Nuclear Technology*, vol. 134, pp. 130–148, May 2001.

[19] "Reprocessing plants, world-wide." http://www.euronuclear.org/info/encyclopedia/r/reprocessing-plants-ww.htm, September 2014.

[20] W. I. Ko, H. Choi, and M. S. Yang, "Economic analysis on direct use of spent pressurized water reactor fuel in CANDU reactors – IV: DUPIC fuel cycle cost," *Nuclear Technology*, vol. 134, pp. 130–148, May 2001.

[21] P. G. Boczar, G. R. Dyck, P. Chan, and D. Buss, "Recent advances in thorium fuel cycles for CANDU reactors," in *Thorium Fuel Utilization: Options and Trends*, no. IAEA-TECDOC-1319, (Austria), IAEA, November 1997.

[22] M. Milgram, "Once-through thorium cycles in CANDU reactors," Tech. Rep. AECL-7516, AECL, Canada, January 1982.

[23] S. S. Drera, K. I. Bjork, and J. F. Kelly, "Thorium fuel production and results from beginning of life irradation," *Progress in Nuclear Energy*, vol. 72, pp. 5–10, 2014.

[24] B. Bromley, "Heterogeneous core designs and thorium based fuels for heavy water reactors." http://www.google.com/patents/CA2839084A1?cl=en, July 17 2014. CA Patent App. CA 2,839,084.

[25] X. Zhonsheng and P. G. Boczar, "CANDU fuel-cycle vision," Tech. Rep. AECL-11937, AECL, Canada, May 1998.

[26] J. J. Duderstadt and L. J. Hamilton, *Nuclear Reactor Analysis*. John Wiley & Sons, 1976.

[27] G. Marleau, "DRAGON theory manual part 1: Collision probability calculations," Tech. Rep. IGE-236 Revision 1, École Polytechnique de Montréal, Canada, October.

[28] A. Hébert, *Applied Reactor Physics*. Canada: Presses Internationales Polytechnique, 2009.

[29] G. Marleau, A. Hébert, and R. Roy, "A user guide for DRAGON 3.06," Tech. Rep. IGE-174 Revision 9, École Polytechnique de Montréal, December 2011.

[30] B. Rouben, "CANDU fuel management," November 2003. Presented to McMaster University.

[31] E. Varin, A. Hébert, R. Roy, and J. Koclas, "A user guide for DONJON version 3.01," Tech. Rep. IGE-208 Revision 4, École Polytechnique de Montréal, August 2005.

[32] National Nuclear Data Center, "Chart of Nuclides." `http://www.nndc.bnl.gov/`, 2015.

[33] B. Rouben, "Xenon effect." class notes for EP6D03.

[34] Y. Friedlander, "A scoping study of advanced thorium fuel cycles for CANDU reactors," Master's thesis, Dept. Eng. Phys., McMaster University, Hamilton, Ontario, 2011.

[35] R.D. Page, "Canadian power reactor fuel," tech. rep.

[36] CNSC, "Science and reactor fundamentals – reactor physics." `https://canteach.candu.org/Content%20Library/20030101.pdf`, 2002.

[37] D. Serghiuta and O. Nainer, "The Application of the Goal Programming to CANDU Fuel Management Optimization," in *Proceedings of the 19th CNS Simulation Symposium*, Canadian Nuclear Society, October 1995.

[38] B. Rouben, "CANDU Fuel Management Course." `https://canteach.candu.org/Content%20Library/20031101.pdf`, 1999.

[39] D. Rozon, "CANDU fuel management and advanced fuel cycles: Reasearch at Ecole Ploytechnique." `https://canteach.candu.org/Content%20Library/20043403.pdf`, December 1997.

[40] M. Younis and P. Boczar, "Equilibrium fuel-management simulations for 1.2% SEU in a CANDU 6," in *Proceedings of the 29th annual conference of the Canadian Nuclear Association and 10th annual conference of the Canadian Nuclear Society*, vol. 2, Canadian Nuclear Society, 1989.

[41] J. Luxat. personal communication, April 2014.

[42] B. Rouben, "DIFC6 computer program." class notes for EP784.

Appendix A

Reference Material

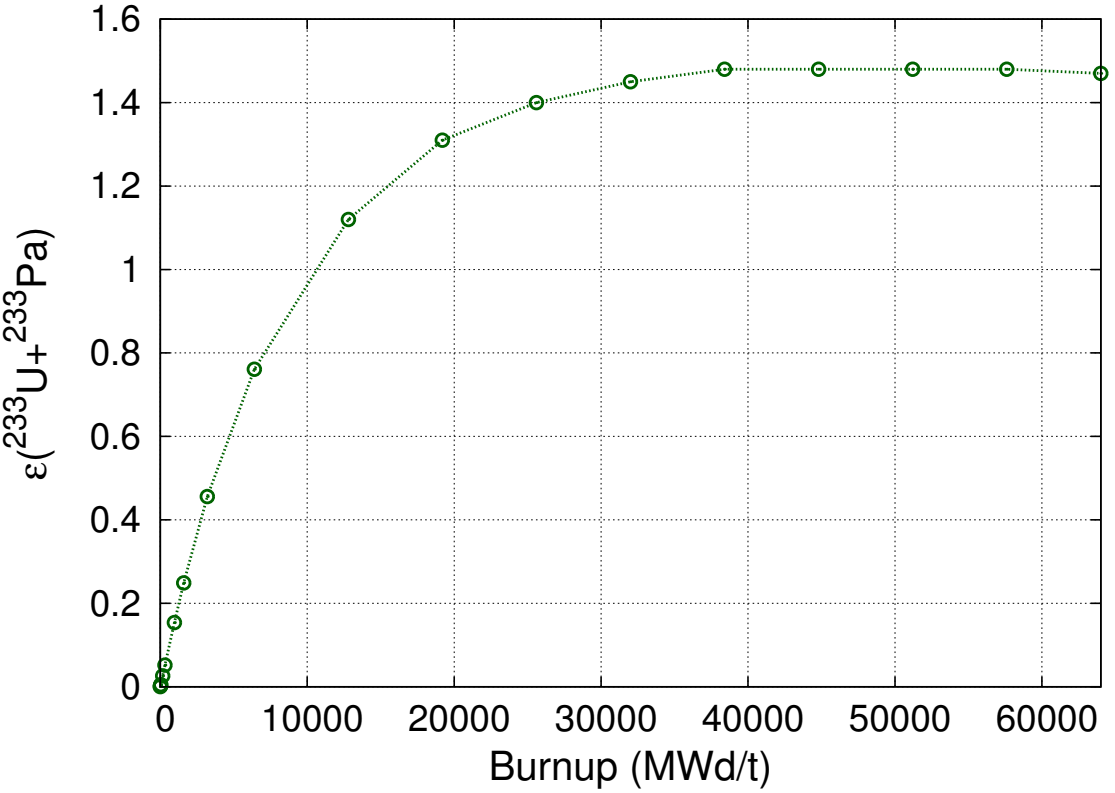

Figure A.1: U-233 + Pa-233 enrichment in thorium bundle over extended burnup using 1.2% driver bundles

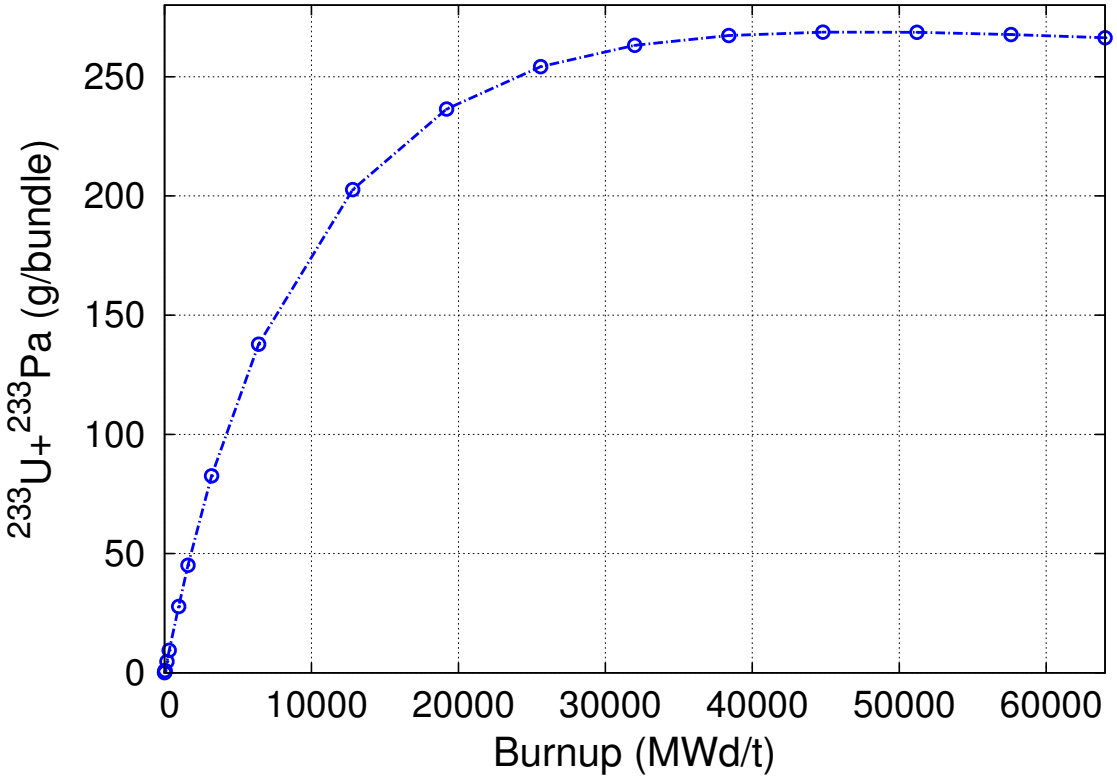

Figure A.2: U-233 + Pa-233 weight in thorium bundle over extended burnup using 1.2% driver bundles

Table A.1: Burnup values for various shifts schemes at an exit burnup of 22 GWd/t

	Burnup (MWd/t)					
Bundle Position	2 Bundle Shift	4 Bundle Shift	6 Bundle Shift	8 Bundle Shift	10 Bundle Shift	12 Bundle Shift
1	22010.42	20761.84	21037.71	21980.8	6537.523	8.181668
2	21989.57	21865.1	25591.7	21636.45	5189.154	6032.822
3	20268.49	23203.95	26562.41	16282.57	14972.88	19298.49
4	16955.23	22169.1	22827.58	18125.44	24370.89	29644.87
5	12550.27	17928.29	17983.98	23086.04	30771.78	36710.59
6	7649.077	13677.95	17996.63	25901.35	34021.1	40305.04
7	3412.923	10594.65	17471.67	25901.35	34021.1	40305.04
8	805.7356	6801.02	15051.2	23086.04	30771.79	36710.6
9	48.80201	2405.415	10274.14	17527.61	24370.89	29644.87
10	13.11703	201.4894	3711.84	9389.978	14972.89	19298.5
11	6.736923	11.30401	60.98563	889.2483	3321.716	6032.818
12	2.295698	3.79189	4.844299	5.987214	7.18993	8.181684

Table A.2: Bundle power for various shifts schemes at an exit burnup of 22 GWd/t for a 12 thorium bundle loading

	Power (kW)					
Bundle Position	2 Bundle Shift	4 Bundle Shift	6 Bundle Shift	8 Bundle Shift	10 Bundle Shift	12 Bundle Shift
1	269.0012	226.2406	209.206	188.3383	70.6841	0.048942
2	664.4625	566.3236	546.8316	456.4289	98.44853	116.8601
3	825.0781	751.0468	734.5762	454.4307	385.6687	447.7383
4	739.3812	753.3834	695.184	525.1445	611.1732	656.167
5	505.1313	592.6993	524.7111	612.0689	715.7711	744.1865
6	257.2285	421.5255	498.3982	636.6873	742.083	760.291
7	90.52637	337.4051	480.7438	625.5624	729.2094	747.0971
8	9.77646	231.591	443.7952	580.9943	680.1293	707.1306
9	0.28251	63.43766	335.086	472.7233	563.8886	605.4594
10	0.229038	0.866471	102.8026	259.2346	347.274	403.8323
11	0.171129	0.150286	0.183587	7.072379	50.15262	103.8859
12	0.067419	0.0577	0.053396	0.048344	0.040076	0.040122

Table A.3: Burnup values for various shifts schemes at an exit burnup of 37 GWd/t for a 12 thorium bundle loading

	Burnup (MWd/t)					
Bundle Position	2 Bundle Shift	4 Bundle Shift	6 Bundle Shift	8 Bundle Shift	10 Bundle Shift	12 Bundle Shift
1	36970.73	37545.3	34008.68	36632.05	18729.86	36.97425
2	37029.25	37943.07	40923.78	38577.45	13470.08	16438.69
3	34804.66	36105.36	43746.88	34223.57	27621.11	34683.71
4	30696.11	36406.25	41461.01	30495.18	39991.8	48811.64
5	24811.69	33795.04	32661.63	37205.13	48479.18	58532.3
6	17950.52	26988.74	29197.99	40830.74	52807.95	63496.68
7	10736.92	18940.31	28910.47	40830.74	52807.95	63496.68
8	4709.356	14542.99	25948.29	37205.13	48479.17	58532.29
9	1009.662	9338.875	20112.13	30081.33	39991.8	48811.64
10	28.94846	3258.487	11594.02	19665.46	27621.11	34683.71
11	7.934091	56.15088	1813.155	6357.585	11634.24	16438.7
12	2.701524	4.685569	6.423384	8.29651	12.20208	36.97355

Table A.4: Core A-4F-12BS bundle burnup values in channel K10

	Average Channel Exit Burnup (MWD/t)				
Bundle	22000	25000	27000	32000	37000
Position	Bundle Burnup (MWD/t)				
1	6027.12158	6711.06006	7167.2251	8304.18457	9431.8418
2	15823.4814	17453.4375	18535.0781	21223.3066	23894.1445
3	23457.0879	25852.2676	27453.2852	31470.7324	35510.0312
4	29366.5547	32400.9414	34436.9922	39566.5234	44742.6602
5	27168.5156	32144.6172	35454.8789	43710.3203	51941.9648
6	30157.2207	35437.6719	38952.5195	47724.9297	56479.3789
7	30157.2207	35437.6719	38952.5195	47724.9297	56479.3789
8	27168.5215	32144.625	35454.8906	43710.3242	51941.9727
9	29366.5547	32400.9414	34436.9922	39566.5234	44742.6602
10	23457.0938	25852.2754	27453.2891	31470.7324	35510.0312
11	15823.4775	17453.4316	18535.0723	21223.3027	23894.1387
12	6027.1333	6711.07324	7167.23535	8304.19922	9431.85938

Table A.5: Core A-6D-12BS bundle burnup values in channel K10

	Average Channel Exit Burnup (MWD/t)				
Bundle	22000	25000	27000	32000	37000
Position	Bundle Burnup (MWD/t)				
1	6314.00244	6950.26025	7375.17383	8436.13281	9491.15527
2	16509.0723	18021.4297	19027.627	21535.5586	24035.377
3	24461.8516	26691.7617	28185.2402	31940.5684	35724.5977
4	23110.3711	27190.2285	29904.4414	36676.4531	43432.7344
5	29242.3848	33871.9961	36957.3711	44667.8086	52375.3477
6	32362.3164	37274.3203	40550.1562	48743.4609	56940.7773
7	32362.3164	37274.3203	40550.1562	48743.4609	56940.7773
8	29242.3848	33871.9961	36957.3672	44667.8086	52375.3477
9	23110.3711	27190.2285	29904.4414	36676.4531	43432.7344
10	24461.8574	26691.7676	28185.2441	31940.5684	35724.6055
11	16509.0684	18021.4258	19027.6211	21535.5508	24035.3711
12	6314.0127	6950.27393	7375.18262	8436.14648	9491.16992

Table A.6: Core A-8C-12BS bundle burnup values in channel K10

	Average Channel Exit Burnup (MWD/t)				
Bundle	22000	25000	27000	32000	37000
Position	Bundle Burnup (MWD/t)				
1	6663.74121	7264.02783	7665.27441	8668.48926	9668.03027
2	17341.748	18764.6992	19713.5605	22085.0625	24455.9395
3	15890.5244	18998.4492	21063.3203	26205.1543	31325.4414
4	25311.166	29166.9629	31735.1133	38151.3047	44563.8477
5	31756.8965	36130.2266	39048.5156	46353.1758	53669.0039
6	35035.9258	39675.6172	42774.2148	50536.793	58317.6992
7	35035.9258	39675.6172	42774.2148	50536.793	58317.6992
8	31756.9043	36130.2266	39048.5234	46353.1797	53669.0117
9	25311.166	29166.9629	31735.1133	38151.3047	44563.8477
10	15890.5293	18998.457	21063.3262	26205.1602	31325.4551
11	17341.7441	18764.6934	19713.5508	22085.0547	24455.9336
12	6663.75293	7264.0376	7665.28857	8668.50586	9668.0459

Table A.7: Core A-4F-8BS bundle burnup values in channel K10

	Average Channel Exit Burnup (MWd/t)			
Bundle	22000	26000	30000	34000
Position	Bundle Position (MWd/t)			
1	25926.0859	29050.6816	32221.5156	35421.6953
2	27339.3789	30645.5664	34012.9844	37421.1602
3	27231.9023	30494.2637	33818.8125	37188.6406
4	25804.2773	28866.2031	31966.8945	35093.1719
5	16248.7227	20925.1562	25548.0645	30133.1641
6	18600.4492	23546.4824	28441.8262	33304.5234
7	18600.4492	23546.4824	28441.8262	33304.5234
8	16248.7246	20925.1602	25548.0684	30133.168
9	22883.0859	25621.4766	28388.1113	31171.3105
10	18290.8535	20481.9277	22681.9258	24882.9414
11	12264.7734	13780.4551	15293.2617	16795.6328
12	4559.07715	5179.06494	5805.89648	6434.49316

Table A.8: Core A-6D-9BS bundle burnup values in channel K10

	Average Channel Exit Burnup (MWd/t)			
Bundle	22000	26000	30000	34000
Position	Bundle Position (MWd/t)			
1	24408.0664	27066.8125	29761.3164	32480.8516
2	24939.1699	27640.2168	30384.793	33163.0508
3	24300.4941	26905.7109	29539.1133	32193.0703
4	16329.21	20549.0918	24739.4062	28907.3555
5	21587.125	26348.3848	31092.5215	35825.5195
6	24259.791	29296.1484	34325.4609	39348.6484
7	24259.791	29296.1484	34325.4609	39348.6484
8	21587.125	26348.3848	31092.5234	35825.5234
9	16329.21	20549.0918	24739.4062	28907.3555
10	20817.998	23075.7051	25350.8281	27636.4219
11	14012.2949	15563.0029	17113.5781	18658.5078
12	5274.49414	5918.17871	6567.93506	7219.30957

Table A.9: Core A-8C-10BS bundle burnup values in channel K10

	Average Channel Exit Burnup (MWd/t)			
Bundle	22000	26000	30000	34000
Position	Bundle Position (MWd/t)			
1	20067.2383	22074.207	24099.9727	26139.5547
2	20022.8906	22001.7402	23992.3633	25990.916
3	12354.7656	15879.5098	19380.2188	22863.123
4	20949.1562	25303.791	29645.5449	33980.3828
5	26831.8223	31749.9336	36674.5664	41603.1328
6	29819.1953	35028.7852	40253.5117	45488.1328
7	29819.1953	35028.7852	40253.5117	45488.1328
8	26831.8242	31749.9336	36674.5664	41603.1367
9	20949.1562	25303.791	29645.5449	33980.3828
10	12354.7734	15879.5137	19380.2246	22863.125
11	15741.293	17339.3555	18941.5312	20543.2461
12	5992.09961	6662.69482	7338.81738	8016.46094

Table A.10: Core B-4F-12BS bundle burnup values in channel K10

	Average Channel Exit Burnup (MWD/t)				
Bundle	20000	24000	28000	32000	37000
Position	Bundle Burnup (MWD/t)				
1	5572.64697	6482.94873	7395.12354	8304.18457	9431.8418
2	14732.3975	16911.1055	19074.4531	21223.3066	23894.1445
3	21864.8691	25053.0059	28255.0234	31470.7324	35510.0312
4	27358.7207	31386.7441	35458.6328	39566.5234	44742.6602
5	23841.5098	30487.4824	37108.1641	43710.3203	51941.9648
6	26629.8398	33678.7031	40708.5781	47724.9297	56479.3789
7	26629.8398	33678.7031	40708.5781	47724.9297	56479.3789
8	23841.5137	30487.4785	37108.1719	43710.3242	51941.9727
9	27358.7207	31386.7441	35458.6328	39566.5234	44742.6602
10	21864.8652	25053.0098	28255.0273	31470.7324	35510.0312
11	14732.3965	16911.0996	19074.4531	21223.3027	23894.1387
12	5572.65771	6482.96045	7395.13867	8304.19922	9431.85938

Table A.11: Core B-6D-12BS bundle burnup values in channel K10

	Average Channel Exit Burnup (MWD/t)				
Bundle	20000	25000	30000	35000	40000
Position	Bundle Burnup (MWD/t)				
1	5891.77393	6950.26025	8012.21924	9070.08789	10120.0176
2	15499.7363	18021.4297	20533.5977	23036.1367	25533.168
3	22983.5098	26691.7617	30434.8789	34207.6719	38007.6992
4	20381.918	27190.2285	33969.7344	40731.8477	47480.4648
5	26154.1289	33871.9961	41584.0273	49292.7109	56998.5
6	29088.9395	37274.3203	45465.5547	53661.5195	61860.1094
7	29088.9395	37274.3203	45465.5547	53661.5195	61860.1094
8	26154.1328	33871.9961	41584.0312	49292.7109	56998.5078
9	20381.918	27190.2285	33969.7344	40731.8477	47480.4648
10	22983.5117	26691.7676	30434.8809	34207.6836	38007.7031
11	15499.7354	18021.4258	20533.5898	23036.1348	25533.1582
12	5891.78271	6950.27393	8012.23291	9070.10938	10120.0312

Table A.12: Core B-8C-12BS bundle burnup values in channel K10

	Average Channel Exit Burnup (MWD/t)					
Bundle	20000	24000	25000	28000	30000	32000
Position	Bundle Burnup (MWD/t)					
1	6265.74707	7063.63818	7264.02783	7865.99658	8267.40723	8668.48926
2	16394.6406	18290.2422	18764.6992	20187.9648	21136.5938	22085.0625
3	13809.7588	17964.0352	18998.4492	22093.9082	24151.6445	26205.1543
4	22735.959	27882.3086	29166.9629	33018.7148	35585.3242	38151.3047
5	28844.4941	34671.8672	36130.2266	40508.4336	43429.8125	46353.1758
6	31949.4004	38127.8945	39675.6172	44324.9727	47429.2188	50536.793
7	31949.4004	38127.8945	39675.6172	44324.9727	47429.2188	50536.793
8	28844.4922	34671.8711	36130.2266	40508.4336	43429.8125	46353.1797
9	22735.959	27882.3086	29166.9629	33018.7148	35585.3242	38151.3047
10	13809.7666	17964.0449	18998.4492	22093.9102	24151.6484	26205.1602
11	16394.6387	18290.2383	18764.6992	20187.957	21136.5898	22085.0547
12	6265.76025	7063.65186	7264.02783	7866.00928	8267.41992	8668.50586

Table A.13: Core B-4F-8BS bundle burnup values in channel K10

	Average Channel Exit Burnup (MWd/t)									
Bundle	18000	20000	24000	28000	29000	30000	31000	32000	36000	37000
Position	Bundle Burnup (MWd/t)									
1	22887	24391	27481	30632	31426	32222	33019	33819	37030	37836
2	24138	25721	28983	32323	33167	34013	34862	35713	39137	39997
3	24070	25634	28854	32150	32983	33819	34658	35499	38887	39740
4	22817	24297	27329	30413	31189	31967	32746	33527	36664	37451
5	11478	13880	18595	23242	24396	25548	26697	27845	32415	33554
6	13566	16098	21081	25999	27221	28442	29660	30877	35726	36935
7	13566	16098	21081	25999	27221	28442	29660	30877	35726	36935
8	11478	13880	18595	23242	24396	25548	26697	27845	32415	33554
9	20205	21533	24248	27002	27695	28388	29083	29778	32567	33267
10	16134	17205	19384	21581	22132	22682	23232	23782	25983	26533
11	10767	11511	13022	14538	14916	15293	15670	16046	17542	17914
12	3956	4254	4868	5492	5649	5806	5963	6120	6749	6905

Table A.14: Core B-6D-9BS bundle burnup values in channel K10

	Average Channel Exit Burnup (MWd/t)					
Bundle	27000	28000	29000	30000	31000	35000
Position	Bundle Burnup (MWd/t)					
1	27737.7	28410.5	29085.0	29761.3	30439.1	33163.9
2	28322.8	29007.8	29695.2	30384.8	31076.5	33862.2
3	27561.9	28219.5	28878.7	29539.1	30200.8	32859.4
4	21599.2	22647.5	23694.2	24739.4	25783.2	29946.7
5	27535.7	28722.0	29907.6	31092.5	32276.8	37007.2
6	30554.0	31811.5	33068.7	34325.5	35581.9	40603.4
7	30554.0	31811.5	33068.7	34325.5	35581.9	40603.4
8	27535.7	28722.0	29907.6	31092.5	32276.8	37007.2
9	21599.2	22647.5	23694.2	24739.4	25783.2	29946.7
10	23643.3	24211.7	24780.9	25350.8	25921.4	28209.1
11	15951.0	16338.8	16726.4	17113.6	17500.4	19043.7
12	6080.3	6242.6	6405.2	6567.9	6730.7	7382.1

Table A.15: Core B-8C-10BS bundle burnup values in channel K10

	Average Channel Exit Burnup (MWd/t)					
Bundle	27000	28000	29000	30000	31000	35000
Position	Bundle Burnup (MWd/t)					
1	21570.4	22074.2	22579.2	23085.2	23592.1	24100.0
2	21505.6	22001.7	22498.6	22996.0	23493.9	23992.4
3	15001.0	15879.5	16756.6	17632.4	18506.9	19380.2
4	24216.7	25303.8	26390.1	27475.7	28560.9	29645.5
5	30519.6	31749.9	32980.6	34211.6	35442.9	36674.6
6	33724.6	35028.8	36333.8	37639.7	38946.3	40253.5
7	33724.6	35028.8	36333.8	37639.7	38946.3	40253.5
8	30519.6	31749.9	32980.6	34211.6	35442.9	36674.6
9	24216.7	25303.8	26390.1	27475.7	28560.9	29645.5
10	15001.1	15879.5	16756.6	17632.4	18506.9	19380.2
11	16939.1	17339.4	17739.8	18140.3	18540.9	18941.5
12	6494.3	6662.7	6831.4	7000.4	7169.5	7338.8